Inhibition of the bacterial ribosome by nascent and antimicrobial peptides

Alexandra Seefeldt

université de BORDEAUX

THÈSE PRÉSENTÉE

POUR OBTENIR LE GRADE DE

DOCTEUR DE L'UNIVERSITÉ DE BORDEAUX

ÉCOLE DOCTORALE SCIENCES DE LA VIE ET DE LA SANTÉ

SPÉCIALITÉ BIOCHIMIE et BIOLOGIE STRUCTURALE

Par Alexandra Carolin SEEFELDT

Master of Science in Biochemistry (LMU, Munich, Germany)

Née le 20. Août 1988 à Heidelberg, Allemagne

Inhibition of the bacterial ribosome by nascent and antimicrobial peptides

Sous la direction du: Dr C Axel INNIS

Soutenue le 14. Décembre 2017

Membres du jury :

Prof. KRAMER, Ijsbrand	Professeur, Université de Bordeaux	Président
Dr. SCHMITT, Emmanuelle	Directeur de recherche 2, École polytechnique (Paris)	Rapporteur
Prof. SUGA, Hiroaki	Professeur, University of Tokyo	Rapporteur
Dr. FRONZES, Rémi	Directeur de recherche 2, Université de Bordeaux	Examinateur
Dr. HASHEM, Yaser	Chargé de recherche, Université de Strasbourg	Examinateur

To

my mom Bärbel Seefeldt,

my grandma Trude Kurz,

my grandfather Rolf Kurz,

my uncle Frieder Kurz,

and music.

"The way to get good ideas is to get lots of ideas and throw the bad ones away."

Linus Pauling

Acknowledgments

Firstly, I would like to thank all members of the jury, **Prof Ijsbrand Kramer, Dr. Emmanuelle Schmitt, Prof Hiroaki Suga, Dr. Rémi Fronzes** and **Dr. Yaser Hashem**, for taking the time to read and evaluate my thesis. My research was funded with a pre-doctoral fellowship from INSERM and the region Aquitaine.

During the last three years, I was often asked the question why I decided to come to Bordeaux and my answer was always the same, I wanted to work on ribosomes and Structural Biology and that I chose the project not the city. By now, I know that this city and its location are just incredible and I had a great opportunity to get to know the South-West of France. The last three years have been a wonderful journey and I had the honor to work with so many inspiring people and here I would like to take the opportunity to acknowledge everyone.

Firstly, I would like to express my sincere gratitude to my thesis supervisor **Axel Innis** for giving me this great opportunity to come to Bordeaux and to work on these wonderful projects. It has been my pleasure and honor to be your first PhD student. Your passion for science was inspiring. Your constant guidance and our knowledge exchanges helped me during the whole of my research and writing and inspired me to pursue an academic career.

Next, I am especially grateful to **Britta Seip**. I will never forget your welcoming smile when I first arrived in Bordeaux. From the start, you were there for me to discuss with me and giving me constant input throughout the entire time of my thesis and during the writing process. You were there when I needed a push to finish an experiment or to post-pone it to the next day. I would like to thank you for being an inspiring colleague and more importantly becoming a wonderful and close friend. It was a lot of fun to discover France with you.

I owe a special thanks to **Kishore Inampudi** for establishing the flexizyme reaction and $tRNA_i^{Met}$ purification, for cloning $tRNA^{Pro}$ into pUC19 and cloning the proline-tRNA synthetase. Thanks to your work, I had a huge advantage when I started my thesis. A special thank goes to **Natacha Pérébaskine** for ribosome and tRNA purification and teaching me how to crystallize ribosomes. Our synchrotron trips were always special, and we came back to Bordeaux often with more than one exciting story to tell. I had a great time working with you.

I would like to thank **Alba Herrero del Valle** for her support and positive energy. We had a lot to talk and laugh about. You always found a new way to improve my figures and slides (😊) make them look better. I had a great time working with you and I am happy to call you my friend. I want to thank **Justine Charon** for helping me write the French sections and bringing a great spirit into the lab. I want to thank **Guénaël Sacheau** for his help with sequencing reactions, correcting my French sections of my thesis and for providing a good mood including OOOOOh yeah, tons of despacito and "Je peux pas, j'ai aqua cloning". A special thanks to **Mélanie Gillard, Elodie Leroy** and **Aitor Manteca**. I know you just arrived but it has been a fun time working with you and spent time with you during lunch and coffee breaks. A big thanks to **Elodie Leroy** for her help with the summary in French.

I want to acknowledge **Gilles Guichard** and his group for fruitful collaboration over the last years that resulted directly in many positive results. I want to thank in particular **Caterina Lombardo** and **Christophe André** for the synthesis of the flexizyme compounds and constant discussions to increase the yield of the peptidylation and to overcome problems with proline. Furthermore, I would like to thank **Céline Douat** and **Stéphanie Antunes** for their work during the Onc112 project. It was a great pleasure to work with you.

Next, I want thank **Daniel Wilson** and his group for constant input, knowledge exchanges and sending the plasmid expressing EF-P and EF-G from *E. coli*. Additionally, I want to thank **Fabian Nguyen**, **Michael Graf** and **Stefan Arenz** for their work during the PrAMP project. A special thanks to **Marco Scocchi** and **Mario Mardirossian** for working with us on the further characterization of PrAMPs.

I owe also thanks to **Alexander Shura Mankin** and his team for their help in input. I especially want to thank **Nora Vazquez-Laslop**. It was always inspiring discussing with you during conferences. A special thanks to **Tanja Florin** and **James Marks III** for your ideas to improve my toeprinting experiments. My sincere thanks to **Thomas Steitz** and **his group** for providing plasmids, protocols and advice for tRNA purification.

I want to thank **Derek McCusker** and his team for providing material and **Emmaunelle Schmitt** for providing the pBSTNAV plasmids for tRNA purification. A special thanks to **Brice Kaufmann** and **Stéphane Massip** for their support during crystal freezing and fishing. It was always a very exciting moment after weeks of sample preparation. During crystal screening and data collection, I want to acknowledge **Pierre Legrand** and **Leonard Chavas** from PX1 and **William Shepard** and **Martin Savko** from PX2a beamline at the Soleil synchrotron for their advice and support during data processing.

I learned a lot from all of you. I started with cryo-EM in January 2017 without experience in sample preparation, data collection and data processing. I want to thank **Armel Bézault** for training me in sample preparation and data collection. A special thanks to **Rémi Fronzes** and his team for sharing the cluster for data processing and constant discussion through-out all the steps. In particular, I want to thank **Chiara Rapisdara** for long and extensive discussions about structural biology and life and for giving me tons of positive energy. I want to thank **Valerie Gabélica** and **Frédéric Rosu** for mass spectrometry analysis of $tRNA^{Pro}$ and for their support during data interpretation.

My longest and most constant lunch group member **Lionel Beaurepaire** had more than once the one or the other idea to get me further with my experiments. Sometimes a lunch break can solve most of the problems with experiments. More importantly, thank you for listening and teaching me about France. Nearly every morning (except when she was on holidays) I was greeted with a warm smile. Thank you **Mariline Yot** for being there and for being my best French teacher. I want to acknowledge **Myriam Mederic** for her positive energy every time she came to our lab. A special thanks to **Patricia Martin** and **Kati Ba-Pierozzi** for helping me with all the administration, refunding and mission order. Special thanks to **Gerald Canet** and **Eric Roubin** for solving all the computer problems, I was facing during the last years. The printer was always happy to see you, too.

I want thank the whole unit Inserm U1212, CNRS UMR5320 under the direction **of Jean-Louis Mergny**. It was a pleasure to discuss and exchange knowledge due to different expertise. In particular, I want to thank **Fabien Darfeuille, Cameron Mackereth** and **Denis Dupuy** for answering a lot of questions. In addition, I want to thank the team of **Martin Teichmann** in particular **Stéphanie Durrieu, Camila Perrot** and **Wiebke Bretting** for their help improving protocols.

I would like to acknowledge all members of the JJC organization committee 2015 and 2016. I was a great experience to work together and organize two exciting conferences. I want to thank in particular **Diane Bécart** for a wonderful friendship, 1000000 PhD student dinners, long discussions about life and science. I loved playing music with you and just being around you.

Thank you for convincing me to start dancing Batchata, it was each time a great experience even if I am not the most talented dancer. I want to thank **Birgit Habenstein** and **Joséphine Abi-Ghanam** for their advice, wonderful discussions and constant support. Furthermore, I want to thank **Laura Mauran** for hours of surfing and wonderful times on the Sunday market in Pessac. A special thanks to **Sonia Cuidad**, **Martí Ninot**, **Eduard Puig** and **Thomas Perry** for their constant support, encouragement and for increasing my knowledge about penguins. It was always lots of fun to do things together.

Ein großes Dankeschön geht an meine Familie, die mich immer ermutigt und unterstützt hat meinen eigenen Weg zu finden und mich gegen jeglichen Wiederstand durchzusetzen. Meiner Mama **Bärbel Seefeldt** möchte ich für ihr beeindruckendes Druchhaltevermögen und offenes Ohr danken auch wenn ich meinen eigenen Kopf durchsetzen wollte. Ich möchte meiner Oma **Trude Kurz** dafür danken, dass sie immer wieder die richtigen Worte findet egal ob auf Deutsch oder Französisch. Meinen Großvater **Rolf Kurz** möchte ich danken, dass er die Begeisterung für Naturwissenschaften mit mir teilt und mir sehr viel beigebracht hat. Zusätzlich möchte ich meinem Onkel **Frieder Kurz** danken, dass er immer einen Rat für mich übrighatte. Ohne euch wäre diese Arbeit nicht möglich gewesen. Ich möchte zusätzlich meiner längsten Freundin **Anna Neubauer**, danken, dass sie mich durch alle Höhen und Tiefen bisher begleitet hat und die sich einfach nur freut, wenn ich anrufe.

Studying chemistry and biochemistry made it possible to meet **Thomas Leissing, Michaela Wipper, Katharina Essig, Stefanie Herrmann, Kerstin Lippl** and **Janina Andreß**. I want to acknowledge them for their constant support throughout the complete time of my studies but more importantly for their friendship. In the three years you showed me no matter where we will live we will find our way to stay in touch. Five years ago, I went to Riverside California and was lucky to meet **Tamara Mielke**. I want to thank you for being my best friend ever since. I can thank you enough for listening through all the up and downs of a thesis, for going back with me to California. You are the person to be hiking on a volcano in a volcano, finding our inner sunflower as well as being in a kayak while being surrounded by sea otters, sea lions and humpback whales. I also want to thank **Raissa** and **Jarren Kay** for their constant support and **Nicola Cellini** for reminding me about my personal reasons to keep on going with science.

Je tiens à remercier tous **les membres de la chorale croq'notes** d'être la meilleure classe de français et une merveilleuse compagnie à chanter avec beaucoup de joie tous les mardis soirs et de voyager à travers l'Italie. En particulier, je tiens à remercier **Anne-Marie Garcia** pour être l'une des meilleures chefs de chorale avec qui j'ai travaillé et pour nous avoir motivé à participer deux fois au projet Tutti.

A special thanks to the whole team of the Black Valvet Bar, **Barry, Will, Marta, Angi, Nick** and **Langi** for the best entertainment on Wednesdays nights increasing important knowledge about penguins and constant training for blind test. The Black Valvet Bar is the best Irish pub in Bordeaux and there is only one real catzapplin. I want to acknowledge **Ian Ruigrok** for introducing me to this particular pub and for the one and other great discussion.

Table of content

List of Figures and Tables

Conventions

mRNA, DNA oligos, and Open Reading Frames (ORF) are listed from 5′ to 3′ end. For standard amino acids, the three letters code or one letter code is used. Amino acid positions within the growing peptide chain are described using the amino acid attached to the P-site tRNA as position 0. The numbering towards the N-terminus decreases, and amino acid that have not yet been incorporated are labeled with increasing numbering towards the stop codon. This is illustrated in the following figure:

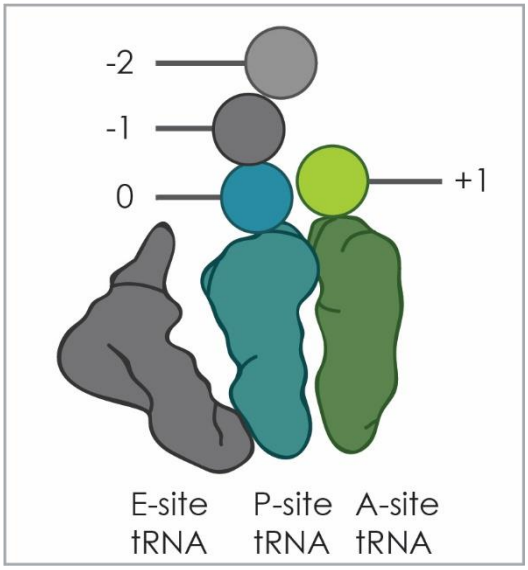

Figure 1: tRNA positions and correct labeling of the nascent chain, as used in this work.

Arrest peptide sequences are listed by using the one letter code starting from the N-terminus. The amino acid located in the A-site is reported in brackets. Ribosomal residues are listed using the *Escherichia coli* (*E. coli*) numbering.

For toeprinting experiments, sequencing lanes are located on the left, with the bases in the following order: CUAG. The following lanes are the individual reactions and will be referred to by number, with the lowest number next to the sequencing. Structures of arrested ribosomes are referred to as arrest peptide-70S structures.

Abbreviations

Table 1: Summary of abbreviations used in this work.

Abbreviations	Full name
7	7-methylguanosine
%	Percent
$(CH_3CO_2)^-$	Acetate
°C	Degrees Celsius
µ	Micro
A	Adenine
A or Ala	Alanine
aa	Amino acids
ABT	Amino-modified benzyl thioester
Ac	Acetyl
aFx	Amino based flexizyme
Amp	Ampicillin
AMP	Antimicrobial peptide
Approx.	Approximately
APS	Ammonium persulfate
A-site	Aminoacyl tRNA binding site
ATP	Adenosine triphosphate
B. subtilis	*Bacillus subtilis*
BLAST	Basic Local Alignment Search Tool
BME	β-mercaptoethanol
bp	Base pairs
BSA	Bovine serum albumin
C	Cytosine
C, Cys	Cysteine
CAM	Chloramphenicol
CBT	4-chlorobenzyl thioester
Cl^-	Chloride
CME	Cyanomethylester
cryo-EM	Cryo-electron microscopy
CTF	Cross transfer function
CTP	Cytosine triphosphate
CV	Column volume
D	Dihydrouridine
D, Asp	Aspartate
Da	Dalton
dATP	Desoxy adenosine triphosphate
DBE	3,5 dinitrobenzyl ester

Abbreviations	Full name
dCTP	Desoxy cytosine triphosphate
ddATP	Didesoxy adenosine triphosphate
ddCTP	Didesoxy cytosine triphosphate
ddGTP	Dideoxy guanosine triphosphate
ddNTP	Dideoxynucleotide triphosphate
ddTTP	Dideoxy thymine triphosphate
DEPC	Diethyl pyrocarbonate
dFx	Dinitro flexizyme
dGTP	Desoxy guanosine triphosphate
DMSO	Dimethyl sulfoxide
DNA	Deoxyribonucleic acid
DNAP	DNA polymerase
dNTP	Desoxy nucleotide triphosphate
DT	Drift tube
dTTP	Desoxy thymine triphosphate
E, Glu	Glutamate
E. coli	*Escherichia coli*
e.g.	For example
EDTA	Ethylenediaminetetraacetic acid
EF	Elongation factor
eFx	Enhanced flexizyme
erm	Erythromycin resistance methylase
ERY	Erythromycin
ESI	Electrospray ionization
E-site	Exit, deaminoacyl tRNA binding site
ESRF	European Synchrotron Radiation Facility
EtOH	Ethanol
ExPASy	The Expert Protein Analysis System
f	Formyl, femto (10^{-15})
F, Phe	Phenylalanine
FRET	Fluorescence (Förster) resonance energy transfer
FSC	Fourier shell correlation
Fx	Flexizyme
g	Gramm
G	Guanine
G, Gly	Glycine
GTP	Guanosine triphosphate
gu	*N,N,N',N'*-tetramethylguarnidino
h	Hours
H, His	Histidine
H_2O	Water

Abbreviations	Full name
HCl	Hydrochloric acid
HEPES	4-(2-hydroxyethyl)-1-piperazineethanesulfonic acid
HF	High fidelity
HPLC	High-pressure liquid chromatography
I, Ile	Isoleucine
IF	Initiation factor
IPTG	Isopropyl β-D-1-thiogalactopyranoside
K	1-methylguanosine, Potassium
K. pneumoniae	*Klebsiella pneumoniae*
KAN	Kanamycin
K_d	Dissociation constant
KLB	Klebsazolicin
KOH	Potassium hydroxide
L	Liter
L, Leu	Leucine
LB	Luria Broth
LIN	Linezolid
log	Logarithmus
m	Mili (10^{-3})
M	mol/L
M, Met	Methionine
mAU	Mili absorption units
MD	Molecular dynamics
MeOH	Methanol
MES	2-(N-morpholino)ethanesulfonic acid
Mg^{2+}	Magnesium bivalent cation
min	Minutes
mRNA	Messenger RNA
MS	Mass spectrometry
n	Nano (10^{-9})
N, Asn	Asparagine
Na^{+}	Sodium cation
NaOH	Sodium hydroxide
NCS	Non-crystallographic symmetry
NEB	New England Biolabs
NGS	Next-generation sequencing
nm	Nanometer
NRPS	Non-ribosomal protein synthetases
nt	Nucleotides
NTP	Nucleotide triphosphate
O, Orn	Ornithine
OD_{600}	Optical density at 600 nm

Abbreviations	Full name
ORF	Open reading frame
P	Pseudouridine
p	Pico
P, Pro	Proline
PAGE	Polyacrylamid gel elecetrophoresis
PCR	Polymerase chain reaction
PDB	Protein data bank
pH	Log_{10} of the proton concentration
PHENIX	Python-based Hierarchical ENvironment for Integrated Xtallography
pK_a	Logarithmic acid constant
PMSF	Phenylmethanesulfonyl fluoride
PrAMP	Proline-rich antimicrobial peptide
P-Site	Peptidyl-tRNA binding site
px	Pixel
Q, Gln	Glutamine
r	D-arginine
R, Arg	Arginine
RBS	Ribosomal binding site
RCF	Relative centrifugal force
RELION	REgularized LIkelihood OptimizatioN
RF	Release factor
rmsd	Root-mean-square deviation
RNA	Ribonucleic acid
RNAP	RNA polymerase
RNase	RNA degradation enzyme
RNC	Ribosome nascent-chain complexes
RP	Reverse phase
rpm	Revolutions per minute
RRF	Ribosomal recycling factor
rRNA	Ribosomal RNA
RT	Room temperature
s	Seconds
S	Svedberg
SD	Shine Dalgarno sequence
SDS	Sodium dodecyl sulfate
SILAC	Stable isotopic labeling of amino acids in cell culture
SLIC	Sequence and ligation independent cloning
SPAR	Sparsomycin
Str	Streptomycin
T	Thymine
T, Thr	Threonine

Abbreviations	Full name
T. thermophilus	*Thermus thermophilus*
TAE	Tris Acetate EDTA
TB	Terrific Broth
TBE	Tris Boric acid EDTA
TBU	Tris Boric acid Urea
TCA	Trichloroacetic acid
TEMED	Tetramethylethylenediamine
Tet	Tetracycline
tmRNA	Transfer-messenger RNA
ToF	Time of flight
Tris	Trizma Base
tRNA	Transfer RNA
Tu	Temperature unstable
U	Uracil
UTP	Uracil triphosphate
V	Volt, Volume
V, Val	Valine
V. alginolyticus	*Vibrio alginolyticus*
v/v	Volume per volume
VdW	Van der Waals
Vol	Volumes
W	Watt
W, Trp	Tryptophane
w/v	Weight per volume
wt	Wild-type
X	Any amino acid
ʎ	Wavelength
Δ	Deletion
ε	Extinction coefficient

1. Introduction

1.1 Bacterial translation

1.1.1 Gene expression and the bacterial ribosome

The central dogma of molecular biology was elucidated by Francis Crick in 1958 (Crick, 1958) and summarizes the general steps from a gene to a functional protein. The genetic material is encoded as deoxyribonucleic acid (DNA) and is transcribed into messenger ribonucleic acid (mRNA) by RNA polymerases (RNAP). Subsequently, the mRNA is translated into the corresponding amino acid (aa) sequence by the ribosome (Crick, 1970). Over the years, discoveries like for example non-coding RNAs (Blattner et al., 1997) or post-transcriptional and post-translational modifications revealed the complexity of this process (Mohanty and Kushner, 2006).

Ribosomes were first observed in electron microscopy (EM) micrographs of mammalian cell cross sections and were described as dense particles or granules (Palade, 1955). Further investigations showed that ribosomes are abundant in all kingdoms of life and are the key players in protein biosynthesis as reviewed by Schmeing and Ramakrishnan, 2009. In prokaryotes, ribosomes are 2.5 megadaltons (MDa) ribonucleoprotein complexes, termed the 70S (Svedberg) ribosomes, which dissociate into two subunits at low magnesium bivalent cations (Mg^{2+}) concentrations (Chao, 1957). In *Escherichia coli*, the large (50S) subunit consists of 34 proteins, 23S ribosomal RNA (rRNA) and 5S rRNA. The length of the 23S rRNA is approx. 2900 nucleotides (nt) while the length of the 5S rRNA is approx. 120 nt. The small (30S) subunit consists of an approx. 1500 nt long 16S rRNA and 21 proteins (Ban et al., 2014; Kurland, 1960; Schuwirth et al., 2005; Wilson and Nierhaus, 2005, (Figure 2). Among those 55 proteins, 34 are conserved in all kingdoms of life and 44 proteins are conserved among bacteria (study included 995 bacterial genomes) (Yutin et al., 2012).

During translation, the mRNA sequence is translated into the corresponding amino acid sequence utilizing amino acid-specific transfer RNAs (tRNA) as adaptors (Crick, 1958; Hoagland et al., 1958). The ribosome has three distinct binding positions for tRNAs: the aminoacyl-site (A-site) is the binding site for the aminoacylated tRNA, the peptidyl-site (P-site) is the position

in which the tRNA is connected to the nascent chain and the exit site (E-site) is the position from which the deacylated tRNA is released (Agrawal et al., 1996). The decoding process is carried out by the small subunit (Ogle et al., 2003; Wimberly et al., 2000) whereas peptide bond formation is catalyzed in the large subunit within the peptidyl transferase center (PTC) (Maden et al., 1968; Monro, 1967; Traut and Monro, 1964). A structure of the 70S *E. coli* ribosome is shown in the following figure:

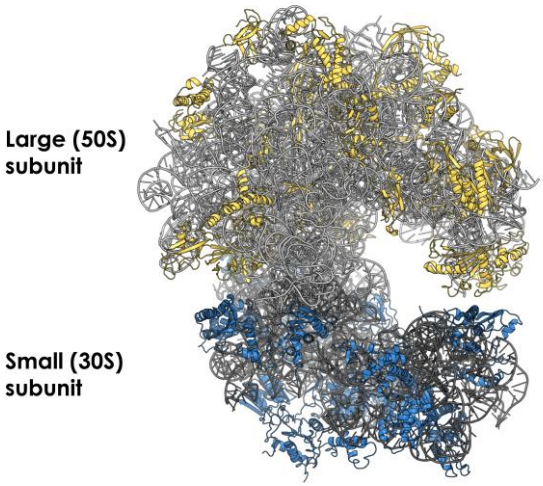

Figure 2: Structure of 70S ribosome from *E. coli.* The bacterial 70S ribosome is a ribonucleoprotein complex formed of a large (50S) and a small (30S) subunit. The 50S subunit consists of 23S rRNA, 5S rRNA (light gray) and 31 proteins (yellow). The 30S subunit consists of a 16S rRNA (gray) and 20 proteins (blue). (PDB code: 4U27, (Noeske et al., 2014)).

The peptidyl transferase center (PTC) is mainly composed of rRNA and so the ribosome was termed as a ribozyme meaning the catalysis is performed by RNA (Ban et al., 2000; Nissen et al., 2000; Noller, 1993). From the PTC, the nascent peptide chain passes through the ribosomal exit tunnel to reach the cytoplasm. This ribosomal exit tunnel, spanning the 50S subunit, was first described in initial cryo-electron microscopy (cryo-EM) structures (Frank et al., 1995). The ribosomal exit tunnel is about 100 Å long (Nissen et al., 2000) which is equivalent to a growing peptide chain of 30-35 aa as revealed by a proteolytic protection assay (Malkin and Rich, 1967). The ribosomal tunnel features different regions, subdivided into the upper tunnel, lower tunnel and the vestibule (Figure 3). It is mainly formed of 23S rRNA and at its narrowest point (constriction site) the ribosomal proteins L4 and L22 reach into the cavity (Gabashvili et al., 2001). The average diameter of the tunnel is 15 Å, with a minimum of 10 Å at the constriction site (Nissen et al., 2000; Voss et al., 2006). The diameter of the tunnel is sufficient to allow co-

translational folding of α-helices in the upper and lower tunnel (Bhushan et al., 2010; Lu and Deutsch, 2005; Su et al., 2017; Voss et al., 2006) and even the formation of tertiary structure in the vestibule (Nilsson et al., 2015). Figure 3 shows a schematic view of the tunnel (Seip and Innis, 2016):

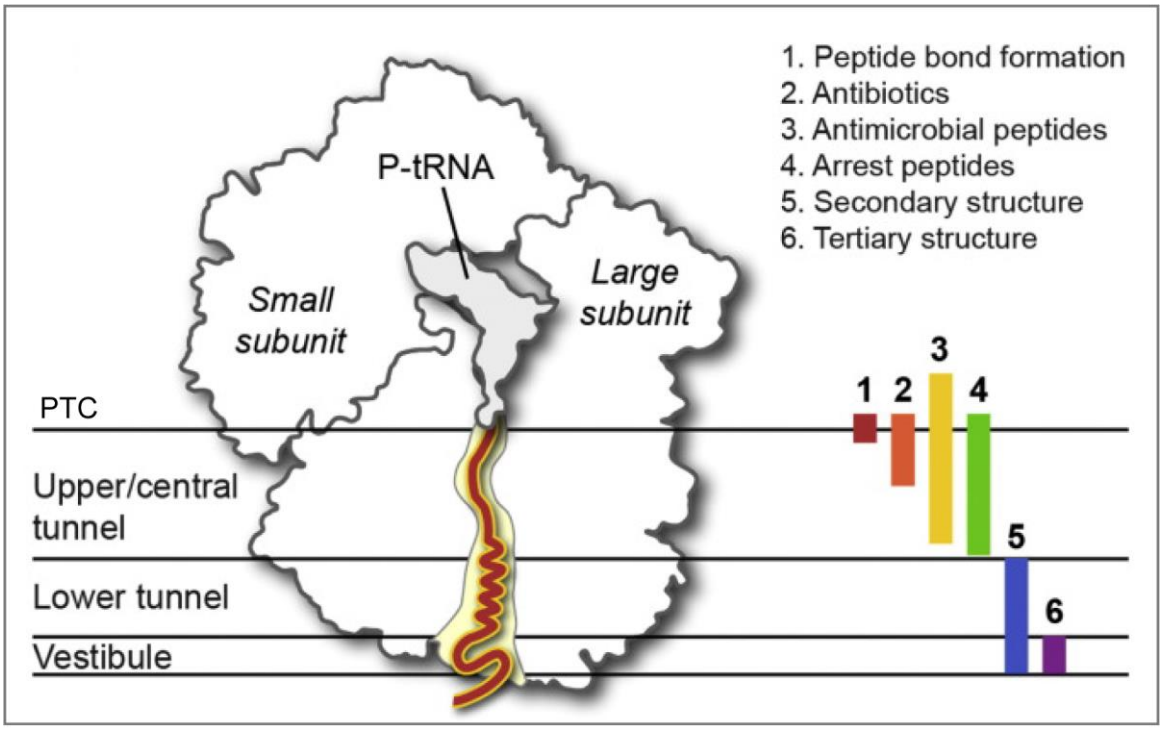

Figure 3: Schematic view of the ribosomal exit tunnel. The tunnel spans the whole large subunit connecting the PTC to the cytoplasm. It can be divided into the upper tunnel, lower tunnel, and the vestibule. Figure is taken from Seip and Innis, 2016.

To ensure the production of all encoded proteins in equal amounts, it was originally hypothesized that the tunnel wall has "Teflon like" properties, meaning no interactions of the nascent chain with the tunnel (Nissen et al., 2000). However, studies have shown that certain nascent peptides can interact with the tunnel and induce nascent chain-mediated translational arrest of the translating ribosome as reviewed by (Ito and Chiba, 2013; Seip and Innis, 2016; Wilson et al., 2016) (Figure 3).

Although the catalytic process of the ribosome is mainly performed by rRNA, additional ribosomal proteins and protein factors are needed to increase the processivity of the translational cycle as reviewed by Schmeing and Ramakrishnan, 2009. Many classes of antibiotics target the bacterial ribosome, in particular, the PTC and ribosomal tunnel. As antibiotic resistances are becoming a bigger threat it is important to understand the molecular

regulation of the bacterial ribosome as well as the action of antibiotics for further drug development as reviewed (Wilson, 2009, 2014).

1.1.2 The prokaryotic translation cycle

The bacterial translation cycle can be divided into initiation, elongation and termination phases, the latter being divided into the release of the produced protein and the recycling of the ribosomal subunits, as reviewed by Schmeing and Ramakrishnan, 2009. Figure 4 illustrates the translation cycle including all essential protein factors:

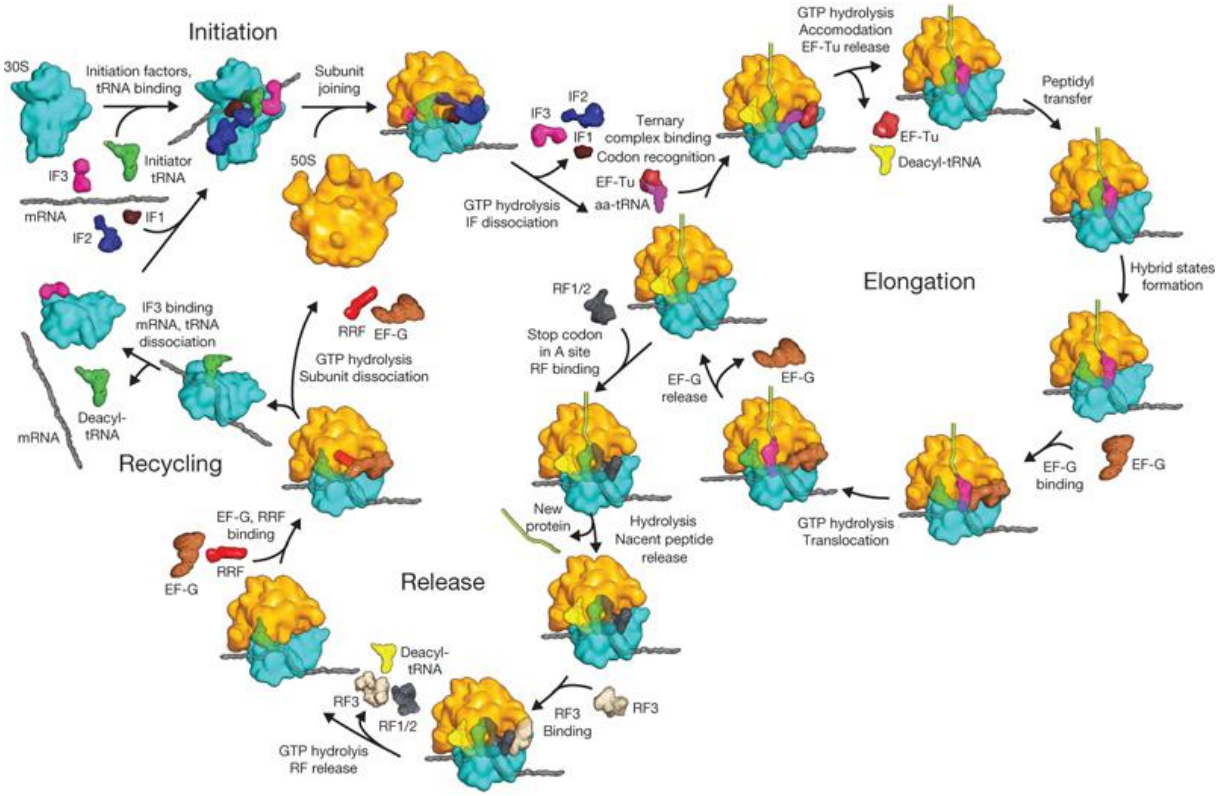

Figure 4: Overview of the bacterial translation cycle as reviewed by Schmeing and Ramakrishnan, 2009. The prokaryotic translation cycle can be divided into three phases: Initiation, elongation, and termination (Release and recycling). The 30S subunit is shown blue and the 50S subunit is shown in yellow. All canonical translation factors are listed illustrating their function in the translation cycle.

1.1.2.1 Initiation

The rate-limiting step of the translation cycle is the initiation step. During this step, as reviewed by Laursen et al., 2005, both ribosomal subunits and the initiator $tRNA_i^{Met}$ needs to be recruited to the start codon and assembled. During initiation three initiation factors (IF1, 2, 3) ensure the correct assembly of the ribosome on the mRNA (Figure 4). The mRNA contains at the 5'end of

the open reading frame (ORF) a ribosomal binding site (RBS), termed in bacteria Shine-Dalgarno (SD) sequence which is six to seven nucleotides (nts) upstream from the start codon (Ringquist et al., 1992; Shine and Dalgarno, 1974) The consensus SD sequence is AGGAGG. The 3' end of the 16S rRNA in the small ribosomal subunit contains an anti-SD-sequence forming base pairs with the SD-sequence thus resulting in right positioning of the small subunit (Shine and Dalgarno, 1974).

In *E. coli*, 82.6% genes start with an "AUG", encoding Met, as a start codon and are initiated by $tRNA_i^{Met}$. Alternative start codons in *E. coli* are GUG (14.7%, Val), UUG (3.0%, Leu) and two possible rare ones (Blattner et al., 1997). In order to prevent premature subunit joining IF3 is bound to the E-site of the small subunit (Carter et al., 2001; Dallas and Noller, 2001; Karimi et al., 1999; Shine and Dalgarno, 1974). Binding of IF1 to the A-site of the small subunit prevents the binding of elongator tRNA as well as premature subunit joining (Antoun et al., 2006a; Antoun et al., 2006b). The initiator-tRNA has a different sequence than the elongator-$tRNA^{Met}$, resulting in higher rigidity and affinity for the P-site. Furthermore, the methionine attached to the $tRNA_i^{Met}$ is formylated. The fMet-$tRNA_i^{Met}$ is delivered to the initiation complex by the translational GTPase (trGTPase) IF2 in its GTP-bound state. (Antoun et al., 2003). Once fMet-$tRNA_i^{Met}$ is positioned properly, GTP hydrolysis is triggered and IF1 and IF3 are released from the 30S subunit followed by the recruitment of the 50S subunit and the release of IF2 (Simonetti et al., 2013).

1.1.2.2 Elongation

The following step, elongation, is the most repeated one in the translational cycle as the ribosome has to go through it for the incorporation of each amino acid. During elongation, the mRNA is decoded by the aid of tRNAs and the 30S subunit. Base triplets encode for a particular amino acid termed genetic code (Crick et al., 1961). Amino acids are attached to their cognate tRNA through the activity of specific aminoacyl-tRNA synthetases in an ATP-dependent process. Aminoacylation is a process with high enzymatic selectivity. Next, to their synthetase activity these enzymes have also and editing domain for the specific removal of wrongly attached amino acids as a proof-reading domain (Ibba et al., 1999). Specificity is ensured by e.g. a double sieve mechanism (Ibba et al., 1997; Nureki et al., 1998; Schmidt and Schimmel,

1994) or the presence of cations (Dock-Bregeon et al., 2000) ensuring the discrimination of the chemical properties of similar amino acids.

Aminoacylated-tRNAs are recognized and bound by Elongation Factor (EF)-Tu in its GTP bound state (Nissen et al., 1995). The genetic code contains 64 possible codon combinations for only 20 amino acids and two release factors. The consequence is that multiple codons encode the same amino acid. To reduce the number of tRNAs within the cell, only the first two bases of the codon form Watson-Crick base pairs with the mRNA while the third base can form wobble base pairs (Ebel et al., 1973; Speyer et al., 1963). The aminoacylated-tRNA in complex with EF-Tu is then recruited to the ribosome allowing the tRNA to form codon-anticodon interactions with the mRNA. The decoding process involves the small subunit detecting the right base pairing by flipping the bases A1493 and A1492 of helix 44, resulting in conformational changes within the L7/12 stalk and sarcin-ricin loop, triggering GTP hydrolysis within EF-Tu and its release from the ribosome (Diaconu et al., 2005; Ogle et al., 2003; Schmeing et al., 2009). For peptide bond formation to occur, the amino acid attached to the 3'CCA end of the A-site tRNA needs to be well positioned in the A-crevice within the PTC. During A-site tRNA accommodation, the tRNA has to go through large conformational changes rendering it the rate-limiting step of peptide bond formation (Pape et al., 1998; Valle et al., 2002).

Processes studied during the work of this thesis are known to target and influence peptide bond formation and so the following paragraphs discuss this process in detail. During A-site tRNA accommodation, the residues of the 23S rRNA undergo large conformational changes switching from the uninduced to the induced state (Schmeing et al., 2005c). In the uninduced state, the ester bond between the P-site tRNA and the peptide needs to be protected from premature hydrolysis. The ester bond is sequestered by the bases of the 23S rRNA U2585, A2451, and C2063 (Schmeing et al., 2005c). A-site tRNA accommodation induces a rearrangement of 23S ribosomal RNA residues due to base pairing of C75 of the A-site tRNA with G2553 resulting in movement of U2585 and the reorientation of the ribose of A76 of the P-site tRNA (induced fit) (Schmeing et al., 2005c). The induced fit brings the carbonyl ester carbon of the P-site tRNA in close proximity of the α-amino (NH_2) group of the following amino acid (Schmeing et al., 2005c). As a consequence, a peptide bond can be formed by the nucleophilic attack of the α-amino (NH_2) group of the A-site amino acid to the carbonyl ester carbon of the peptidyl-tRNA. The nucleophilic attack leads to a tetrahedral oxyanion transition

state that breaks down leaving the peptide chain attached to the A-site tRNA. The ribosome acts as an entropic trap that changes binding affinities for the different binding sites thus enhancing the reaction by a factor of 10^7 (Sievers et al., 2004).

To enhance the nucleophilicity of the α-NH_2 group of the A-site amino acid, it needs to be deprotonated. Early X-ray crystallography structures showed that no ribosomal protein was observed within 15 Å of the PTC (Ban et al., 2000; Nissen et al., 2000). Consequently, the ribosome is deemed to act as a ribozyme which was postulated first in 1993 (Noller, 1993). The resulting possible reaction mechanisms that can be catalyzed by RNA are acid-base catalysis, metal catalysis and a substrate-induced mechanism as reviewed by (Leung et al., 2011). The acid-base mechanism based on a crystal structure of the *Haloarcula martismortui* 50S subunit in complex with the Yarus inhibitor that mimics the transition state of peptide bond formation. It was proposed due to the close proximity of the N3 of A2451 to the Yarus inhibitor (Nissen et al., 2000). A2451 is one of the five universally conserved bases located in the PTC (Thompson et al., 2001; Youngman et al., 2004). It was also hypothesized that the base of G2447 lowers the pK_a of A2451 due to hydrogen bonding increasing the basicity of the N3 atom and this will facilitate the deprotonation of the α-amino group (Nissen et al., 2000). Mutation of these two bases led to a growth defect but mutant ribosomes are still capable of peptide bond formation (Beringer et al., 2003; Beringer et al., 2005; Polacek et al., 2001; Thompson et al., 2001). The pH independence of the peptide bond formation was demonstrated by replacing α-amino acids by α-hydroxy acids allowing to perform the reaction at different pH ranges. The result was that the reaction rate of the ribosome is independent of the pH of the solution (Bieling et al., 2006). This makes an acid-base catalyzed mechanism unlikely (Bieling et al., 2006) and is consistent with results from molecular dynamics studies (Trobro and Åqvist, 2005). X-ray crystallography structures containing substrate and transition state mimics showed that no Mg^{2+} or other cations could be localized within the PTC and that instead well-ordered water molecules could be detected (Schmeing et al., 2005b). This fact makes a metal-catalyzed mechanism also unlikely.

This leaves substrate induced mechanism as a mechanism that can be catalyzed by RNA. In this case, tRNAs deliver the amino acids to the A-site and are attached to the growing peptide chain in the P-site. Biochemical and molecular dynamics studies have shown that the 2'OH group of A76 is necessary for peptide bond formation when the tRNA is located in the P-site

(Dorner et al., 2003; Dorner et al., 2002; Trobro and Åqvist, 2005; Weinger et al., 2004). The 2′OH group of A76 could be a part of a six-membered proton shuttle between the nascent chain and the α-NH_2 group of A-site amino acid ensuring its deprotonation and stabilization of the oxyanion transition state (Dorner et al., 2002). The well-ordered water molecule in close proximity to the 2′OH group of A76 of the P-site tRNA could possibly form an eight-membered proton shuttle with a second water molecule that stabilizes potentially the oxyanion transition state (Schmeing et al., 2005b). Molecular dynamics showed that the eight-membered proton shuttle is preferred over the six-membered proton shuttle (Wallin and Åqvist, 2010)

Lacking of the 2′OH group of A2451 leads to reduction in peptide bond formation by a factor of 1000 fold as shown biochemically (Erlacher et al., 2005; Erlacher et al., 2006; Lang et al., 2008) and in molecular dynamics studies (Trobro and Åqvist, 2005) which was not a part of the proton shuttle models. A recent study involving high-resolution X-ray structures of the PRE- and POST-catalysis state of the 70S *T. thermophilus* ribosome with full-length tRNAs revealed three trapped water molecules within the PTC. This led to the postulation of the proton wire model, which takes into account the involvement of the 2′OH of A2451 in contrast to previous models (Polikanov et al., 2014).

After the peptide bond is formed, the nascent peptide is attached to the A-site tRNA and the P-site tRNA is deaminoacylated. The consequence is that the binding affinities of the tRNAs for their current positions are decreased. This results in movement of the tRNAs between two PRE-translocation states: The classical PRE-state (A/A, P/P) and the hybrid state (A/P, P/E) meaning that the CCA-ends of the tRNAs move towards the next codon leading to the rotation of the 50S subunit compared to the 30S subunit by 6° (Frank and Agrawal, 2000; Munro et al., 2007). As the last step of the elongation cycle, the ribosome needs to be translocated exactly one codon further towards the 3′ end of the ORF. This step is catalyzed by EF-G, which recognizes the hybrid state of the ribosome in its GTP-bound form (Agrawal et al., 1998). Time-resolved cryo-EM as well as high-resolution structures of EF-G bound to the bacterial ribosome and trapped in PRE-, intermediated and POST-translocation states gave great insights into movements of the protein factor, tRNAs, mRNA and the ribosome Due to GTP hydrolysis triggered by the L7/12 stalk and sarcin-ricin loop, EF-G undergoes a large conformational change (Chen et al., 2013; Fischer et al., 2010; Gao et al., 2009; Lin et al., 2015; Pulk and Cate, 2013; Tourigny et al., 2013; Zhou et al., 2013). EF-G was reported to act as Brownian ratchet

directing the movement of the ribosome along the mRNA as reviewed in detail by Rodnina and Wintermeyer, 2011 while a recent X-ray crystallographic study suggests that the conformational change of EF-G applies a power stroke resulting in translocation of the bacterial ribosome (Lin et al., 2015). A recent high resolution single molecular study led to the observation that translocation is driven by EF-G acting as a Brownian ratchet and by using a power stroke (Chen et al., 2016). The elongation cycle is a very fast step due to the fact that the bacterial ribosome incorporates 10-20 aa per second (s) (Sørensen et al., 1989).

1.1.2.3 Peptide release and recycling

Termination is the last step of the translation cycle. Therefore, the stop codon has to be recognized, the peptide has to be released and the ribosome has to be disassembled into its subunits as reviewed by (Korostelev, 2011). The three stop codons (UGA, UAA, UAG) (Brenner et al., 1967; Brenner et al., 1965) are recognized by class I peptide termination factors. The UAA stop codon can be recognized by the two release factors (RF1, 2) found in *E. coli*. Due to a slight difference in the primary structure of the release factors, RF1 recognizes the UAG and RF2 recognizes the UGA stop codon (Klaholz et al., 2003; Petry et al., 2008; Weixlbaumer et al., 2008). The peptide is released by the positioning of a water molecule by the conserved GGQ motif of RF1/2 reaching into the PTC changing its activity to an esterase (Jin et al., 2010; Korostelev et al., 2008; Weixlbaumer et al., 2008). Subsequently, the trGTPase RF3, a class II peptide termination factor, releases RF1 or RF2 from the ribosome under GTP hydrolysis (Freistroffer et al., 1997; Goldstein and Caskey, 1970; Jin et al., 2011). The GTP hydrolysis is triggered by the L7/12 stalk and the sarcin-ricin loop (Diaconu et al., 2005; Zavialov et al., 2001).

As the last step, the deaminoacylated P-site tRNA is released and the 70S ribosome is disassembled into the individual subunits. Therefore, the ribosome recycling factor (RRF) and EF-G work together under NTP hydrolysis (Barat et al., 2007; Pavlov et al., 1997; Weixlbaumer et al., 2007). To prevent the large subunit from reassociation to the small subunit, IF3 binds to its previously described position and the translation cycle can be initiated again (Antoun et al., 2006b).

In summary, peptide bond formation is independent of energy use and catalyzed by rRNA, whereas the steps of subunit assembly, tRNA aminoacylation, and delivery, translocation, the

release of the release factors 1 or 2 and subunit dissociation require the NTP hydrolysis and protein factors (Schmeing and Ramakrishnan, 2009).

1.2 The prokaryotic ribosome as a target for antibiotics

Antibiotics target macromolecular complexes involved in cell wall synthesis, genome maintenance as well as protein synthesis as reviewed by (Kohanski et al., 2010). More than 50% of known antibiotics target the bacterial ribosome affecting all steps of the translational cycle. Known antibiotic binding sites include the decoding center (e.g. Aminoglycosides), sarcin-ricin loop (e.g. Thiopeptides), factor binding (e.g. Fusidic acid), peptidyl transferase center (e.g. Phenicols) and the ribosomal exit tunnel (e.g. Macrolides) as reviewed in detail (Wilson, 2009, 2011, 2014).

The large increase of antibiotic resistance, which is a consequence of excessive antibiotic use over the last decades, represents a global problem. Studies have shown that resistance against antibiotics arises rapidly after their introduction into medical use. The macrolide Erythromycin was introduced into clinical use in 1952 and the first resistant bacterial strain was isolated in 1955 as reviewed by (Lewis, 2013). Strategies of antibiotic resistance can be classified into the following categories as reviewed in detail by (Roberts, 2008; Wilson, 2014): disruption of the binding site by mutation or modification, enzymatic modification/degradation of the drug or active export of the drug.

The following chapter will focus on antibiotics that target specifically the PTC and macrolides targeting the ribosomal exit tunnel. In addition, they can act as ligands during nascent-chain mediated translational arrest (chapter 1.3.2).

1.2.1 Antibiotics targeting the PTC

The PTC is a major target for antibiotics. Classes that target specifically the PTC are Phenicols (Chloramphenicol, CAM), Oxazolidinones (Linezolid, LIN), Lincosamides (Clindamycin, CLN), Sparsomycin (SPAR), Puromycins, Pleuromutilins (Tiamulin, TIA), Hygromycin A, A203A and Blasticidin S (BlaS) as reviewed (Arenz and Wilson, 2016; Wilson, 2011).

Most of these classes bind to the A-site within the PTC. Puromycin is an antibiotic that reacts covalently with the nascent chain and results in premature termination as reviewed (Darken, 1964). Puromycin is active against eukaryotic as well as prokaryotic ribosomes meaning it cannot be used for treatments (Darken, 1964). Nevertheless, puromycin or its derivatives are used in several biochemical, kinetic and structural studies to study peptide bond formation and nascent chain-mediated translational arrest (Muto et al., 2006; Schmeing et al., 2002; Sievers et al., 2004; Traut and Monro, 1964). Other antibiotics that bind to the A-site, like chloramphenicol and clindamycin, bind to or in close proximity to the A-site crevice, the binding pocket for the A-site aminoacyl moiety, thus preventing the accommodation of the aminoacyl-tRNA as shown in X-ray crystal structures (Bulkley et al., 2010; Dunkle et al., 2010; Wilson et al., 2008). The antibiotic Hygromycin A binds to the CCA binding pocket of the A-site resulting in the inhibition of A-site tRNA accommodation (Polikanov et al., 2015b).

Sparsomycin is an antibiotic that, like puromycin, is potent against eukaryotic as well as prokaryotic ribosomes. It was reported that Sparsomycin induces precise translocation of the ribosome in the absence of EF-G (Fredrick and Noller, 2003). In addition, Sparsomycin stabilizes the growing peptide chain and prevents further A-site accommodation. This particular property is used in structural biology to force the binding short peptidyl-RNA fragments, that mimic peptidyl chain and the 3′ CCA end of tRNAs, to the P-site (Melnikov et al., 2016a; Schmeing et al., 2005a). Pleuromutilins like Tiamulin bind to the A as well as the P-site blocking the elongation of peptide growth due to steric hindrance (Gürel et al., 2009). Blasticidin S binds to the P-site and deforms the 3′ CCA-end of the P-site tRNA. This protects the peptide chain from elongation and release (Svidritskiy et al., 2013).

All in all, antibiotics that target the PTC inhibit peptide bond formation by hydrolysis of the peptide chain, stabilization of the peptide chain, preventing A-site tRNA accommodation or steric hindrance of prolongation of the growing peptide chain (Wilson, 2011).

1.2.2 Macrolides and ketolides binding to the ribosomal tunnel

Macrolides and ketolides form a valuable class of broad-spectrum antibiotics, with the first representative pikromycin isolated from a *Streptomyces* strain in 1950 (Brockmann and Henkel, 1950). Erythromycin (ERY), a well-studied and widely used macrolide, introduced to medical use in 1952 (Mcguire JM et al., 1952), was originally isolated from *Streptomyces erythraea* (as reviewed by (Kannan and Mankin, 2011)). Macrolides are active against a broad range of Gram-positive and a limited range of Gram-negative bacteria (Nakayama, 1984). They have a high binding specificity for the bacterial ribosome over the eukaryotic one, making macrolides a valuable group of antibiotics (Böttger et al., 2001; Taubman et al., 1966). The chemical structures of erythromycin (macrolide) and telithromycin (ketolide) are shown in Figure 5:

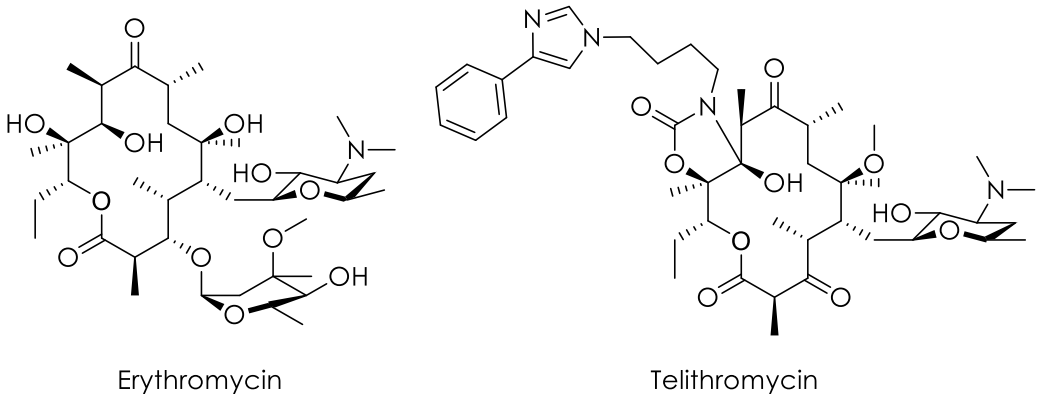

Figure 5: Chemical structure of Erythromycin (macrolide) and Telithromycin (ketolide). Erythromycin and Telithromycin consist of a 14-membered lactone ring. ERY has also a C5 desosamine and a C3 cladinose sugar. In the case of telithromycin, the C3-cladinose sugar is replaced by a keto-group and an N-aryl-alkyl acetamide.

The chemical structure of erythromycin consists of a 14-membered lactone ring, a C3 cladinose and a C5 desosamine sugar (Figure 5). The size of the lactone ring can adopt 12-, 14-, 15- or 16-membered rings and macrolides are classified accordingly. To overcome resistance and to increase bioavailability, rounds of drug development led to the isolation 2nd and 3rd generation, macrolide/ketolide antibiotics (reviewed by George, 2017). Ketolides are 3rd generation antibiotics and have a keto group instead of the cladinose sugar. Telithromycin, a member of this group is shown in Figure 5 (Katz and Ashley, 2005; Zhong and Shortridge, 2001). These class of antibiotics binds to the ribosomal exit tunnel (Moazed and Noller, 1987) and its binding site is illustrated in the following figure:

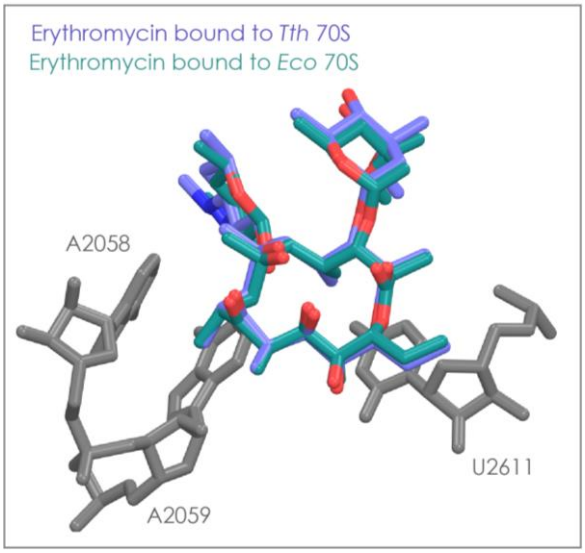

Figure 6: Binding site of erythromycin within the bacterial ribosome. Overlay of the 70S *E. coli* ribosome (turquoise; PDB code: 4V7U) and 70S *T. thermophilus* ribosome (blue; PDB code: 4V7X) in complex with erythromycin illustrates the similar conformations of the drug bound to the ribosomal tunnel. The bases of the 23S rRNA that form the binding site are shown in gray. For simplification reasons, only the bases from the *T. thermophilus* 70S ribosome structure are shown. A2059 and U2611 form a hydrophobic surface resulting in stacking interactions with the lactone ring (Bulkley et al., 2010; Dunkle et al., 2010).

Extensive biochemical studies identified the upper ribosomal exit tunnel as the binding site for erythromycin allowing the accommodation of the A-site tRNA (Celma et al., 1971; Moazed and Noller, 1987). Several X-ray crystallography studies identified and proved the biochemical binding sites but different orientations of the lactone ring were observed (Berisio et al., 2003; Schlunzen et al., 2001; Tu et al., 2005). More recent studies have shown that different macrolides and telithromycin bound to the 70S *E. coli* (Dunkle et al., 2010) and *T. thermophilus* (Bulkley et al., 2010) ribosome have similar conformation of the lactone ring independently from drug and species (Figure 6). Erythromycin forms stable interactions with the ribosomal exit tunnel via base A2058 while the lactone ring stacks against the hydrophobic surface formed by A2059 and U2611 (Bulkley et al., 2010; Dunkle et al., 2010; Figure 6).

This binding site within the ribosomal tunnel originally suggested that macrolides work like a plug, inhibiting protein synthesis in the early elongation phase and leading to peptidyl-tRNA drop-off (Menninger, 1995; Menninger and Otto, 1982; Tenson et al., 2003). Further investigations identified nascent chain peptide sequences that lead to the arrest of the ribosome in the presence of the macrolides (Gryczan et al., 1980; Horinouchi and Weisblum, 1980) (more detailed chapter 2). More recent studies have shown that cells, which are exposed

to erythromycin or telithromycin, can still produce a subset of proteins. The by-passing of the drug is possible due to a specific amino acid composition of these proteins in their N-terminus (ILNNIR or IGQQVR) (Kannan et al., 2012). Another effect is drug-induced frameshifting that can be observed in the presence of ketolides like telithromycin (Gupta et al., 2013).

1.3 Proline-rich antimicrobial peptides (PrAMPs) as possible new therapeutics

All organisms produce substances to protect themselves against competitors for nutrients and against pathogens. Peptides or glycopeptides like Vancomycin represent a large proportion of these defense substances. They can be produced by the ribosome or by large multiprotein complexes called non-ribosomal synthetases, which are capable of incorporating nonproteinogenic amino acids into peptides or macrocycles (Hur et al., 2012). Antimicrobial peptides (AMPs) can be classified by their structure, such as α-helices, β-sheets or macrocycles, by their mode of action, like lytic or non-lytic, or by their amino acid composition, like hydrophobic, amphiphilic or specific amino acid-rich as reviewed in detail by (Epand and Vogel, 1999; Otvos, 2005).

One class of AMPs are proline-rich antimicrobial peptides (PrAMPs) which are produced as a part of the innate immune system of higher eukaryotes (Otvos, 2002). Representative members have been isolated and characterized from the milkweed bug (*Oncopeltus fasciatu*s, (Schneider and Dorn, 2001)), honey bees (*Apis mellifera,* (Casteels et al., 1990)), green shield bug (*Palomena prasina,* (Chernysh et al., 1996)), Firebug (*Pyrrhocoris apterus,* (Cociancich et al., 1994)) and even domestic mammals like cows (*Bos taurus,* (Scocchi et al., 1994)). As PrAMPs are incapable of entering the eukaryotic cell (Hansen et al., 2012) and therefore, represent a promising class of antimicrobials. Additionally, these peptides can also be used to treat infections affecting the brain as they can cross the blood-brain barrier (Stalmans et al., 2014). A representative list of sequences is shown in Figure 7:

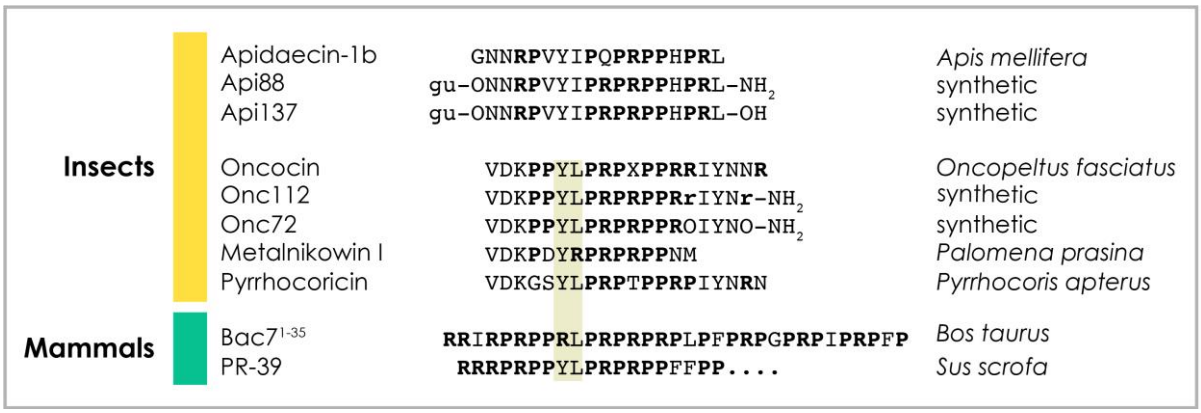

Figure 7: Sequence alignments of PrAMPs isolated from different species (insects and mammalian) or derived from drug development. Proline and arginine are highlighted in bold to visualize their high content. The light-yellow box indicates the two most important residues for antimicrobial activity. O stands for L-ornithine, D-amino acids are indicated with a letter in lower case, gu stands for N,N,N',N'-tetramethylguanidine**.**

The main sequence characteristic of PrAMPs is a high proline content, in particular, proline arginine repeats (Figure 7). This results in a restricted backbone geometry that does not allow the formation of α-helices, in addition, their positive charge preventing the PrAMPs from passing through eukaryotic cell membranes (Hansen et al., 2012). PrAMPs are potent growth inhibitors of Gram-negative bacteria with an intracellular target. The peptide uptake is coupled to the SbmA transporter that is present in the cell membrane of Gram-negative bacteria e.g. *E. coli* or *Klebsiella pneumoniae* (Ostorhazi et al., 2014). The exact function of the SbmA transporter remains unknown (Mattiuzzo et al., 2007).

The first presumed intracellular target of the insect-derived PrAMPs drosocin, pyrrhocoricin and apidaecin, identified by co-immunoprecipitation, was the heat shock protein and chaperone DnaK (Otvos et al., 2000). Crystal structures of PrAMPs, oncocin and Bac7, in complex with DnaK were solved and used as the basis for further drug development (Zahn et al., 2013; Zahn et al., 2014). Optimization of the peptide sequences included the incorporation of non-proteinogenic amino acids such as L-ornithine, D-amino acids and chemical modification of the C-terminus and N-terminus, as shown in Figure 7, to increase the stability of the peptides against serum proteases. It should be noted that all-D peptides are inactive (Knappe et al., 2010).

A recent study revealed that *dnaK* knockout cells are still sensitive to the synthetic derivatives of oncocin, Onc112 and Onc72, as well as Apidaecin 1b, Api88 and Api137, suggesting that some PrAMPs have a different target (Krizsan et al., 2014). To identify the target by cross-

linking, Tyr7 of Api88 was replaced by *p*-benzoylphenyl alanine, a photoactive derivative. In addition, Api88 was biotinylated for the purification of the crosslinking products. The direct result was that Api88 was cross-linked to the ribosomal protein L10 (Krizsan et al., 2014). Follow-up *in vitro* protein synthesis assays revealed that these peptides inhibit protein biosynthesis and show a lower dissociation constant (K_d) for the bacterial 70S ribosome than for DnaK (Krizsan et al., 2014). A different study, working with the mammalian-derived PrAMP $Bac7^{1-35}$, the shortened form of the normally 60 aa long Bac7 peptide, identified by pulse-labeling experiments that the peptide is transported into the cell and blocks the production of proteins. Additionally, this $Bac7^{1-35}$ was co-sedimented with 70S ribosomes (Mardirossian et al., 2014). However, the molecular mechanism of action remains unknown.

1.4 Nascent chain-mediated translational arrest

During protein synthesis, the translating ribosome can stall along the mRNA due to various reasons including rare codons, amino acid starvation, antibiotic binding, mRNA secondary structure or the amino acid sequence of the nascent peptide. A stalling event that is mediated by the translated amino acid sequence is termed nascent chain-mediated translational arrest. This arrest is induced by the particular interactions of the nascent chain with the tunnel wall resulting in a rearrangement of ribosomal bases and can result in a specific path or fold of the nascent chain within the tunnel. This process can be aided by the binding of a small ligand, antibiotic or metabolite. Thus, the nascent chain acts as a sensor for the presence or absence of this particular ligand within the cell and so gene expression can be modulated in prokaryotes as well as eukaryotes (reviewed in detail Chiba et al., 2011; Ramu et al., 2009; Seip and Innis, 2016; Wilson et al., 2016). This section will focus on nascent chain-mediated translational arrest in bacteria.

After the identification of the first arrest peptide, *ermCL*, in 1980 (Gryczan et al., 1980; Horinouchi and Weisblum, 1980) different methods were developed to study nascent chain-mediated translational arrest *in vitro* as well as *in vivo*. *In vitro* methods include toeprinting, which uses *in vitro* translation systems that give at nucleotide resolution of the position of the ribosome along the mRNA under stalling and nonstalling conditions using primer extension (detailed description chapter 3.8) (Hartz et al., 1988; Orelle et al., 2013a). Arrest peptides are less sensitive to puromycin treatment and can be analyzed by acidic gel electrophoresis (Muto and Ito, 2008). The nature of the P-site tRNA can be identified using northern blotting (Chiba and Ito, 2012; Muto et al., 2006). Fluorescence resonance energy transfer (FRET) studies can give great insights into conformational changes of the ribosomes while arrest complex formation (Johansson et al., 2014; Tsai et al., 2014).

In vivo methods include the expression of a reporter gene, in many studies lacZ that encodes for β-galactosidase. The arrest can be investigated by fusing the arrest peptide directly to the reporter gene, meaning if the arrest occurs LacZ is not produced (Martínez et al., 2014; Ude et al., 2013). Another approach uses the mechanism of translational regulation by replacing the downstream gene by the reporter gene. In contrast to the fusion protein approach, LacZ is produced only if the arrest occurs (Gupta et al., 2016).

Ribosome profiling is a high-throughput method to analyze translation events occurring on a genome-wide scale *in vivo* (Ingolia et al., 2009) and has shown to be a valuable tool to study nascent chain-mediated translational arrest. Total mRNA bound to ribosomes is isolated from cells and digested by nucleases. The remaining mRNA fragments are purified, reverse transcribed, analyzed by next-generation sequencing (NGS) and mapped to the genome (Ingolia et al., 2009).

Another method to gain a deepened understanding of the molecular mechanism of nascent chain-mediated translation arrest is solving the structure of arrested ribosomes using cryo-EM (Arenz et al., 2016; Arenz et al., 2014a; Arenz et al., 2014b; Bhushan et al., 2011; Bischoff et al., 2014; Seidelt et al., 2009; Sohmen et al., 2015; Su et al., 2017; Zhang et al., 2015).

In prokaryotes, one mRNA often encodes multiple genes and is thus termed as a polycistronic mRNA. ORFs regulated by nascent chain-mediated arrest peptides are organized following: The arrest peptide, termed leader peptide, is encoded at the 5′ end of the mRNA followed by the ORFs of the regulated genes. The expression of downstream genes can be regulated through transcriptional or translational mechanisms (Gong and Yanofsky, 2002; Vazquez-Laslop et al., 2008).

1.4.1 Ligand-independent arrest peptides

The following table summarizes known sequences that lead to a ribosomal arrest, their biological relevance and how they are released:

Table 2: Peptide sequences that lead to a nascent chain-mediated translational arrest in bacteria. The amino acid attached to the P-site tRNA is underlined. [1]Citation is about the discovery of the listed arrest sequence. [2] Citation is describing the residues necessary for the arrest.

Name[1]	**Sequence[2]**	**Biological significance, Release mechanism**	**Species**
SecM (Nakatogawa and Ito, 2001)	FXXXXWIXXXXGIRAG(P) (Nakatogawa and Ito, 2002)	Regulation of SecA expression	*E. coli* and others
MifM (Chiba et al., 2009)	RIXXWIXXXXXMNXXXXDEED(AGS) (Chiba et al., 2009)	Regulation of membrane integration of $YidC_2$	*Bacillus subtilis*
VemP (Ishii et al., 2015)	HRIXGWKETNAMYVALNXS(Q) (Ishii et al., 2015)	Modulation of protein composition of the protein translocation machinery in low salt, $SecDF_1$	*Vibrio alginolyticus*

Characterized long ligand-independent arrest peptides regulate the expression of membrane or membrane-associated proteins in bacteria. The arrest is released by applying a mechanical force to the nascent chain, resulting in the translocation of the arrest peptide through the membrane or its insertion into the lipid bilayer.

1.4.1.1 SecM

The secretion monitor (SecM), formerly known as gene X, is encoded upstream of the ATP-dependent preprotein translocase SecA in bacteria and regulates the expression of SecA via a translational mechanism (McNicholas et al., 1997; Oliver et al., 1998). SecM has an N-terminal signal sequence for membrane translocation (Nakatogawa and Ito, 2001) for the recruitment of the translating ribosome to the membrane and an independent C-terminal arrest sequence. In the absence of SecA, ribosomes translating the SecM ORF get arrested. This leads to a rearrangement of the secondary structure of the translated mRNA freeing the SD sequence for SecA (Nakatogawa and Ito, 2001). Consequently, SecA is expressed directly at the membrane (Nakatogawa et al., 2005). SecA regulates its own expression over a negative feedback loop by applying a pulling force on the SecM peptide resulting in the relieve of the arrested ribosome (Butkus et al., 2003). SecM is translocated resulting in the translocation of SecM into the periplasm and fastly degraded by proteases (Nakatogawa and Ito, 2001). This allows a refolding of the secondary structure of the mRNA and the sequestering of the SD of *secA*. The crucial residues for nascent chain-mediated translational arrest by SecM (Table 1) were identified by alanine mutation screens and deletion of parts of the peptide (Nakatogawa and Ito, 2002).

Cryo-electron microscopy showed that SecM arrest peptide can form contacts with the ribosomal tunnel wall, leading to a rearrangement of 23S rRNA bases like A2062 having an allosteric effect on the PTC. The A76 ribose of the P-site tRNA is shifted by 2 Å making a peptide bond formation unlikely (Bhushan et al., 2011). The structure also shows the bound A-site Pro-tRNA^{Pro} which was identified to be crucial for SecM-mediated arrest. As discussed earlier the N-alkyl properties of proline reduces peptide bond formation, indicating that this property is crucial for SecM arrest (Bhushan et al., 2011; Muto et al., 2006). Recent higher resolution structures (3.3-3.7 Å) revealed that the specific contacts of the peptide with the tunnel wall lead additionally to a rearrangement of the ribosomal bases within the PTC mimicking an uninduced state (Zhang et al., 2015). A lot of particles had the peptide chain attached to the in the A-site tRNA^{Pro} resulting in a different set of interactions that were predicted by MD to be more favored compared to contacts observed in previous studies (Gumbart et al., 2012; Zhang et al., 2015). Due to peptide contacts and rearrangements of the PTC, base pairing between the D-loop and the tRNA^{Pro} is prevented and so the ribosome cannot adopt the hybrid conformation and so translocation is inhibited (Zhang et al., 2015). The results are consistent with a FRET study investigating the kinetics of SecM-mediated arrest (Tsai et al., 2014).

1.4.1.2 MifM

MifM is an arrest peptide that arrests specifically the *B. subtilis* ribosome (Chiba et al., 2011) and regulates the expression of the membrane insertase $YidC_2$ through a translational mechanism (Chiba et al., 2009). *B. subtilis* has two homologs of YidC, SpoIIIJ ($YidC_1$) and $YidC_2$. Studies have shown that MifM arrested ribosomes are released by the insertion of MifM into the membrane by SpoIIIJ (Chiba and Ito, 2015). In the absence of SpoIIIJ, MifM arrests and this results in the activation of $YidC_2$. $YidC_2$ itself can release the MifM arrested ribosomes as well, thus repressing its own expression (negative feedback loop) (Chiba and Ito, 2015). MifM has a multiple stalling sites consisting of consecutive acidic amino acids (Chiba and Ito, 2012).

The cryo-EM structure of MifM-arrested 70S *B. subitilis* ribosome (3.5-3.9 Å resolution) showed that MifM forms interactions with L22, L4 and the bases of the 23S rRNA. It has been shown that MifM arrests specifically the *B. subitilis* ribosome and not the *E. coli* ribosome (Chiba et al., 2011). This can be explained by the fact that L22 has a species-specific sequence. Biochemical studies have shown that in particular, M80 is crucial for MifM arrest. Mutations of this amino acid to a negatively charged amino acid leads to the loss of the translational arrest. M80 does not form a direct contact with the arrest peptide but its location indicates that it stabilizes the orientation of rRNA bases and the L22 loop (Sohmen et al., 2015). The cryo-EM structure contains no A-site tRNA. The interactions of the arrest peptide with the tunnel wall led to an allosteric rearrangement of the PTC that inhibits A-site tRNA accommodation due to the orientation of A2602 and U2506 pointing into the A-site binding pocket (Sohmen et al., 2015).

1.4.1.3 VemP

The marine Gram-negative bacteria *V. alginolyticus* has two paralogs of the SecDF protein. The leader peptide VemP is encoded upstream of $SecDF_2$ and regulates its expression through a translational mechanism (Ishii et al., 2015). VemP-mediated arrest is released by $SecDF_1$ applying a mechanical force to the nascent chain while translocating the peptide into the periplasm. $SecDF_1$ is active at high Na^+-concentration. If the Na^+ concentration drops, $SecDF_1$ becomes inactive and VemP-arrested ribosomes cannot release anymore. This leads to a rearrangement of the secondary structure of the mRNA freeing the SD sequence of the ORF encoding $SecDF_2$ and so it can be translated (Ishii et al., 2015). Recently, the structure of VemP-arrested *E. coli* ribosomes was solved at a resolution of 2.9 Å by cryo-EM (Su et al., 2017). The

VemP peptide forms two helices, one in the upper and one in the lower tunnel. The two helices are connected over an linking region forming two consecutive turns through the constriction site (Su et al., 2017). Residues forming the α-helix within the upper tunnel can form interactions with the tunnel wall, leading to an allosteric rearrangement within the PTC that stabilizes the uninduced state of the ribosome. Consequently, the accommodation of the A-site tRNA is prevented by the orientation of U2506 (Su et al., 2017).

1.4.2 Ligand-dependent arrest peptides

In contrast to ligand-independent arrest peptides, ligand-dependent arrest peptides act as sensors for the presence of ligands. Ligands can be metabolites or antibiotics binding to the ribosomal exit tunnel (Seip and Innis, 2016). A nascent chain-mediated translational arrest can also be induced by specific amino acid sequences and the presence of a ligand, such as an antibiotic or a metabolite. The ribosome-nascent chain complex (RNC) acts as a sensor for the ligand. The following table includes ligand-dependent arrest peptides, their ligand, biological significance and their mechanism of inhibition during the translational cycle:

Table 3: Summary of well-characterized ligand-dependent arrest peptides in bacteria. The amino acid located in the P-site is underlined. [1]citation describing the discovery of the listed arrest sequence. [2]citation identified important residues. +No alanine screen is published for ErmDL.

Name[1]	Sequence[2]	Biological significance, ligand	Inhibition point
TnaC (Konan and Yanofsky, 1997)	WXXXDXXIXXXXP(*) (Gong and Yanofsky, 2002) (Cruz-Vera et al., 2005)	Regulation of the transcription of the tnaBC operon, tryptophan	Termination
Cat86 leader (Brückner and Matzura, 1985)	MVKTD(K) (Alexieva et al., 1988)	Regulation of chloramphenicol resistance (drug modification enzymes), chloramphenicol	Peptidyl transfer
CmlA leader (Dorman and Foster, 1985)	MSTSKNAD(K) (Gu et al., 1994; Gu et al., 1993)		Peptidyl transfer

Name[1]	Sequence[2]	Biological significance, ligand	Inhibition point
ErmA leader (Murphy, 1985)	MXXXIAVV(E,D,K,R,H) (Ramu et al., 2011)	Regulation of macrolide resistance genes that methylate A2058, macrolides	Peptidyl transfer
ErmB leader (Horinouchi et al., 1983)	MXXXXXVD(K) (Arenz et al., 2014b)		Peptidyl transfer
ErmC leader (Gryczan et al., 1980; Horinouchi and Weisblum, 1980)	MXXXXIFVI(S) (Arenz et al., 2014a)		A-site tRNA binding
ErmD leader[3] (Hue and Bechhofer, 1992)	MTHSMRL(R) minimal motif MRL(R) (Sothiselvam et al., 2014)		Peptidyl transfer

1.4.2.1 TnaC acts as a sensor for tryptophan

Metabolic pathways are tightly regulated. In *E. coli*, the tryptophan degradation pathway is regulated by the arrest peptide TnaC that is encoded upstream of tryptophanase (TnaB) and the tryptophan-specific permease (TnaA) (Konan and Yanofsky, 1997). TnaC regulates the expression of TnaB and TnaA on a transcriptional level. In the absence of tryptophan, TnaC is translated and the peptide is released from the ribosome. This allows mRNA to adopt a specific secondary structure and its transcription is pre-mature terminated by Rho-factor binding. In the presence of free tryptophan, TnaC arrests when it reaches the stop codon preventing its release by RF2 in *E. coli* (Gong et al., 2001). In *Proteus vulgaris*, the arrest occurs during elongation and not during termination (Cruz-Vera et al., 2009). The arrest allows results in a different mRNA fold and the Rho-binding site is sequestered and the full-length mRNA is transcribed.

Insights into the underlying molecular arrest mechanism were obtained by cryo-EM. The structure was solved for *E. coli* TnaC sequence and *E. coli* ribosomes. A first cryo-EM study showed that the TnaC peptide can form possible specific contacts with the tunnel wall (Seidelt et al., 2009). A more recent cryo-EM structure identified two Trp molecules bound within the hydrophobic pockets formed by the TnaC peptide and located 15-20 Å away from the PTC (Bischoff et al., 2014) which is in agreement with a recent biochemical study (Martínez et al.,

2014). The peptide forms specific contacts with L22, L4 and 23S rRNA. The PTC is inactivated due to distinct positions of U2585 and A2602 preventing release factor binding. U2586 forms stacking interactions with one of the bound Trp-ligands restricting possibly the movement of U2585. Furthermore, the orientation of the penultimate amino acid clashes with the GGQ motif of the release factor (Bischoff et al., 2014).

1.4.2.2 Erm leader peptides sense the presence of macrolide antibiotics

The expression of antibiotic resistance genes can be regulated by short leader peptides. Macrolide and ketolide resistance genes encoding a methyltransferase (*erythromycin resistance methylase, erm*), are regulated by upstream encoded leader peptides (Ramu et al., 2009). Different leader peptide sequences were identified which showed differences in arrest motifs and could be sorted accordingly. Expression of the downstream *erm* gene can be regulated using a translational or transcriptional mechanism. The resistance gene methylates specifically A2058 resulting in the disruption of the erythromycin binding site (Katz et al., 1987; Roberts et al., 1999). The first *erm* leader gene to have been characterized is *ermCL* (Gryczan et al., 1980; Horinouchi and Weisblum, 1980). The ErmCL peptide itself has been studied biochemically and by cryo-EM (Arenz et al., 2014a). The 3.9 Å structure of the arrested 70S *E. coli* ribosome reveals stable contacts of the peptide with erythromycin and the ribosomal tunnel wall resulting in a unique orientation of A2062. This results in a reorientation of bases within the PTC. U2585 adopts a unique orientation and U2586 forms direct contacts with the growing peptide chain. A2602 points into the A-site binding pocket prevent A-site tRNA accommodation (Arenz et al., 2014a).

Another erm leader peptide studied by cryo-EM is ErmBL. The path of the peptide in the absence of the drug is significantly different from that of ErmCL. ErmBL does not form direct contacts with the drug but with the tunnel wall (Arenz et al., 2014b). ErmBL adopts a unique path in the ribosomal tunnel as a consequence of the fact that Asp10 is rotated resulting in a displacement of A76 of the P-site tRNA. The conformation results in a suboptimal geometry for the nucleophilic attack of the A-site amino acid (Arenz et al., 2016). The A-site $tRNA^{Lys}$ is bound in the structure in a different conformation compared to the fully accommodated state and U2585 is trapped between uninduced and induced states. Molecular dynamics simulations have shown that allosteric rearrangement of the PTC due to the presence of erythromycin leads

to a trapped lysine side chain, while small hydrophobic sidechains could overcome this effect and the ribosome would not arrest (Arenz et al., 2016).

In bacteria, long arrest peptides are involved in the expression of membrane proteins, metabolic enzymes, and antibiotic resistance genes. The arrest peptides form interactions with the ribosomal tunnel wall and potential ligand. Consequently, this leads to an allosteric rearrangement of the PTC resulting in the inhibition of A-site tRNA or RF accommodation by stabilization of the uninduced state, formation of secondary structure within the PTC and reorientation of the 3' end of the P-site tRNA.

1.4.3 Short ligand-dependent ribosomal arrest peptides in bacteria

To gain a broader understanding of the abundance of macrolide dependent arrest sequences, ribosome profiling was performed with *E. coli* cells which were exposed for a short time to erythromycin or telithromycin (Kannan et al., 2014). Another independent study used *Staphylococcus aureus* exposed to sublethal concentration of the macrolide azithromycin (Davis et al., 2014). The ribosome profiling data identified the motif +X(+), which arrests once the X (any amino acid) is bound to the P-site tRNA within proteins for both studies. This resulted in the conclusion that the nature of the amino acids within the PTC determines the arrest of the peptide, and suggested that macrolide binding leads to the formation of a restrictive PTC (Davis et al., 2014; Kannan et al., 2014).

The arrest peptide ErmDL contains this particular motif, namely MRL(R), and arrests accordingly in the presence of erythromycin. Sequential shortening of the ErmDL sequence revealed the minimal stalling motif MRL(R) (Sothiselvam et al., 2014). The peptide is too short to reach the binding site of the drug, leading to the assumption that the drug and the peptide could induce an allosteric rearrangement of the ribosomal residues within the PTC. Residues that were identified previously as being crucial for the arrest of ErmAL and ErmCL like A2062 or C2610 do not seem to have a direct impact on the stalling efficiency (Sothiselvam et al., 2014; Vázquez-Laslop et al., 2011; Vázquez-Laslop et al., 2010). In contrast base U2585, which adopts different, distinct conformations during translation elongation to prevent premature peptide hydrolysis and allow A-site tRNA accommodation (Schmeing et al., 2005a; Voorhees et al., 2009), seems to adopt a specific conformation as a consequence of erythromycin binding, as

suggested by molecular dynamics (MD) simulations and ribosomal residue protection assays (Sothiselvam et al., 2014).

Further biochemical studies revealed that the fMRL(R) motif represents only one possible stalling sequence and that it can be generalized as the motif fM+X(+) that was identified within nascent peptide chains by ribosome profiling (Sothiselvam et al., 2016). Using unnatural amino acids attached to the CCA end mimics, it was shown that the positive charge of the A-site amino acid is crucial for the arrest while the length of the side chain has only a minor effect (Sothiselvam et al., 2016), as shown in Figure 8.

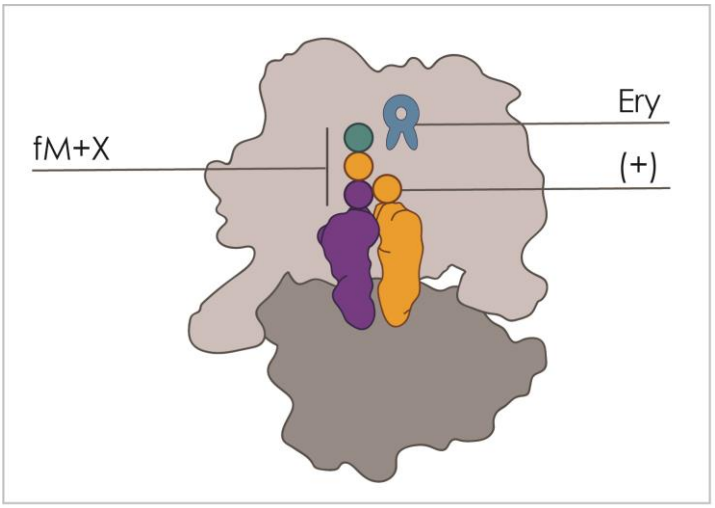

Figure 8: fM+X(+) arrests the ribosome in the presence of the antibiotic erythromycin. The peptide barely touches the binding site of the drug.

In summary, fM+X(+) is an arrest peptide that stalls the ribosome in the presence of macrolide antibiotics (Figure 8). The binding of the drug leads to rearrangements within the PTC and to ribosomal arrest through what appears to be an allosteric mechanism.

1.4.4 Polyproline induced arrest is relieved by the protein factor EF-P

In contrast to SecM, VemP and MifM, polyproline-mediated arrest is induced by the amino acid composition within a short distance to the PTC (Peil et al., 2013; Starosta et al., 2014a; Woolstenhulme et al., 2015) and might be mainly induced by the chemistry and stereochemistry of proline (Muto and Ito, 2008). Among all canonical amino acids, proline is the only *N*-alkyl amino acid which has a higher alkalinity and its imino group is more likely to be protonated at physiological pH compared to other canonical amino acids. Additionally, proline is also the only canonical amino acid that can form *cis* as well as *trans* peptide bonds introducing possible kinks in secondary structure elements (Muto and Ito, 2008; Pavlov et al., 2009).

While fast kinetic studies have shown, that proline is incorporated at a slower peptide bond formation rate compared to other canonical amino acids (Pavlov et al., 2009) recent *in vivo* and *in vitro* studies have shown that the translation of proteins containing three consecutive prolines is severely reduced in the absence of a specific protein factor (Doerfel et al., 2013; Ude et al., 2013; Woolstenhulme et al., 2013). Three consecutive prolines are encoded in the primary structure of approximately 100 proteins in *E. coli*, among which are important housekeeping factors like valinyl-tRNA-synthetase (ValS) (Starosta et al., 2014b). These proteins can be still produced due to the presence of the protein factor EF-P. EF-P can specifically recognize ribosomes that are arrested by polyproline motifs and catalyze their rescue (Doerfel et al., 2013; Ude et al., 2013). Similar results were observed for the eukaryotic homolog initiation factor 5A (eIF5A) (Gutierrez et al., 2013). Further proteomic studies using stable isotope labeling of amino acids in cell culture (SILAC) on EF-P deletion strains (Δ*efp*) revealed a higher number of down-regulated genes than the 100 encoding three consecutive prolines (Peil et al., 2013). Further analysis using *in vivo* reporter systems and *in vitro* translation assays revealed the full complexity of polyproline-mediated arrest. The strength of the polyproline-mediated arrest is modulated by the nature of the amino acid in the -2, -1 or +1 position (Peil et al., 2013; Starosta et al., 2014a) (Table 2) and Figure 9 represents strong arrest sequences Figure 9:

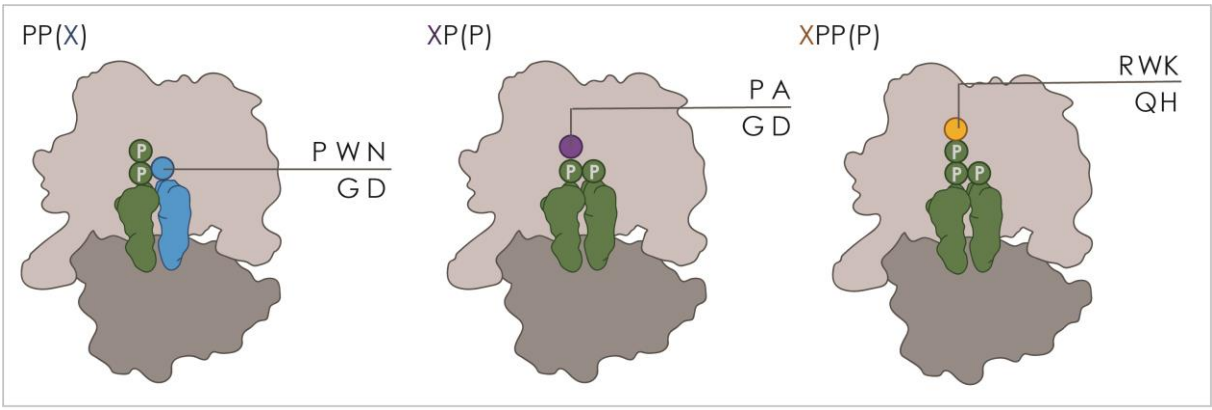

Figure 9: Summary of the sequence variants that can induce polyproline-mediated ribosomal arrest. 0 the proline and its corresponding tRNA are highlighted in green. The amino acid in the A-site (PP(X)), in the -1 position (XP(P)) and -2 positions (XPP(P)) directly influence the strength of the arrest. The figure summarizes strong polyproline arrest motifs identified by (Doerfel et al., 2013; Peil et al., 2013; Starosta et al., 2014a; Woolstenhulme et al., 2015)**.**

The resulting sequences were validated by recent ribosome profiling experiments comparing the data obtained from wild-type cells with Δ*efp* (Woolstenhulme et al., 2015). It has been shown that EF-P and its homologs need to be post-translationally modified to gain activity. The modification is species-specific and can vary from glycosylation to β-lysinylation (Bailly and de Crécy-Lagard, 2010; Bullwinkle et al., 2013; Lassak et al., 2015; Park et al., 2012). Bacterial cells lacking EF-P or its modification enzymes show defects in fitness, mobility, membrane integrity and virulence (Navarre et al., 2010).

To gain insights into the function of EF-P and its eukaryotic homolog, several structures were determined by cryo-EM and X-ray crystallography. The first structural information of the function of EF-P was obtained by co-crystallization of 70S *T. thermophilus* ribosomes, unmodified EF-P from *T. thermophilus* and $tRNA_i^{Met}$ from *E. coli* resulting in a structure at 3.5 Å resolution (Blaha et al., 2009). The structure was solved under the assumption that EF-P promotes and enhances the formation of the first peptide bond (An et al., 1980; Glick et al., 1979; Glick and Ganoza, 1975). The factor binds next to the P-site tRNA stabilizing the orientation of the 3'CCA end of the P-site tRNA (Blaha et al., 2009).

More recently, the Beckmann group published a cryo-EM structure with 3.9 Å resolution of the 80S yeast (*Saccharomyces cerevisiae*) ribosome pulled down from cells to study non-stop decay (NSD) to study the Ski complex (His-tagged). During cryo-EM data processing, a large number of particles contained two tRNAs and eIF5A, the eukaryotic homolog of EF-P. Like EF-

P, eIF5A needs to be modified to be active. The eukaryotic modification is the unusual amino acid hypusine, which is formed by transferring a 4-aminobutyl moiety on the corresponding Lys residue followed by hydroxylation (Dever et al., 2014; Gutierrez et al., 2013). The structure showed that the hypusine modification of eIF5A forms direct contact with the CCA end of the P-site tRNA. This aids the correct orientation of the peptide chain for peptide bond formation (Schmidt et al., 2015).

Recently, a study from the Yusupov group utilized tRNA mimics, a short peptide attached to the RNA fragment ACCA which mimics the 3'CCA end of the tRNA, in complex with the 80S *S. cerevisiae* ribosome giving a greater understanding of the conformation of proline within the PTC (Melnikov et al., 2016a). The structures solved by X-ray crystallography have a resolution range of 3.1 to 3.5 Å. To obtain greater insights into the conformation of a diproline peptide the tRNA mimic was stabilized with the antibiotic Sparsomycin. The backbone of the dipeptide is bent with the N-terminus pointing towards the tunnel wall while the N-terminus of the control peptide (Phe-Leu) points into the exit tunnel (Melnikov et al., 2016a). In addition, proline does not bind in the same orientation like other amino acids to the A-site crevice leading to wrong orientation for peptide bond formation (Melnikov et al., 2016a). Further studies, including the eIF5A in complex with the yeast ribosome, showed that eIF5A binds at the same position even if the P-site tRNA mimic is absent and the hypusine modification points towards the PTC. In addition, the binding of the factor results in a conformational change of the ribosome (Melnikov et al., 2016b).

All in all, EF-P is non-canonical translation factor that presents a possible target for antibiotic research. Even if there are many published structures of EF-P or its eukaryotic homolog in complex with the ribosome, there is no high-resolution structure containing the native substrate Pro-tRNA^{Pro} as well as the orientation of a prokaryotic modification remains unknown.

1.5 Flexizyme as a tool to study translation

1.5.1 Identification and sequence optimization

One major aim of this thesis is to study short nascent-chain arrest peptides by structural characterization. In doing so, the arrest peptide needs to be attached to the 3′CCA end of tRNAs. To obtain peptidylated tRNA, the flexizyme methodology was used. The flexizyme methodology, a method to transfer activated amino acids and derivatives specifically to the 3′ CCA end of a tRNA, was developed overcome limitations of genetic reprogramming *in vitro* (Goto et al., 2011). These limitations included the high substrate sensitivity of aminoacyl-tRNA synthetases and so only a limited number of amino acids could be used to produce novel potential therapeutic peptides by the bacterial ribosome (Hartman et al., 2007; Hartman et al., 2006).

RNA is involved in many reactions like splicing and peptide bond formation and are indicators of an "RNA-world" before protein enzymes were evolved. It has been hypothesized that processes like aminoacylation of tRNAs have been originally catalyzed by ribozymes (as reviewed by Hager et al., 1996). First attempts to identify RNA sequences that can aminoacylate and recognize tRNAs resulted in the identification of sequences that can transfer the amino acid onto their own 5′ end or internally onto 2′OH groups (Lohse and Szostak, 1996; Suga et al., 1998a; Suga et al., 1998b). Further experiments and optimization steps resulted in the identification of an RNA sequence that uses activated Biotin-L-glutamine adenylate and Biotin-L-phenylalanine-adenylate to act in *cis* (self-amino acylation) or in *trans* (aminoacylation of a different RNA) (Lee et al., 2000). The natural leaving group, adenylate, was replaced by a cyanomethyl ester (CME) to ensure that the chemical properties of the amino acid are forming the interactions with the ribozyme (Lee et al., 2000).

For incorporation of an amino acid into the nascent chain by the ribosome, the amino acid is specifically attached to the 3′ CCA end of its tRNA by the aminoacyl-tRNA synthetase (ARS). To site-direct, the aminoacylation reaction catalyzed ARS like ribozymes a tRNA precursor molecule was used (Saito et al., 2001a). In cells, tRNAs get produced as long precursors that are processed post-transcriptionally. In particular, the 5′ end gets processed by the ribozyme RNase P (Meinnel and Blanquet, 1995). The 5′ end sequence might have had the capability of aminoacyl synthetase by aminoacylating its own 3′CCA end that got lost after the evolution of

protein-based aminoacyl-tRNA synthetases. Several rounds of *in vitro* selection were performed on a pre-tRNA with a randomized 5′ region. The selected 5′ region of the pre-tRNA is capable of recognizing L-phenylalanine-adenylate or L-phenylalanine-cyanomethyl ester (CME) and can then transfer the amino acid specifically to its own 3′CCA-end acting in *cis* (Saito et al., 2001a). Furthermore, the identified 5′ region folds independently from the tRNA region and after RNase P cleavage the site-directed aminoacylation reactivity is preserved (acting in *trans*) (Saito et al., 2001b).

Moreover, the identified ribozyme can specifically aminoacylate also a microhelix mimicking the CCA end of a tRNA meaning the reaction is independent of the folding of the target molecule (Saito et al., 2001b). The reaction can be enhanced by Mg^{2+} cations which preserve the folding of the ribozyme (Saito and Suga, 2002). Further sequence optimization led to the identification of a flexizyme (Fx) that forms three base pairs with the target tRNA (Fx3). The three base pairs are formed with the RCCA 3′ end of tRNAs (base pairing underlined). The reaction is faster in cases base 73 (R) is an A, U or G base in contrast to C, which results in a longer reaction duration. Fx3 binds specifically enough for efficient aminoacylation without disrupting the acceptor stem of the tRNA resulting a flexizyme that can recognize all tRNAs (Murakami et al., 2003; Ramaswamy et al., 2004). To understand the underlying reaction mechanism the structure of Fx3 fused to a microhelix that mimics the 3′ acceptor stem of a tRNA in complex with the protein U1A was solved at 2.8 Å resolution. Fx3 flexizyme forms four helices. Three of them adopt compact right-handed helices, termed A-form helices and one irregular helix. The irregular helix is necessary for substrate. Base pairing between the CCA end and the flexizyme give rise to additional stacking interactions as well as a defined network of hydrogen bonds which results in the accessibility of the 3′OH for substrate binding (Xiao et al., 2008).

To increase the substrate variety and the reaction yields, the Fx3 sequence was used as a template for further rounds *in vitro* selection using a randomized sequence in the substrate binding site. The identified sequences are listed in Figure 10:

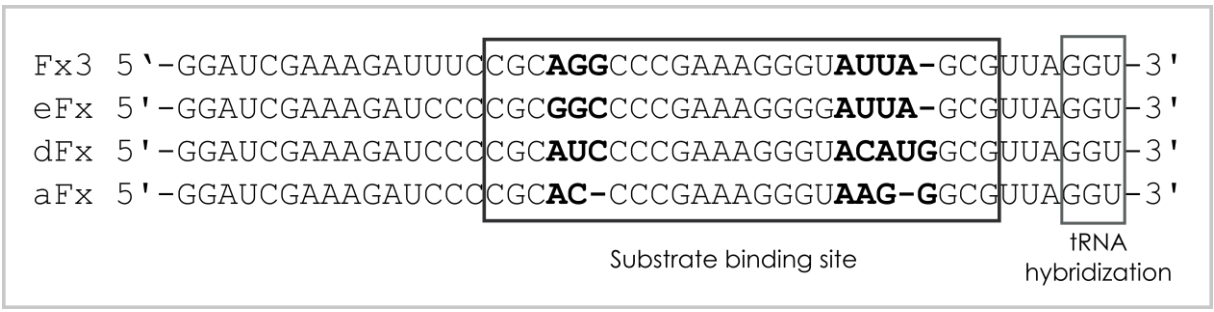

Figure 10: Sequence alignments of the different *in vitro* selected flexizymes Fx3, eFx, dFx, and aFx. The tRNA hybridization and substrate recognition site are marked with gray and black boxes, respectively. Minimal changes in the sequences leading to the change in recognition of different leaving groups.

The *in vitro* selected flexizymes have high sequence similarities. However, mutations within the substrate recognition site allow the recognition of three different benzyl-based leaving groups (Figure 10). Figure 11 illustrates the different flexizymes with their corresponding activation group and the chemical properties of amino acid derivatives (Goto et al., 2011):

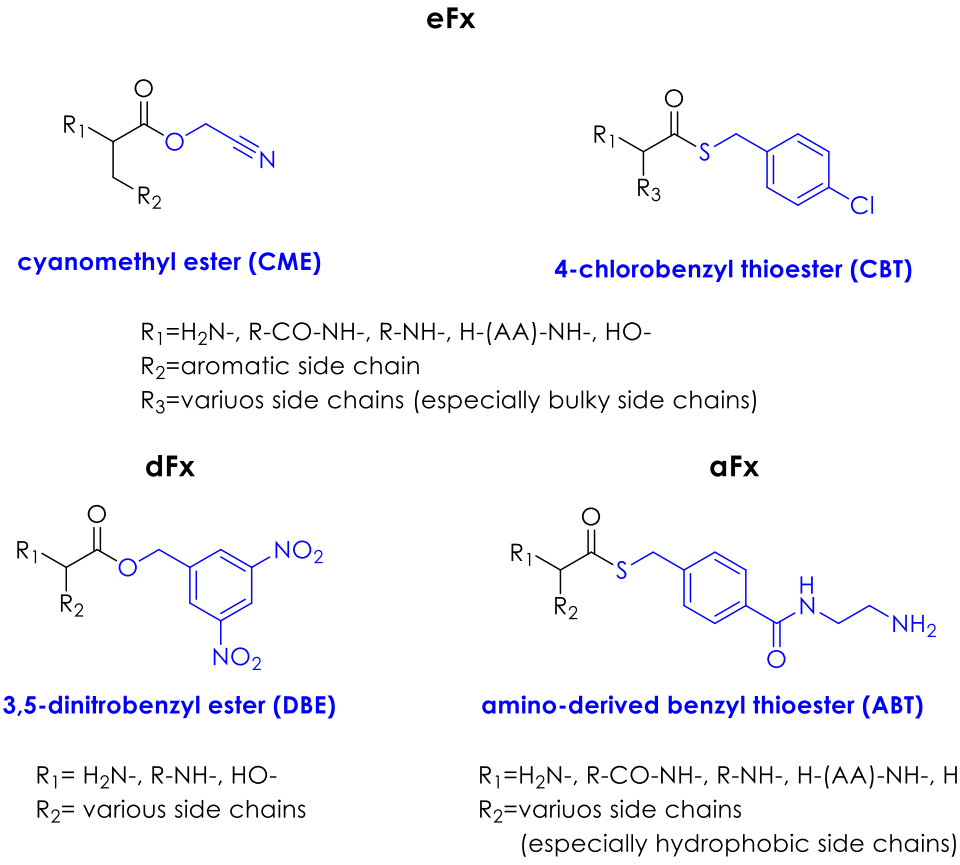

Figure 11: Different flexizymes (eFx, dFx, and aFx) were selected *in vitro* to recognize different leaving groups to increase reactivity and complexity in the substrate. The leaving group is marked in blue. The different leaving groups allow different chemical properties of the activated peptide or amino acid derivative (figure after Goto et al., 2011).

As shown in Figure 11, enhanced Fx (eFx) is more active than Fx3 and recognizes two different leaving groups. On one hand aromatic amino acids are activated by CME, the same leaving group as Fx3, and on the other hand, bulky amino acids can be activated by using 4-chloro benzyl thioester (CBT). The dinitro flexizyme (dFx) recognizes the leaving group 3,5-dinitrobenzyl ester (DBE) and transfers various amino acids and activated peptides onto tRNAs (Murakami et al., 2006a). Already dFx and eFx increased the accessibility to a wider variety of activated peptides for further experiments whereas hydrophobic amino acids activated with CBT or DBE are insoluble in water, inducing poor reactivity of the activated peptide. To overcome this issue of very hydrophobic amino acids, like those with long alkyl side chains, they can be activated with amino-derived benzyl thioester (ABT) as leaving the group (Niwa et al., 2009).

1.5.2 Case studies

Flexizyme-mediated charging led to a great variety of substrates that could be incorporated into a growing nascent peptide. To do so, *in vitro* translation was performed in a reconstituted *in vitro* translation system (Shimizu et al., 2001; Shimizu et al., 2005). Reactions were performed using an aminoacylated tRNA in an *in vitro* translation system lacking these tRNAs, the natural amino acid, and the corresponding aminoacyl-tRNA synthetase. This system is called flexible *in vitro* translation (FIT) (Goto et al., 2011) and can be used to initiate translation using any L- or D-amino acid (Goto et al., 2008; Murakami et al., 2006a), short peptides and peptide-like structures (Goto and Suga, 2009). Unnatural amino acids can also be incorporated into the growing peptide chain by charging the molecule onto an elongator tRNA (Murakami et al., 2006b). To ensure that all native amino acids can be included in the reaction, a $tRNA_{SNN}$ library can be produced by *in vitro* transcribing individually each tRNA with an SNN anticodon. In some cases, one amino acid, like alanine or proline, can be delivered by multiple tRNAs to the ribosome. One of the tRNAs can be aminoacylated with the native amino acid using the corresponding aminoacyl tRNA synthetase and the others by non-proteinogenic amino acids or derivatives using flexizyme (Iwane et al., 2016); all charged tRNAs can be mixed and incorporated while the ribosome is translating an NNS library.

A recent study (Katoh et al., 2016) used the flexizyme approach to identify the nucleotides of $tRNA^{Pro}$, that are crucial for the recognition of EF-P and the release of polyproline-mediated translational arrest. Different mutants of $tRNA^{Pro}$, $tRNA^{Ser}$, $tRNA^{Val}$ and $tRNA_i^{Met}$ were *in vitro* transcribed and prolinylated using flexizyme. The reactivity of EF-P was quantified by measuring the incorporation of downstream radioactive labeled Asp and kinetic parameters were obtained by measuring Pro incorporation rates in the presence or absence of EF-P. The major result of this study was that the D-loop structure of $tRNA^{Pro}$ and $tRNA_i^{Met}$ is crucial for EF-P recognition and thus needs to be included for further structural studies to understand the detailed mechanism of EF-P (Katoh et al., 2016).

In summary, extensive studies have shown that flexizymes can be used specifically to transfer amino acids or small peptides onto the 3′ CCA end of any tRNA and incorporate them into the growing peptide chain during initiation and elongation.

1.6 Aims

The bacterial ribosome is one of the major targets for antibiotics (Wilson, 2009, 2011, 2014). The rise of multiple bacterial resistant genes against clinically used antibiotics is an increasing threat and there is need for the development of new therapeutic strategies. Certain peptides can inhibit bacterial translation, either as free peptides that are produced as a part of defense mechanisms against other organisms such as PrAMPs or during their own translation (nascent chain-mediated translational arrest).

PrAMPs are antimicrobial peptides which are produced by insects and mammals as a part of their innate immune system (Otvos, 2002). Though recent studies have shown that PrAMPs inhibit protein biosynthesis through binding to the bacterial ribosome (Krizsan et al., 2014; Mardirossian et al., 2014) the molecular mechanism remains unknown. In order to obtain detailed insights into the molecular mechanism, the structures of different PrAMPs in complex with the 70S *T. thermophilus* ribosome are determined here using X-ray crystallography.

During the nascent-chain mediated translational arrest the bacterial ribosome is inhibited by the translating peptide. Structural information of long nascent chain arrest peptides such as SecM (Zhang et al., 2015) and ErmCL (Arenz et al., 2014a) has been obtained recently using cryo-EM. The underlying mechanisms of how short arrest peptides, including polyproline motifs as well as fM+X(+)arrest the ribosome in the presence of erythromycin, remain unknown. To investigate this further, the aim of this work was to study these arrest complexes using the flexizyme methodology for complex formation for structural and biochemical characterization. Obtaining high-resolution or near atomic resolution structures will give insights into the molecular conformation of the nascent chain as well as into their allosteric effect on the bacterial ribosome. The knowledge to be obtained from this will enable a greater understanding how peptide bond formation can be inhibited specifically and could lead to the development of novel highly specific antibiotics targeting this process.

2. Materials

2.1 Chemicals

Table 4: List of chemicals

Name	Elemental formula	Company	Experiment
(+/-)-2-Methyl-2,4-pentanediol (MPD)	$C_6H_{14}O_2$	Hampton Research	Crystallography
(R)-γ-(3-chloro-benzyl)-L-proline hydrochloride	$C_{12}H_{15}Cl_2NO_2$	Sigma Aldrich, St Louis, MO, USA	Amino acid derivative
1,4-Dithiothreitol (DTT)	$C_4H_{10}O_2S_2$	Euromedex, Souffelweyersheim, France	*in vitro* transcription/ translation
2-(N-morpholino)-ethanesulfonic acid (MES)	$C_6H_{13}NO_4S$	Sigma Aldrich, St Louis, MO, USA	Buffer
2-Mercaptoethanol (BME)	C_2H_6OS	Sigma Aldrich, St Louis, MO, USA	Ribosome purification
4-(2-hydroxyethyl)-1-piperazineethanesulfonic acid (HEPES)	$C_8H_{18}N_2O_4S$	Sigma Aldrich, St Louis, MO, USA	Buffer for protein purification, crystallography
Acetic acid	$C_2H_4O_2$	Sigma Aldrich, St Louis, MO, USA	PH adjustment
Acetone	C_3H_6O	Sigma Aldrich, St Louis, MO, USA	TCA precipitation
Acetonitril	C_2H_5N	Sigma Aldrich, St Louis, MO, USA	HPLC
Acrylamide/bis-acrylamide 30% solution 19:1		Euromedex, Souffelweyersheim, France	PAGE (Protein)
Acrylamide/bis-acrylamide 40% solution 19:1		Dutscher, Brumath, France	PAGE (DNA, RNA)
Adenosine 5'-triphosphate disodium salt hydrate	$Na_2C_{10}H_{14}N_5O_{13}P_3$	Sigma Aldrich, St Louis, MO, USA	*In vitro* transcription/ translation, amino acylation reaction
Agar		Sigma Aldrich, St Louis, MO, USA	Bacterial selection
Agarose type D-5		Euromedex, Souffelweyersheim, France	DNA electrophoresis

Name	Elemental formula	Company	Experiment
Ammonium acetate	$(NH_4)C_2H_3O_2$	Sigma Aldrich, St Louis, MO, USA	RNA extraction, purification, precipitation
Ammonium chloride	NH_4Cl	Euromedex, Souffelweyersheim, France	Protein purification, sucrose gradients
Ammonium persulfate	$(NH_4)2S_2O_8$	Sigma Aldrich, St Louis, MO, USA	PAGE
Ammonium sulfate	$(NH_4)2SO_4$	Euromedex, Souffelweyersheim, France	Protein, RNA purification
β-Nicotinamide adenine dinucleotide hydrate (NAD)	$C_{21}H_{27}N_7O_{14}P_2 \cdot XH_2O$	Sigma Aldrich, St Louis, MO, USA	*In vitro* translation
Bacto-Agar		Sigma Aldrich, St Louis, MO, USA	*E. coli* growth
Bicine (>99%)	$C_6H_{13}NO_4$	Sigma Aldrich, St Louis, MO, USA	Buffer
Bis-Tris	$C_8H_{19}NO_5$	Sigma Aldrich, St Louis, MO, USA	Buffer for flexizyme reaction
Boric Acid	H_3BO_3	Sigma Aldrich, St Louis, MO, USA	DNA/RNA electrophoresis
Brillant blue R	$Na(C_{45}H_{44}N_3O_7S_2)$	Sigma Aldrich, St Louis, MO, USA	Protein PAGE staining
Bromophenol blue	$C_{19}H_{10}Br_4O_5S$	Fisher chemicals	Loading dye
Butyl-65OS		Tosho, Tokyo, Japan	RNA and protein purification
Calcium chloride dihydrate	$CaCl_2 \cdot 2H_2O$	Euromedex, Souffelweyersheim, France	Chemical competent cells, toeprinting
Chloroform: Isoamyl alcohol (24:1)	CCl_2H_2	Sigma Aldrich, St Louis, MO, USA	tRNA purification, enzymatic reaction
Cobalt(II) chloride hexahydrate	$CoCl_2 \cdot 6H_2O$	Sigma Aldrich, St Louis, MO, USA	*Thermus* growth
Coenzyme A disodium salt	$Na_2(C_{21}H_{34}N_7O_{16}P_3S)$	Sigma Aldrich, St Louis, MO, USA	*In vitro* translation
Copper (II) chloride dihydrate	$CuCl_2 \cdot 2H_2O$	Sigma Aldrich, St Louis, MO, USA	*Thermus* growth
Copper (II) sulfate pentahydrate	$CuSO_4 \cdot 5H_2O$	Sigma Aldrich, St Louis, MO, USA	*Thermus* growth
Cytidine monophosphate (CMP)	$C_9H_{16}N_3O_8P$	Jenabioscience, Jena, Germany	*In vitro* transcription/translation
Cytidine triphosphate (CTP)	$C_9H_{16}N_3O_{14}P_3$	Jenabioscience, Jena, Germany	*In vitro* transcription/translation

Name	Elemental formula	Company	Experiment
D-(+)-Glucose	$C_6H_{12}O_6$	Sigma Aldrich, St Louis, MO, USA	Cell culture
Deoxyribonucleic acid sodium salt from salmon testes (DNA)	DNA	Sigma Aldrich, St Louis, MO, USA	Northern Blotting
Diethyl pyrocarbonate (DEPC)	$C_6H_{10}O_5$	Sigma Aldrich, St Louis, MO, USA	RNase inactivation
Dimethyl sulfoxide (DMSO)	$C_2\ H_6\ OS$	Sigma Aldrich, St Louis, MO, USA	Solvent for flexizyme compounds and antibiotics
Di-tert-butyl dicarbonate	$C_{10}H_{18}O_5$	Sigma Aldrich, St Louis, MO, USA	
DL-3-Phenyllactic acid	$C_9H_{10}O_3$	Sigma Aldrich, St Louis, MO, USA	Amino acid derivative
DL-Indole-3-lactic acid	$C_{11}H_{11}NO_3$	Sigma Aldrich, St Louis, MO, USA	Amino acid derivative
Ethanol	C_2H_5OH	Sigma Aldrich, St Louis, MO, USA	Nucleic acid precipitation, HPLC
Ethylenediaminetetraacetic acid disodium salt dihydrate (EDTA)	$Na_2(C_{10}H_{14}N_2O_8)\cdot 20H_2O$	Sigma Aldrich, St Louis, MO, USA	Ion chelator
Folic acid	$C_{19}H_{19}N_7O_4$	Sigma Aldrich, St Louis, MO, USA	*In vitro* translation
Folinic acid calcium salt hydrate	$Ca(C_{20}H_{21}N_7O_7)\cdot xH_2O$	Sigma Aldrich, St Louis, MO, USA	*In vitro* translation
Formamide	CH_3NO	Sigma Aldrich, St Louis, MO, USA	Denaturing RNA loading dye
Gelzan		Sigma Aldrich, St Louis, MO, USA	*Thermus* growth
Glycerol	$C_3H_8O_3$	VWR, Radnor, PA, USA	Protein protectant
Glycine	$C_2H_5NO_2$	Sigma Aldrich, St Louis, MO, USA	Amino acid, protein running buffer
Guanosine monophosphate (GMP)	$C_{10}H_{16}N_5O8P$	Jenabioscience, Jena, Germany	*In vitro* transcription/translation
Guanosine triphosphate (GTP)	$C_{10}H_{16}N_5O_{14}P_3$	Jenabioscience, Jena, Germany	*In vitro* transcription/ translation
Hydrochloric acid solution	HCl_{aq}	Sigma Aldrich, St Louis, MO, USA	PH adjustment
Imidazole	$C_3H_4N_2$	Sigma Aldrich, St Louis, MO, USA	Protein purification

Name	Elemental formula	Company	Experiment
Iron chloride hexahydrate	$FeCl_3 \cdot 6H_20$	Sigma Aldrich, St Louis, MO, USA	*Thermus* growth
Isopropanol	C_3H_7OH	Sigma Aldrich, St Louis, MO, USA	Nucleic acid precipitation, HPLC
Isopropyl-β-D-thiogalactopyranoside (IPTG)	$C_9H_{18}O_5S$	Euromedex, Souffelweyersheim, France	Cell culture
L-(+)-Arabinose	$C_5H_{10}O_5$	Sigma Aldrich, St Louis, MO, USA	Cell culture
L-Alanine	$C_3H_7NO_2$	Sigma Aldrich, St Louis, MO, USA	*In vitro* translation
L-Arginine monohydrochloride	$C_6H_{14}N_4O_2 \cdot HCl$	Sigma Aldrich, St Louis, MO, USA	*In vitro* translation, crystallization
L-Asparagine	$C_4H_8N_2O_3$	Sigma Aldrich, St Louis, MO, USA	*In vitro* translation
L-Aspartic Acid	$C_4H_7NO_4$	Sigma Aldrich, St Louis, MO, USA	*In vitro* translation
LB-Powder		Sigma Aldrich, St Louis, MO, USA	*E. coli* growth
L-Cysteine hydrochloride	$C_3H_7NO_2S \cdot xHCl$	Sigma Aldrich, St Louis, MO, USA	*In vitro* translation
L-Glutamic acid monopotassium salt monohydrate	$K(C_5H_9NO_4) \cdot H_20$	Sigma Aldrich, St Louis, MO, USA	*In vitro* translation
L-Glutamic acid	$C_5\,H_9\,NO_4$	Sigma Aldrich, St Louis, MO, USA	*In vitro* translation
L-Glutamic acid hemimagnesium salt tetrahydrate	$Mg(C_{10}H_{16}N_2O_8) \cdot 4H_2O$	Sigma Aldrich, St Louis, MO, USA	*In vitro* translation
L-Glutamine	$C_5H_{10}N_2O_3$	Sigma Aldrich, St Louis, MO, USA	*In vitro* translation
L-Histidine monohydrochloride monohydrate	$C_6H_9N_3O_2$	Sigma Aldrich, St Louis, MO, USA	*In vitro* translation
L-Isoleucine	$C_6H_{13}NO_2$	Sigma Aldrich, St Louis, MO, USA	*In vitro* translation
Lithium chloride	LiCl	Sigma Aldrich, St Louis, MO, USA	tRNA precipitation
L-Leucine	$C_6\,H_{13}NO_2$	Sigma Aldrich, St Louis, MO, USA	*In vitro* translation
L-Lysine monohydrochloride	$C_6H_{14}N_2O_2 \cdot HCl$	Sigma Aldrich, St Louis, MO, USA	*In vitro* translation
L-Methionine	$C_5H_{11}NO_2S$	Sigma Aldrich, St Louis, MO, USA	*In vitro* translation, tRNA purification, aminoacylation

Name	Elemental formula	Company	Experiment
L-Ornithine dihydrochloride	$C_5H_{12}N_2O_2 \cdot 2HCl$	Sigma Aldrich, St Louis, MO, USA	*In vitro* translation, ligand
L-Phenylalanine	$C_6H_{11}N0_2$	Sigma Aldrich, St Louis, MO, USA	*In vitro* translation, tRNA purification, aminoacylation
L-Proline	$C_5H_9NO_2$	Sigma Aldrich, St Louis, MO, USA	*In vitro* translation, tRNA purification, aminoacylation
L-Serine	$C_3H_7NO_3$	Sigma Aldrich, St Louis, MO, USA	*In vitro* translation
L-Threonine	$C_4H_9NO_3$	Sigma Aldrich, St Louis, MO, USA	*In vitro* translation
L-Tryptophan	$C_{11}H_{12}N_2O_2$	Sigma Aldrich, St Louis, MO, USA	*In vitro* translation
L-Tyrosine	$C_9H_{11}NO_3$	Sigma Aldrich, St Louis, MO, USA	*In vitro* translation
L-Valine	$C_5\,H_{11}\,NO_2$	Sigma Aldrich, St Louis, MO, USA	*In vitro* translation
Magnesium acetate tetrahdrate	$Mg(C_2H_3O_2)_2 \cdot 4H_2O$	Sigma Aldrich, St Louis, MO, USA	tRNA purification, *in vitro* translation, structure biology
Magnesium chloride hexahydrate	$MgCl_2 \cdot 6H_2O$	Sigma Aldrich, St Louis, MO, USA	tRNA purification, *in vitro* translation, structure biology
Magnesium sulfate heptahydrate	$Mg(SO_4) \cdot 7H_2O$	Sigma Aldrich, St Louis, MO, USA	tRNA purification
Manganese (II) chloride tetrahydrate	$MnCl_2 \cdot 4H_2O$	Sigma Aldrich, St Louis, MO, USA	*Thermus* growth
Manganese (II)sulfate monohydrate	$MnSO_4$	Sigma Aldrich, St Louis, MO, USA	*Thermus* growth
Methanol	CH_3OH	Sigma Aldrich, St Louis, MO, USA	HPLC
Molecular Biology water	H_2O	Merck, Kenilworth, NJ, USA	Enzymatic reactions
N,N,N',N'-Tetramethylethylene diamine (TEMED)	$C_6H_{16}N_2$	Euromedex, Souffelweyersheim, France	PAGE
N-acetyl-L-phenylalanine	$C_{11}H_{13}NO_3$	Sigma Aldrich, St Louis, MO, USA	Amino acid derivative
Nickel chloride hexahydrate	$NiCl_2 \cdot 6H_2O$	Sigma Aldrich, St Louis, MO, USA	*Thermus* growth
Nitrilotriacetic acid	$C_6H_9NO_6$	Sigma Aldrich, St Louis, MO, USA	*Thermus* growth
Phenol solution, 10 mM Tris-HCl pH 8.0	C_6H_6O	Sigma Aldrich, St Louis, MO, USA	DNA extraction

Name	Elemental formula	Company	Experiment
Phenol solution, 100 mM citric acid pH 4.3	C_6H_6O	Sigma Aldrich, St Louis, MO, USA	RNA extraction, enzymatic reactions
Phenylmethanesulfonyl fluoride (PMSF)	$C_7H_7FO_2S$	Sigma Aldrich, St Louis, MO, USA	Protease inhibitor
Polyethylene Glycol 20 000	$HO(C_2H_4O)_nH$	Hampton Research, Aliso-Viejo, CA, USA	Crystallography
Potassium acetate	$K(C_2H_3O_2)$	Euromedex, Souffelweyersheim, France	Cryo-EM
Potassium chloride	KCl	Euromedex, Souffelweyersheim, France	tRNA purification, *in vitro* translation, structure biology
Potassium hydroxide	KOH	Sigma Aldrich, St Louis, MO, USA	pH adjustment
Potassium nitrate	KNO_3	Sigma Aldrich, St Louis, MO, USA	*Thermus* growth
Potassium phosphate monobasic	$K(H_2PO_4)$	Sigma Aldrich, St Louis, MO, USA	*Thermus* growth
Putrescine	$C_4H_{12}N_2$	Sigma Aldrich, St Louis, MO, USA	*In vitro* translation
Sodium acetate	$Na(C_2H_3O_2)$	Sigma Aldrich, St Louis, MO, USA	Flexizyme reaction, RNA precipitation
Sodium chloride	NaCl	Sigma Aldrich, St Louis, MO, USA	tRNA purifcation
Sodium dihydrogen phosphate	NaH_2PO_4	Sigma Aldrich, St Louis, MO, USA	Northern Blotting
Sodium dodecyl sulfate (SDS)	$Na(C_{12}H_{25}SO_4)$	Euromedex, Souffelweyersheim, France	Protein purification
Sodium hydroxide	NaOH	Sigma Aldrich, St Louis, MO, USA	pH adjustment, toeprinting
Sodium molybdate	$Na_2(MoO_4)$	Sigma Aldrich, St Louis, MO, USA	*Thermus* growth
Sodium nitrate	$NaNO_3$	Sigma Aldrich, St Louis, MO, USA	*Thermus* growth
Sodium oxalate	$Na_2(C_2O_4)$	Sigma Aldrich, St Louis, MO, USA	*In vitro* translation
Sodium phosphate dibasic	$Na_2(HPO_4)$	Sigma Aldrich, St Louis, MO, USA	Northern Blotting
Sodium phosphate dibasic dihydrate	$Na_2(HPO_4)$	Sigma Aldrich, St Louis, MO, USA	Northern Blotting

Name	Elemental formula	Company	Experiment
Sodium pyrophosphate tetrabasic decahydrate (NaPPi)	$Na_4(P_2O_7)\cdot 10H_2O$	Sigma Aldrich, St Louis, MO, USA	CCA end modification
Sodium pyruvate	$Na(C_3H_3O_3)$	Sigma Aldrich, St Louis, MO, USA	*In vitro* translation
Spermidine	$C_7H_{19}N_3$	Sigma Aldrich, St Louis, MO, USA	*In vitro* translation
Spermine	$C_{10}H_{26}N_4$	Sigma Aldrich, St Louis, MO, USA	*In vitro* transcription/ translation
Sucrose	$C_{12}H_{22}O_{11}$	Sigma Aldrich, St Louis, MO, USA	Ribosome purification
TB Powder		Dutscher, Brumath, France	*E. coli* growth
Tetraethylammonium chloride	$(C_2H_5)_4N(Cl)$	Sigma Aldrich, St Louis, MO, USA	Buffer
Tetrahydro-2-furoic acid (THFA)	$C_5H_8O_3$	Sigma Aldrich, St Louis, MO, USA	Amino acid derivative
Trans-4-Hydroxy-L-proline	$C_5H_9NO_3$	Sigma Aldrich, St Louis, MO, USA	Amino acid derivative
Trichloroacetic acid (TCA)	$C_2HCl_3O_2$	Sigma Aldrich, St Louis, MO, USA	RNA/protein precipitation
Trifluoroacetic acid (TFA)	$C_2HO_2F_3$	Sigma Aldrich, St Louis, MO, USA	HPLC cleaning
Trisodium citrate dihydrate	$Na_3(C_6H_5O_7)\cdot 2H_20$	Sigma Aldrich, St Louis, MO, USA	Northern Blotting
Trizma base	$C_4H_{11}NO_3$	Sigma Aldrich, St Louis, MO, USA	Buffer
Tween 20		Sigma Aldrich, St Louis, MO, USA	Molecular crowding
Urea	CH_4N_2O	Sigma Aldrich, St Louis, MO, USA	Denaturing PAGE
Uridine triphosphate (UTP)	$C_9H_{15}N_2O_{15}P_3$	Jenabioscience, Jena, Germany	*In vitro* transcription/translation
Xylene cyanol	$C_{25}H_{27}N_2NaO_6S_2$	BioSolve	Loading dye
Zinc sulfate monohydrate	$Zn(SO_4)\cdot H_2O$	Sigma Aldrich, St Louis, MO, USA	*Thermus* growth experiments

2.2 Antibiotics

Table 5: List of antibiotics

Antibiotic	Provider	Experiment	Stock concentration	Solvent
Ampicillin	Euromedex, Souffelweyersheim, France	Cell culture	100 mg/mL	Water
Chloramphenicol	Sigma Aldrich, St Louis, MO, USA	Cell culture	30 mg/mL	Ethanol
Erythromycin	Sigma Aldrich, St Louis, MO, USA	*In vitro* translation, structure biology	2 mM	Ethanol
Kanamycin	Euromedex, Souffelweyersheim, France	Cell culture	50 mg/mL	Water
Puromycin	Sigma Aldrich, St Louis, MO, USA	*In vitro* translation	10 mM	Water
Streptomycin	Sigma Aldrich, St Louis, MO, USA	Cell culture	20 mg/mL	Water
Telithromycin	Glenthan	*In vitro* translation		DMSO
Tetracycline	Sigma Aldrich, St Louis, MO, USA	Cell culture	20 mg/mL	Water 0.1% EtOH
Thiostrepton	Merck	*In vitro* translation		DMSO

2.3 Enzymes

Table 6: Enzymes used for cloning, toeprinting and RNA purification

Enzyme	Company	Experiment	Stock solution
AMV RTase	Promega, Medison, WI, USA	Toeprinting	10,000 u /mL
BSA	Euromedex, Souffelweyersheim, France	Northern Blot	
CCA adding enzyme	Purified in the lab	CCA end modification	
DpnI	New England Biolabs (NEB), Ipswich, MA, USA	Mutagenesis	20,000 u/mL
EcoRI HF	NEB, Ipswich, MA, USA	Plasmid digestion	20,000 u/mL
EF-G	Purified in the lab	*In vitro* translation	
EF-P	Purified in the lab	*In vitro* translation	

Enzyme	Company	Experiment	Stock solution
Hemoklen Taq DNAP	NEB, Ipswich, MA, USA	Sequencing	
HindIII HF	NEB, Ipswich, MA, USA	Plasmid digestion	20,000 u/mL
Lysozyme	Sigma Aldrich, St Louis, MO, USA	Genomic DNA extraction	10 mg/Ml
MetS	Purified in the lab	Aminoacylation	
NcoI HF	NEB, Ipswich, MA, USA	Plasmid digestion	20,000 u/mL
NdeI HF	NEB, Ipswich, MA, USA	Plasmid digestion	20,000 u/mL
PheRS	Purified in the lab	Aminoacylation	
Phosphodiesterase I, Western Diamond rattlesnake venom	Sigma Aldrich, St Louis, MO, USA	CCA end modification	10 mg/ml
Phusion High fidelity DNA Polymerase	NEB, Ipswich, MA, USA	PCR	2,000 u/mL
ProS	purified in the lab	aminoacylation	15 mg/mL
PstI HF	NEB, Ipswich, MA, USA	Plasmid digestion	20,000 u/mL
Q5 Hot Start high fidelity DNA polymerase	NEB, Ipswich, MA, USA	PCR based Ligation/mutagenesis	2,000 u/mL
SacI	NEB, Ipswich, MA, USA	Plasmid digestion	20,000 u/mL
T4 DNA Polymerase	NEB, Ipswich, MA, USA	Exonuclease based ligation	3,000 u/mL
T7 RNA Polymerase	Purified in the lab	*In vitro* transcription	20 mg/mL
DNase I	NEB, Ipswich, MA, USA	Protein purification	

2.4 Kits

Table 7: List of Kits

Kits	Company	Experiment
PCR purification kit	Qiagen, Hilden, Germany	DNA purification
Nucleotide removal kit	Qiagen, Hilden, Germany	Toeprinting, linker ligation
Minipreparation kit	Qiagen, Hilden, Germany	extraction of Plasmids from *E coli* cells
Gel extraction kit	Qiagen, Hilden, Germany	DNA purification from agarose gels
Midipreparation kit	Macherey & Nagel, Düren, Germany	Extraction of Plasmids from *E. coli* cells

2.5 Equipment

2.5.1 Columns

Table 8: List of used columns for RNA and protein purification

Column (material)	Company	Experiment
C4-RP-column (analytical)	Grace, Columbia, MD, USA	RNA purification
C4-RP-column (preparative)	Grace, Columbia, MD, USA	RNA purification
C16-RP-column (analytical)	Phenomedex, Torrance, CA, USA	RNA purification
C16-RP-column (semi-preparative)	Phenomedex, Torrance, CA, USA	RNA purification
C16-RP-column (preparative)	Phenomedex, Torrance, CA, USA	RNA purification
Q-Sepharose (90 mL)	GEHeathcare, Chicago, IL, USA	RNA purification
Superdex 200 16/600	GEHeathcare, Chicago, IL, USA	Protein purification
Superdex 75 16/600	GEHeathcare, Chicago, IL, USA	Protein purification
HIS-Select® Cobalt Affinity Gel	Sigma Aldrich, St Louis, MO, USA	Protein purification
HIS-Select® Nickel Affinity Gel	Sigma Aldrich, St Louis, MO, USA	Protein purification

3. Methods

3.1 General methods

3.1.1 Microbiological handling

During work with bacteria, all steps were performed under sterile conditions. When growing *E. coli* in liquid media Lysogeny Broth (LB, (Bertani, 1951)) or Terrific Broth (TB, (Tartof and Hobbs, 1987)) were used. The media was prepared as listed in the following table:

Table 9: Media composition of LB and TB

Name	Composition of 1 L
LB media	5 g LB powder 5 g NaCl
TB media	5 g TB powder 100 mL glycerol

Plates for bacterial growth contained 1.5% (w/v) Bacto-Agar. All solutions for liquid and solid media were autoclaved. Antibiotics were prepared as 1000x stock solutions and added to plates and liquid media in 1x end concentration. *E. coli* cells were grown at 37°C under optimal aerobe conditions in baffled shaking flasks. Cells used in this thesis are listed in the following table:

Table 10: List of used E. coli strains with specifics on genotypes and usage

E. coli strain	Genotype	Experiment	Citation
DH5α	*fhuA2 lac(del)U169 phoA glnV44 Φ80' lacZ(del)M15 gyrA96 recA1 relA1 endA1 thi-1 hsdR17*	Plasmid amplification, tRNA overexpression	(Hanahan, 1983)
XL-1 blue	*rec*A1 *end*A1 *gyr*A96 *thi*-1 *hsd*R17 *sup*E44 *rel*A1 *lac* Phage: F´ *pro*AB l*ac*IqZΔM15 Tn10 Tet^{r}	Plasmid amplification	Invitrogen
HB101	F^{-} Lambda^{-} araC14 leuB6(Am) DE(gpt-proA)62 lacY1 glnX44(AS) galK2(Oc) recA13 rpsL20(strR) xylA5 mtl-1 thiE1 hsdS20(r_B^-, m_B^-)	tRNA overexpression	(Hanahan, 1985)
BL21 gold	B F^{-} *ompT gal dcm lon hsdS$_B$*(r_B^- m_B^-) λ(DE3 [*lacI lacUV5-T7p07 ind1 sam7 nin5*]) [*malB*$^{+}$]$_{K-12}$(λ^{S}) pLysS[*T7p20 ori*$_{p15A}$](Cm^{R})	Protein overexpression	(Studier and Moffatt, 1986) pLysS (Moffatt and Studier, 1987)

E. coli strain	Genotype	Experiment	Citation
BL21 AI	B F$^-$ *ompT gal dcm lon hsdS$_B$*(r_B^- m_B^-) [*malB*$^+$]$_{K\text{-}12}$(λ^S) *araB*::*T7RNAP-tetA*	tRNA overexpression	Invitrogen
KC6	A19 Δ*speA* Δ*tnaA* Δ*sdaA* Δ*sdaB* Δ*gshA* Δ*tonA* Δ*endAmet*$^+$	Ribosome isolation	(Calhoun and Swartz, 2006)

Ribosomes were purified by Natacha Pérébaskine from *Thermus thermophilus* HB8 cells (wild-type, (Oshima and Imahori, 1974)). The cells were ordered from the Bioexpression and fermentation facility of the University of Georgia (USA). For extraction of total *T. thermophilus* tRNA and genomic DNA, cells were grown at 70°C under optimal aerobic conditions in the 689 media. The media composition is shown in the following table:

Table 11: 689 media composition

Name	Composition (listed amounts for 1 L)
689 media	8 g Tryptone 4 g Yeast Extract 2 g NaCl 1x Castenholz Salts 20 mL Nitch Trance elements
10x CARSTENHOLTZ salts	1 g Nitrilotriacetic acid 1g 16 mL 0.03% (w/v) $FeCl_3$ 0.6 g $CaSO_4$ 0.08 g NaCl 1 g $MgSO_4$ 1.03 g KNO_3 6.89 g $NaNO_3$ 1.11 g Na_2HPO_4
Nitch trace elements	0.5 mL H_2SO_4 (conc.) 2.2 g $MnSO_4$ 0.5 g $ZnSO_4 \cdot 7\ H_2O$ 0.5 g boric acid 16 mg $CuSO_4 \cdot 5H_2O$ 25 mg Na_2MoO_4 46 mg $CoCl_2 \cdot 6H_2O$

Cells were plated on 689 solid media supplemented with 1% Gelzan and incubated for 24 h at 70°C. Single colonies had an orange color.

3.1.2 Extraction of genomic DNA from *E. coli and T. thermophilus*

Genomic DNA was extracted from 5 mL of *E. coli* or *T. thermophilus* overnight culture. The cells were harvested for 10 min at 4000 g in a 5424R Eppendorf centrifuge (Eppendorf, Hamburg, Germany). The pellet was resuspended in 500 µL TES buffer (50 mM Tris HCl pH 7.4, 1 mM EDTA, 1% SDS) and cells were lysed by adding 500 µL phenol (pH 8.0): chloroform: isoamyl alcohol (25:24:1). Phenol denatures proteins and pH 8.0 facilitates the degradation of RNA. The resuspension was carefully inverted until a homogeneous solution was formed, followed by spinning at 13000 revolutions per minute (rpm, 18 000 relative centrifugal force (rcf)) in a tabletop centrifuge (Thermofisher, Waltham, MA, USA) at 4°C for 20 min. This resulted in the separation into three phases: The aqueous phase containing the DNA, the interphase containing denatured proteins and the organic phase containing lipids and other hydrophobic compounds. The aqueous phase, which contains the extracted DNA, was washed twice with chloroform: isoamyl alcohol (24:1).

The DNA was precipitated by adding end concentrations of 300 mM $Na(CH_3CO_2)$ pH 4.8 and 50% Isopropanol. The solution was incubated for 1 h at -20°C to enhance the amount of precipitation. Subsequently, the DNA was pelleted by spinning at full speed for 30 min at 4°C in a tabletop centrifuge. The pellet was washed with 70% ethanol (EtOH) to remove ions. The DNA was resuspended in 200 µL TE Buffer (10 mM Tris·HCl pH 8.0, 1 mM EDTA). To enhance dissolution, the sample was incubated for 1 h at 65°C and overnight at 4°C. The extracted DNA was used for polymerase chain reaction (PCR, Chapter 3.3).

3.2 Analytical procedures

3.2.1 Standard gel electrophoresis

The purity and concentration of nucleic acids and proteins were analyzed by gel electrophoresis. To do so biomolecules are exposed to an electric field and are separated due to their charge.

3.2.1.1 Nucleic acid gels

DNA samples were analyzed either by agarose TAE gels or native Polyacrylamide gel electrophoresis (PAGE). DNA fragments with a minimal length of 500 bp were analyzed on 1.5-3 % (w/v) agarose gels. Agarose was melted in 70 mL TAE buffer (40 mM Tris, 50 mM Acetate, 1 mM EDTA) and poured into the gel stands. After solidification of the agarose the gel was overlaid with 1x TAE buffer and the DNA samples were loaded by mixing 3 µL PCR product with 0.5 µL 6x DNA loading dye (30% (v/v) Glycerol, 0.25% (w/v) bromophenol blue (BPB), 0,25% (w/v) xylene blue). To be able to estimate the size and concentration of the DNA fragments a DNA size standard (2-log DNA ladder NEB, Ipswich, MA, USA) was loaded. The gel was run at 170V for 60 to 80 min. To detect the DNA the gels were stained afterward with a 2x GelRed solution and detected with the Gel documentation system GelDoc+ (Biorad, Hercules, CA, USA).

DNA fragments shorter than 500 bp were analyzed using TBE (Tris-Borate-EDTA)-PAGE (polyacrylamide gel electrophoresis). The gels were cast using the Bio-Rad gel casting system. The following components were mixed:

Table 12: Composition of a native nucleic acid (TBE)-PAGE

Components (stock concentration)	Final concentration
10x TBE buffer (900 mM Tris, 900 mM Boric acid, 20 mM EDTA)	1x TBE buffer (90 mM Tris, 90 mM Boric acid, 2 mM EDTA)
40% (w/v) acrylamide (19:1)	6-12% (w/v) acrylamide (19:1)
10%(w/v) APS	0.04% (w/v) APS
100% (v/v) TEMED	0.01% (v/v) TEMED

After the gels were polymerized 3 µL PCR sample was mixed with 0.5 µL DNA loading dye and loaded into the wells. Additionally, 1 µL low molecular weight marker (NEB, Ipswich, MA, USA) was loaded to determine the size and concentration of the DNA fragments. The gels were run in 1x TBE buffer (90 mM Tris, 90 mM Boric acid, 2 mM EDTA) at 200V for 1 h at room temperature. The gels were stained afterward with SYBR Gold (Invitrogen, 1:1000 diluted).

RNA samples these were analyzed using TBU (Tris, Boric acid, Urea)-PAGEs. Urea is chaotropic salt that denatures intramolecular hydrogen bonds and van der Waals (VdW) forces resulting in the unfolding of secondary structures of the nucleic acids. Prior to loading the RNA samples were mixed with RNA loading dye (formamide, 250 µM EDTA, 0.25% (w/v) bromophenol blue (BFB), 0.25% xylene blue). EDTA chelates Mg^{2+} ions that could be present in the sample and would lead to degradation of the RNA in the following denaturation step (95°C, 10 min). Formamide is added to enhance the denaturation of the RNA. The TBU-PAGEs were cast using the following mixture:

Table 13: Composition of a denaturing nucleic (TBU)-PAGE

Components (stock concentration)	Final concentration
10x TBE buffer (900 mM Tris, 900 mM Boric acid, 20 mM EDTA)	2x TBE buffer (180 mM Tris, 180 mM Boric acid, 4 mM EDTA)
40% (w/v) acrylamide (19:1)	6-15% (w/v) acrylamide (19:1)
Urea	8 M Urea
10%(w/v) APS	0.02% (w/v) APS
100% (v/v) TEMED	0.01% (v/v) TEMED

To determine the size of the RNA fragments are RNA size standard (NEB, Ipswich, MA, USA or Thermo Fischer, Waltham, MA, USA) was loaded onto the gel. The gels were run for 1 h at 200V at room temperature in 1x TBE buffer. Large gels were run for up to 24 h at 250V. Gels were stained afterward with SYBR Gold (Invitrogen, Carlsbad, CA, USA) and detected with the GelDoc+ (Biorad, Hercules, CA, USA).

TBU-PAGEs have a basic pH which is not suitable for analyzing peptidylated tRNAs bound via an ester bond since the ester bond is pH sensitive. Samples containing peptidylated tRNAs were analyzed on acidic denaturing PAGEs. The PAGEs were prepared as follows:

Table 14: Composition of acidic denaturing PAGE

Stock solutions	Final concentration
3M $Na(CH_3CO_2)$ pH 4.8	100 mM $Na(CH_3CO_2)$
40% (w/v) acrylamide (19:1)	9-20% acrylamide (19:1)
Urea	8 M Urea
10% APS	0.02% (w/v) APS
100% TEMED	0.01%TEMED

Furthermore, to protect the ester bond during the heat denaturation step an acidic RNA loading dye (50 mM $Na(CH_3CO_2)$ pH 4.8, formamide, 250 mM EDTA, 0.25% BPB, 0.25% Xylene blue) was used. The gels were run for 3 h at 160V at 4°C in 100 mM $Na(CH_3CO_2)$. For staining the gels were washed with 1x TBE buffer for 10 min and stained afterward with SYBR Gold (Invitrogen, Carlsbad, CA, USA) and detected with the GelDoc+ (Biorad, Hercules, CA, USA).

3.2.1.2 Protein Gels

Protein purifications were analyzed using SDS-PAGEs. SDS binds to the hydrophobic backbone of proteins and gives the molecule a negative charge that corresponds to its molecular weight. This allows the separation of proteins in a PAGE according to their size. Protein samples were combined with the SDS-loading dye (250 mM Tris·HCl pH 6.8, 1% SDS. 30% glycerol, 1 mM DTT, 0.1% BPB), which This resulted in the denaturation of the proteins by SDS. Gels were prepared using the following mixture:

Table 15: Composition of SDS-PAGE

Stock solutions	Final concentrations
Stacking Gel	
0.5 M Tris HCl pH 6.8	175 mM Tris HCl pH 6.8
30% acrylamide (37.5:1)	4% acrylamide (37,5:1)
20% SDS	0.15% SDS
10% APS	0.042% APS
100% TEMED	0.0014% TEMED
Resolving Gel	
1.5 M Tris HCl pH 8.8	560 mM Tris HCl pH 8.8
30% acrylamide (37.5:1)	12% acrylamide (37.5:1)
20% SDS	0.15% SDS
10% APS	0.075% APS
100% TEMED	0.001% TEMED

Besides the samples, a pre-stained protein marker (NEB, Ipswich, MA, USA) was loaded to determine the molecular size of the proteins. Gels were run for 1 h at 200V at room temperature in 1xSDS running buffer (25 mM Tris, 192 mM glycine, 0.1% SDS) and were stained with Instant Blue™ protein stain (expedeon, San Diego, CA, USA) and detected with the GelDoc+ (Biorad, Hercules, CA, USA).

3.2.2 Northern Blot

Northern Blot is a method in Molecular Biology, that allows detecting specific RNAs using a labeled DNA probe that is reverse complementary to the RNA of interest. During this process, the RNA is separated by gel electrophoresis and subsequently transferred onto a membrane (Alwine et al., 1977; Thomas, 1980).

Northern Blotting was used to analyze the overexpression of specific tRNAs as well as monitoring the elution fractions during the tRNA purification. During the process, RNAs were separated and denatured by gel electrophoresis. Subsequently, the RNA is transferred and fixed to a membrane. A fluorescently labeled DNA probe, which is reverse complementary to the anticodon loop of the tRNA of interest with an optimal annealing temperature of 65°C, was used to detect specifically the tRNA of interest. The anticodon loop is specific for each tRNA and is the least structured part. The optimal amount of the detection varies from 1 pmol to 100 pmol of tRNA.

First, the RNA was separated on a 9% TBU-PAGE and the gel was run for 45 min at room temperature. For the blotting, the membrane Hybond-N+ (GE Healthcare, Chicago, IL, USA) and TBU-PAGE were assembled and prepared for blotting as shown in the following figure:

Figure 12: Assembly of Northern Blot, the RNA was separated in the TBU-PAGE prior to the blotting. The RNA is transferred onto the membrane by applying an electric field. Due to the negative charge of the RNA, the sample migrates towards the plus pole and onto the membrane.

After assembly of the blot according to the order shown in Figure 12 Biorad Trans-Blot® cell (Biorad, Hercules, CA, USA), the transfer of the RNA onto the membrane was performed. The transfer was run overnight at 10V in 1xTBE buffer at 4°C with constant stirring of the buffer in a. After the transfer, the membrane was moved onto a Whatman paper and baked for 2 h at 80°C to fix the RNA onto the membrane. In the next step, the membrane was incubated in for at least 2 h at 28°C with Recette church buffer (250 mM sodium phosphate buffer pH 7.2, 1 mM EDTA, 7% (w/v) SDS, 0,5 (w/v) Bovine serum albumin (BSA) ,4 µg/mL DNA from salmon testicles) (Kim et al., 2010). This blocking step of the membrane prevents unspecific binding of the labeled oligonucleotide and reduces background signal. 1 nmol of the fluorescent probe was denatured for 2 min at 95°C and then added to the blocking solution. The Blot was incubated overnight at 28°C on a tube rotator.

Before detection the blot was washed twice with 300 mM NaCl, 30 mM Na_3citrate (2x SSC buffer) and 0.2% (w/v) SDS and once with 150 mM NaCl, 15 mM Na_3citrate (1x SSC buffer) and 0.1% SDS. The blot was detected using the blue laser of the Pharos detection system from Bio-Rad.

Table 16: List of used probes

Name	Sequence	Modification
Initiator tRNA	GATGTGCTCTAACCAACTGAGCT	3' 6 FAM
$tRNA^{Val}$	CCGACCCCCGACACCCCATG	3' 6 FAM
$tRNA^{Arg}$	CCTCCGACCGCTCGGTTCGTAG	3' 6 FAM
$tRNA^{Trp}$	TCCCAACACCCCGTTTTGG	3' 6 FAM
$tRNA^{Phe}$	GAATCGAACCAAGGACACGGGGATTTTC	3' 6 FAM
$tRNA^{Pro}$	GACCCCTTCGTCCCGAAC	5' 6FAM

3.2.3 Macromolecule concentration determination

Macromolecule concentrations were determined using a Nanodrop (Thermofisher) The Nanodrop was blanked with the buffer in which the macromolecules were dissolved in. For the measurement 1-2 µL of the sample was pipetted onto the probe. Nucleic acid concentrations were determined by measuring the absorbance at 260 nm and the purity was monitored by the ratio of the absorbance at A_{260}: A_{280} . A ratio of 1.8 indicates pure DNA while a ratio of 2.0 indicates a pure RNA sample.

Protein concentrations were determined at 280 nm. Depending on the amino acid composition the absorbance can variate. To encounter the amino acid composition the extinction factor ε was calculated using the bioinformatic tool ProtParam (Gasteiger et al., 2003). The exact concentration can be calculated by the following equation:

$$c\left(\frac{\mu g}{\mu L}\right) = \left(\frac{A_{260}}{\varepsilon}\right) \quad (1)$$

The following table lists all proteins purified in this thesis including their molecular weight and extinction coefficient:

Table 17: List of proteins purified in this thesis, their corresponding extinction coefficients and molecular weight were determined using the bioinformatic platform ProtParam. If the complex consists of two subunits, the values are listed independently.

Protein	Number of amino acids	Molecular weight [kDa]	Extinction coefficient [$M^{-1}cm^{-1}$]
Tth EF-P	184	20.22	15.93
E. coli EF-P	188	20.50	25.44
Tth EF-P HQ	184	20.22	14.44
Tth EF-P loop	184	20.20	14.44
E. coli ProS	572	63.67	54.32
E. coli EF-G	750	82.88	61.31
E. coli PheST	S 327 T 795	S 36.83 T 87.38	87.17
E. coli GlySQ	S 689 Q 303	S 76.81 Q 34.77	118.19
E. coli AsnS	466	52.57	62.59
E. coli AspS	590	65.91	43.11
E. coli TrpS	334	37.44	32.11
T7-RNAP	883	98.86	141.01

3.2.4 Native mass spectrometry

Native mass spectrometry (MS) is used study biomolecules within the gas phase perceiving the folding of the biomolecule prior to ionization. The method was used to study DNA folding, protein-protein interaction and ribosomes as reviewed by (Leney and Heck, 2017).

The technique was used to validate the purity, the molecular weight and the presence of modifications of $tRNA^{Pro}$. Therefore, 1 µmol (final concentration: 10 µM) tRNA were washed eight times through 10 kDa Amicon concentrators (Merck Millipore, Billerica, MA, USA) with a buffer containing 100 mM $NH_4(CH_3CO_2)$. Next, 50 µL of the sample was injected into Agilent 6560-DTIMS-Q-TOF mass spectrometer and the spectrum was detected. The machine was set to negative mode due to the charge of the RNA and the source temperature was set at 200°C and 600V for desolvation termed "soft ionization" condition. The soft ionization condition prevents the tRNA from fragmentation.

3.3 Cloning

DNA templates were generated by Polymerase Chain Reaction (PCR), which allows exponential amplification of DNA fragments (Mullis et al., 1987). The reaction uses DNA polymerases (DNAP) that were isolated from thermophiles and remain active after incubation at high temperatures. Other compounds of the reactions are two short DNA oligomers (primer) that are a reverse complement to 3′ ends of the sense and antisense strand of the gene of interest. DNAP prolongs the DNA oligonucleotides by incorporating dNTPs from the 5′ to the 3′ end complementary to the template strand. The reaction cycle can be divided into DNA denaturation, primer annealing and primer extension phase (Saiki et al., 1988).

All primers are listed in the supplemental material according to their downstream application.

3.3.1 Amplification of gene of interest from genomic DNA

To amplify a gene of interest, for example, an aminoacyl-tRNA synthetase, DNA megaprimers were from Eurogentec (Lüttich, Belgium) or Eurofins (Ebersberg, Germany). A megaprimer is a DNA oligomer overlapping 30 nt (nucleotides) with the multiple cloning site (MCS) of in this case the pBAT4 and 18 nt with the gene of interest (Miyazaki, 2011). For cloning translation

factors, histidine$_6$ tags (H_6-tag) were introduced at the N- or C-terminus as reported in (Shimizu et al., 2001; Shimizu et al., 2005).

The amplification was performed by PCR using *Phusion* DNA polymerase (*Phu*DNAP). The pipetting scheme is showing the following table:

Table 18: Pipetting scheme for gene amplification from genomic DNA

Component [stock concentration]	Final concentration
HF-Buffer (NEB, Ipswich, MA, USA) [5x]	1x
dNTPs [10 mM each]	200 µM each
Forward primer [10 µM]	200 nM
Reverse primer [10 µM]	200 nM
Genomic DNA	2 µM
*Phu*DNAP [2 000 u/mL]	0.02 u/µL
Nuclease-free water	To final volume

The corresponding PCR program is shown in the following table:

Table 19: PCR program for gene extraction

Temperature	Time	Function	Cycles
98°C	30 s	Enzyme activation	1x
98°C	30 s	Denaturation of the vector and PCR fragment	30x
50-60°C	30 s	Primer annealing	
72°C	2 min	Primer extension	
4°C	∞	Incubation until further usage	1x

For gene operons like *glySQ* longer than 750 bp, the temperature during primer extension was reduced to 68°C and the reaction time was increased to 3 min. The PCR products were analyzed on 1.5% TAE-agarose gels (chapter 3.8.1) by loading 3 µL per reaction together with the 2-log DNA ladder (NEB, Ipswich, MA, USA). Depending on its purity, the product was purified by PCR purification kit (Qiagen, Hilden, Germany) or gel extraction kit (Qiagen, Hilden, Germany) following the manufacturer's instructions.

3.3.2 Amplification of gene of interest by oligo assembly

DNA templates for cell-free protein synthesis and tRNA genes were amplified from oligo assembly. To do so, the sequence was divided into several reverse and forward primers overlapping with each other to be able to result in a full-length synthetic gene. to obtain tRNA gene for cloning into pBASTNAV or pUC19 plasmids, the primers were overlapping 30 nt with the vector for insertion. For cell-free protein synthesis and *in vitro* transcription, the construct encoded a T7 promoter in the 5' region in order to initiate transcription. The product was assembled from six to eight primers. The outer primers were added in ten times excess over the other primers to amplify the whole fragment. The pipetting scheme is shown in the following table:

Table 20: Pipetting scheme for primer annealing PCR

Component [stock concentration]	Final concentration
HF-Buffer [5x]	1x
dNTPs [10 mM each]	200 µM each
Forward amplifying primer [10 µM]	20 nM
Forward primer 1 [1 µM]	2 nM
Reverse primer 1 [1 µM]	2 nM
Forward primer 2 [1 µM]	2 nM
Reverse primer 2 [1 µM]	2 nM
Reverse amplifying primer [10 µM]	20 nM
*Phu*DNAP [2 000 u/mL]	0.2 u
Nuclease-free water	to a final volume

The following PCR program was used to amplify the genes:

Table 21: PCR program for primer annealing

Temperature	Time	Function	Cycles
98°C	30 s	Enzyme activation	1x
98°C	15 s	Denaturation of the vector and PCR fragment	20X
45-60°C	15 s	Primer annealing	
72°C	15-30 s	Primer extension	
4°	∞	Incubation until further usage	1x

The PCR products were analyzed by on 9% TBE-PAGE by loading 3 µL per reaction. Depending on the purity of the product, it was purified by PCR purification kit (Qiagen, Hilden, Germany) or gel extraction kit (Qiagen, Hilden, Germany) following the manufactory's instructions.

3.3.3 Vector restriction and ligation

For cloning, vectors were amplified in *E. coli* DH5α cells and purified using the minipreparation kit from Qiagen, (Hilden, Germany). The isolated vector was restricted using 1 µg of vector together with 1x CutSmart buffer and the 1 µL of each restriction enzymes (NEB,) as listed in the following table:

Table 22: List of vectors with their corresponding restriction enzymes and downstream application

Vector name	Antibiotic resistance	Restriction enzymes	Experiment
pBAT4	Amp	*NdeI, NcoI*	Protein overexpression
pUC19	Amp	*EcoRI, HindIII*	tRNA overexpression
pBSTNAV2OK	Amp	*EcoRI, PstI*	
pBSTNAV3S	Amp	*SacI, PstI*	

For optimal vector digestion, the high fidelity (HF) version of the enzymes was used, when available. These enhanced enzymes have a reduced star activity and higher efficiency. The reaction product was analyzed on a 1% TAE-agarose gel (chapter 3.8) and purified via PCR purification kit (Qiagen, Hilden, Germany).

The previously obtained insert was inserted by PCR using MEGAWHOP (Miyazaki, 2003, 2011) or by sequence and ligation independent cloning (SLIC) (Li and Elledge, 2012). For MEGAWHOP cloning, the insert overlaps on both sites 18 nt with the digested vector. The following PCR mixture was used to ligate the insert into the restricted plasmid:

Table 23: Pipetting scheme for insertion of gene into pUC19 or pBAT4

Component [stock concentration]	Final concentration
Q5-Reaction Buffer [5x]	1x
Q5 High GC Enhancer [5x]	1x
dNTPs [10 mM each]	200 µM each
Insert	60 nM
Digested vector	0.6 nM
Q5-DNAP [2 u/µL]	0.2 u
Nuclease-free water	To 100 µL

The following PCR program was used and the 100 µL master mix was split into two reactions of 50 µL each. For one reaction the annealing temperature was set to 50°C and the other to 60°C:

Table 24: PCR program for MEGAWHOP

Temperature	Time	Function	Cycles
98°C	30 s	Enzyme activation	1x
98°C	30 s	Denaturation of the vector and PCR fragment	25x
50-60°C	30 s	Primer annealing	
72°C	2 min	Primer extension	
4°C	Hold	Incubation until further usage	1x

The two reactions were pooled and the PCR product was purified by PCR purification kit (Qiagen, Hilden, Germany). The eluate was directly used for chemical transformation into *E. coli* DH5α without further analysis.

For cloning tRNA genes into the plasmids pBSTNAV2OK and pBSTNAV3S, this approach did not work, probably due to the high AT content in the overlapping region between the insert and the plasmid. In order to clone the tRNA genes into these plasmids, the sequence and ligation independent cloning (SLIC) strategy was used, which relies on the 3'→5' exonuclease activity of T4 DNAP in the absence of dNTPs. 100 ng of the insert were mixed with 60 ng of digested vector and 0.5 µL T4-DNAP (NEB) and was incubated for 2 min at room temperature (RT) followed by 5 min incubation on ice. During the reaction, the enzyme creates long sticky ends on the digested vector and on the insert. When the temperature is reduced in the next

step the insert and plasmid anneal (Li and Elledge, 2012). The product was used directly for transformation into competent *E. coli* DH5α cells.

3.3.4 Mutagenesis of *Thermus thermophilus* Elongation Factor P

To date, the post-translational modification of *T. thermophilus* EF-P remains unknown. To study the orientation of an EF-P modification within the 70S *T. thermophilus* ribosome, *T. thermophilus* EF-P was mutated systematically following the MEGAWHOP protocol (Miyazaki, 2003) using megaprimers. reverse complementary to each other. The forward primer anneals 24 nt downstream the mutated region and the reverse primer overlaps 24 nt upstream the mutated region. The reaction contained the following mixture:

Table 25: Pipetting scheme for PCR based mutagenesis

Component [stock concentration]	Final concentration
Q5-Reaction Buffer NEB [5x]	1x
Q5 High GC Enhancer [5x]	1x
dNTPs [10 mM each]	200 µM each
Forward sequencing primer [10 µM]	200 nM
Reverse sequencing primer [10 µM]	200 nM
Vector with wild typ sequence	0.6 nM
Q5-DNAP [2 u/µL]	0.2 u
Nuclease-free water	To final volume

The following PCR program was used:

Table 26: PCR program for PCR based mutagenesis

Temperature	Time	Function	Cycles
98°C	30 s	Enzyme activation	1x
98°C	30 s	Denaturation of the vector and PCR fragment	25x
50-60°C	30 s	Primer annealing	
68°C	3 min	Primer extension	
4°C	∞	Incubation until further usage	1x

The template plasmid was isolated from *E. coli* DH5α cells and was thus methylated. Since PCR products are not methylated the template DNA can be degraded specifically using the

restriction enzyme *DpnI*. *DpnI* recognizes and cuts specifically methylated and hemimethylated DNA double strands. To do so, the PCR reaction was mixed with CutSmart buffer (final concentration 1x) and 10 units *DpnI*. The reaction was incubated for 2 h at 37°C. The DNA fragments were purified using the PCR purification kit (Qiagen, Hilden, Germany) and eluted in30 µL DNase-free water. 15 µL of this DNA was subsequently used for transformation into competent *E. coli* XL1-blue cells.

3.3.5 Preparation of chemically competent cells

For cloning, protein and tRNA expression the corresponding plasmids were transformed into *E. coli* cells. To enhance uptake of the plasmid DNA the cells were treated with $MgCl_2$, which leads to permeabilization of the cell wall.

For the preparation of chemically competent cells, a liquid LB culture (containing the required antibiotic; see Table 10) was inoculated with the respective cells and was grown overnight at 37 °C with 200 rpm shaking. This overnight culture was subsequently used to inoculate 200 mL LB media to a starting OD_{600} between 0.05 and 0.1, which was grown at 37 °C until the culture reached an OD600 of 0.4-0.6. After pelleting the cells (4000g, 10 minutes, 4 °C, Eppendorf 5804R) the pellets were resuspended in 100 mL 100 mM $MgCl_2$ solution and were incubated for 30 min on ice. Subsequently, the cells were pelleted and resuspended in 10 mL 100 mM $CaCl_2$ and 15% glycerol. The cells were aliquoted in 100 µL and flash-frozen in liquid nitrogen (N_2) and stored at -80°C until further use.

3.3.6 Plasmid transformation into chemically competent cells

For the chemical transformation, the cells were thawed on ice. After adding the plasmid solution (15 µL of PCR products or SLIC products or 0.5 µL of plasmids) the cells were incubated on ice for 30 min. After a heat shock at 42°C for 1 min, the cells were placed on ice immediately and incubated for another 1.5 min. To allow recovery of the cells 500 µL of LB media was added and the cells were incubated at 37 °C for at least one hour. After the incubation, the cells were plated on LB agar plates containing the plasmid-specific antibiotic for cell selection. The agar plates were incubated overnight at 37 °C.

3.3.7 Colony identification

After cloning, clones, containing the insert, were identified by colony PCR. In a first step master mix was prepared using sequencing primers as amplifying primers, but lacking the Phusion DNA polymerase. The sequencing primers are designed to be plasmid specific and should not bind to the genomic DNA of the cells. The master mix was aliquoted into PCR tubes. As a control, one PCR reaction contained empty purified plasmid. The master mix is listed in the following table:

Table 27: Pipetting scheme for Colony PCR

Component [stock concentration]	Final concentration
HF-Buffer NEB [5x]	1x
dNTPs [10 mM each]	200 µM each
Forward sequencing primer [10 µM]	200 nM
Reverse sequencing primer [10 µM]	200 nM
*Phu*DNAP [2 000 u/mL]	0.2 u
Nuclease-free water	To final volume

Single colonies were picked using sterile pipet tips and transferred into the reaction tubes. In order to keep the cells, they were also streaked out onto a fresh LB agar plate containing the required antibiotic. The agar plates were incubated at 37 °C overnight to allow growth of the colonies. The PCR was performed with the following program:

Table 28: Reaction scheme for Colony PCR

Temperature	Time	function	cycles
98°C	10 min	Cell lysis	1x
98°C	30 s	Denaturation of the vector and PCR fragment	25x
52°C'	30 s	Primer annealing	
72°C	10 s to 2 min	Primer extension	
4°C	Hold	Incubation until further usage	1x

The PCR cycler was stopped after the cell lysis step and continued after the addition of 0.25 µL *Phu* DNAP in each reaction. As the size of the insert varied between 100 bp and 2000 bp, the reactions were analyzed depending on the size of the insert either by a 1.5% TAE-agarose gel

or a 9% TBE-PAGE (chapter 3.2). Colonies corresponding to reactions giving rise to a band on the gel with the size of the insert were used for further steps.

3.3.8 Plasmid extraction and sequencing

The potential colonies, containing potentially the insert, were transferred into 5 mL LB containing the respective antibiotic and grown overnight at 37 °C and shaking at 200 rpm. The cells were harvested by centrifugation (4000 g, 10 min) and the plasmids purified using the plasmid purification kit following the manufacturer's instructions. The plasmid DNA was eluted in30 µL water and the concentration was determined using a NanoDrop (2000c, Thermofisher, Waltham, MA, USA).

Plasmids were sequenced by SANGER sequencing (GATC Biotech, Konstanz, Germany) The resulting sequences were confirmed by comparing with the planned sequences using Basic Local Alignment Search Tool (BLAST, (Altschul et al., 1990)) and Multalign (Toulouse, France,).

3.4 Protein expression and purification

All proteins purified in this thesis were overexpressed in *E. coli* BL21 Gold. The genes encoding the proteins were cloned to be under the regulation of a T7 RNAP promoter. In *E. coli* BL21 Gold the T7 RNAP gene is under the control of a LacI repressor and can be induced by the addition of the lactose derivative, isopropyl β-D-1-thiogalactopyranoside (IPTG).

The process of protein purification can be divided into a capture step, an intermediate step and a polishing step as reported in (Williams, 2001). To purify the proteins, they were tagged with an H_6-tag. The six consecutive H residues form a stable complex with immobilized Co^{2+} ions allowing separation of the protein of interest from the cellular proteins (capture step) (Petty, 2001; Williams, 2001). Since the purity of the protein samples, purified proteins after the Co^{2+}-NTA column was already high. Subsequently, the buffer was exchanged using a size exclusion chromatography directly as polishing step. In this step, the sample components are separated by their overall size (Hagel, 2001; Williams, 2001).

3.4.1 Expression vectors

Table 29: List of expression vectors used for protein purification

Protein (organism)	Vector	Citation
EF-G (*E. coli*)	pET46-Ek/LIC	(Mikolajka et al., 2011)
EF-P (*E. coli*)	pET14b	(Peil et al., 2012)
EF-P (*T. thermophilus*) +mutants	pET14b	(Blaha et al., 2009)
YjeA/K (*E. coli*)	pRSFDuet	(Ude et al., 2013)
ProS (*E. coli*)	pBAT4	Cloned by Dr. KK Inampudi
TrpS (*E. coli*)	pBAT4	This work
GlySQ (*E. coli*)	pBAT4	This work
AsnS (*E. coli*)	pBAT4	This work
AspS (*E. coli*)	pBAT4	This work
PheST (*E. coli*)	pQE3	Provided by the Steitz lab
T7RNAP (P226L)	pAR1219	(Guillerez et al., 2005)

3.4.2 Expression and purification of aminoacyl tRNA synthetases, T7 RNAP and EF-G

Aminoacyl-tRNA synthetases were cloned into pBAT4 plasmids and H_6-tagged as reported in (Shimizu et al., 2001; Shimizu et al., 2005). After confirming the sequences of the vectors by SANGER sequencing, the plasmids were transformed into competent *E. coli* BL21 gold cells and selected on LB containing ampicillin and chloramphenicol (Amp-CAM) plates. For expression experiments, cells were grown in an overnight culture (preculture). The main culture was used to inoculate the main culture to an OD_{600} of 0.05 which was grown at 37°C (shaking at 180 rpm) until it reached an OD_{600} of 0.6. Next, the expression was induced by the addition of 1 mM IPTG (end concentration). After induction, the cells were incubated at 30°C and harvested after 4 h by centrifugation at 4,000 rcf for 15 min at 4°C. The harvested cells were flash frozen in liquid nitrogen and stored at -80°C until protein purification.

The cells were resuspended in 25 mL of protein lysis buffer (50 mM HEPES·KOH pH 7.6, 10 mM $MgCl_2$, 1 M NH_4Cl). To lyse the cells, they were sonicated at 40%, 45 s sonication 45 s recovering on ice for 7 min. The cell debris was removed by centrifugation in JA 25-50 rotator for 45 min at 4°C at 40,000 g in the Avanti J26XP Beckmann centrifuge. The lysate was then mixed with cobalt-agarose (Sigma Aldrich, St Louis, MO, USA) (1 mL per 2 L LB expression culture) and incubated for 1 h at 4°C to allow binding of the His-tagged proteins to the immobilized

Co^{2+}-ions. After binding of the protein, the beads were transferred onto a gravity column and were washed with 60 mL protein lysis buffer to remove loosely bound proteins from the Cobalt-agarose beads. The proteins were eluted by adding 5 mL protein elution buffer (protein lysis buffer with 250 mM imidazole).

The eluate was concentrated using Amicon centrifugation concentrators (Merck Millipore, Billerica, MA, USA). The molecular weight cut off of the concentrators was chosen depending on the size of the purified protein. Subsequently, the sample was loaded onto a gel filtration column to exchange the buffer to protein storage buffer (20 mM HEPES KOH pH 7.6, 10 mM $MgCl_2$, 50 mM KCl, 50 mM NH_4Cl). Depending on the molecular weight of the protein, the gel filtration was performed using a Superdex 75 (16/600) or Superdex 100 through the NGC medium pressure liquid chromatography system (Biorad, Hercules, CA, USA) collecting 1 mL elution fractions. Elution fractions were analyzed by SDS-PAGE. Fractions containing the protein of interest were pooled and concentrated using centrifugal filters to a concentration of 20 mg/mL. For long-term storage, 100% glycerol was added to a final concentration of 50% glycerol and the samples were flash-frozen in liquid nitrogen and stored at -80°C.

3.4.3 Expression and purification of Elongation factor-P

Elongation factor-P (EF-P) from *E. coli* was overexpressed as published (Ude et al., 2013). To ensure that the expressed protein is fully modified the plasmid encoding for H_6-tagged EF-P was co-expressed with the pRSF plasmid encoding for the untagged modification enzymes YjeA and YjeK. The expression of all three proteins is under the control of a T7 promoter (Doerfel et al., 2015). 7 *T. thermophilus* EF-P was expressed as published in (Blaha et al., 2009) was used. Plasmids encoding mutated versions of *T. thermophiles* EF-P were also co-expressed with the modification enzymes for *E. coli* EF-P. The proteins were overexpressed in *E. coli* BL21 Gold cells. and the expression was induced by addition of 1mM IPTG (end concentration) at an OD_{600} of 0.6. After induction, the cells were grown for 4 h at 30°C. The cells were harvested by centrifugation at 4,000 g for 15 min at 4°C and flash frozen in liquid nitrogen and stored at -80 °C until further use.

For EF-P purification the cells were thawed and resuspended protein lysis buffer and lysed as described in the previous chapter 3.4.2. For the purification of *E. coli* EF-P, the cell lysate was

incubated directly with Co^{2+}-NTA beads. The cell lysate containing the *T. thermophilus* EF-P or one of the mutants was first treated with a heat shock to remove *E. coli* proteins, using the expected thermal stability of the protein. For the heat shock, the lysate was transferred into an Erlenmeyer flask that was put in a water bath at a temperature of 60°C. The cell lysate was incubated for 20 min followed by removal of cell debris and denatured *E. coli* proteins by centrifugation in JA 25.50 (Beckmann) rotor for 45 min at 40,000 g at 4°C. The following steps were performed as described in chapter 3.4.2. Since these proteins were mainly used for crystallography experiments the proteins were flash-frozen and stored at -80 °C without the addition of glycerol.

3.5 RNA handling

All reactions containing RNA were performed in DEPC treated water or molecular biology grade water (Merck, Billerica, MA, USA) to avoid degradation of the RNA by RNases. Glassware used for these reactions was baked for several hours to degrade potential RNase contaminations.

3.5.1 *In vitro* transcription and purification *in vitro* transcribed RNA

Unmodified tRNAs, flexizymes and mRNA templates for toeprinting were transcribed *in vitro* using the T7 RNAP mutant P266L (Guillerez et al., 2005). This mutant of the T7 RNAP synthesized more full-length product compared to the wt T7 RNAP. The DNA templates were synthesized by PCR as described in chapter 3.2 encoding the genes under the T7 promoter. *In vitro* transcription was performed using 5-10 µg/mL of DNA template, 7.5 mM of each NTP, 10 µg/mL of T7 RNAP in Ribomax buffer (80 mM Tris·HCl pH 7.6, 2 mM spermidine, 24 mM $MgCl_2$),.and was incubated for 2 h at 37°C. The reaction was stopped by phenol-chloroform extraction (chapter 3.5.2) and nucleic acids and nucleotides were precipitated with 1 M $NH_4(CH_3CO_2)$ and 70% ethanol end concentration

Unincorporated nucleotides were removed by washing the RNA several times with RNase-free water over Amicon centrifugation filters (Merck Millipore, Billerica, MA, USA) using a molecular weight cut-off smaller than the produced RNA. The success of the washing was monitored by measuring the absorption in the flow-through on the NanoDrop. After recovery of the RNA

from the centrifugal filters, the concentration was determined using the Nanodrop 2000c (Thermofisher, chapter 3.2) and the purity was determined by gel electrophoresis (chapter 3.2).

3.5.2 Phenol-Chloroform extraction

Purification of RNA from enzymatic reactions was performed by phenol-chloroform extraction using. acidic phenol (pH 4.3, Na_3citrate solution, Sigma Aldrich, St Louis, MO, USA). The low pH prevents hydrolysis of RNA. The reactions were extracted by adding one volume phenol: chloroform: isoamyl alcohol (25:24:1) and mixing it vigorously by vortexing. The organic phase was separated from the aqueous phase by centrifugation. The denatured proteins then locate at the interphase between the organic and the aqueous phase. The aqueous phase was re-extracted three times with chloroform: isoamyl alcohol (24:1). All phases were washed with reaction, stabilization buffer or molecular biology water to ensure the recovery of the RNA sample. To remove residual organic solvents, the RNA was precipitated by NH_4Ac/ethanol precipitation, as described in chapter 3.5.3.

3.5.3 Precipitation of RNA

3.4.3.1 Alcohol precipitation of RNA

An important step in the RNA purification is the removal of salts, buffer exchange as well as concentrating the sample. Nucleic acids can be precipitated specifically in the presence of monovalent cations such as Na^+ and NH_4^+. The ions bind to the phosphate-sugar backbone of the nucleic acid and neutralize its negative charges. By the addition of 2.5 Vol EtOH or one volume isopropanol, the RNA precipitates at low temperatures due to its decreased solubility. For precipitation, the samples were incubated for 1 h at -20°C and then spun down for 30 min at 18,000 rcf in a cooled tabletop centrifuge. The pellet was washed with 70% EtOH to remove remaining salt and spun down again. The pellet was dried at room temperature for 10-15 minutes and finally. resuspended in the desired buffer.

The salt for RNA precipitation was chosen depending on the downstream application and properties of the sample. In most cases, $NH_4(CH_3CO_2)$ was used due to its volatile properties. For aminoacylated and peptidylated tRNA samples $Na(CH_3CO_2)$ pH 4.8 was used to protect the

product from uncontrolled hydrolysis. Chloride as a counterion was avoided since it shows inhibitory properties in downstream reactions such as *in vitro* transcription or the initiation of *in vitro* translation.

3.5.3.2 TCA precipitation of RNA

tRNA samples from analytical HPLC runs were often too low concentrated for the following Northern Blot analysis. In order to increase the concentration, the RNA was precipitated using a 100% (w/v) trichloroacetic acid (TCA) solution to. to obtain a final TCA concentration of 10%. The samples were incubated for 1 h on ice to ensure complete precipitation. After the incubation, the RNA was pelleted and washed with 100% acetone to remove residual TCA. After the washing step, the pellet was dried briefly and resuspended in RNA loading dye. If TCA was still left in the sample, which was indicated by a color change of the RNA loading dye, small amounts of 1 M Trizma base were added to ensure a basic pH for optimal separation on TBU-PAGE.

3.6 tRNA expression and purification

A specific tRNA can either be produced by *in vitro* transcription or by overexpression of the corresponding gene *in vivo* and subsequent purification from cells. tRNAs function as an adaptor between the mRNA and the amino acid sequence (Crick, 1958) and are modified post-transcriptionally. These modifications are important decoding capacity, decreasing codon sensitivity and maintaining open reading frame. The advantage of the purification of tRNAs from cells is that these tRNAs are modified. In contrast to protein purification, the length of the tRNA is crucial for the modification, meaning the tRNA cannot be tagged. In order to purify a specific tRNA species from a crude tRNA purification, the tRNA can be aminoacylated using the corresponding aminoacyl-tRNA synthetase. This reaction is tRNA specific since the enzyme recognizes specific features of the tRNA and the chemical properties of the amino acid (Ibba et al., 1997). The aminoacylation of a tRNA changes its binding properties on a reverse phase (RP) high-performance liquid chromatography (HPLC) column (Cayama et al., 2000) enabling separation from the deaminoacylated-tRNAs in the mixture. The column matrix is formed by hydrophobic residues that bind biomolecules due to hydrophobic residues exposed on the

surface. The sample is eluted by gradually increasing concentrations of an organic solvent allowing separation of the different compounds according to their hydrophobicity (Aguilar, 2004). The addition of the amino acid changes the hydrophobic character of the tRNA and leads to a different elution profile. By cycling the deaminoacylation and aminoacylation, the tRNA of interest can be enriched (Cayama et al., 2000).

The used constructs are listed in the following table:

Table 30: List of tRNA constructs for purification and expression

Gene	Vector	Induction	Citation
$tRNA_i^{Met}{}_{AUG}$	pBS	consecutive	(Schmitt et al., 1999)
$tRNA^{Phe}{}_{UUU}$	pBR322	consecutive	(Jünemann et al., 1996)
$tRNA^{Pro}{}_{CCG}$	pUC19	L-arabinose	Dr. KK Inampudi
	pBSTNAV2OK	consecutive	This thesis
	pBSTNAV3S	consecutive	This thesis
$tRNA^{Trp}{}_{UGG}$	pUC19	L-arabinose	This thesis
$tRNA^{Gly}{}_{GGG}$	pUC19	L-arabinose	This thesis
$tRNA^{Asp}{}_{GAC}$	pUC19	L-arabinose	This thesis
$tRNA^{Asn}{}_{AAC}$	pUC19	L-arabinose	This thesis

3.6.1 Test expression of $tRNA^{Pro}$ overexpression

To identify the optimal expression conditions for $tRNA^{Pro}$ small-scale expression tests were performed in 25 mL LB culture. To test the expression efficiency the plasmids pBSTNAV2OK and pBSTNAV3S, as well as the $tRNA^{Pro}$ containing plasmids, were transformed into *E. coli* HB101 and *E. coli* DH5α cells. The preculture was grown for 8 shaking at 180 rpm and was used to inoculate the main culture (25 mL LB) to a starting OD_{600} of 0.1. The cells were harvested after 16 h of growth at 37°C under optimal aerobic conditions and the OD_{600} was measured using Nanodrop 2000c (Thermofisher). 10 mL of cell culture were harvested and flash frozen in liquid N_2.

To test the expression capacity of the pUC19-$tRNA^{Pro}$ constructs the plasmid was transformed into *E. coli* BL21AI cells. The preculture was grown overnight (37 °C, shaking at 180 rpm) and main cultures were inoculated to an OD_{600} of 0.1. When the cells reached an OD_{600} of 0.6 the expression of the tRNA was induced by the addition of L-arabinose (1%, 0.1%, and 0.01%, end concentration). An uninduced sample served as control. 10 mL time points were taken after 4 h and after 19 h of overexpression. The OD_{600} was measured and the cells were harvested by centrifugation, flash-frozen and stored at -80 °C until further extraction.

Independently from the expression strategy, cells were lysed by phenol/chloroform extraction: In the first step the cells were resuspended in 500 µL tRNA lysis Buffer (50 mM Tris·HCl pH 7.2, 50 mM $Mg(CH_3CO_2)_2$) and mixed with an equal volume of phenol (pH 5.2): chloroform: isoamyl alcohol (25:24:1) solution and centrifuged for 15 min at 18,000 rcf to separate the organic from the aqueous phase. The aqueous phase was washed twice with 500 µL chloroform: isoamyl alcohol (24:1). Subsequently, small RNA species were precipitated specifically with 1 M $NH_4(CH_3CO_2)$ and 70% EtOH (end concentration). After pelleting, the samples were resuspended in RNA loading dye (chapter 3.8) calculated as in the following relation:

$$V_{loading\ dye} = OD_{600} \cdot 16.4\ \mu L \quad (2)$$

The expression levels were analyzed by Northern Blot (chapter 3.2).

3.6.2 Large-scale expression of $tRNA^{Pro}$ and total tRNA extraction

For large scale expression $tRNA^{Pro}$, eight main cultures of 1 L LB (100 µg/mL ampicillin) were inoculated with an overnight preculture of *E. coli* HB101 pBSTNAV3S-$tRNA^{Pro}$. The cultures were grown overnight (approximately 16 h) at 37°C under aerobe conditions. The cells were harvested by centrifugation in a JLA 9.100 rotor at 4 000 rcf for 20 min at 4°C (Avanti J26XP centrifuge, Beckmann, Brea, CA, USA). The cell pellets were washed with tRNA lysis buffer (20 mM Tris·HCl pH 7.4, 20 mM $Mg(CH_3CO_2)_2$) and pelleted by a second centrifugation step using the same conditions. Per 1 L LB culture, the cell pellet weighed approximately 5 g. For storage, cells were flash-frozen in liquid nitrogen and stored at -80°C. The following figure highlights the different steps during $tRNA^{Pro}$ extraction and purification:

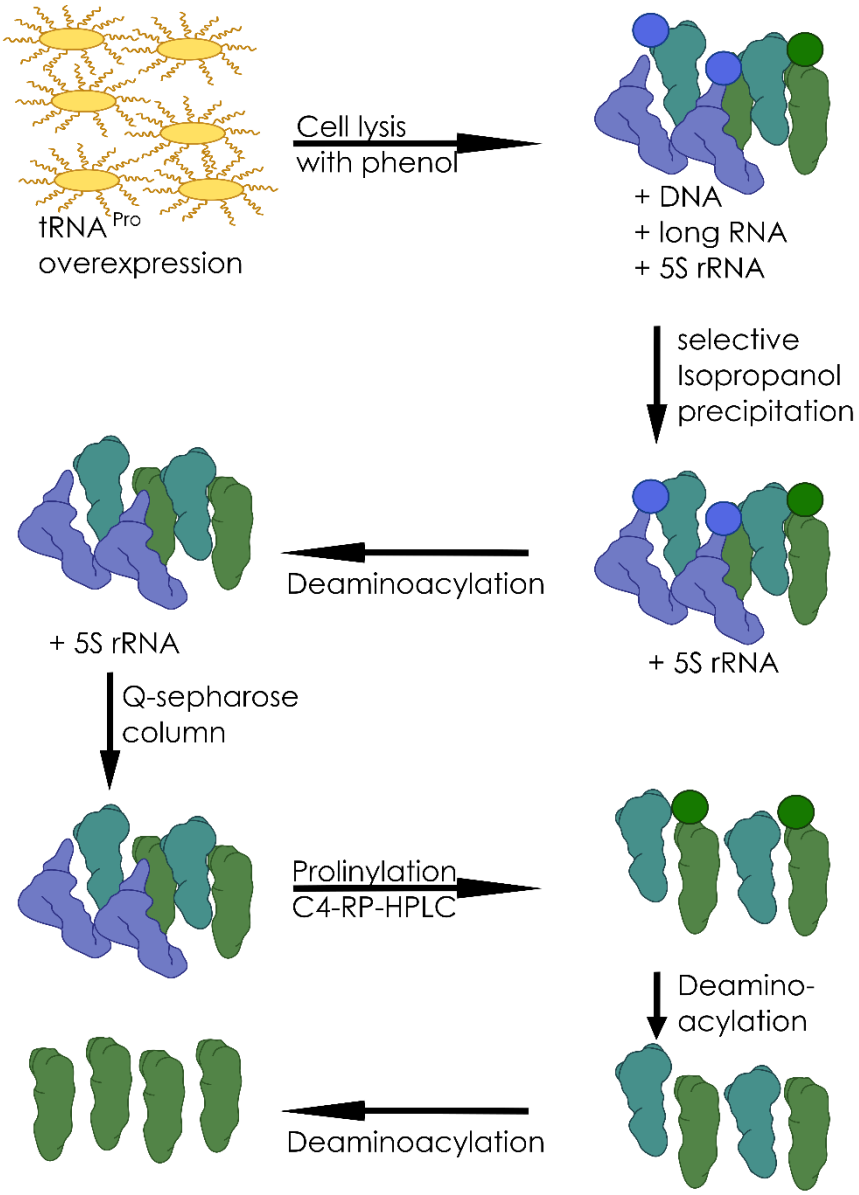

Figure 13: Summary of tRNA^{Pro} extraction and purification. tRNA^{Pro} was overexpressed in *E. coli* HB101 cells and cells were lysed by phenol/chloroform extraction. DNA and long RNA species were removed by selective isopropanol precipitation. Total tRNA sample was deaminoacylated by incubation at pH 8.0. Subsequently, the 5S rRNA was removed by Q-sepharose column. tRNA^{Pro} was purified further by changing its chemical properties using aminoacylation and deaminoacylation and C4 RP-HPLC.

To purify the tRNA the cells were thawed and resuspended in tRNA lysis buffer (25 mL per 10 g of cells). The cells were lysed and the proteins were denatured by adding acidic phenol (pH 4.2 citric acid, Sigma Aldrich, St Louis, MO, USA) to the resuspension (25 mL per 10 g of cells). The resuspension was incubated on a tube rotator for 1 h at 4°C to ensure complete lysis of the cells. Subsequently, the lysate was centrifuged for 30 min in Eppendorf 5804R centrifuge (Hamburg, Germany). The aqueous phase was extracted once with chloroform: isoamyl alcohol

(24:1, Sigma). The organic phases were washed once with fresh tRNA lysis buffer. The DNA was removed by precipitation with 300 mM $Na(CH_3CO_2)$ pH 4.8 and 20% isopropanol for 1 h at 4°C. After centrifugation for 1 h at 5,170 g (JLA 8.100, Avanti J26XP, Beckmann, Brea, CA, USA) at 4°C, pellets, containing the genomic DNA of the cells, were discarded and the concentration of isopropanol in the supernatant was increased to 60% to precipitate the RNA. The solution was incubated overnight at 4°C to ensure precipitation. The RNA was pelleted by centrifugation and washed with 70% ethanol to remove remaining salts. The pellet was briefly dried on air by placing the centrifugation bottle under the hood for 20 min.

This extracted tRNA sample contains aminoacylated, deaminoacylated tRNAs and other RNA species. To deaminoacylate all tRNAs and obtain a homogeneous preparation the pellet was resuspended in 200 mM Tris·acetate pH 9.0 at 37°C for 1 h. In the last step of the total tRNA extraction, small RNA species were precipitated specifically by adding 1 M $NH_4(CH_3CO_2)$ and 70% ethanol. The pellet was dissolved in RNase-free water and the concentration was determined on the NanoDrop (see chapter 3.2).

3.6.3 Chromatography of $tRNA^{Pro}$

The total tRNA extraction (chapter 3.6.2) still contains longer rRNA species that will bind tighter to the reverse phase (RP) column as they present a larger hydrophobic surface and might prevent binding of the tRNA to the column material. Therefore, these and other long RNA species were removed specifically by loading the RNA onto a Q-sepharose (GE Healthcare, Chicago, IL, USA) column, which is an anion exchange column. Negatively charged biomolecules bind to the positively charged matrix and can be eluted specifically by increasing concentrations of Cl^- ions in the elution buffer. Due to the lower charge, the shorter tRNAs elute before the rRNA species. The purification protocol was adopted from the published protocol (Mechulam et al., 2007). The binding buffer contained 20 mM HEPES·NaOH pH 7.5, 100 µM EDTA, 6 mM $MgCl_2$, 200 mM NaCl. The sample was eluted by increasing the NaCl concentration over four column volumes slope into 1 M NaCl. The $tRNA^{Pro}$ containing fractions were identified by Northern Blot analysis (chapter 3.8) and pooled for further purification.

In the next purification step, the $tRNA^{Pro}$ was prolinylated specificially by using the *E. coli* prolyl-tRNA synthetase ProS (purification chapter 3.4.1, reaction chapter 3.6.5). This modification

changes the binding behavior of $tRNA^{Pro}$ to the C4-RP-HPLC column (Grace, Columbia, MD, USA). The total tRNA was bound to the column using the RP-buffer A (20 mM $NH_4(CH_3CO_2)$ pH 5.5, 10 mM $Mg(CH_3CO_2)_2$, 400 mM NaCl). The different tRNA species were separated by increasing the amount of methanol (MeOH) within the buffer. RP buffer B contained 20 mM $NH_4(CH_3CO_2)$ pH 5.5, 10 mM $Mg(CH_3CO_2)_2$, 400 mM NaCl and 15% MeOH. The tRNA was eluted using a gradient from 0-65% RP-buffer B over 12 column volumes. The $tRNA^{Pro}$ containing fractions were identified by Northern Blotting and in the next step deprolinylated using 200 mM Tris-acetate pH 8.0 for 1 h at 37°C. The sample was rerun using the same program since the deaminoacylation of the $tRNA^{Pro}$ changed its running behavior. Fractions containing $tRNA^{Pro}$ were pooled together and precipitated with 1 M NH_4Ac and 70% EtOH. The purified $tRNA^{Pro}$ was washed several times with H_2O_{DEPC} using a 10 kDa centrifugal filter to remove all sodium cations that potentially interfere with downstream reactions. As a final step, the sample was lyophilized and resuspended in a small volume of RNase-free water. The concentration was determined and the tRNA was stored at -80°C.

The protocol for $tRNA_i^{Met}$ purification was optimized by Dr. K. Kishore Inampudi following the same principle. $tRNA_i^{Met}$ preparations for this thesis were done by Dr. K. Kishore Inampudi, Dr. Axel Innis, Natacha Pérébaskine and myself. $tRNA^{Phe}$ was purified by Natacha Pérébaskine.

3.6.4 CCA end modification of tRNA

In the cell, amino acids are linked via an ester bond to the 3'OH of the tRNA. This linkage is pH sensitive and does hydrolyze during crystallization. In order to prevent deaminoacylation, this bond was modified to an amide bond, the 3'OH has to be exchanged to a $3'NH_2$ group. To do so the purified tRNAs were modified enzymatically by removal and adding back of the 3'CCA end using enzyme phosphodiesterase and CCA-adding enzyme. The following aminoacylation reaction was performed using the corresponding amino acyl-tRNA synthetase. This strategy was used previously to get greater insights into peptide bond formation (Polikanov et al., 2014; Voorhees et al., 2009).

The modification of the 3' end was performed as described previously with minor modifications (Fraser and Rich, 1973; Polikanov et al., 2014; Voorhees et al., 2009). For most tRNAs, the CCA end was be removed by using phosphodiesterase I (Western Diamond rattlesnake, Sigma

Aldrich, St Louis, MO, USA), a 3′-5′ exonuclease that is incapable of degrading double-stranded RNA. For this reaction 10 µM tRNA were mixed with 0.1 mg/mL of the phosphodiesterase I in 50 mM Tris·HCl pH 7,6, 10 mM $MgCl_2$,1 mM DTT. The reaction was incubated for one hour at RT and stopped by phenol-chloroform extraction (chapter 3.52).

In $tRNA_i^{Met,}$ five bases are not base-paired which is one more than in other modified tRNAs. Consequently, phosphodiesterase I would remove an additional nucleotide and thus cannot be used for the removal of the CCA end. To overcome this problem, the CCA-adding enzyme was used, which, in the presence of pyrophosphate, specifically removes the CCA end. For this reaction 10 µM tRNA were mixed with 0.1 mg/mL CCA adding enzyme and 250 µM $NaPP_i$ in the same buffer as for the phosphodiesterase I treatment and incubated for 1 h at 37°C. The reaction was stopped by phenol-chloroform extraction and the tRNA was precipitated with 1 M $NH_4(CH_3CO_2)$/70% EtOH precipitation. In the last step, the free nucleotides were removed by washing the RNA over a 10 kDa Amicon centrifugal concentrator (Merck Millipore).

The CCA-end was added back by reversing the enzymatic activity of the CCA adding an enzyme, which was done in the presence of CTP and 3′-amino adenosine-triphosphate (3′NH_2-ATP, Biolog Inc, Hayward, CA, USA). As the name indicates, 3′NH_2-ATP has an amino group instead of the 3′ OH group. The reaction to incorporate 3′NH2-ATP into the CCA end of the tRNA was performed using 10 µg $tRNA^{-CCA}$ together with 30 µM CTP, 40 µM 3′NH_2-ATP and 2 µM CCA adding enzyme in 50 mM Tris·HCl pH 7.6, 12 mM $MgCl_2$ and 30 mM KCl (Fraser and Rich, 1973; Polikanov et al., 2014; Voorhees et al., 2009). The reaction was incubated for 2 h at 37°C and was stopped by phenol-chloroform extraction. Depending on the downstream application, the product was directly purified by C4-HPLC or was first aminoacylated and then purified by C4-HPLC. All products of the reactions were analyzed on 15% denaturing TBU-PAGE to monitor the process.

3.6.5 Aminoacylation with aminoacyl-tRNA synthetases

For solving structures, tRNA purification and biochemical assays it was necessary to aminoacylate tRNAs using their aminoacyl-tRNA synthetases. The reactions were performed in 100 mM HEPES·KOH pH 7.5, 20 mM $MgCl_2$, 30 mM KCl, 4.15 mM ATP, and 0.42 mM amino acid using 0.1 mg/mL aminoacyl-tRNA synthetase. The reaction was incubated for 20 to 30 min at 37°C and stopped by phenol-chloroform extraction.

3.6.6 Peptidylation of $tRNA_i^{Met}$ with flexizyme technique

As described in chapter 1.5, flexizyme can be used to specifically peptidylate and aminoacylate tRNA on the CCA end forming an ester bond (Goto et al., 2011; Ramaswamy et al., 2004).For the reaction 75 µM flexizyme and 25 µM $tRNA_i^{Met}$ or microhelix, a short tRNA mimic, were mixed in 50 mM HEPES·KOH buffer (pH 7.5) or 50 mM Bicine·KOH buffer (pH 8.5) and were incubated for 2 min at 95°C followed by incubation at room temperature for 5 min to allow the flexizyme to fold. In the next step, the MgCl2 concentration in the reaction was increased to 50-600 mM $MgCl_2$ (sample-specific) and the reaction was incubated for another 5 min at room temperature followed by an incubation for 3 min on ice (Goto et al., 2011). To start the reaction 5 mM activated peptide solubilized in 100% dimethyl sulfoxide (DMSO) were added, resulting in a final concentration of 20% DMSO (v/v). The reactions were incubated at 4 °C on ice. The reaction time and activity depended on the nature of the activated amino acid and varied from 2 h up to several days.

For screening and optimizing the reaction conditions n optimization, the reaction was set up using a microhelix and 1 µLtime points were taken directly into 20 µL acidic RNA loading dye over the course of eight days. All samples were analyzed at the end on a 20% acidic denaturing PAGE (see chapter 3.2). Once the reaction conditions were optimized the reaction size was scaled-up to a total volume of 200 µL. The reactions were stopped by addition of 300 mM $Na(CH_3CO_2)$ pH 4.8 and 70% ethanol. The aminoacylated-tRNA was recovered in 500 µL reverse phase buffer A (20 mM $NH_4(CH_3CO_2)$ pH 5.5, 10 mM $Mg(CH_3CO_2)_2$, 400 mM NaCl). The peptidylated-tRNA was separated by running the sample over an analytical C4 reverse phase column (Grace) by performing a 14 CV gradient into 50-80% reverse phase buffer B (20 mM $NH_4(CH_3CO_2)$ pH 5.5, 10 mM $Mg(CH_3CO_2)_2$, 400 mM NaCl, 40% MeOH). The slope of the gradient depended on the hydrophobicity of the peptide. Elution fractions were followed by detecting the UV-Vis profile and analyzed by 9% acidic denaturing PAGE. Fractions containing the peptidylated tRNA were pooled together and washed multiple times using centrifugal filters with 20 mM $NH_4(CH_3CO_2)$ pH 5.5 to completely remove Na^+ cations. The peptidylated-tRNA was flash-frozen and stored at -80°C.

3.7 Ribosome purification

70S *T. thermophilus* ribosomes were purified from the strain *T. thermophiles* HB8 for X-ray crystallography by Natacha Pérébaskine as published (Selmer et al., 2006).

E. coli ribosomes were isolated for toeprinting and structure determination by cryo-EM from *E. coli* KC6 cells. The cells were grown at an OD_{600} of 0.6 to ensure that the cells are in exponential growth phase. Using an ice-cooled water bath the cells were cooled down quickly and then harvested by centrifugation (4500 rpm JLA 9.100 Beckmann rotor, 4°C). The cells were frozen in liquid nitrogen and stored at -80°C until ribosome purification.

The ribosomes were isolated following the published protocol (Blaha et al., 2000) with minor modifications. *E. coli* KC6 cells were thawed and washed once with ribosome resuspension buffer (50 mM HEPES·KOH pH 7.5, 10 mM $Mg(CH_3CO_2)_2$, 100 mM NH_4Cl and 4 mM β-mercaptoethanol (BME)). For cell lysis 2 mL ribosome resuspension buffer per 1 g of cells were added and the cells were lysed using an EmulsiFlex-C5 (Avestin, Ottawa, ON, Canada). The cell debris was removed by centrifuging the supernatant twice at 4 °C at 48 000 g for 1 h (JA 25.50 rotor Beckmann). The cleared cell lysate was overlaid a sucrose cushion (30% (w/v) sucrose in ribosome resuspension buffer) and spun by ultra-centrifugation at 40 000 rpm in a 50.2 Ti rotor (Beckmann) for 20 h at 4°C to pellet the ribosomes. The sucrose was removed by washing the pellet for 5 min with ribosome dissociation buffer (50 mM HEPES·KOH pH 7.5, 1 mM $Mg(CH_3CO_2)_2$, 100 mM NH_4Cl) followed by resuspending the pellet in ribosome dissociation buffer by continuously shaking on ice in the cold room. The low Mg^{2+} concentration in the buffer leads to dissociation of the two subunits (Chao, 1957). The absorption was determined at 260 nm using the Nanodrop (Thermofisher).

To separate the subunits, gradients from 10 to30% sucrose were prepared and overlaid with 200 A_{260} units of ribosomes. The gradients were centrifuged using a swinging bucket rotor (SW28) at 19 000 rpm for 17 h (Optima L80XP, Beckmann, Brea, CA, USA). The gradients were then fractionated using a peristaltic pump combined with the detector and fraction collector of the NGC medium pressure liquid chromatography system (Bio-Rad). The fraction volume was set to 1 mL. Fractions for the 50S and 30S subunits were pooled separately and pelleted by ultracentrifugation in a 50.2 Ti rotor (Beckmann) by spinning at 40 000 rpm for 24 h.

The colorless pellets were resuspended in ribosome re-association buffer (50 mM HEPES·KOH pH 7.5, 10 mM $Mg(CH_3CO_2)_2$, 30 mM KCl). The concentration of the purified subunits was determined and the subunits were mixed in an equal ratio of absorption units. This leads to an excess of the 30S over 50S subunits and thus allows proper separation of re-associated 70S ribosomes from the 30S subunits in the analysis of the sucrose gradient of these samples. The mixture was diluted to a concentration of 50 A_{260} per mL and incubated for 1 h at 40°C to allow 70S ribosome formation. 100 A_{260} units were loaded per gradient (10-30% sucrose in the re-association buffer) and centrifuged for 18 h at 18 000 rpm using an SW28 (Beckmann) rotor. Gradients were collected as before, pooled and pelleted by ultracentrifugation in 50.2 Ti rotor. The pellets were resuspended in a minimal volume of re-association buffer and incubated for another 15 min at 40°C to ensure the re-association (Blaha et al., 2000). The absorption was determined using the Nanodrop 2000c and converted into molar concentration according to the following equation:

$$c\left(\frac{mg}{mL}\right) = A_{260} \cdot 0.06\ \frac{mg}{mL} \tag{3}$$

The ribosome solution was aliquoted, flash-frozen and stored at -80°C until further use.

3.8 Toeprinting

Toeprinting is an *in vitro* method to identify the position of an arrested ribosome along a mRNA with nucleotide resolution. Originally the reaction was performed using an S30 cell extract (Hartz et al., 1988), but recent developments led to a protocol using a reconstituted *in vitro* translation system (Orelle et al., 2013b). This system contains all components necessary for *in vitro* transcription from a T7 promoter as well as for canonical translation and offers well-defined reaction conditions. During the toeprinting reaction, a 5'fluorescently labeled oligonucleotide complementary to the 3' end of the template mRNA is extended using a reverse transcriptase until the enzyme reaches the arrested ribosome. The synthesized cDNA is then purified and analyzed on a sequencing gel (Orelle et al., 2013b; Starosta et al., 2014a).

3.8.1 In vitro translation

Depending on the experiment different variants of the PURExpress kit (NEB, Ipswich, MA, USA) were used. The nascent chein-medtiated translational arrest of *E. coli* ribosomes was tested using the full kit or the ΔRF1,2,3 kit. To analyze the possibility to use 70S *T. thermophilus* ribosomes or peptidylated-tRNAs during the translation reaction the ΔtRNA, Δribosomes, ΔRF1,2,3 kit was used. The following table lists the PURExpress systems used in this thesis as well as the corresponding experiments:

Table 31: List of used PURExpress systems from NEB, Ipswich, MA, USA with the corresponding experiments

Name	Separated factors	Experiments
PURExpress system, no release factors	ΔRF1, 2, 3	• Characterization of arrest peptides • EF-P activity
Custom made PURExpress system	Δribosomes ΔRF1, 2, 3 ΔtRNA Δaa	• fMet-control • tRNA activity tests • activity test of peptidylated tRNA • testing the secondary structure of mRNA

The reactions were assembled as recommended for a total volume of 5 µL per reaction. Additionally, 2 pmol Yakima yellow labeled DNA oligonucleotide, which is a reverse complement oligo to the 3' end of the mRNA, 1 pmol DNA template or 5 pmol mRNA template and 25 µM antibiotic (Orelle et al., 2013b; Starosta et al., 2014a) were used in the reaction. The

following table lists the reaction compositions of the control reactions are listed in the following table:

Table 32: Reaction mixture for toeprinting control reactions

Reaction	PURExpress system	Reaction mix	Toeprint corresponds to step in translational cycle
fMet-control	Δribosomes, ΔRF1, 2, 3, ΔtRNA, Δaa	1 µL factor A$^-$ 0.8 µL factor mix 0.6 µL ribosomes 150 µM L-methionine 100 µM $tRNA_i^{Met}$	Start codon
Onc112 control	ΔRF1, 2, 3	2 µL Solution A 1.5 µL Solution B 100 µM Onc112	
tRNA activity	Δribosomes, ΔRF1, 2, 3, ΔtRNA, Δaa	Same mix as fMet-control 150 µM amino acid 100 µM purified tRNA	Elongation
Non-released ribosomes	ΔRF1, 2, 3	2 µL Solution A 1.5 µL Solution B	Termination
mRNA secondary structure	Δribosomes, ΔRF1, 2, 3, ΔtRNA, Δaa	1 µL factor A$^-$ 0.8 µL factor mix 0.5 µL total tRNA 0.5 µL amino acids	Secondary structure of mRNA

All components were combined, and the reaction was incubated for 15 min at 37°C to allow transcription and translation. During this time potential arrest complexes can be formed. To detect arrest complexes the 5' labeled oligonucleotide was extended by reverse transcription.1 µL reverse transcriptase mix (100 µM dNTPs, four volumes of PURE system buffer (9 mM $Mg(CH_3CO_2)_2$, 5 mM K-phosphate pH 7.3, 95 mM K-glutamate, 5 mM NH_4Cl, 0.5 mM $CaCl_2$, 1 mM spermidine, 8 mM putrescine, 1 mM DTT) and five volumes of AMV reverse transcriptase) was added to the reaction which was incubated for further 20 min at 37°C. The mRNA was degraded in the next step by addition of 0.5 M NaOH and incubation at 37°C for 15 minutes. The reaction was neutralized with 0.5 M HCl and diluted with resuspension buffer (300 mM $Na(CH_3CO_2)$ pH 5.5, 5 mM EDTA, 0.5% SDS) (Orelle et al., 2013b; Starosta et al., 2014a). Proteins and nucleotides were removed using a nucleotide removal kit (Qiagen, Hilden, Germany). Per reaction 100 µL PNI buffer were added and the sample was loaded onto the spin columns provided by the kit. Subsequently, the column was washed once with 750 µL PE buffer.

The cDNA was eluted with 100 µL molecular biology grade water (Merck) and dried by vacuum centrifugation. The dried cDNA was resuspended in 6 µL toeprinting loading dye.

3.8.2 Sanger sequencing for toeprinting experiment

To be able to determine the exact arrest position of the ribosome on the mRNA, a sequencing reaction was performed according to the method of Sanger (Sanger and Coulson, 1975; Sanger et al., 1977). In the reactions, dGTP was replaced by deazaGTP which leads to an enhanced capability of the HemoKlen Taq DNAP overcome secondary structure elements. The addition of ddNTPs leads to interrupted reactions and thus during several cycles of PCR to the generation of all lengths of DNA fragments. The following stock solutions were used:

Table 33: List of 3x ddNTP stock solutions

Stock solution	Composition
ddGTP	20 µM of each dNTP 30 µM ddGTP
ddATP	20 µM of each dNTP 350 µM ddATP
ddTTP	20 µM of each dNTP 600 µM ddTTP
ddCTP	20 µM of each dNTP 200 µM ddCTP

The ddNTP mixtures were mixed with the sequencing reaction master mix which is listed in the following table:

Table 34: Mastermix for sequencing reaction

Component	Concentration
1x fmol sequencing buffer	50 mM Tris·HCl pH 9.0, 2 mM $MgCl_2$
Yakima yellow NV primer (2 µM)	0.3 µM Primer
HemoKlen Taq DNAP (NEB, Ipswich, MA, USA)	1 µL per 17 µL master mix
DNA template	0.06 µM DNA
Water	To final volume

The following PCR program was used:

Table 35: Program for sequencing reaction

Temperature	Time	Function	Cycles
95°C	30 s	Heat activation of enzyme	1x
95°C	30 s	Denaturation of PCR fragments	30x
42°C	30 s	Primer annealing	
70°C	1 min	Primer extension	
72°C	5 min	Final extension	1x
4°C	∞	Incubation until further usage	1x

3.8.3 Analysis and interpretation

Sequencing reactions were evaporated by vacuum centrifugation and resuspended in 6 µL toeprinting loading dye. Samples were heated for 5 min at 95°C to enhance solvation and to denature the cDNA. The samples were loaded onto a denaturing sequencing PAGE that was prepared according to the following protocol:

Table 36: Gel mix for sequencing PAGE

Components (stock concentration)	Final concentration
10x TBE buffer (900 mM Tris, 900 mM Boric acid, 20 mM EDTA)	2x TBE buffer (180 mM Tris, 180 mM Boric acid, 4 mM EDTA)
40% (w/v) acrylamide (19:1)	7.5% (w/v) acrylamide (19:1)
Urea	8 M Urea
10%(w/v) APS	0.075% (w/v) APS
100% (v/v) TEMED	0.075% (v/v) TEMED

The sequencing PAGE was run at 40 W for 2.5 h at room temperature. The bands were detected using a fluorescent scanner (Typhoon, GE Healthcare, Chicago, IL, USA) using the green laser, detecting +3 mm and default settings.

The ribosome covers 16-18nt between the P-site and the position where the reverse transcriptase stops. Thus, the band in the sequencing gel is 16-18nt shorter than the corresponding fragment in the sequencing reaction. This difference in length needs to be taken into account for the analysis and interpretation of toeprinting gels.,.

3.9 X-ray crystallography and structure determination

Crystallography is a biophysical technique that is commonly used to obtain the structure of proteins and nucleic acids. During crystallization, the biomolecular complexes adopt well-ordered, regular orientations. The obtained crystals are exposed to X-rays from a local source or a synchrotron. The way in which the X-rays interact with the crystal is dependent on the structure of the macromolecule and thus by analyzing the pattern, the 3-dimensional structure can be solved.

First high-resolution structures of ribosomal subunits and full 70S *T. thermophilus* ribosome complexes gave great insights into the molecular mechanism of translation. These crystals can diffract to high resolution to obtain information about e.g. ribosomal modifications (Polikanov et al., 2015a) and or mechanistic insights into peptide bond formation (Polikanov et al., 2014). This degree of resolution is necessary to understand the underlying mechanism of action of arrest peptides and proline-rich antimicrobial peptides.

Hindrances of this method include that variation of the sample composition can lead to decrease in resolution or the sample does not crystallize at all. Another disadvantage includes, that the obtained structure derived from molecules that are forced into a specific orientation due to crystal packing and partial dehydration of the biomolecular complex. This might result in artifacts within the structure. However, high-resolution data can be obtained from well-diffracting crystals giving great insights into the underlying molecular mechanism of the biomolecular complex studied. In addition, data sets from multiple experiments can be obtained in relatively short amounts of time and the data processing involves less computational power compared to cryo-EM.

3.9.1 Complex formation and crystallography

Ribosome complexes were formed in the presence of a short, synthetic RNA to allow tRNA binding and selection. The RNAs (Eurogentec) were composed of a Shine-Dalgarno sequence followed by a short ORF, and are listed in the following table:

Table 37: List of synthetic mRNAs for structural biology studies

Name	Sequence	Project
mRNA_MRFR	GGCAAGGAGGUAAAA AUG CGG UUU CGG UAA	M(+)F(+)
mRNA_MRFR_AGG	GGCAAGGAGGUAAAA AUG AGG UUU AGG UAA	M(+)F(+)
mRNA_MFR_AGG	GGCAAGGAGGUAAAA AUG UUU AGG UAA	M(+)F(+)
mRNA_MPP	GGCAAGGAGGUAAAA AUG CCG CCG	Poly-prolines
mRNA_PP	GGCAAGGAGGUAAAA CCG CCG	Poly-prolines
mRNA_MF	GGCAAGGAGGUAAAA AUG UUC UAA	PrAMPs/Poly-prolines

To form the complex of interest, 5 µM 70S *T. thermophilus* ribosomes were incubated with 10 µM mRNA and 25 µM of potential antibiotic for 10 min at 55°C in *T. thermophilus* ribosome buffer (5 mM HEPES·KOH pH 7.5, 30 mM KCl, 10 mM $MgCl_2$, 50 mM NH_4Cl). This step allows the mRNA to bind to small subunit and the antibiotic to its binding site. Subsequently, 20 µM of initiator and elongator tRNAs were added and the complex was incubated further 15 min at 37°C. Complexes without tRNAs were co-crystallized with 50 µM of the hibernation factor YfiA to increase the resolution by preventing ratcheting (Polikanov et al., 2015a). As a final step, the complex was kept at room temperature for at least 15 min before setting up the crystallization drops (Polikanov et al., 2014; Seefeldt et al., 2015; Selmer et al., 2006).

Ribosomes were crystallized using vapor diffusion in sitting drops crystallization plates. In doing so, the concentration of the ribosomes within crystallization drop increased steadily and slowly over several days in a closed environment. The crystallization process is divided into nucleation and crystal growth. Nucleation occurs when the concentration of the biomolecular complex reaches the unstable state in a supersaturated solution. With the formation of small nuclei crystals, the concentration of the biomolecular complex within the solution drops gets reduced and reaches the metastable state and the crystal grows. The challenge is to find the right balance to obtain a good number of crystals and good-sized ones for diffraction to high

resolution. The reservoir solution consisted of 100 mM Tris·HCl pH 7.6, 2.9% (v/v) polyethylene glycol (PEG) 20 000, 7-10% v/v) 2-methyl-2,4-pentanediol (MPD) and 175 mM arginine. PEG 20 000 and MPD act as precipitants to reach the supersaturated state of the solution. While the concentration of PEG was kept constant, the MPD concentration was optimized depending on the ribosome preparation and the complex composition. Crystallization drops consisted of 3 µL of pre-formed complex and 3-4 µL reservoir solution. The drops contain a lower concentrated reservoir buffer. During the crystallization process, the concentration differences are equilibrated by water diffusion from the drop towards the reservoir, increasing the ribosome concentration slowly within the drop solution resulting in crystallization. Crystals appeared after 2 to 3 days incubation at 20°C and after approximately a week, crystals grew to their full sizes of ~1000 × 100 × 100 µm.

Subsequently, crystals were stabilized to prevent ice formation and drying of the crystals.by replacing water with MPD. The concentration of MPD was increased stepwise: 25%, 30%, 35% and 40% (v/v) MPD in 100 mM Tris·HCl, pH 7.6, 2.9% (v/v) PEG 20,000, 50 mM KCl, 10 mM NH_4Cl and 10 mM $Mg(CH_3COO)_2$. The reservoir solution was completely removed during this step. For the first three steps, 5 µL of the cryo-protectant solution was added an incubated for 15 min at room temperature. For the last step, 15 µL of the drop solution was removed and replaced by 40 µL of the cryo-protectant solution containing 40% MPD. The crystals were stabilized minimum 1 h. Crystals were fished into nylon loops and flash frozen using a cryo-stream set to a temperature of 100 K.

3.9.2 Data collection and processing

Data were collected at the Soleil Synchrotron (Saclay, France) at the beamlines Proxima 1 and Proxima 2A and at the European Synchrotron Radiation Facility (ESRF, Grenoble, France) at the beamlines ID23 and ID29. The data were collected at 100 K and at a wavelength around 0.98 Å. Slight differences in wavelength, due to the set-up of the different beamlines, were taken into account during processing. While collecting the crystal was rotated by 0.1° per image and exposed for 0.1 s. Data were obtained using helical data collection mode. Alternatively, individual wedges of 30° were collected and merged at the end into one data set. For each data set at least 180° were collected.

The data were processed using xdsme, which is a collection of python scripts to process the data with X-ray detector software (XDS) facilitating its usage (Legrand, 2017). XDS is a data processing program that facilitates processing of data with weak reflections and high mosaicity (Kabsch, 2010). The processing is divided in the localization of the spots, indexing, integration, scaling and merging. Ribosome crystals from *T. thermophilus* have a large number of weak spots due to large unit cells which were taken into account during spot localization. During this step, spots were identified and separated from noise. The specific localization of each spot arises from the orientation of the molecular complexes within the crystal and the position is crucial for indexing. 70S *T. thermophilus* ribosomes crystallize in most cases in the point group $P2_12_12_1$ with the cell dimensions of 210 × 450 × 625 Å with the corresponding angles of $\alpha=\beta=\gamma=90°$.

Spots were integrated over all collected frames to re-create the 3D profile of each spot that passed through the EWALD sphere. During merging and scaling, the multiple data sets can be combined into one and converted into *.mtz-format which is necessary for downstream applications. During this step, 5% of all spots were selected for R_{free} calculation. These spots were excluded from the refinement. R_{free} is a factor to prevent over-refinement. To avoid artifacts during refinement, the same set of spots were used for R_{free} calculations for each processed data set. As a molecular replacement (MR) was used for phasing and so heavy atom soaking was not necessary for phasing, FRIEDEL's law was set to true meaning that each spot has a corresponding spot in point symmetry.

The final resolution was determined using signal to noise ratio (I/σ) of 1.0, significant value for CC1/2 of > 15 and high completeness (> 95%) for all resolution shells

3.9.3 Phasing, refinement and model building

During the detection of X-ray diffraction, the intensity of the X-ray wave while hitting the detector gets collected while the phase of the wave gets lost. The phases are necessary for structure determination and as they are crucial for the FOURIER transformation needed to calculate the electron density from the integrated spots. Different techniques have been developed to experimentally determine the phases. Crystals can be soaked with heavy atoms (MAD, MIRAS) or existing models can be used as a template for structure determination (molecular replacement, MR). In our case, a known ribosome structure was available (PDB code: 4Y4O, (Polikanov et al., 2015a) that, when stripped of flexible bases, protein factors and tRNA to prevent model bias, was sufficient to phase the data and obtain a complete electron density of our complex. PrAMPs, tRNAs or protein factors were subsequently built on such a model and rRNA geometry of the input model was improved using the ERRASER-phenix pipeline and its deposited structure factors (Chou et al., 2016). The initial electron density map was obtained by refining the model obtained from ERRASER against the processed data set using PHENIX refine pipeline (Adams et al., 2010). The refinement was divided into rigid-body fitting, positional and B-factor refinement. Rigid body fitting is moving the whole complex or domains of a biomolecular complex into the density. The different domains are highlighted in the following figure:

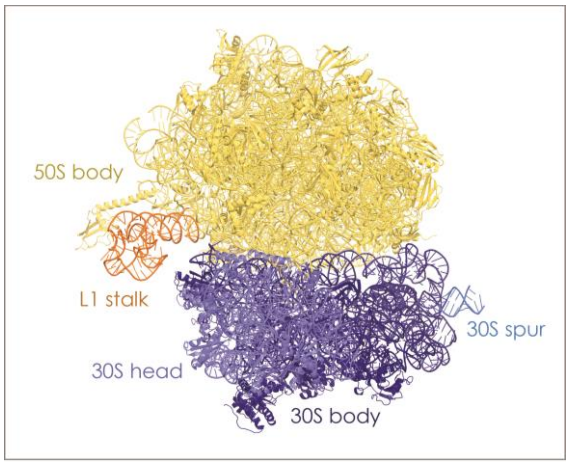

Figure 14: Ribosomal domains for rigid-body fitting. The large subunit is divided into the 50S body (yellow) and the L1 stalk (orange). The small subunit is divided into the 30S head (slate), 30S body (dark blue) and the 30S spur (marine) domain.

In the case of the 70S *T. thermophilus* ribosome, the small subunit was divided into the head, body, spur and helix h44 and the large subunit was divided into the body, L1 stalk and the C-

terminus of ribosomal protein L9, which is extended in the crystal structure due to crystal contacts. Positional refinement was performed applying multiple restraints, including base pairing restraints and non-crystallographic symmetry (NCS) due to the presence of two ribosomes *per* asymmetric unit. The base pairing restraints were generated using the online interface from the RNA center in Santa Cruz, CA (Laurberg et al., 2008). The last step of each macrocycle included B-factor refinement. B-factors indicate the possible movement of each atom. Prior to the first refinement, the B-factor of all atoms was set to the Wilson B-factor as a starting point. Ribosomal modifications were restrained using cif files created by phenix elbow describing the chemical properties of modified residues e.g. tRNA or rRNA modification.

In between refinement cycles, the density and the corresponding model were visualized in the program COOT (Emsley and Cowtan, 2004). Using a minimally biased difference map (F_o-F_c), missing parts of a model were modeled manually into the density, which was displayed as positive difference map. Additional information and wrongly modeled parts were surrounded by a negative density and removed. The model was refined against the processed data set over several cycles, maintaining values for R and R_{free} factor to stay in a different range of under 5% and making sure that their values decrease with each refinement cycle. The MolProbity server was used to validate the geometry of the structure (Chen et al., 2010).

3.10 Cryo-Electron microscopy (cryo-EM)

Cryo-EM is a method used to study the structure of large biomolecules and has proven to be a valuable tool for the study the underlying mechanism of translation as reviewed in (Razi et al., 2017). Early studies provided information on the overall shape of the ribosome including the ribosomal tunnel and tRNA binding sites as well as its large conformational changes during the translational cycle at a resolution of 25 Å (Agrawal et al., 1999; Frank et al., 1995) The recent development of direct electron detectors that allow movie collection mode and the constant improvement of processing software made it possible to obtain near-atomic resolution structures from cryo-EM data. The "Resolution revolution", as it has been called, led to the solution of structures by cryo-EM with resolutions comparable to X-ray crystallography and NMR (Kühlbrandt, 2014). Limitations of this technique include long data collection time per data set and the computational power needed for processing thousands of movies, compared to X-ray crystallography. Advantages include the low amounts of sample required and the visualization of the protein in solution which allows seeing different conformations in the same sample.

The structure is solved by shining electrons through the specimen to be observed. The electrons that are transmitted through because they have not interacted with the specimen result in 2D projections in different orientations in the ice of the sample. To prepare cryo-grids, the protein is quickly frozen at a concentration range of 5 nM to 1 µM depending on the size of the specimen in its optimal buffer. The images are processed to reconstruct the single particles followed by the interpretation of the electron density obtained.

3.10.1 Sample preparation

The desired complex was formed using the same concentrations as for the toeprinting assay (chapter 3.7) and the dilution buffer was substituted with Arg-tRNA^{Arg} to ensure that the dilution has no impact on the occupancy of the A-site tRNA. Therefore, 2.5 µM 70S *E. coli* ribosomes were incubated with 5 µM synthetic RNA (Eurogentec, Lüttich, Belgium) and 25 µM erythromycin. As erythromycin was dissolved in EtOH, the antibiotic was dried into the reaction tube prior to the complex formation. 10 µM fMKF-tRNA$_i^{Met}$ was added together with 20 µM Arg-tRNA^{Arg}. The complex was then incubated for 15 min at 37°C. As a final step, the complex was diluted to a final concentration of 240-480 nM of ribosomes in cryo-EM dilution buffer

(50 mM HEPES·KOH pH 7.5, 20 mM $Mg(CH_3CO_2)_2$, 100 mM $K(CH_3CO_2)$) in the presence of 25 µM erythromycin and 20 µM Arg-$tRNA^{Arg}$.

The sample was placed on a support surface, the grid. For this project, lacey holey carbon grids were used as the thickness of the vitreous ice was optimal to obtain high-resolution information (Cho et al., 2013). The grids are carbon coated and its hydrophobicity does not allow for a homogeneous repartition of the drop onto the grid. The hydrophobicity can be controlled, treating the grids with a low-energy plasma (Passmore and Russo, 2016). The grids were glow-discharged for 1 min with an ELMO machine (Cordouan, Pessac, France) at a pressure of $2*10^{-2}$ mbar and a charge of 2 mA.

3.5 µL of the mixture was transferred to a Lacey holey carbon coated grid, blotted for 5 s and frozen with a Vitrobot™ (FEI, Hillsboro, CA, USA). The Vitrobot™ is an automatic freezing machine that allows fast plunging of the grids into liquid ethane. The flash-freezing results in vitreous glass-like ice and prevents the formation of ice crystals. The Vitrobot™ chamber was set to 4°C and 100% humidity. The humidity ensures that water does not evaporate from the sample and change the ribosome or salt concentration within the sample. Optimal ice thickness was obtained using a blotting time of 5 s (Passmore and Russo, 2016). The grid was then clipped for insertion in an autoloader and stored in liquid nitrogen until data collection.

3.10.2 Data collection

Data were collected on the Talos™ Arctica transmission electron microscope (FEI) equipped with a Falcon III direct electron detector (FEI) at the IECB (Pessac, France). The Talos™ Arctica runs at 200 kV and has a spherical aberration of 2.7. The magnification was set to 120 k resulting in a pixel size of 1.24 Å. The grids were screened to determine the optimal distribution of the particles and thickness of the ice for data collection. The best squares were identified on the Atlas of the whole grid collected by the EPU software (FEI-Thermo). Due to the irregularity of the holes on lacey carbon grids, the software was set up to collect at regular intervals of 2 µm between spots. Regions of the squares having cracks or thick ice were avoided. A total of 5000 movies were collected, each consisting of 20 frames per second. To obtain information on the whole resolution range, a defocus range between 0.5 µm to 2.5 µm was collected.

3.10.3 Single particle reconstruction using RELION gui

During data collection, the electrons interact with the ribosome and those that pass through are being detected by the camera at the end of the microscope. The resulting micrographs are a collection of 2D projection of each molecule in solution. The particles are boxed and classified by the software according to their orientation in ice. To obtain the electron microscopy density, the 2D projections are used reconstruct the 3D object. To obtain a 3D model, the data were processed using the REgularized LIkelihood OptimizatioN (RELION 2.1) interface following the recommended protocol including slight changes (Fernandez-Leiro and Scheres, 2017; Scheres, 2012a, b).

Image processing consists of aligning movie frames by MotionCorr2 (Zheng et al., 2016; Zheng et al., 2017) and determining of defocus values and astigmatism of the aligned images using CTFFIND4 (Rohou and Grigorieff, 2015). The electron beam induces movement of the particles within the grid which leads to blurred images and thus a low-resolution reconstruction. Due to the development of direct detector, the movement can be detected over the different frames. To correct for this motion, Motioncor2 was used to align each pixel of the 20 frames per second collected. The aligned micrographs were converted into the corresponding power spectra by FOURIER transformation. The background was subtracted using a low pass filter and the obtained Thon rings were compared to theoretical values to obtain the defocus values for each image and astigmatism for further processing.

Further processing requires the selection and classification of particles. To generate references for auto-picking, 1000 to 2000 ribosome particles were selected manually from micrographs of representative defocus values and classified into 2D classes. The contrast of the images increases proportionally with increasing defocus values, thus for the auto-picking program to efficiently recognized particles it is necessary to cover the whole range when manually selecting the images. The box size was set to 340 Å which is larger than the diameter of the ribosomes. Auto-picking values were optimized for each data set. The picking threshold used, varied from 0.4-0.8 and maximum standard deviation used was 1.1-1.5 to avoid picking on the carbon. As Lacey grids were used for the analysis, some of the particles stuck to the carbon resulting in loss of information. The minimum inner particle distance was set to 120 Å to avoid picking particles on carbon.

The picked particles were extracted and downscaled by a factor of 3 to speed up the processing time. The picked particles were classified into 100 different 2D classes over 25 iteration cycles. The alignment and classification were performed using an algorithm based on maximum likelihood resulting (Scheres, 2010). To further improve the quality of the picked articles, 2D Classes that appeared to be 70S ribosomes were selected and reclassified into 100 2D classes as a second cleaning step.

The particles were re-extracted at their original box size of 320 px and used as an input for 3D auto-refinement using a low-resolution map of a bacterial ribosome. The refinement was performed using the gold-standard FSC calculations. This means that the data set was split in half and all reconstruction steps were performed independently. By comparing the reconstructions, the FOURIER shell correlation is determined and with this the resolution. As recommended the resolution cut off was set to an FSC value of 0.143. The 3D auto-refinement was performed without solvent masking to prevent overfitting. However, including the disordered solvent increases the noise resulting in a lower resolution. By removing solvent regions with the help of a mask, results directly in an increase of the FSC values and with it the resolution of the reconstruction. The resulting map was used as an input for masked 3D classification sorting all particles for the abundance of tRNAs in the A-, P- and E-site (Scheres, 2016). Therefore, a mask around the tRNAs and a mask for the ribosome without tRNAs were created. By using particle subtraction, particles were classified according to the occupancy of tRNA in the A, P or E-site These polished particles can be used as an input for further refinement.

The movement of individual particles was accounted for through movie refinement. Another important step to improve the final quality of the map is particle polishing. During data collection, in our case 20 frames per spot, the particles get damaged and loose high-resolution information. Still, low-resolution information can be necessary to improve reconstruction. Each frame gets a calculated B-factor and dependent on its value the frame gets taken into account for the final reconstruction (Scheres, 2016). The shiny particles were used for another round of 3D-refinement using a mask for the 50S subunit as the arrest peptide is located in the ribosomal exit tunnel, followed by postprocessing and the determination of the local resolution.

3.10.4 Model building

For model building and refinement the resulting *.mrc was renamed to *.ccp4. An initial model, a 2.8 Å resolution structure of a 70S *E. coli* ribosome (PDB code: 4U27, (Noeske et al., 2014)) was a rigid-body fitted into the density using the program Situs (Wriggers, 2012). In an initial fit, the whole structure is fitted into the density setting the resolution to 15 Å. The structure was divided into the same domains as used for PHENIX refine. The domains are fitted over multiple cycles into the density while increasing stepwise the resolution. This task is performed using the program "collage" within the Situs package (Wriggers, 2012).

Flexible bases were rotated into the density, the peptide and the drug were modeled using the program COOT (Emsley and Cowtan, 2004). The P-site tRNA (PDB code: 4VY5) was a rigid body fitted to the density using COOT. The backbone geometry of the rRNAs was improved using the program ERRASER (Chou et al., 2016). The resulting coordinates were refined against the map using PHENIX real space refinement (Afonine et al., 2013). To increase the amount of restrains, the input model was used as a reference model. The connection between the peptide and the tRNA was modeled as a data-link and a corresponding cif file was provided. Base pairing restraints were applied as geometry restraints. The base pairing restraints were generated using the online interface from the RNA center in Santa Cruz, CA (Laurberg et al., 2008).

3.11 Bioinformatic databases and programs

The graphics programs, Pymol (DeLano, 2010) and Chimera (Pettersen et al., 2004), were used to generate figures for structural interpretation. Sequencing data were analyzed using basic local alignment tool (BLAST, (Altschul et al., 1990)) and Multalign (Corpet, 1988). The DNA sequence for tRNA cloning was taken from the tRNA database (Leipzig, Germany, Jühling et al., 2009).

To calculate the theoretical mass spectrum, the sequence containing the modifications *proK* were taken from the MODOMICs database (Bujnicki et al., 2013; Dunin-Horkawicz et al., 2006). Next, the theoretic electrospray series were generated by Mongo Oligo mass calculator (Rozenski, 1999).

The ExPASy (The Export Protein Analysis System) online tool was used to calculate the molecular weight, extinction factors and isoelectric points (ProtParam). Nucleic acid sequences encoding for proteins were translated into the corresponding amino acid sequence using the Translate tool (Gasteiger et al., 2003).

4. Results

4.1 Proline-rich antimicrobial peptides inhibit the bacterial ribosome

Due to the increased prevalence of multidrug-resistant bacteria, the development of new therapeutic agents has become a public health priority. In this respect, proline-rich antimicrobial peptides (PrAMPs) are potent bacteriostatic agents that are effective against Gram-negative pathogens and have been the focus of numerous studies to improve their properties as potential drugs. As the name indicates, PrAMPs show a high content of prolines and at least one Pro-Arg-Pro motif which leads to a disordered conformation of the peptide in solution (Otvos, 2002). Recent studies have shown that PrAMPs, like Bac7 and Onc112, can inhibit protein biosynthesis *in vivo* and *in vitro*. In addition, these peptides can be cross-linked to, or co-purified with the bacterial ribosome (Krizsan et al., 2014; Mardirossian et al., 2014).

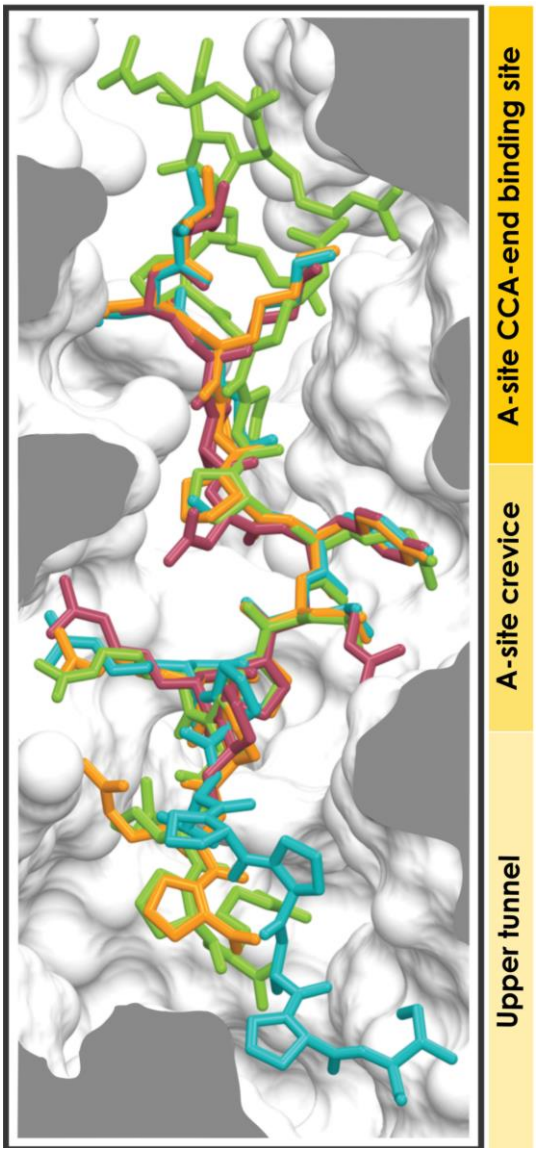

Figure 15: PrAMPs bind to the ribosomal exit tunnel. Onc112 (orange), Bac7 (green), Met I (raspberry) and Pyr bind to the ribosomal tunnel in a reverse orientation compared to the nascent chain. The binding site covers the A-site tRNA binding site, A-site crevice

The underlying molecular mechanism of action of PrAMPs was still unknown when I began my doctoral studies. To investigate this further, I solved the crystal structures of *T. thermophilus* 70S ribosomes in complex with the PrAMPs Onc112, Bac7$^{1-16}$, Pyrrhocoricin (Pyr) and metalnikowin I (Met I). The resolution ranges from 2.8 Å to 3.2 Å. Compared to the growing nascent peptide chain, PrAMPs bind in a reverse orientation to the ribosomal exit tunnel (Gagnon et al., 2016; Roy et al., 2015; Seefeldt et al., 2016; Seefeldt et al., 2015).

A network of potential hydrogen bonds and stacking interaction of the peptide with ribosomal

residues stabilize the peptides within the ribosomal exit tunnel resulting in well-structured peptides. In particular, residues Y6 and L7 in Onc112, which were previously identified to be crucial for antimicrobial activity (Knappe et al., 2011), adopt a specific conformation whereby they point into the A-site crevice. In $Bac7^{1-16}$ (green, Figure 15), the corresponding residue to Y6 is an arginine adopting a similar orientation. In Met I (raspberry, Figure 15), L7 is replaced by an arginine residue pointing in a similar orientation and allows further interactions with ribosomal residues. The orientation of these residues is stabilized by U2506 forming potential hydrogen bonds with the peptide backbone. Additional interactions of PrAMPs with ribosomal tunnel include the binding site of the 3′ CCA end of the A-site tRNA and the upper tunnel region. From the binding site, which overlaps with the incoming aminoacyl-tRNA, we could hypothesize that PrAMPs inhibit the transition from initiation towards elongation. This hypothesis was investigated biochemically by our collaborators, the group of Prof. Daniel N Wilson (Gene center, Munich by now University of Hamburg) using toeprinting, disome assays and cell-free protein synthesis assays to confirm the proposed mechanism. Our studies showed that PrAMPs inhibit specifically the transition from initiation towards elongation and destabilize the post-initiation complex.

For the C-terminus of Onc112, Met I and Pyr, no density was detected due to the reason that it might be disordered in the tunnel and potentially not necessary for the inhibition of protein biosynthesis. To investigate this further, Onc112-ΔC7/9, lacking C-terminally seven or nine amino acids, were used for bacterial growth inhibition experiments and cell-free protein synthesis assays. The results showed that PrAMPs need a certain length for the uptake by the SbmA transporter and to a certain extent for ribosome binding, which is longer than that required to inhibit protein biosynthesis. The resulting mechanism is summarized in Figure 16:

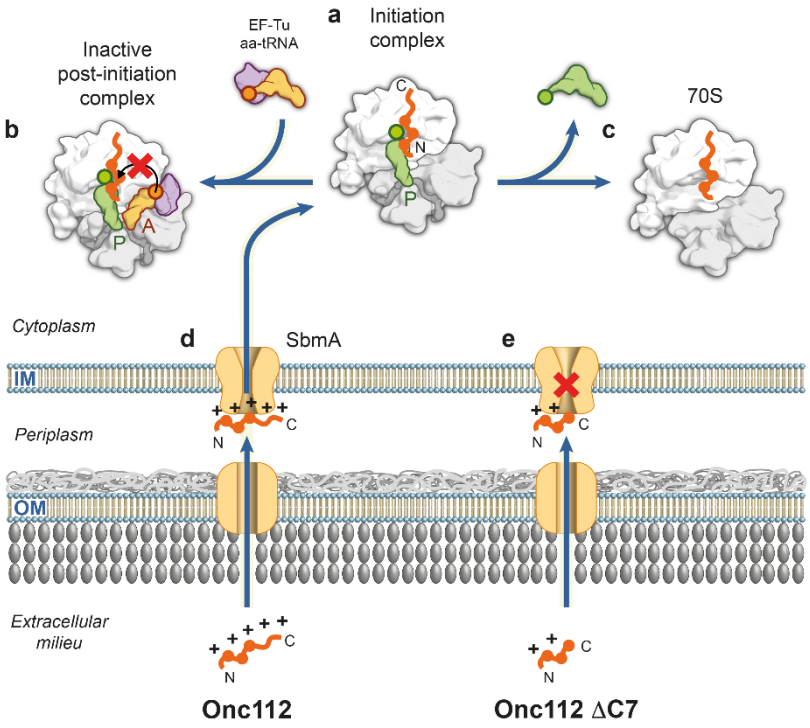

Figure 16: Mechanism of action of proline-rich antimicrobial peptides. PrAMPs are taken up specifically by Gram-negative bacteria through the SbmA transporter. C-terminal truncations lead to up-take inhibition. Inside the cytoplasm, they bind to the ribosomal exit tunnel in the reversed orientation compared to the growing peptide chain. This results in the inhibition of the transition from initiation towards elongation and destabilizes the initiation complex. Figure is taken from (Seefeldt et al., 2015).

Comparing the structure Bac7$^{1-16}$-70S *T. thermophilus* ribosome with mammalian ribosome showed that the peptide could potentially bind to the mammalian exit tunnel. Using cell extract from rabbits, we were able to show that Bac7$^{1-16}$ inhibits the eukaryotic protein biosynthesis (Seefeldt et al., 2016). However, Bac7 has been shown to be not toxic for eukaryotic cells and might be taken up during endocytosis (Tomasinsig et al., 2006) and stored after its production in granules (Zanetti et al., 1990). This prevents the contact of the Bac7 with the eukaryotic ribosome and it is believed that insect-derived PrAMPs might act in a similar way (Seefeldt et al., 2016). PrAMPs are taken up by Gram-negative bacteria via the SbmA transporter.

The work was published back to back with results from the group of Prof Thomas A. Steitz, which corroborated our findings.

nature structural & molecular biology

The proline-rich antimicrobial peptide Onc112 inhibits translation by blocking and destabilizing the initiation complex

A Carolin Seefeldt[1,2,6], Fabian Nguyen[3,6], Stéphanie Antunes[1,4,6], Natacha Pérébaskine[1,2], Michael Graf[3], Stefan Arenz[3], K Kishore Inampudi[1,2], Céline Douat[1,4], Gilles Guichard[1,4], Daniel N Wilson[3,5] & C Axel Innis[1,2]

The increasing prevalence of multidrug-resistant pathogenic bacteria is making current antibiotics obsolete. Proline-rich antimicrobial peptides (PrAMPs) display potent activity against Gram-negative bacteria and thus represent an avenue for antibiotic development. PrAMPs from the oncocin family interact with the ribosome to inhibit translation, but their mode of action has remained unclear. Here we have determined a structure of the Onc112 peptide in complex with the *Thermus thermophilus* 70S ribosome at a resolution of 3.1 Å by X-ray crystallography. The Onc112 peptide binds within the ribosomal exit tunnel and extends toward the peptidyl transferase center, where it overlaps with the binding site for an aminoacyl-tRNA. We show biochemically that the binding of Onc112 blocks and destabilizes the initiation complex, thus preventing entry into the elongation phase. Our findings provide a basis for the future development of this class of potent antimicrobial agents.

Antimicrobial peptides form a diverse group of molecules that are produced as part of the innate immune response of all multicellular organisms[1]. Among these, PrAMPs have garnered considerable attention as a possible means of countering the rapid increase in bacterial resistance to classical antibiotics[2,3]. Unlike many peptides that kill bacteria by disrupting their cell membrane, PrAMPs are transported into the cytoplasm by specialized transporters, such as SbmA in Gram-negative bacteria[4,5], where they inhibit specific intracellular targets. Given that such transport mechanisms are absent in mammalian cells, and only limited interactions with intracellular eukaryotic proteins have been detected, PrAMPs are generally considered to be nontoxic[6] and therefore an attractive alternative to existing antimicrobials. Interestingly, some PrAMPs can cross the blood-brain barrier to selectively target brain cells, thus further highlighting their potential for the treatment of cerebral infections or for brain-specific drug delivery[7].

Initial efforts to locate bacterial targets for PrAMPs led to the identification of the heat-shock protein DnaK as the prime candidate for inhibition[8]. Short proline-rich peptides (of 18–20 amino acids (aa)) such as oncocin, drosocin, pyrrhocoricin or apidaecin were previously shown to bind to this bacterial chaperone in a stereospecific manner, thus leading to the development of improved PrAMP derivatives with increased affinity for DnaK[9–12]. However, subsequent studies into the antimicrobial properties of PrAMPs[13] have suggested that these peptides are likely to use additional modes of action to inhibit growth. For example, a C-terminally truncated version of the apidaecin 1b peptide results in a loss of antimicrobial activity but no observable decrease in DnaK binding or cellular uptake[13]. Similarly, oncocin (Onc72 and Onc112) and apidaecin (Api88 and Api137) derivatives were found to inhibit the growth of a *dnaK*-deletion strain as efficiently as that of the *dnaK*-containing parental strain[14]. Further investigation revealed that these PrAMPs have an additional target within the bacterial cell, namely the ribosome[14]. Although such PrAMPs have been shown to bind to the ribosome and inhibit translation[14], the mechanism by which they inhibit translation has so far not been determined.

Here, we set out to address this issue by obtaining a 3.1-Å-resolution X-ray crystallography structure of the *Thermus thermophilus* 70S ribosome (*Tth*70S) in complex with a peptidyl (P)-site–bound deacylated $tRNA_i^{Met}$ and Onc112, a representative of the oncocin family of PrAMPs produced by the milkweed bug (*Oncopeltus fasciatus*)[15]. The structure reveals that the N-terminal residues 1–12 of Onc112 bind to the upper region of the ribosomal exit tunnel, overlapping the binding site for the CCA end of an aminoacyl (A)-site tRNA at the peptidyl transferase center. Consistently with this, we showed biochemically that Onc112 allows translation to initiate but destabilizes the initiation complex and thus prevents subsequent entry of affected ribosomes into the translation-elongation phase. Moreover, we demonstrated that although truncation of the C-terminal portion of Onc112 is dispensable for ribosome binding, it is essential for antimicrobial activity. We believe that these findings will provide an excellent basis for the design of improved antibacterial compounds, either peptidic or peptidomimetic, that inhibit translation by targeting the ribosomal exit tunnel.

[1]Institut Européen de Chimie et Biologie, Université de Bordeaux, Pessac, France. [2]INSERM U869, Bordeaux, France. [3]Gene Center, Department of Biochemistry, University of Munich, Munich, Germany. [4]Université de Bordeaux, CNRS, Institut Polytechnique de Bordeaux, UMR 5248, Institut de Chimie et Biologie des Membranes et des Nano-objets (CBMN), Pessac, France. [5]Center for Integrated Protein Science Munich (CiPSM), University of Munich, Munich, Germany. [6]These authors contributed equally to this work. Correspondence should be addressed to C.A.I. (axel.innis@inserm.fr) or D.N.W. (wilson@lmb.uni-muenchen.de).

Received 26 February; accepted 22 April; published online 18 May 2015; doi:10.1038/nsmb.3034

RESULTS

Onc112 binds in a reverse orientation within the exit tunnel

We obtained the structure herein referred to as *Tth*70S–Onc112 by soaking the 19-aa Onc112 peptide (VDKPPYLPRPRPPRrIYNr-NH_2, in which r denotes D-arginine) into crystals of *Tth*70S ribosomes in complex with a P-site–bound deacylated $tRNA_i^{Met}$ and a short mRNA (**Table 1**). Using a minimally biased $F_o - F_c$ map calculated after refinement of a model comprising *Tth*70S ribosomes, $tRNA_i^{Met}$ and mRNA but lacking Onc112, we could see clear density that could be attributed to the N-terminal two-thirds of the Onc112 peptide (**Fig. 1**). Interestingly, the peptide is bound inside the tunnel with a reversed orientation relative to the growing polypeptide chain during protein synthesis, i.e., with its N terminus located near the peptidyl transferase center and its C terminus extending into the exit tunnel toward the constriction formed by ribosomal proteins L4 and L22. Despite the reversed orientation, the location of the Onc112 peptide overlaps to varying extents with the path of nascent polypeptide chains that have been visualized within the ribosomal tunnel[16–18] (**Supplementary Fig. 1**). The conformation of Onc112 bound to the ribosome is extended, in a manner similar to but distinct from that observed previously for oncocin in complex with DnaK[10] (**Supplementary Fig. 2**). Our CD studies suggest that, in solution, the Onc112 peptide adopts an essentially random conformation, with short stretches of poly(Pro)II helix, specifically, 6% α-helix, 54% random coil, 30% PPII and 6% β-sheet (**Supplementary Fig. 3**).

Table 1 Data collection and refinement statistics

	*Tth*70S–Onc112[a]
Data collection	
Space group	$P2_12_12_1$
Cell dimensions	
a, *b*, *c* (Å)	209.30, 452.29, 624.12
α, β, γ (°)	90.0, 90.0, 90.0
Resolution (Å)	50 (3.1)
R_{merge}	25.5% (166.4%)
$I / \sigma I$	5.47 (0.95)
Completeness (%)	99.1 (98.8)
Redundancy	3.8 (3.6)
Refinement	
Resolution (Å)	3.1
No. reflections	3,999,403
R_{work} / R_{free}	23.08 / 27.13
No. atoms	
Protein / RNA	91,758 / 195,737
Ligand/ion	2,333
B factors	
Protein / RNA	64.81 / 63.15
Ligand/ion	51.31
r.m.s. deviations	
Bond lengths (Å)	0.015
Bond angles (°)	0.809

[a]Structure determined from a single crystal.

Interaction between Onc112 and 23S rRNA of the exit tunnel

Comparison of the *Tth*70S–Onc112 structure with that of a *Tth*70S ribosome featuring $tRNA_i^{Met}$ bound to the P site[19] reveals that several nucleotides of the 23S rRNA undergo a conformational change upon binding of Onc112 to the ribosome (**Fig. 2a**). U2506 shifts to occupy a position similar to that observed upon binding of aminoacyl-tRNA to the A site of the ribosome[20,21]. In the presence of Onc112, U2585, which is very flexible in many crystal structures, adopts a defined position similar to that modeled in the structure of a vacant *Escherichia coli* 70S ribosome[22]. In addition, A2062 shifts to provide space for Onc112, adopting a similar conformation to that observed previously in the presence of the ErmBL nascent chain[23]. Thus, binding of Onc112 to the ribosome is accompanied by an induced fit involving several 23S rRNA nucleotides that are generally known for their dynamic behavior within the peptidyl transferase center and ribosomal tunnel.

Electron density for the Onc112 peptide was strongest for residues Val1–Pro8 and became weaker after Pro10, thus making it difficult to model the peptide beyond Pro12 (**Fig. 1**). We observed three sets of interactions between the N-terminal 10 aa of Onc112 and nucleotides of the 23S rRNA (**Fig. 2b**). The first set involves aa 1–3 of Onc112 and encompasses eight potential hydrogen-bond interactions (**Fig. 2b**,**c**). Val1 of Onc112 can form three hydrogen bonds with nucleotides of the 23S rRNA; two via its α-amine to the N3 atom of C2573 and the O3′ atom of C2507; and one via its carbonyl oxygen to the N4 atom of C2573. Three additional hydrogen bonds are possible between the side chain carboxylic acid of Asp2 and the N1 and N2 atoms of G2553 or the 2′-OH of C2507. The positively charged side chain of Lys3 extends into a negatively charged cavity, displacing a hydrated magnesium ion that is present at this site in other *Tth*70S ribosome structures[20], and it interacts with the backbone phosphates of A2453 (**Fig. 2c**) and U2493 (not shown). Substitution of Val1, Asp2 and especially Lys3 by alanine in Onc72 leads to a loss of antimicrobial activity[10], whereas, as expected, a D2E mutant of Onc112 retained both *in vitro* and *in vivo* activity (**Supplementary Fig. 4**). The K3A substitution in Onc72 reduced its ribosome binding affinity by a factor of 4.3 and lowered the half-maximal inhibitory concentration (IC_{50}) for *in vitro* translation more than 18-fold[14].

The second set of interactions involves the side chains of Tyr6 and Leu7 of Onc112 (**Fig. 2b**,**d**). The aromatic side chain of Tyr6 establishes a π-stacking interaction with C2452 of the 23S rRNA (**Fig. 2d**). In addition, the side chain hydroxyl of Tyr6 hydrogen-bonds with an undetermined ion that is coordinated by the backbone phosphate of U2506 and the O2 atoms of C2452 and U2504. The hydrophobic cavity occupied by the Tyr6 side chain also accommodates the side chain of Leu7 of Onc112, which packs against the phenol moiety of Tyr6, whereas the backbone of Leu7 forms two hydrogen bonds with U2506 (**Fig. 2b**,**d**). The compact hydrophobic core formed by Tyr6 and Leu7 is likely to be key in anchoring the Onc112 peptide to the tunnel because mutagenesis experiments have shown that alanine substitution of either residue in Onc72 reduces the ribosome binding affinity by a factor of 7 and results in a complete loss of inhibitory activity on translation *in vitro*[14]. In contrast, mutation of Leu7 in Onc112 to cyclohexylalanine, which would preserve the hydrophobic environment, resulted in retention of inhibitory activity on translation *in vitro* but unexpectedly led to a loss of antimicrobial activity (**Supplementary Fig. 4**).

Additional interactions with the ribosome encompass the PRPRP motif of Onc112 (**Fig. 2b**) and include a π-stacking interaction between the guanidino group of Arg9 of Onc112 and the base of C2610 (**Fig. 2e**). Although substitution of Arg11 with alanine in Onc72 also reduces the ribosome binding affinity and inhibitory properties of the peptide[14], we observed very little density for the side chain of this residue, thus suggesting that it could be important for the overall electrostatic properties of the peptide rather than for a defined interaction with the ribosome (**Fig. 1**). The high conservation of the 23S rRNA nucleotides that comprise the ribosome-binding site of Onc112 is consistent with the broad spectrum of antimicrobial

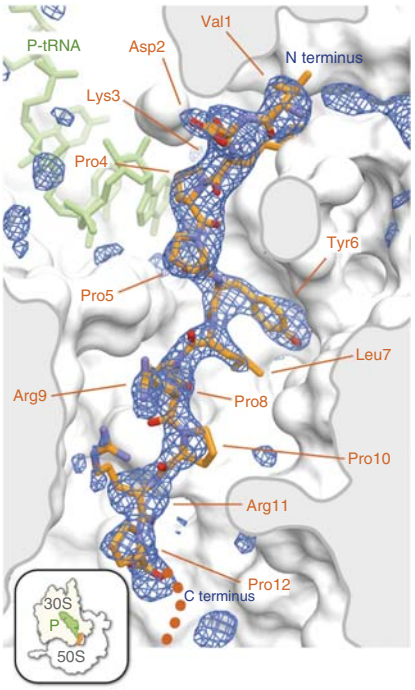

Figure 1 Onc112-binding site within the exit tunnel of the ribosome. Transverse section of the exit tunnel of the *Tth*70S ribosome showing the binding site for the Onc112 peptide (orange). Minimally biased $F_o - F_c$ difference map contoured at +3.0σ (blue) is observable for the first 12 amino acids of Onc112 (**VDKPPYLPRPRP**PRrIYNr-NH_2; residues 1–12 are bold and underlined). Initiator $tRNA_i^{Met}$ bound at the P site is shown in green. Inset shows the view chosen to display the Onc112 peptide relative to the complete 70S ribosome.

activity displayed by this and related PrAMPs against a range of Gram-negative bacteria[10,24].

Onc112 allows translation to initiate but blocks elongation

Comparison of the *Tth*70S–Onc112 structure with that of the *Tth*70S ribosome in the preattack state of peptide-bond formation[20] indicated that the binding of Onc112 to the ribosome would prevent accommodation of the CCA end of an incoming aminoacyl-tRNA via steric occlusion of the ribosomal A site at the peptidyl transferase center (**Fig. 3a**). Indeed, Asp2 of Onc112 directly interacts with G2553, a residue located within helix H92 of the 23S rRNA, termed the A loop, that normally stabilizes the A site tRNA at the peptidyl transferase center via Watson-Crick base-pairing with nucleotide C75 of its CCA end.

In order to determine the step of translation that Onc112 inhibits, we performed cell-free protein synthesis and monitored the location of the ribosomes on the mRNA (**Fig. 3b** and **Supplementary Data Set 1**), by using toe-printing assays[25,26]. In the absence of Onc112 or antibiotic, ribosomes were able to initiate at the AUG start codon and translate through the open reading frame, but they became trapped on the downstream isoleucine codon because isoleucine was omitted from the translation mix. In the presence of the antibiotics clindamycin or thiostrepton, ribosomes accumulated at the start codon and could not translate down to the isoleucine codon because these antibiotics prevent delivery and/or accommodation of the first aminoacyl-tRNA directly following the initiation codon[27]. We observed similar results when performing the toe-printing assay with increasing concentrations of the Onc112 peptide, namely a loss of the band corresponding to ribosomes stalled at the isoleucine codon and an increase in the band corresponding to the ribosomes accumulating at the start codon. These findings indicate that Onc112 allows subunit joining and formation of the 70S initiation complex but prevents accommodation of the first aminoacyl-tRNA at the A site, as suggested by steric overlap between Onc112 and an A-site tRNA (**Fig. 3a**). This contrasts with a bona fide translation-initiation inhibitor, such as edeine, which interferes with the stable binding of fMet-$tRNA_i^{Met}$ to the 30S subunit and thus prevents 70S initiation-complex formation[28], in agreement with the lack of a toe-print band at the start codon in the presence of edeine (**Fig. 3b**).

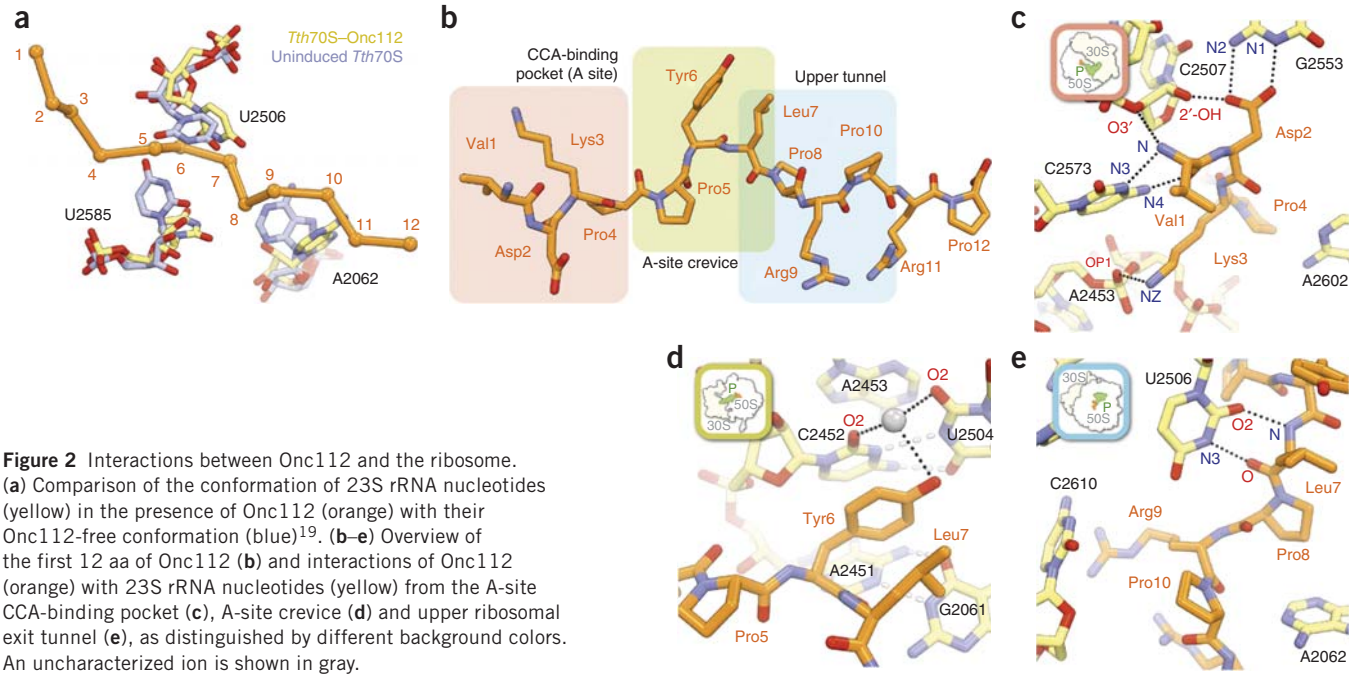

Figure 2 Interactions between Onc112 and the ribosome. (**a**) Comparison of the conformation of 23S rRNA nucleotides (yellow) in the presence of Onc112 (orange) with their Onc112-free conformation (blue)[19]. (**b**–**e**) Overview of the first 12 aa of Onc112 (**b**) and interactions of Onc112 (orange) with 23S rRNA nucleotides (yellow) from the A-site CCA-binding pocket (**c**), A-site crevice (**d**) and upper ribosomal exit tunnel (**e**), as distinguished by different background colors. An uncharacterized ion is shown in gray.

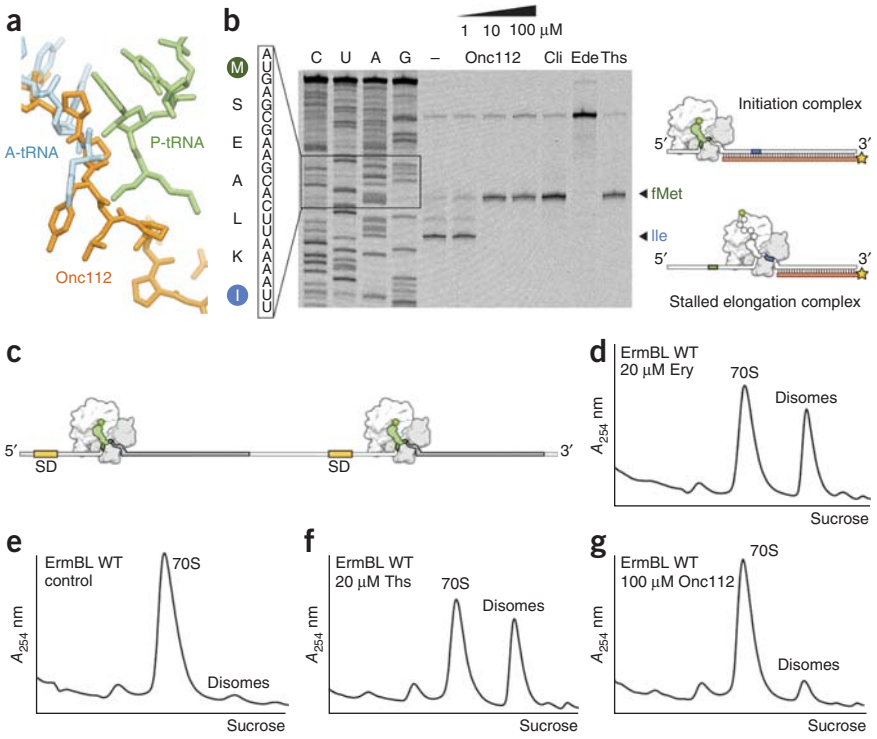

Figure 3 Onc112 blocks and destabilizes the initiation complex. (**a**) Structural comparison of Phe-tRNA^{Phe} (blue) in the A site and fMet-tRNA$_i^{Met}$ in the P site (green)[20] with the binding site of Onc112 (orange). (**b**) Toe-printing assay performed in the absence (–) or presence of increasing concentrations (1 μM, 10 μM and 100 μM) of Onc112, 50 μM clindamycin (Cli), 50 μM edeine (Ede) or 100 μM thiostrepton (Ths). Sequencing lanes for C, U, A and G and the sequence surrounding the toe-print bands (arrows) when ribosomes accumulate at the AUG start codon (green, initiation complex) or the isoleucine codon (blue, stalled elongation complex) are included for reference, as illustrated graphically. The uncropped gel image for the toe-printing assay is in **Supplementary Data Set 1**. (**c**–**g**) Schematic (**c**) showing the dicistronic ErmBL mRNA that was used to monitor disome formation with sucrose gradients in the presence (**d**) or absence (**e**) of 20 μM erythromycin (Ery) or the presence of 20 μM thiostrepton (**f**) or 100 μM Onc112 (**g**). In **c**, SD denotes the Shine-Dalgarno sequence. *A*, absorbance.

Onc112 destabilizes the translation-initiation complex

We noticed that the toe-print bands at the start codon in the presence of Onc112 were consistently weaker than those observed in the presence of clindamycin or thiostrepton (**Fig. 3b** and data not shown), thus suggesting that Onc112 may also perturb the placement of fMet-tRNA$_i^{Met}$ at the P site. In the *Tth*70S–Onc112 structure, the P-site tRNA is uncharged, and its terminal A76 residue undergoes a conformational change that positions it ~3.4 Å away from the Onc112 peptide. *In vivo*, however, we would expect fMet-tRNA$_i^{Met}$ to bind to the peptidyl transferase center in the same manner as in the *Tth*70S ribosome preattack complexes[20], such that the formyl group of the fMet moiety would sterically clash with residues Tyr6 and Leu7 of the Onc112 peptide (**Fig. 3a**). Consequently, we used sucrose gradients to monitor disome formation upon translating a dicistronic ErmBL mRNA *in vitro*, in order to investigate the stability of the translation-initiation complex formed in the presence of Onc112 (**Fig. 3c**–**g**). As a positive control, we performed translation in the presence of the macrolide antibiotic erythromycin, which acts synergistically with the ErmBL polypeptide chain within the ribosomal tunnel to stall translation at a specific site on the mRNA[29]. Because the mRNA was dicistronic, two stalled ribosomes on a single mRNA led to the formation of disomes that could be visualized on a sucrose gradient (**Fig. 3d**), as shown previously[16,23]. We observed negligible disome formation in the absence of erythromycin because the ribosomes rapidly translated the short ORF and were released from the mRNA (**Fig. 3e**). As expected, thiostrepton, which allows 70S initiation-complex formation but prevents elongation (**Fig. 3b**), also led to efficient disome formation (**Fig. 3f**). In contrast, the presence of Onc112, even at concentrations as high as 100 μM, resulted in only a small increase in disomes (**Fig. 3g**). This leads us to suggest that the 70S initiation complexes formed in the presence of Onc112 are unstable, presumably because the Onc112 peptide encroaches onto fMet-tRNA$_i^{Met}$, thus causing it to dissociate from the ribosome under the nonequilibrium conditions (centrifugation and sucrose density) used in the disome assay.

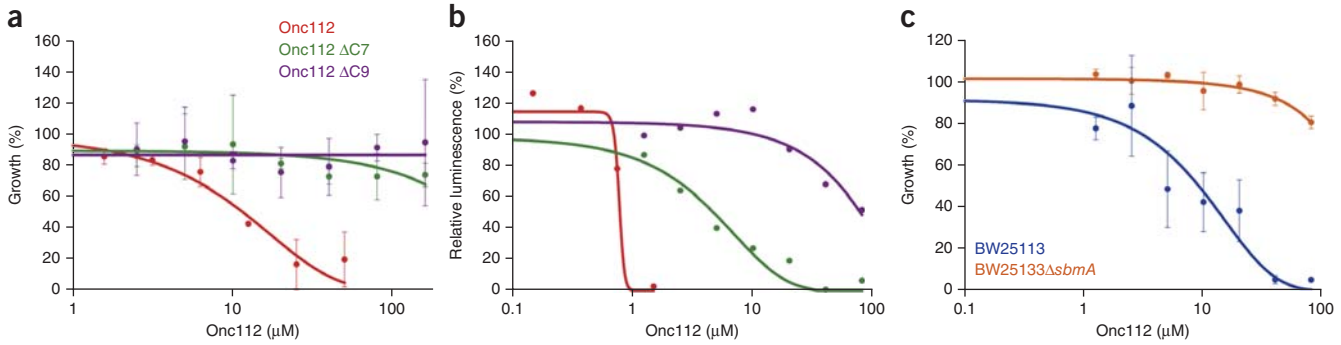

Figure 4 Characterization of Onc112, its C-terminally truncated derivatives and its membrane transporter in Gram-negative bacteria. (**a**,**b**) Effect of Onc112 (red) and C-terminally truncated Onc112 derivatives Onc112 ΔC7 (green) and Onc112 ΔC9 (purple) on overnight growth of *E. coli* strain BL21(DE3) (**a**) and the luminescence resulting from the *in vitro* translation of Fluc (**b**). (**c**) Effect of Onc112 on overnight growth of *E. coli* strain BW25113 (blue) or BW25113Δ*sbmA* (orange). In **a** and **c**, error bars represent mean ± s.d. for triplicate experiments, whereas the experiment in **b** was performed in duplicate, with the plotted points representing the mean value. The growth or luminescence measured in the absence of peptide was assigned as 100% in all cases.

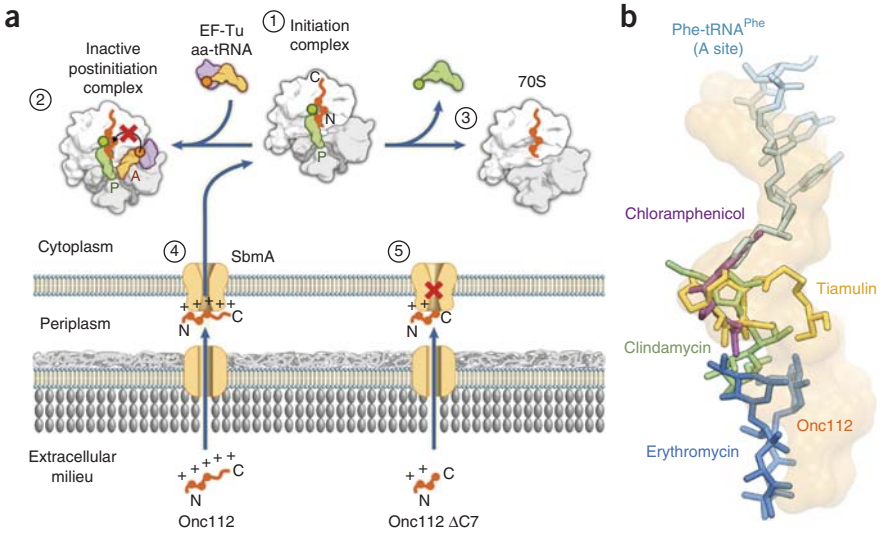

Figure 5 Mechanism of action and overlap of Onc112 with antibiotics that target the large subunit of the ribosome. (**a**) Model for the mechanism of action of Onc112. (1) Onc112 binds within the exit tunnel of the ribosome with a reverse orientation relative to a nascent polypeptide chain. (2) Onc112 allows formation of a translation-initiation complex but prevents accommodation of the aminoacyl-tRNA (aa-tRNA) at the A site of the peptidyl transferase center. (3) The initiation complex is destabilized, thus leading to dissociation of the fMet-tRNA$_i^{Met}$ from the P site. Although full-length Onc112 can efficiently penetrate the bacterial cell membrane by using the SbmA transporter (4), C-terminal truncation of Onc112 reduces its antimicrobial activity (5), presumably owing to impaired uptake. (**b**) Relative binding position of Onc112 (orange) on the ribosome, compared with those of well-characterized translation inhibitors chloramphenicol (purple)[32,33], clindamycin (green)[33], tiamulin (yellow)[34] and erythromycin (blue)[32,33] as well as an A site–bound Phe-tRNA^{Phe} (ref. 20).

Onc112 C terminus is needed for uptake, not ribosome binding

The lack of density for the C terminus of Onc112 (residues 13–19) hinted that this region is dispensable for ribosome binding, yet its high degree of conservation suggested that it may nevertheless be necessary for antimicrobial activity. In order to assess the role of the C-terminal region of Onc112, we prepared truncated versions of this peptide, Onc112 ΔC7 and Onc112 ΔC9, which lacked the last 7 and 9 aa, respectively. We then determined the half-minimal inhibitory concentration (MIC$_{50}$) for the growth of *E. coli* strain BL21(DE3) in the presence of full-length Onc112 and compared it with those of the truncated Onc112 ΔC7 and Onc112 ΔC9 derivatives (**Fig. 4a**). As expected, the full-length Onc112 displayed good activity, inhibiting growth with an MIC$_{50}$ of 10 μM, a value similar to that reported previously[14]. In contrast, truncation of 7 or 9 aa from the C terminus of Onc112 led to a complete loss of inhibitory activity, even at concentrations above 100 μM (**Fig. 4a**). To ascertain whether the truncated Onc112 peptides could still bind to the ribosome and inhibit translation, we monitored *in vitro* translation of firefly luciferase (Fluc) by measuring luminescence after 60 min of translation in the presence of increasing concentrations of either full-length Onc112 or the truncated Onc112 ΔC7 and Onc112 ΔC9 derivatives (**Fig. 4b**). As expected, the full-length peptide displayed excellent activity, inhibiting translation of Fluc with an IC$_{50}$ of 0.8 μM (**Fig. 4b**), a value similar to that reported when the same system was used for well-characterized translation inhibitors such as chloramphenicol[30]. In contrast to their lack of antimicrobial activity (**Fig. 4a**), both truncated Onc112 peptides displayed some inhibitory activity with the *in vitro*–translation system (**Fig. 4b**), albeit with a reduced efficiency relative to that of full-length Onc112. Specifically, the Onc112 ΔC7 peptide consisting of residues 1–12 of Onc112 had an IC$_{50}$ of 5 μM, which was only six times greater than that of full-length Onc112, a result consistent with our structure-based prediction that these residues comprise the major ribosome binding determinants. In contrast, the Onc112 ΔC9 peptide consisting of aa 1–10 of Onc112 had an IC$_{50}$ of 80 μM, which was 16 times greater than that of Onc112 ΔC7 and two orders of magnitude greater than that of full-length Onc112. These results illustrate the contribution of Arg11 to efficient ribosome binding and translation inhibition, as reported previously[14].

Although the inner-membrane protein SbmA has been shown to be responsible for the uptake of the eukaryotic PrAMPs Bac7 and PR39 (refs. 4,5), the only insect PrAMP tested so far was apidaecin Ib[4]. In order to assess the role of SbmA in the uptake of Onc112, we compared the growth of an *E. coli* strain lacking the *sbmA* gene (Δ*sbmA*) with the parental strain BW25113 in the presence of increasing concentrations of Onc112 (**Fig. 4c**). As expected, the full-length Onc112 displayed excellent activity against the susceptible SbmA-containing parental strain, inhibiting growth with an MIC$_{50}$ of 8 μM (**Fig. 4c**), a value similar to that observed with the BL21(DE3) strain (**Fig. 4a**). In contrast, the Δ*sbmA* strain displayed increased resistance to Onc112, such that even with 100 μM Onc112, growth was reduced by only 20% (**Fig. 4c**). These findings indicate that SbmA is indeed necessary for the uptake of Onc112 into Gram-negative bacteria, such as *E. coli*, and provide further support for the proposition that the SbmA transporter is involved in the mechanism of action of the entire group of the PrAMPs[4].

DISCUSSION

From our structural and biochemical data, we propose a model to explain the mechanism by which PrAMPs such as oncocin inhibit translation (**Fig. 5a**). We have shown that the binding of Onc112 to the ribosomal exit tunnel allows formation of the 70S initiation complex but prevents accommodation of the aminoacyl-tRNA into the A site (**Fig. 5a**, steps 1 and 2). Additionally, we propose that Onc112 destabilizes the postinitiation complex by inducing dissociation of fMet-tRNA$_i^{Met}$ from the P site (**Fig. 5a**, step 3). Finally, our data also suggest that positively charged residues distributed along the entire length of the Onc112 sequence are necessary for ensuring the efficient SbmA-mediated uptake of Onc112 into the cell, whereas residues from the N-terminal moiety of Onc112 are responsible for targeting this peptide to the ribosome (**Fig. 5a**, steps 4 and 5). We believe that this mechanism of action is likely to be the same for other PrAMPs, such as drosocin, pyrrhocoricin and apidaecin, which share many of the residues of Onc112 that are important for its ribosome binding and antimicrobial function.

The binding site for Onc112 within the ribosomal exit tunnel overlaps with the binding sites for a majority of the antibiotics that target the large subunit of the ribosome (**Fig. 5b**), such as the

chloramphenicols, pleuromutilins (for example, tiamulin) and lincosamides (for example, clindamycin), which inhibit peptide-bond formation by preventing the correct positioning of the tRNA substrates, as well as the macrolides (for example, erythromycin), which abort translation by interfering with the movement of the nascent polypeptide chain through the ribosomal exit tunnel[27]. Given the substantial spatial overlap that exists between the binding sites for these antibiotics and the regions of the tunnel that interact with Onc112 (**Fig. 5b**) and presumably with several other PrAMPs, it appears likely that such antimicrobial peptides represent a vast, untapped resource for the development of new therapeutics. Several strategies have been pursued to design improved or entirely new antimicrobials that target the exit tunnel of the ribosome[31]. One approach consists of modifying existing antibiotics to create semisynthetic compounds that possess enhanced antimicrobial properties, including better affinity for mutated or modified ribosomes, the ability to evade drug modification or degradation pathways, increased solubility, improved uptake and reduced efflux. Other strategies involve designing chimeric antibiotics from drugs with adjacent binding sites (for example, macrolide-chloramphenicol or linezolid-sparsomycin) or developing entirely new scaffolds, as exemplified by the oxazolidinone linezolid. The ability to produce new scaffolds based on peptides, such as Onc112, that display potent activity against a diverse range of Gram-negative bacteria represents an exciting avenue for the development of future antimicrobials.

METHODS

Methods and any associated references are available in the online version of the paper.

Accession codes. Coordinates and structure factors have been deposited in the Protein Data Bank under accession code 4ZER.

Note: Any Supplementary Information and Source Data files are available in the online version of the paper.

ACKNOWLEDGMENTS

We thank the staff at the European Synchrotron Radiation Facility (beamline ID-29) for help during data collection and B. Kauffmann and S. Massip at the Institut Européen de Chimie et Biologie for help with crystal freezing and screening. We also thank C. Mackereth for discussions and advice. This research was supported by grants from the Agence Nationale pour la Recherche (ANR-14-CE09-0001 to C.A.I., G.G. and D.N.W.), Région Aquitaine (2012-13-01-009 to C.A.I.), the Fondation pour la Recherche Médicale (AJE201133 to C.A.I.), the European Union (PCIG14-GA-2013-631479 to C.A.I.), the CNRS (C.D.) and the Deutsche Forschungsgemeinschaft (FOR1805, WI3285/4-1 and GRK1721 to D.N.W.). Predoctoral fellowships from the Direction Générale de l'Armement and Région Aquitaine (S. Antunes) and INSERM and Région Aquitaine (A.C.S.) are gratefully acknowledged.

AUTHOR CONTRIBUTIONS

A.C.S. performed structure solution, model building and analysis. N.P. prepared and crystallized ribosomes. N.P. and C.A.I. collected X-ray crystallography data. F.N. performed growth and *in vitro*–translation inhibition assays. S. Antunes and C.D. synthesized the peptides and performed NMR, CD and electrospray ionization high-resolution MS experiments. M.G. performed toe-printing assays. S. Arenz performed disome assays. K.K.I. prepared $tRNA_i^{Met}$. G.G., D.N.W. and C.A.I. designed experiments, interpreted data and wrote the manuscript.

COMPETING FINANCIAL INTERESTS

The authors declare no competing financial interests.

1. Wang, G. *et al.* Antimicrobial peptides in 2014. *Pharmaceuticals (Basel)* **8**, 123–150 (2015).
2. Casteels, P., Ampe, C., Jacobs, F., Vaeck, M. & Tempst, P. Apidaecins: antibacterial peptides from honeybees. *EMBO J.* **8**, 2387–2391 (1989).
3. Li, W. *et al.* Proline-rich antimicrobial peptides: potential therapeutics against antibiotic-resistant bacteria. *Amino Acids* **46**, 2287–2294 (2014).
4. Mattiuzzo, M. *et al.* Role of the *Escherichia coli* SbmA in the antimicrobial activity of proline-rich peptides. *Mol. Microbiol.* **66**, 151–163 (2007).
5. Runti, G. *et al.* Functional characterization of SbmA, a bacterial inner membrane transporter required for importing the antimicrobial peptide Bac7 (1–35). *J. Bacteriol.* **195**, 5343–5351 (2013).
6. Hansen, A., Schäfer, I., Knappe, D., Seibel, P. & Hoffmann, R. Intracellular toxicity of proline-rich antimicrobial peptides shuttled into mammalian cells by the cell-penetrating peptide penetratin. *Antimicrob. Agents Chemother.* **56**, 5194–5201 (2012).
7. Stalmans, S. *et al.* Blood-brain barrier transport of short proline-rich antimicrobial peptides. *Protein Pept. Lett.* **21**, 399–406 (2014).
8. Otvos, L. *et al.* Interaction between heat shock proteins and antimicrobial peptides. *Biochemistry* **39**, 14150–14159 (2000).
9. Czihal, P. *et al.* Api88 is a novel antibacterial designer peptide to treat systemic infections with multidrug-resistant Gram-negative pathogens. *ACS Chem. Biol.* **7**, 1281–1291 (2012).
10. Knappe, D. *et al.* Rational design of oncocin derivatives with superior protease stabilities and antibacterial activities based on the high–resolution structure of the oncocin–DnaK complex. *ChemBioChem* **12**, 874–876 (2011).
11. Zahn, M. *et al.* Structural studies on the forward and reverse binding modes of peptides to the chaperone DnaK. *J. Mol. Biol.* **425**, 2463–2479 (2013).
12. Zahn, M. *et al.* Structural identification of DnaK binding sites within bovine and sheep bactenecin Bac7. *Protein Pept. Lett.* **21**, 407–412 (2014).
13. Berthold, N. & Hoffmann, R. Cellular uptake of apidaecin 1b and related analogs in Gram-negative bacteria reveals novel antibacterial mechanism for proline-rich antimicrobial peptides. *Protein Pept. Lett.* **21**, 391–398 (2014).
14. Krizsan, A. *et al.* Insect-derived proline-rich antimicrobial peptides kill bacteria by inhibiting bacterial protein translation at the 70 S ribosome. *Angew. Chem. Int. Ed. Engl.* **53**, 12236–12239 (2014).
15. Schneider, M. & Dorn, A. Differential infectivity of two *Pseudomonas* species and the immune response in the milkweed bug, *Oncopeltus fasciatus* (Insecta: Hemiptera). *J. Invertebr. Pathol.* **78**, 135–140 (2001).
16. Arenz, S. *et al.* Drug sensing by the ribosome induces translational arrest via active site perturbation. *Mol. Cell* **56**, 446–452 (2014).
17. Bischoff, L., Berninghausen, O. & Beckmann, R. Molecular basis for the ribosome functioning as an L-tryptophan sensor. *Cell Reports* **9**, 469–475 (2014).
18. Shao, S. & Hegde, R.S. Reconstitution of a minimal ribosome-associated ubiquitination pathway with purified factors. *Mol. Cell* **55**, 880–890 (2014).
19. Jenner, L. *et al.* Structural basis for potent inhibitory activity of the antibiotic tigecycline during protein synthesis. *Proc. Natl. Acad. Sci. USA* **110**, 3812–3816 (2013).
20. Polikanov, Y.S., Steitz, T.A. & Innis, C.A. A proton wire to couple aminoacyl-tRNA accommodation and peptide-bond formation on the ribosome. *Nat. Struct. Mol. Biol.* **21**, 787–793 (2014).
21. Schmeing, T.M., Huang, K.S., Strobel, S.A. & Steitz, T.A. An induced-fit mechanism to promote peptide bond formation and exclude hydrolysis of peptidyl-tRNA. *Nature* **438**, 520–524 (2005).
22. Schuwirth, B.S. *et al.* Structures of the bacterial ribosome at 3.5 A resolution. *Science* **310**, 827–834 (2005).
23. Arenz, S. *et al.* Molecular basis for erythromycin-dependent ribosome stalling during translation of the ErmBL leader peptide. *Nat. Commun.* **5**, 3501 (2014).
24. Knappe, D. *et al.* Oncocin (VDKPPYLPRPRPPRRIYNR-NH2): a novel antibacterial peptide optimized against Gram-negative human pathogens. *J. Med. Chem.* **53**, 5240–5247 (2010).
25. Hartz, D., McPheeters, D.S., Traut, R. & Gold, L. Extension inhibition analysis of translation initiation complexes. *Methods Enzymol.* **164**, 419–425 (1988).
26. Starosta, A.L. *et al.* Translational stalling at polyproline stretches is modulated by the sequence context upstream of the stall site. *Nucleic Acids Res.* **42**, 10711–10719 (2014).
27. Wilson, D.N. The A–Z of bacterial translation inhibitors. *Crit. Rev. Biochem. Mol. Biol.* **44**, 393–433 (2009).
28. Dinos, G. *et al.* Dissecting the ribosomal inhibition mechanisms of edeine and pactamycin: the universally conserved residues G693 and C795 regulate P-site RNA binding. *Mol. Cell* **13**, 113–124 (2004).
29. Vázquez-Laslop, N., Ramu, H., Klepacki, D., Kannan, K. & Mankin, A.S. The key function of a conserved and modified rRNA residue in the ribosomal response to the nascent peptide. *EMBO J.* **29**, 3108–3117 (2010).
30. Starosta, A.L. *et al.* Interplay between the ribosomal tunnel, nascent chain, and macrolides influences drug inhibition. *Chem. Biol.* **17**, 504–514 (2010).
31. Wilson, D.N. Ribosome-targeting antibiotics and mechanisms of bacterial resistance. *Nat. Rev. Microbiol.* **12**, 35–48 (2014).
32. Bulkley, D., Innis, C.A., Blaha, G. & Steitz, T.A. Revisiting the structures of several antibiotics bound to the bacterial ribosome. *Proc. Natl. Acad. Sci. USA* **107**, 17158–17163 (2010).
33. Dunkle, J.A., Xiong, L., Mankin, A.S. & Cate, J.H. Structures of the *Escherichia coli* ribosome with antibiotics bound near the peptidyl transferase center explain spectra of drug action. *Proc. Natl. Acad. Sci. USA* **107**, 17152–17157 (2010).
34. Schlünzen, F., Pyetan, E., Fucini, P., Yonath, A. & Harms, J.M. Inhibition of peptide bond formation by pleuromutilins: the structure of the 50S ribosomal subunit from *Deinococcus radiodurans* in complex with tiamulin. *Mol. Microbiol.* **54**, 1287–1294 (2004).

ONLINE METHODS

Peptide synthesis. Commercially available reagents were used throughout without purification. *N*,*N*-dimethylformamide (DMF, peptide synthesis–quality grade) was purchased from Carlo Erba, and piperidine and trifluoroacetic acid (TFA) were purchased from Alfa Aesar. Rink amide PS resin was purchased from PolyPeptide Laboratories. *N*,*N*′-diisopropylcarbodiimide (DIC), Oxyma and all standard *N*-Fmoc–protected L and D amino acids were purchased from Iris Biotech. *N*-Fmoc-cyclohexylalanine-OH (Fmoc-Cha-OH) was purchased from PolyPeptide laboratories. RP-HPLC–quality acetonitrile (CH_3CN, Sigma-Aldrich) and MilliQ water were used for RP-HPLC analyses and purification. Analytical RP-HPLC analyses were performed on a Dionex U3000SD with a Macherey-Nagel Nucleodur column (4.6 × 100 mm, 3 µm) at a flow rate of 1 ml min^{-1} at 50 °C. The mobile phase was composed of 0.1% (v/v) TFA-H_2O (solvent A) and 0.1% TFA-CH_3CN (solvent B). Purification was performed on a Gilson GX-281 with a Macherey-Nagel Nucleodur VP250/21 100–5 C18ec column (21 × 250 mm, 5 µm) at a flow rate of 20 mL min^{-1}. The solid-phase syntheses of peptides were conducted on an automated Liberty Blue System synthesizer (CEM µWaves S.A.S.). ^1H NMR spectra were recorded on a DPX-400 NMR spectrometer (Bruker Biospin) with a vertical 9.4T narrow-bore/ultrashield magnet operating at 400 MHz for ^1H observation by means of a 5-mm direct QNP $^1H/^{13}C/^{31}P/^{19}F$ probe with gradient capabilities (**Supplementary Fig. 5**). ESI-MS analyses were carried out on a Thermo Exactive from the Mass Spectrometry Laboratory at the European Institute of Chemistry and Biology (UMS 3033–IECB), Pessac, France (**Supplementary Fig. 5**).

All peptides were synthesized on Rink Amide PS resin (0.79 mmol/g) with a five-fold excess of reagents for the coupling step (0.2 M *N*-Fmoc–amino acid solution (in DMF) with 0.5 M DIC (in DMF) and 1.0 M Oxyma (in DMF)). Coupling of *N*-Fmoc–protected L- and D-arginine-OH was performed twice at 25 °C without microwaves for 1,500 s. Other amino acid couplings were performed first at 90 °C, 170 W, 115 s then at 90 °C, 30 W, 110 s. Fmoc removal was performed with a solution of 20% piperidine in DMF at 75 °C with 155 W for 15 s then 90 °C, 35 W, 50 s. After completion of the synthesis, the peptide resin was washed three times with DCM. Cleavage was performed by treatment with 5 mL of a freshly prepared TFA/TIS/H_20 solution for 240 min at room temperature. The resin was then filtered off, and the TFA solution was concentrated under reduced pressure. The crude products were precipitated as TFA salts in the presence of Et_2O and purified with the appropriate gradient (10–30% of B in 20 min) by semipreparative RP-HPLC. The compounds were freeze dried, and TFA was exchanged with HCl by two repetitive freeze-drying cycles in 0.1 N HCl solution[35].

The list of peptides prepared for this study and details concerning their synthesis is as follows:

Onc112. H-Val-Asp-Lys-Pro-Pro-Tyr-Leu-Pro-Arg-Pro-Arg-Pro-Pro-Arg-(D-Arg)-Ile-Tyr-Asn-(D-Arg)-NH_2 (2,389.85 g mol^{-1}). Synthesis of Onc112 (0.1-mmol scale): 24 mg (10% yield); RP HPLC t_R 4.11 min (gradient 10–50% of B in 10 min); ESI HRMS (*m/z*): found 1,195.70 $[M + 2H]^{2+}$, 797.47 $[M +3 H]^{3+}$, 598.35 $[M + 4H]^{4+}$, and 478.88 $[M + 5H]^{5+}$.

Onc112 ΔC7. H-Val-Asp-Lys-Pro-Pro-Tyr-Leu-Pro-Arg-Pro-Arg-Pro-NH_2 (1,433.73 g mol^{-1}). Synthesis of Onc112 ΔC7 (0.15-mmol scale): 79.4 mg (37% yield); RP HPLC t_R 3.54 min (gradient 10–50% of B in 10 min); ESI HRMS (*m/z*): $[M + H]^+$ calcd for $C_{67}H_{108}H_{20}O_{15}$, 1,433.83758 found 1,433.84017, with 717.42 $[M + 2H]^{2+}$ and 478.61 $[M + 3H]^{3+}$.

Onc112 ΔC9. H-Val-Asp-Lys-Pro-Pro-Tyr-Leu-Pro-Arg-Pro-NH_2 (1,180.42 g mol^{-1}). Synthesis of *Onc112 ΔC9.* (0.1-mmol scale): 22.6 mg (19% yield); RP HPLC t_R 4.78 min (gradient 10–50% of B in 10 min); ESI HRMS (*m/z*): $[M + H]^+$ calcd for $C_{56}H_{89}H_{15}O_{13}$, 1,180.63370 found 1,180.68368, with $[M + 2H]^{2+}$ 590.84 and $[M + 3H]^{3+}$ 394.23.

Onc112 D2E. H-Val-Glu-Lys-Pro-Pro-Tyr-Leu-Pro-Arg-Pro-Arg-Pro-Pro-Arg-(D-Arg)-Ile-Tyr-Asn-(D-*Arg*)-NH_2 (2,403.88 g mol^{-1}). Synthesis of Onc112 D2E (0.05-mmol scale): 11.6 mg (10% yield); RP HPLC t_R 5.75 min (gradient 10–50% of B in 10 min); ESI HRMS (*m/z*): found 1316.70 $[M + 2H]^{2+}$, 840.14 $[M + 3H]^{3+}$ and 601.86 $[M + 4H]^{4+}$.

Onc112 L7Cha. H-Val-Asp-Lys-Pro-Pro-Tyr-Cha-Pro-Arg-Pro-Arg-Pro-Pro-Arg-(D-Arg)-Ile-Tyr-Asn-(D-Arg)-NH_2 (2,429.92 g mol^{-1}). Synthesis of Onc112 L7Cha (0.05-mmol scale): 6.9 mg (6% yield); RP HPLC t_R 5.28 min (gradient 10–50% of B in 10 min); ESI HRMS (*m/z*): found 1,252.18 $[M + 2H]^{2+}$, 822.80 $[M + 3H]^{3+}$ and 608.36 $[M + 4H]^{4+}$.

CD spectroscopy. CD spectra of peptides were recorded on a J-815 Jasco spectropolarimeter (Jasco France). Data are expressed in terms of total molar ellipticity in deg cm^2 $dmol^{-1}$. CD spectra for the Onc112 peptide were acquired at four different concentrations in phosphate buffer (pH 7.6, 10 mM) between 180 and 280 nm with a rectangular quartz cell with a path length of 1 mm (Hellma 110-QS 1 mm) averaging over two runs. Secondary-structure proportion was estimated from the CD spectra with the deconvolution program CDFriend (S. Buchoux (Unité de Génie Enzymatique et Cellulaire, UMR 6022 CNRS-Université de Picardie Jules Verne) and E. Dufourc (Université de Bordeaux, CNRS, Institut Polytechnique de Bordeaux, UMR 5248 Institut de Chimie et Biologie des Membranes et des Nano-objets (CBMN); available upon request), unpublished). This program uses standard curves obtained for each canonical structure (α-helix, β-sheet, helix-polyproline type II and random coil) with L_iK_j (alternated hydrophobic leucine and hydrophilic/charged lysine residues) peptides of known length, secondary structure and CD spectra. The program implements a simulated annealing algorithm to get the best combination of α-helix, β-sheet, helix-II and random coil that exhibits the lowest normalized r.m.s. deviation with respect to the experimental spectrum[36–38]. The algorithm yielded the following assessment for the Onc112 peptide: 54% random coil, 30% helix-PPII, 6% α-helix and 6% β-sheet content.

Purification of *T. thermophilus* 70S ribosomes. *Tth*70S ribosomes were purified as described previously[39] and resuspended in buffer containing 5 mM HEPES-KOH, pH 7.5, 50 mM KCl, 10 mM NH_4Cl, and 10 mM $Mg(CH_3COO)_2$ to yield a final concentration of 26–32 mg/mL. For storage, *Tth*70S ribosomes were flash frozen in liquid nitrogen and kept at −80 °C.

Preparation of mRNA and $tRNA_i^{Met}$. Synthetic mRNA with the sequence 5′-GGC AAG GAG GUA AAA AUG CGU UUU CGU-3′ was obtained from Eurogentec. This mRNA contains a Shine-Dalgarno sequence and an AUG start codon followed by several additional codons. *E. coli* $tRNA_i^{Met}$ was overexpressed in *E. coli* HB101 cells and purified as described previously[40].

Complex formation. A ternary complex containing *Tth*70S ribosomes, mRNA and deacylated $tRNA_i^{Met}$ was formed by mixing of 5 µM *Tth*70S ribosomes with 10 µM mRNA and incubating at 55 °C for 10 min. For the next step, 20 µM $tRNA_i^{Met}$ was added, and the mixture was incubated at 37 °C for 10 min. Before the complexes for crystallization were used, the sample was incubated at room temperature for at least 15 min. All complexes were centrifuged briefly before use for crystallization. The final buffer conditions were 5 mM HEPES-KOH, pH 7.6, 50 mM KCl, 10 mM NH_4Cl and 10 mM $Mg(CH_3COO)_2$.

Crystallization. Published conditions were used as a starting point for screening crystallization conditions by vapor diffusion in sitting-drop trays at 20 °C (refs. 20,39). Crystallization drops consisted of 3 µl of ternary complex and 3–4 µl of reservoir solution containing 100 mM Tris-HCl, pH 7.6, 2.9% (v/v) PEG 20000, 7–10% (v/v) MPD and 175 mM arginine. Crystals appeared within 2–3 d and grew to ~1,000 × 100 × 100 µm within 7–8 d. For cryoprotection, the concentration of MPD was increased in a stepwise manner to yield a final concentration of 40% (v/v). The ionic composition during cryoprotection was 100 mM Tris-HCl, pH 7.6, 2.9% (v/v) PEG 20000, 50 mM KCl, 10 mM NH_4Cl and 10 mM $Mg(CH_3COO)_2$. *Tth*70S–Onc112 complexes were obtained by soaking 10–20 µM of Onc112 dissolved in the final cryoprotection solution overnight at 20 °C. Crystals were then flash frozen in a nitrogen cryostream at 80 K for subsequent data collection.

Data collection and processing. Diffraction data were collected at beamline ID29 of the European Synchrotron Radiation Facility (ESRF) in Grenoble, France. A complete data set was obtained by merging 0.1° oscillation data collected at 100 K with a wavelength of 0.97625 Å from multiple regions of the same crystal. Initial data processing, including integration and scaling, were performed with XDS[41]. All of the data collected could be indexed in the $P2_12_12_1$ space group, with unit-cell dimensions around 210 Å × 450 Å × 625 Å and an asymmetric unit containing two copies of the *Tth*70S ribosome.

Model building and refinement. Initial phases were obtained by molecular replacement performed with Phaser[42]. The search model was obtained from

a high-resolution structure of the *Tth*70S ribosome (PDB 4Y4O). Restrained crystallographic refinement was carried out with Phenix[43] and consisted of a single cycle of rigid-body refinement followed by multiple cycles of positional and individual *B*-factor refinement. Rigid bodies comprised four domains from the small 30S subunit (head, body, spur and helix h44) and three domains from the large 50S subunit (body, L1 stalk and the C terminus of ribosomal protein L9). Noncrystallographic symmetry restraints between the two copies of the *Tth*70S ribosome in the asymmetric unit were also applied during refinement. After confirming that a single tRNA was bound to the P site and that additional density corresponding to the Onc112 peptide was visible inside the exit tunnel in a minimally biased $F_o - F_c$ map, a model for Onc112 was built with Rapper[44] and Coot[45]. The models for the tRNA and mRNA were obtained from a high-resolution structure of the *Tth*70S ribosome preattack complex (PDB 1VY4). Further refinement and model validation were carried out in Phenix and on the MolProbity server[46], respectively. In the final model, 0.65% of protein residues were classified as Ramachandran outliers, and 94.38% had favorable backbone conformations.

***In vitro*–translation assay.** The inhibition of firefly luciferase (Fluc) synthesis by Onc112 was assessed with an *E. coli* lysate–based transcription-translation coupled assay (RTS100, 5Prime) as described previously for other translational inhibitors[30]. Briefly, 6-µL reactions, with or without Onc112/antibiotic were mixed according to the manufacturer's description and incubated for 1 h at 30 °C with shaking (1,000 r.p.m.). 1 µL of each reaction was stopped with 7 µL kanamycin (50 µg/µl) and then diluted with 40 µL of luciferase assay substrate (Promega) into a white 96-well chimney flat-bottom microtiter plate (Greiner). The luminescence was then measured with a Tecan Infinite M1000 plate reader. Relative values were determined by defining the luminescence value of the sample without inhibitor as 100%.

Growth inhibition assays. Determination of the minimal inhibitory concentration (MIC) of Onc112 was performed as described previously for other antibiotics[30]. Specifically, an overnight culture of *E. coli* strain BL21(DE3) (Invitrogen), BW25113 or Keio deletion strain BW25113Δ*sbmA* (plate 61, well 10E)[47] was diluted 1:100 to an OD_{600} of ~0.02, and 200 µL of the diluted cells was then transferred into individual wells of a 96-well plate (Sarstedt). Either 10 µL of Onc112, Onc112 derivative peptide or water was added to each well. Plates were then incubated overnight in a thermomixer (Eppendorf) at 37 °C/350 r.p.m. The OD_{600} was measured in a Tecan Infinite M1000 plate reader, and the relative growth was calculated by defining the growth of samples without antibiotic as 100%.

Toe-printing assay. The position of the ribosome on the mRNA was monitored with a toe-printing assay based on an *in vitro*–coupled transcription-translation system with the PURExpress *in vitro* protein synthesis kit (NEB)[26]. Briefly, each translation reaction consisted of 1 µL solution A, 0.5 µL Δisoleucine + tryptophan amino acid mixture, 0.5 µL tRNA mixture, 1.5 µL solution B, 1 µL (0.5 pmol) hns40aa template: (5′-*ATTAATACGACTCACTATAGGG*ATATAAGGAGGAAAACAT**ATG**AGCGAAGCACTTAAA**ATT**CTGAACAACATCCGTACTCTTCGTGCGCAGGCAAGAGAATGTACACTTGAAACGCTGGAAGAAATGCTGGAAAAATTAGAAGTTGTTGTTAACGAACGTTGGATTTTG**TAA**GTGATAGAATTCTATC*GTTAATAAGCAAAATTCATTATAACC*-3′, with start codon ATG, catch isoleucine codon ATT and stop codon TAA in bold, the hns40aa ORF underlined and primer-binding sites in italics) and 0.5 µL additional agents (nuclease-free water, Onc112 or antibiotics). Translation was performed in the absence of isoleucine at 37 °C for 15 min at 500 r.p.m. in 1.5-mL reaction tubes. Ile-tRNA aminoacylation was further prevented by the use of the Ile-tRNA synthetase inhibitor mupirocin. After translation, 2 pmol Alexa647-labeled NV-1 toe-print primer (5′-GGTTATAATGAATTTTGCTTATTAAC-3′) was added to each reaction and incubated at 37 °C without shaking for 5 min. Reverse transcription was performed with 0.5 µL of AMV RT (NEB), 0.1 µL dNTP mix (10 mM) and 0.4 µL Pure System Buffer and incubated at 37 °C for 20 min. Reverse transcription was quenched and RNA degraded by addition of 1 µL 10 M NaOH and incubation for at least 15 min at 37 °C and then was neutralized with 0.82 µL of 12 M HCl. 20 µL toe-print resuspension buffer and 200 µL PN1 buffer were added to each reaction before treatment with a QIAquick Nucleotide Removal Kit (Qiagen). The Alexa647-labeled DNA was then eluted from the QIAquick columns with 80 µL of nuclease-free water. A vacuum concentrator was used to vaporize the solvent, and the Alexa647-labeled DNA was then dissolved into 3.5 µL of formamide dye. The samples were heated to 95 °C for 5 min before being applied onto a 6% polyacrylamide (19:1) sequencing gel containing 7 M urea. Gel electrophoresis was performed at 40 W and 2,000 V for 2 h. The GE Typhoon FLA9500 imaging system was subsequently used to scan the polyacrylamide gel.

Disome formation assay. The disome formation assay was performed as described previously[16,23]. Briefly, *in vitro* translation of the 2xermBL construct was performed with the Rapid Translation System RTS 100 *E. coli* HY Kit (Roche). Translations were carried out for 1 h at 30 °C and then analyzed on 10–55% sucrose-density gradients (in a buffer containing 50 mM HEPES-KOH, pH 7.4, 100 mM KOAc, 25 mM $Mg(OAc)_2$ and 6 mM β-mercaptoethanol) by centrifugation at 154,693*g* (SW-40 Ti, Beckman Coulter) for 2.5 h at 4 °C.

Figure preparation. Figures showing electron density and atomic models were generated with PyMOL (http://www.pymol.org/).

35. Brazier, S.P., Ramesh, B., Haris, P.I., Lee, D.C. & Srai, S.K. Secondary structure analysis of the putative membrane-associated domains of the inward rectifier K^+ channel ROMK1. *Biochem. J.* **335**, 375–380 (1998).
36. Jean-François, F. *et al.* Variability in secondary structure of the antimicrobial peptide Cateslytin in powder, solution, DPC micelles and at the air-water interface. *Eur. Biophys. J.* **36**, 1019–1027 (2007).
37. Jobin, M.L. *et al.* The enhanced membrane interaction and perturbation of a cell penetrating peptide in the presence of anionic lipids: toward an understanding of its selectivity for cancer cells. *Biochim. Biophys. Acta* **1828**, 1457–1470 (2013).
38. Khemtémourian, L., Buchoux, S., Aussenac, F. & Dufourc, E.J. Dimerization of Neu/Erb2 transmembrane domain is controlled by membrane curvature. *Eur. Biophys. J.* **36**, 107–112 (2007).
39. Selmer, M. *et al.* Structure of the 70S ribosome complexed with mRNA and tRNA. *Science* **313**, 1935–1942 (2006).
40. Schmitt, E., Blanquet, S. & Mechulam, Y. Crystallization and preliminary X-ray analysis of *Escherichia coli* methionyl-tRNAMetf formyltransferase complexed with formyl-methionyl-tRNAMetf. *Acta Crystallogr. D Biol. Crystallogr.* **55**, 332–334 (1999).
41. Kabsch, W. Xds. *Acta Crystallogr. D Biol. Crystallogr.* **66**, 125–132 (2010).
42. McCoy, A.J. *et al.* Phaser crystallographic software. *J. Appl. Crystallogr.* **40**, 658–674 (2007).
43. Adams, P.D. *et al.* PHENIX: a comprehensive Python-based system for macromolecular structure solution. *Acta Crystallogr. D Biol. Crystallogr.* **66**, 213–221 (2010).
44. de Bakker, P.I., DePristo, M.A., Burke, D.F. & Blundell, T.L. *Ab initio* construction of polypeptide fragments: accuracy of loop decoy discrimination by an all-atom statistical potential and the AMBER force field with the Generalized Born solvation model. *Proteins* **51**, 21–40 (2003).
45. Emsley, P. & Cowtan, K. Coot: model-building tools for molecular graphics. *Acta Crystallogr. D Biol. Crystallogr.* **60**, 2126–2132 (2004).
46. Chen, V.B. *et al.* MolProbity: all-atom structure validation for macromolecular crystallography. *Acta Crystallogr. D Biol. Crystallogr.* **66**, 12–21 (2010).
47. Baba, T. *et al.* Construction of *Escherichia coli* K-12 in-frame, single-gene knockout mutants: the Keio collection. *Mol. Syst. Biol.* **2**, 2006.0008 (2006).

doi:10.1038/nsmb.3034

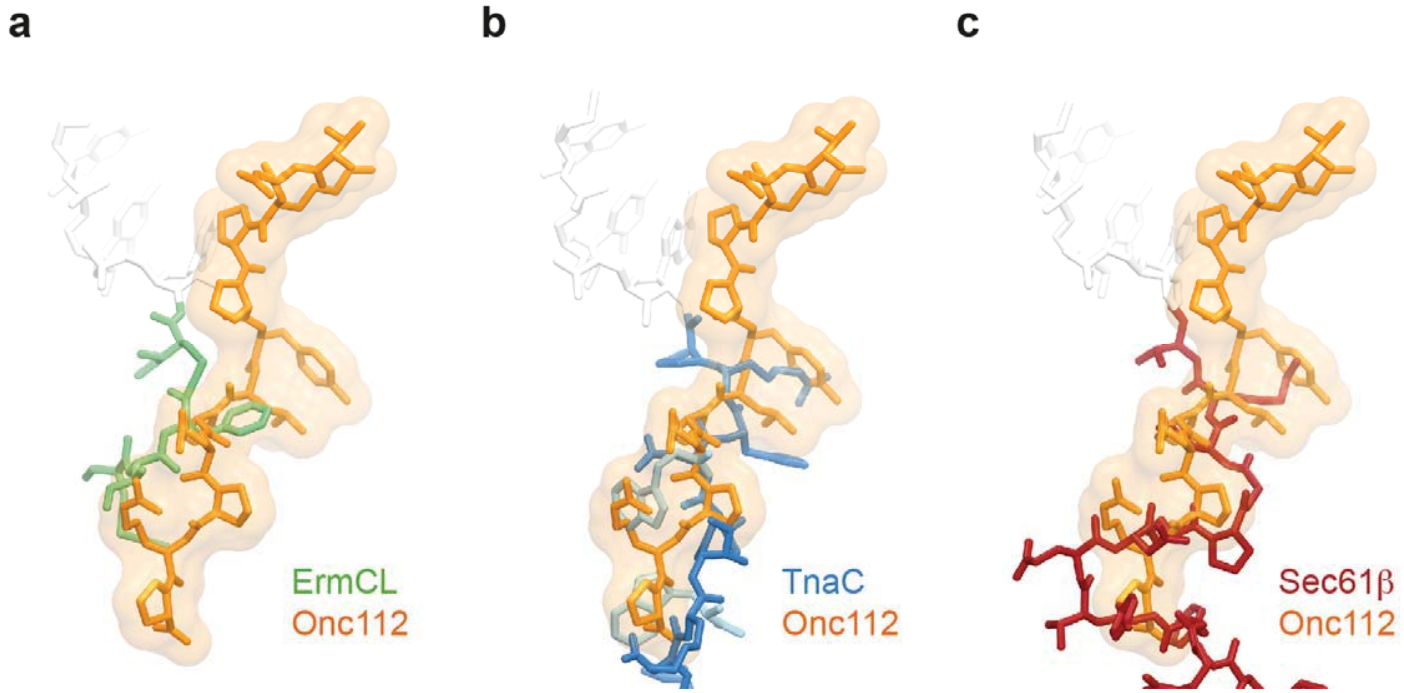

Supplementary Figure 1

Overlap of Onc112 with nascent polypeptide chains in the ribosome exit tunnel.

Comparison of the binding position of Onc112 (orange) with (a) ErmCL (green), (b) TnaC (blue) and Sec61β (red) nascent chains. In (a)-(c), the CCA-end of the P-tRNA is shown in white and in (b) the two tryptophan molecules are in cyan.

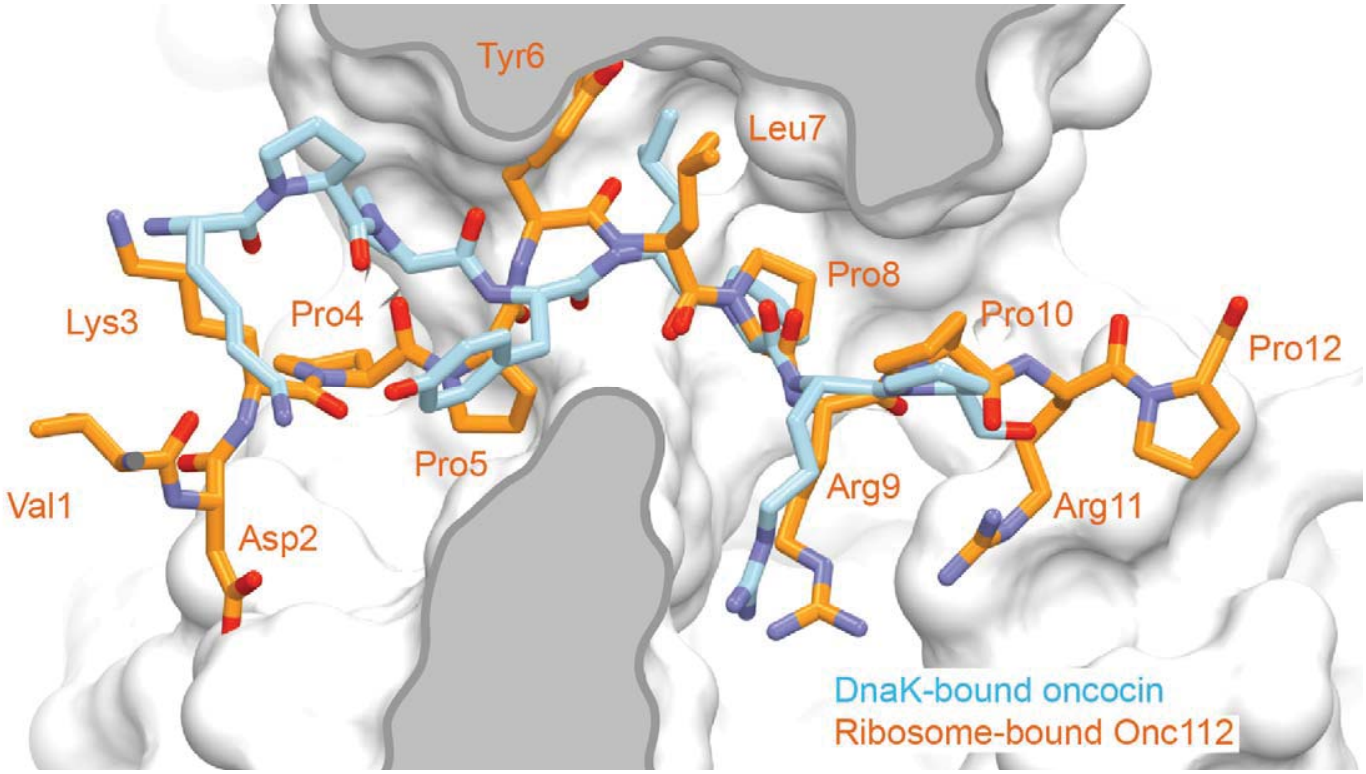

Supplementary Figure 2

Comparison of *Tth*70S–Onc112 with the DnaK–oncocin complex.

The conformation of residues Lys3–Pro10 of the Oncocin peptide O2 (cyan, VD**KPPYLPRP**RPPROIYNO–NH_2, where O represents ornithine) in complex with DnaK (white surface representation) was compared with residues Val1–Pro12 of Onc112 (orange) from the ribosome-bound Onc112 structure.

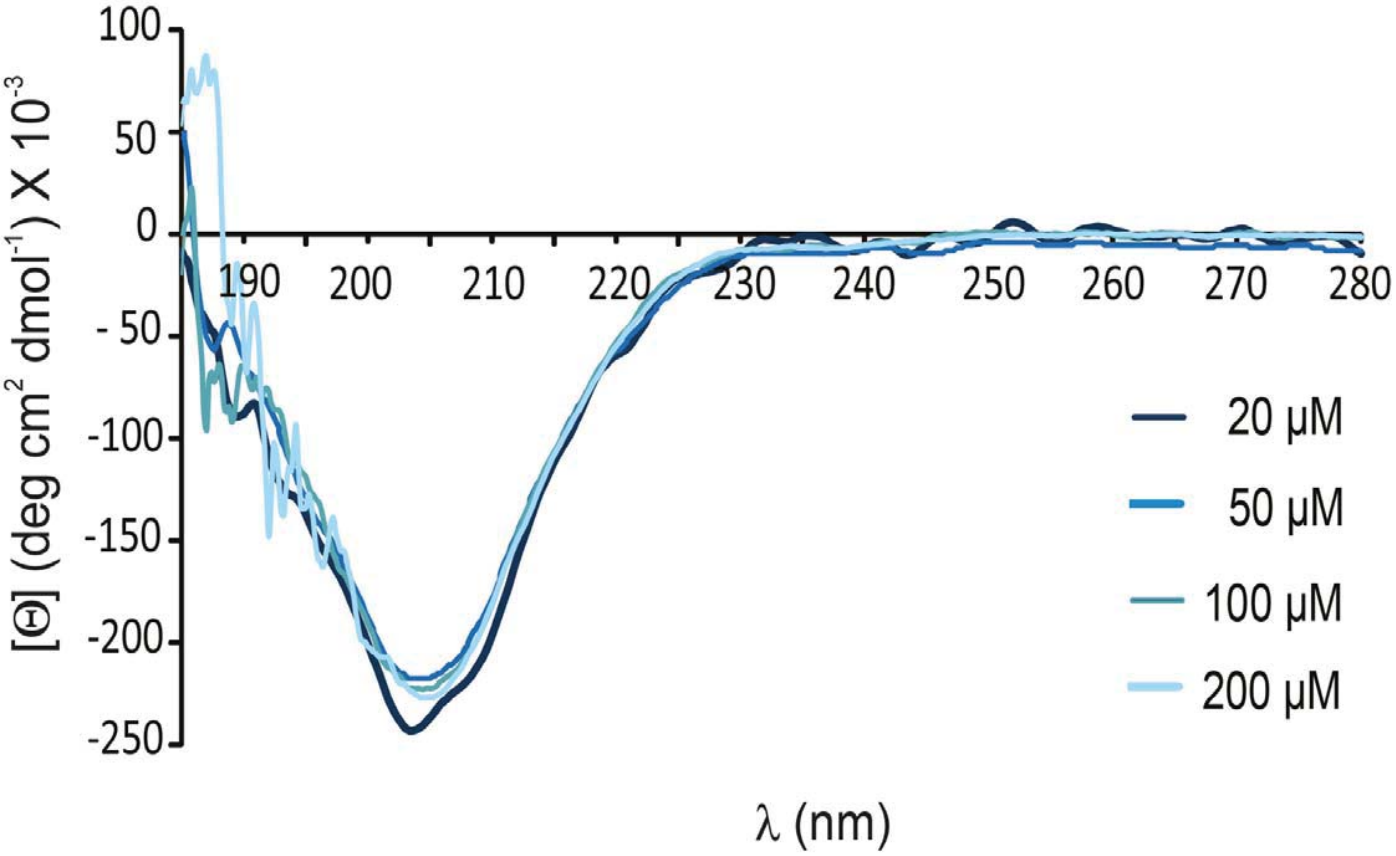

Supplementary Figure 3

Conformation of the Onc112 peptide in solution.

Far-UV circular dichroism (CD) spectra of the Onc112 peptide at concentrations ranging from 20 to 200 μM.

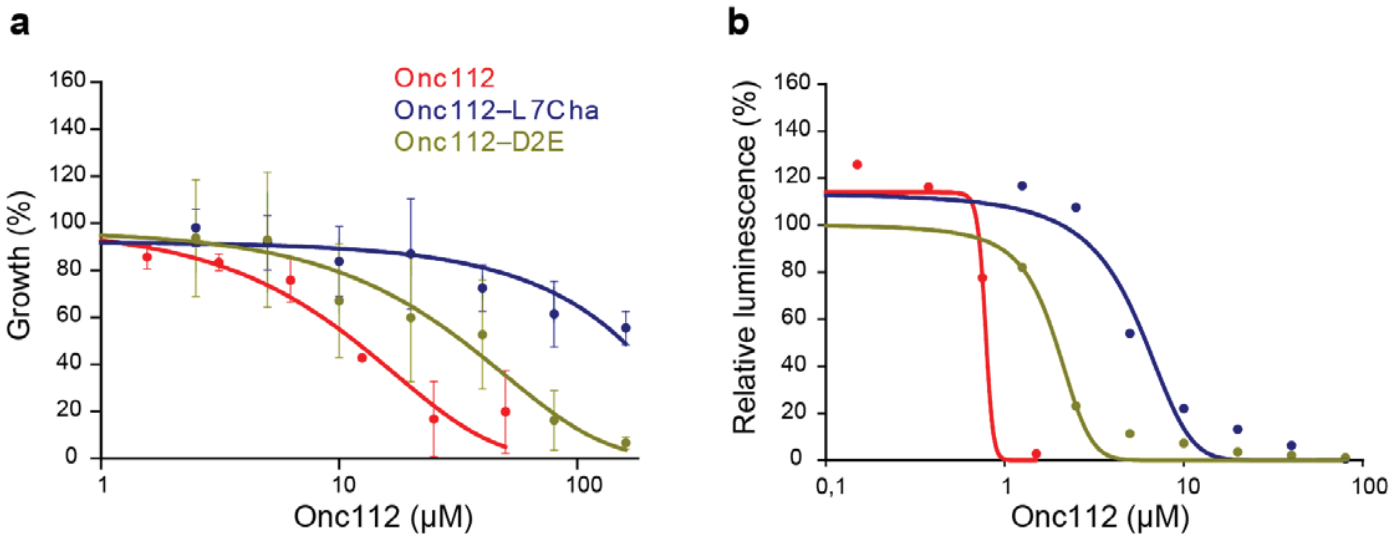

Supplementary Figure 4

Inhibitory activity of Onc112 peptide derivatives.

(a-b) Effect of Onc112 (red) and Onc112 derivatives Onc112–L7Cha (blue) and Onc112–D2E (olive) on (a) the overnight growth of *E. coli* strain BL21(DE3) and (b) the luminescence resulting from the *in vitro* translation of firefly luciferase (Fluc). In (a), the error bars represent the standard deviation (s.d.) from the mean for a triplicate experiment (n=3). In (b), the experiment was performed in duplicate (n=2). The growth or luminescence measured in the absence of peptide was assigned as 100%.

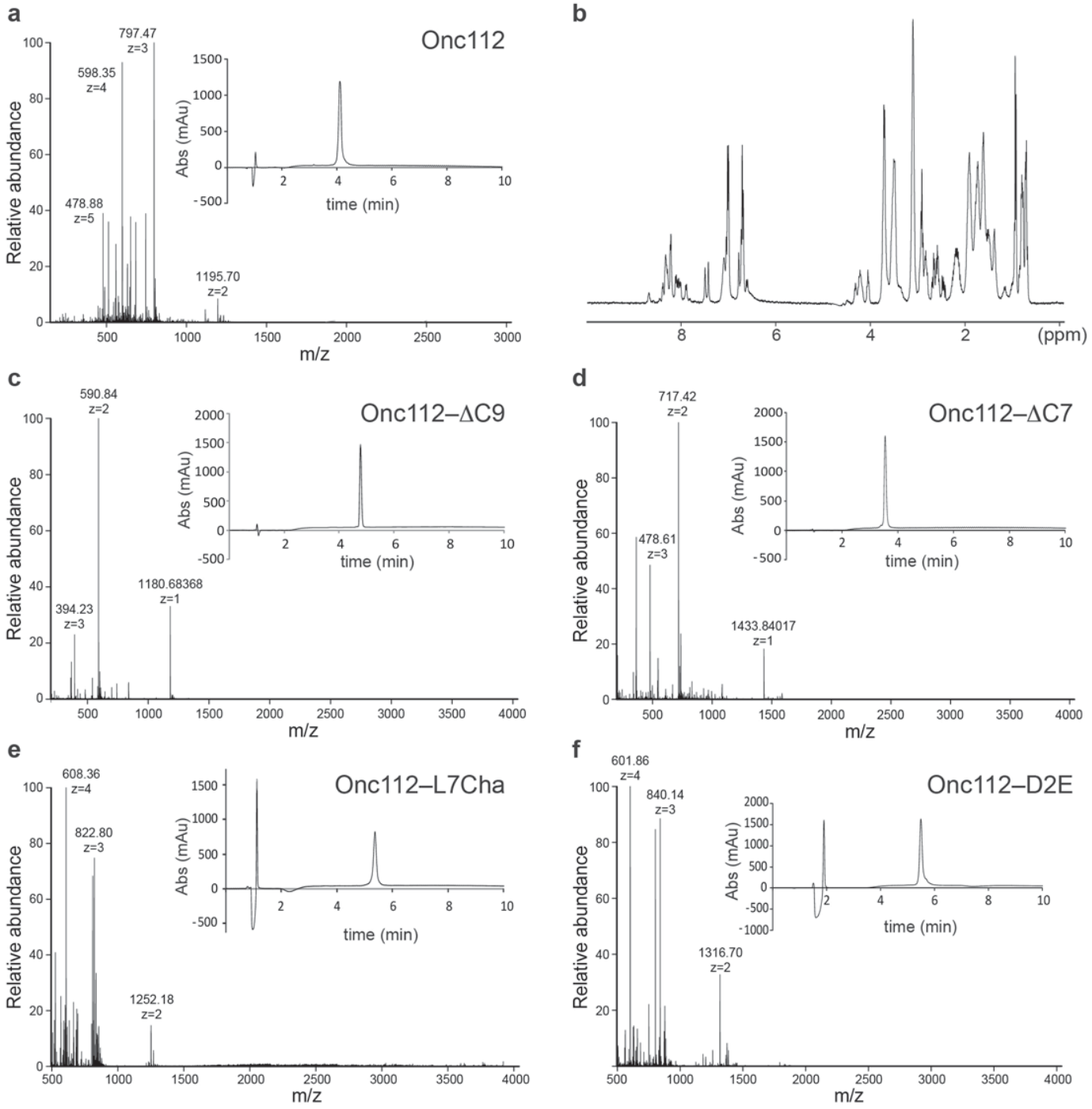

Supplementary Figure 5

Validation of Onc112 and derivatives.

(a) Electrospray ionization high resolution mass spectrometry (ESI-HRMS) and reverse phase (RP) high performance liquid chromatography (HPLC), and (b) ^{1}H nuclear magnetic resonance (NMR) spectra of the Onc112 peptide. (c-f) ESI-HRMS and RP HPLC of the (c) Onc112–ΔC9, (d) Onc112–ΔC7, (e) Onc112–L7Cha and (f) Onc112–D2E peptides.

Nucleic Acids Research Advance Access published January 20, 2016

doi: 10.1093/nar/gkv1545

Structure of the mammalian antimicrobial peptide Bac7(1–16) bound within the exit tunnel of a bacterial ribosome

A. Carolin Seefeldt[1,2,3,†], Michael Graf[4,†], Natacha Pérébaskine[1,2,3], Fabian Nguyen[4], Stefan Arenz[4], Mario Mardirossian[5], Marco Scocchi[5], Daniel N. Wilson[4,6,*] and C. Axel Innis[1,2,3,*]

[1]Institut Européen de Chimie et Biologie, University of Bordeaux, Pessac 33607, France, [2]U1212, Inserm, Bordeaux 33076, France, [3]UMR 5320, CNRS, Bordeaux 33076, France, [4]Gene Center and Department for Biochemistry, University of Munich, Munich 81377, Germany, [5]Department of Life Sciences, University of Trieste, Trieste 34127, Italy and [6]Center for integrated Protein Science Munich (CiPSM), University of Munich, Munich 81377, Germany

Received October 13, 2015; Revised December 22, 2015; Accepted December 28, 2015

ABSTRACT

Proline-rich antimicrobial peptides (PrAMPs) produced as part of the innate immune response of animals, insects and plants represent a vast, untapped resource for the treatment of multidrug-resistant bacterial infections. PrAMPs such as oncocin or bactenecin-7 (Bac7) interact with the bacterial ribosome to inhibit translation, but their supposed specificity as inhibitors of bacterial rather than mammalian protein synthesis remains unclear, despite being key to developing drugs with low toxicity. Here, we present crystal structures of the *Thermus thermophilus* 70S ribosome in complex with the first 16 residues of mammalian Bac7, as well as the insect-derived PrAMPs metalnikowin I and pyrrhocoricin. The structures reveal that the mammalian Bac7 interacts with a similar region of the ribosome as insect-derived PrAMPs. Consistently, Bac7 and the oncocin derivative Onc112 compete effectively with antibiotics, such as erythromycin, which target the ribosomal exit tunnel. Moreover, we demonstrate that Bac7 allows initiation complex formation but prevents entry into the elongation phase of translation, and show that it inhibits translation on both mammalian and bacterial ribosomes, explaining why this peptide needs to be stored as an inactive propeptide. These findings highlight the need to consider the specificity of PrAMP derivatives for the bacterial ribosome in future drug development efforts.

INTRODUCTION

Antimicrobial peptides (AMPs) represent a large and diverse group of molecules that form part of the innate immune response of a variety of invertebrate, plant and animal species (1). While many AMPs kill bacteria by disrupting the bacterial cell membrane, there is growing evidence that some AMPs have intracellular targets (1). Members of one such class of non-membranolytic peptides are referred to as proline-rich AMPs (PrAMPs) and are present in the hemolymph of several species of insects and crustaceans, as well as in the neutrophils of many mammals (2). PrAMPs exhibit potent antimicrobial activity against a broad range of bacteria, especially Gram-negative, and are therefore considered as potential lead candidates for the development of therapeutic antimicrobial agents (3). Well-characterized insect PrAMPs include the apidaecins produced by bees (*Apis melifera*) and wasps (*Apis Vespidae*), pyrrhocoricin from firebugs (*Pyrrhocoris apterus*), drosocins from fruit flies (*Drosophila*), metalnikowins from the green shield bug (*Palomena prasina*) and the milkweed bug (*Oncopeltus fasciatus*) oncocins (2,4,5). PrAMPs are synthesized as inactive precursors, which undergo proteolysis to release the active peptide. In contrast to the active insect peptides, which are generally <21 amino acids in length, the active mammalian mature forms tend to be much longer; for example, the porcine PR-39 is 39 residues long, whereas the bovine bactenecin-7 (Bac7), which is also found in sheep and goats, is 60 residues long (2). Nevertheless, C-terminally truncated versions of the mammalian PrAMPs retain antimicrobial activity (6–9) and exhibit high sequence similarity with the insect PrAMPs. Indeed, the Bac7(1–16) and Bac7(1–35) derivatives corresponding to the first 16 and

*To whom correspondence should be addressed. Tel: +33 540 006 149; Fax: +33 540 002 215; Email: axel.innis@inserm.fr
Correspondence may also be addressed to Daniel N. Wilson. Tel: +49 89 2180 76903; Fax: +49 89 2180 76945; Email: wilson@lmb.uni-muenchen.de
†These authors contributed equally to the paper as first authors.

35 residues of Bac7, respectively, display similar, if not improved, antimicrobial activities compared to the full-length processed Bac7 peptide (6,10,11). For instance, Bac7(1–35) reduces mortality from *Salmonella typhimurium* in a mouse model of infection (12) as well as in a rat model for septic shock (13).

The insect-derived PrAMPs apidaecin and oncocin, as well as the mammalian Bac7, penetrate the bacterial cell membrane mainly via the SbmA transporter present in many Gram-negative bacteria (10,14). Early studies identified interactions between both insect and mammalian PrAMPs and DnaK, suggesting that this molecular chaperone was the common intracellular target (2,15). However, subsequent studies questioned the relevance of this interaction by demonstrating that these PrAMPs also display an equally potent antimicrobial activity against bacterial strains lacking the *dnaK* gene (16–18). Instead, apidaecin, oncocin and Bac7 were shown to bind to the ribosome and inhibit translation (17,19). Subsequent crystal structures of the oncocin derivative Onc112 in complex with the bacterial 70S ribosome revealed that this peptide binds with a reverse orientation in the ribosomal tunnel and blocks binding of the aminoacyl-tRNA to the A-site (20,21). However, there are no crystal structures to date of a mammalian PrAMP in complex with the ribosome.

Here we present 2.8–2.9 Å resolution X-ray structures of the *Thermus thermophilus* 70S (*Tth*70S) ribosome in complex with either the mammalian Bac7 derivative Bac7(1–16) or the insect-derived PrAMPs metalnikowin I or pyrrhocoricin. The structures reveal that Bac7(1–16), metalnikowin I and pyrrhocoricin bind within the ribosomal tunnel with a reverse orientation compared to a nascent polypeptide chain, as observed previously for oncocin (20,21). In contrast to the insect PrAMPs oncocin, metalnikowin I and pyrrhocoricin, the mammalian Bac7(1–16) utilizes multiple arginine side chains to establish stacking interactions with exposed nucleotide bases of the rRNA, and we show that its unique N-terminal RIRR motif is critical for inhibiting translation. Like oncocin, metalnikowin I and pyrrhocoricin, the binding site of Bac7 overlaps with that of the A-tRNA, consistent with our biochemical studies indicating that Bac7(1–16) allows 70S initiation complex formation, but prevents subsequent rounds of translation elongation. Furthermore, we demonstrate that Bac7(1–35) displays activity in a mammalian *in vitro* translation system, providing a possible explanation for why Bac7 is produced as a pre-pro-peptide that is targeted to large granules and phagosomes, thus avoiding direct contact between the active peptide and the mammalian ribosome.

MATERIALS AND METHODS

Peptide synthesis and purification

The Bac7 N-terminal fragments Bac7(1–16; RRIRPRPPRLPRPRPR), Bac7(1–35; RRIRPRPPRLPRPRPRPLPFPRPGPRPIPRPLPFP) and Bac7(5–35; PRPPRLPRPRPRPLPFPRPGPRPIPRPLPFP) were synthesized on solid phase and purified by reversed-phase HPLC as described previously (22). Their concentrations were determined as reported previously (4). All peptides, with a purity of at least 95%, were stored in milliQ water at −80°C until use. The Onc112 peptide was obtained from an earlier study (21). Metalnikowin I (VDKPDYRPRPRPPNM) and pyrrhocoricin (VDKGSYLPRPTPPRPIYNRN) were synthesized to 97.5 and 98.1% purity by NovoPro Bioscience (China).

Purification of *T. thermophilus* 70S ribosomes

*Tth*70S ribosomes were purified as described earlier (23) and resuspended in buffer containing 5 mM HEPES-KOH, pH 7.5, 50 mM KCl, 10 mM NH_4Cl and 10 mM $Mg(CH_3COO)_2$ to yield a final concentration of ∼30 mg/ml. *Tth*70S ribosomes were flash frozen in liquid nitrogen and kept at −80°C for storage.

Preparation of mRNA, $tRNA_i^{Met}$ and YfiA

Synthetic mRNA containing a Shine-Dalgarno sequence and an AUG start codon followed by a phenylalanine codon (5′-GGC AAG GAG GUA AAA AUG UUC UAA -3′) was purchased from Eurogentec. *Escherichia coli* $tRNA_i^{Met}$ was overexpressed in *E. coli* HB101 cells and purified as described previously (24). YfiA was overexpressed in BL21 Star cells and purified as described previously (25).

Complex formation

A quaternary complex containing *Tth*70S ribosomes, mRNA, deacylated $tRNA_i^{Met}$ and Bac7(1–16) peptide was prepared by mixing of 5 μM *Tth*70S ribosomes with 10 μM mRNA and 50 μM Bac7(1–16), and incubating at 55°C for 10 min. After addition of 20 μM $tRNA_i^{Met}$, the mixture was incubated at 37°C for 10 min. The sample was then incubated at room temperature for at least 15 min and centrifuged briefly prior to use. Ternary complexes containing 50 μM metalnikowin I or pyrrhocoricin, 5 μM *Tth*70S ribosomes and 50 μM YfiA were formed by incubation for 30 min at room temperature. The final buffer conditions were 5 mM HEPES-KOH, pH 7.6, 50 mM KCl, 10 mM NH_4Cl and 10 mM $Mg(CH_3COO)_2$.

Crystallization

Published conditions were used as a starting point for screening crystallization conditions by vapour diffusion in sitting-drop trays at 20°C (23,26). Crystallization drops consisted of 3 μl of quaternary or ternary complexes and 3–4 μl of reservoir solution containing 100 mM Tris–HCl, pH 7.6, 2.9% (v/v) PEG 20,000, 7–10% (v/v) 2-methyl-2,4-petanediol (MPD) and 175 mM arginine. Crystals appeared within 2–3 days and grew to ∼1000 × 100 × 100 μm within 7–8 days. For cryoprotection, the concentration of MPD was increased in a stepwise manner to yield a final concentration of 40% (v/v). The ionic composition during cryoprotection was 100 mM Tris–HCl, pH 7.6, 2.9% (v/v) PEG 20,000, 50 mM KCl, 10 mM NH_4Cl and 10 mM $Mg(CH_3COO)_2$. Crystals were flash frozen in a nitrogen cryostream at 80 K for subsequent data collection.

Data collection and processing

Diffraction data for Bac7(1–16) were collected at PROXIMA-2A, a beamline at the SOLEIL synchrotron (Saclay, France) equipped with an ADSC Q315 detector. A complete dataset was obtained by merging 0.25° oscillation data collected at 100 K with a wavelength of 0.98011 Å from multiple regions of the same crystal. Diffraction data for metalnikowin I and pyrrhocoricin were collected at PROXIMA-1, a beamline at the SOLEIL synchrotron equipped with a DECTRIS PILATUS 6M detector. Complete datasets were obtained by merging 0.1° oscillation data collected at 100 K with a wavelength of 0.97857 Å from multiple regions of the crystal. Initial data processing, including integration and scaling, was performed with X-ray Detector Software (XDS) (27). The data could be indexed in the $P2_12_12_1$ space group, with unit-cell dimensions approximating 210 × 450 × 625 Å and an asymmetric unit containing two copies of the *Tth*70S ribosome.

Model building and refinement

Initial phases were obtained by molecular replacement performed with Phaser (28). The search model was obtained from a high-resolution structure of the *Tth*70S ribosome (PDB ID: 4Y4O) (29) where the RNA backbone had been further improved with the ERRASER-Phenix pipeline (30), using the deposited structure factors. Restrained crystallographic refinement was carried out with Phenix (31) and consisted of a single cycle of rigid-body refinement followed by multiple cycles of positional and individual *B*-factor refinement. Rigid bodies comprised four domains from the small 30S subunit (head, body, spur and helix h44) and three domains from the large 50S subunit (body, L1 stalk and the C terminus of ribosomal protein L9). Non-crystallographic symmetry restraints between the two copies of the *Tth*70S ribosome in the asymmetric unit were also applied during refinement. After confirming that a single tRNA was bound to the P site or that YfiA was present at the decoding center, and that additional density corresponding to the PrAMPs was visible within the exit tunnel in a minimally biased F_O–F_C map, models of the corresponding PrAMPs were built in Coot (32). The models for the tRNA and mRNA were obtained from a high-resolution structure of the *Tth*70S ribosome pre-attack complex (PDB ID: 1VY4). The model for YfiA was obtained from a high resolution *Tth*70S ribosome structure (PDB ID: 4Y4O). Further refinement and model validation was carried out in Phenix (31) and on the MolProbity server (33), respectively. In the final models, 0.56–0.95% of protein residues were classified as Ramachandran outliers, and 92.4–94.3% had favourable backbone conformations (Supplementary Table S1). Coordinates and structure factors have been deposited in the Protein Data Bank under accession codes 5F8K (Bac7(1–16)), 5FDU (Metalnikowin I) and 5FDV (Pyrrhocoricin).

In vitro translation assays

Escherichia coli lysate-based transcription-translation coupled assay (RTS100, 5Prime) were performed as described previously for other translational inhibitors (34). Briefly, 6 μl reactions, with or without PrAMP were mixed according to the manufacturer's description and incubated for 1 h at 30°C with shaking (750 rpm). A total of 0.5 μl of each reaction were stopped with 7.5 μl kanamycin (50 μg/μl). The effect of Bac7(1–35) on eukaryotic translation was determined using Rabbit Reticulocyte Lysate System (Promega). A total of 6 μl reactions, with or without Bac7(1–35) were mixed according to the manufacturer´s description and incubated for 1 h at 30°C with shaking (300 rpm). A total of 5 μl of each reaction were stopped in 5 μl kanamycin (50 μg/μl). All samples were diluted with 40 μl of Luciferase assays substrate (Promega) into a white 96-well chimney flat bottom microtiter plate (Greiner). The luminescence was then measured using a Tecan Infinite M1000 plate reader. Relative values were determined by defining the luminescence value of the sample without inhibitor as 100%.

Toe-printing assay

The position of the ribosome on the mRNA was monitored with a toe-printing assay (35) based on an *in vitro*–coupled transcription-translation system with the PURExpress *in vitro* protein synthesis kit (NEB), as described previously (21,36). Briefly, each translation reaction consisted of 1 μl solution A, 0.5 μl Δisoleucine amino acid mixture, 0.5 μl tRNA mixture, 1.5 μl solution B, 0.5 μl (0.5 pmol) hns37aa template: (5′-ATTAAT ACGACTCACTATAGGGATATAAGGAGGAAAAC AT**atg**AGCGAAGCACTTAAA**att**CTGAACAACCTGC GTACTCTTCGTGCGCAGGCAAGACCGCCGCCGC TTGAAACGCTGGAAGAAATGCTGGAAAAATTA GAAGTTGTTGTT**taa**GTGATAGAATTCTATC*GTTA ATAAGCAAAATTCATTATAAC*-3′, with start codon ATG, catch isoleucine codon ATT and stop codon TAA in bold, the hns37aa ORF underlined and toe-print primer binding site in italics) and 0.5 μl additional agents (nuclease-free water, water dissolved Bac7(1–35) Bac7(1–16), Bac7(5–35) (1, 10 or 100 μM final concentration) or antibiotics (100 μM thiostrepton, 50 μM edeine, 50 μM clindamycin final concentration)). Translation was performed in the absence of isoleucine at 37°C for 15 min at 500 rpm in 1.5 ml reaction tubes. After translation, 2 pmol Alexa647-labelled NV-1 toe-print primer (5′-GGTTATAATGAATTTTGCTTATTAAC-3′) was added to each reaction. Reverse transcription was performed with 0.5 μl of AMV RT (NEB), 0.1 μl dNTP mix (10 mM) and 0.4 μl Pure System Buffer and incubated at 37°C for 20 min. Reverse transcription was quenched and RNA degraded by addition of 1 μl 10 M NaOH and incubation for at least 15 min at 37°C and then was neutralized with 0.82 μl of 12 M HCl. 20 μl toe-print resuspension buffer and 200 μl PN1 buffer were added to each reaction before treatment with a QIAquick Nucleotide Removal Kit (Qiagen). The Alexa647-labelled DNA was then eluted from the QIAquick columns with 80 μl of nuclease-free water. A vacuum concentrator was used to vaporize the solvent and the Alexa647-labelled DNA was then dissolved into 3.5 μl of formamide dye. The samples were heated to 95°C for 5 min before being applied onto a 6% polyacrylamide (19:1) sequencing gel containing 7 M urea. Gel electrophoresis was performed at 40 W and 2000 V for 2 h. The GE

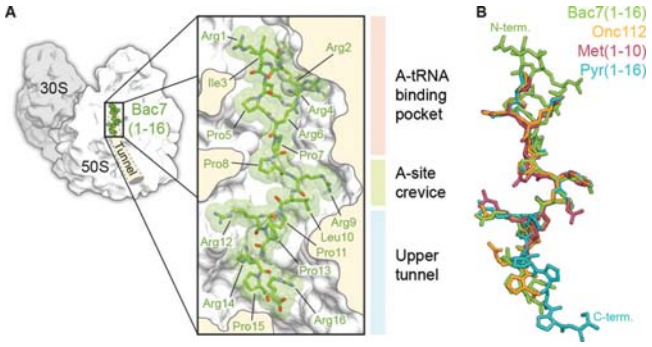

Figure 1. Binding site of Bac7(1–16) on the ribosome and comparison with Onc112. (**A**) Overview and closeup view of a cross-section of the *Tth*70S ribosomal exit tunnel showing the Bac7(1–16) peptide (RRIRPRPPRLPRPRPR) in green and highlighting the three regions of interaction with the ribosome: the A-tRNA binding pocket (light pink), the A-site crevice (light green) and the upper section of the exit tunnel (light blue). (**B**) Structural comparison of Bac7(1–16) (green) with Onc112 (orange)(20,21), Met1(1–10) (burgundy) and Pyr(1–16) (cyan), highlighting the distinct structure of the Bac7 N-terminus (N-term) and the Pyr C-terminus (C-term).

Typhoon FLA9500 imaging system was subsequently used to scan the polyacrylamide gel.

Filter binding assay

Filter binding assays were performed as described previously (34,37). Briefly, 3 pmol of 70S ribosomes purified from BL21 *E. coli* strain were exposed to 30 pmol of radiolabelled [^{14}C]-Erythromycin (Perkin Elmer; 110 dpm/pmol) in presence of 1x filter binding buffer (10 mM HEPES/KOH [pH 7.4], 30 mM $MgCl_2$, 150 mM NH_4Cl and 6 mM β-mercaptoethanol) for 15 min at 37°C. Our controls indicated that approximately 65% of the 70S ribosomes (2 pmol) contained [^{14}C]-Erythromycin previous to the addition of the different PrAMPs. The PrAMPs were diluted in nuclease-free water to a concentration of 1 mM, 100 μM and 10 μM. 2 μl of each PrAMP stock dilution (Onc112, Bac7(1–35), Bac7(1–16) and Bac7(5–35)) were transferred to the respective tube resulting in final concentrations of 100, 10 and 1 μM. Reactions were incubated for an additional 25 min at 37°C. Afterwards the 20 μl samples were passed through a HA-type nitrocellulose filter from Millipore (0.45 μm pore size) and the filter subsequently washed three times with 1 ml 1× filter binding buffer. Scintillation counting was performed in the presence of Rotiszint® eco plus Scintillant. All reactions were performed in duplicate and results were analysed using GraphPad Prism 5. Error bars represent the standard deviation from the mean.

Disome formation assay

The disome formation assay was performed as described previously (38,39). Briefly, *in vitro* translation of the 2xermBL construct was performed using the Rapid Translation System RTS 100 *E. coli* HY Kit (Roche). Translations were carried-out for 1 h at 30°C and then analysed on 10–55% sucrose density gradients (in a buffer containing 50 mM HEPES-KOH, pH 7.4, 100 mM KOAc, 25 mM $Mg(OAc)_2$, 6 mM β-mercaptoethanol) by centrifugation at 154 693 × *g* (SW-40 Ti, Beckman Coulter) for 2.5 h at 4°C.

RESULTS

The N-terminus of Bac7 adopts a compact conformation

We obtained a structure referred to here as *Tth*70S-Bac7 from co-crystals of *Tth*70S ribosomes in complex with deacylated $tRNA_i^{Met}$, a short mRNA and Bac7(1–16) (Supplementary Table S1). In addition, we obtained two additional structures, *Tth*70S-MetI and *Tth*70S-Pyr, from co-crystals of *Tth*70S ribosomes in complex with YfiA and either metalnikowin I or pyrrhocoricin, respectively (Supplementary Table S1). The quality of the electron density in the minimally biased F_O–F_C difference maps calculated after refinement of a model comprising *Tth*70S ribosomes and $tRNA_i^{Met}$/mRNA or YfiA, made it possible to build a model for the entire Bac7(1–16; RRIRPRPPRLPRPRPR), the first 10 (of 15; VDKPDYRPRPRPPNM) residues of metalnikowin I (MetI) and the first 16 (of 20; VDKGSYLPRPTPPRPIYNRN) residues of pyrrhocoricin (Pyr), as well as to position several neighbouring solvent molecules (Supplementary Figure S1). Like the insect-derived Onc112 peptide (20,21), MetI, Pyr and Bac7(1–16) all bind to the ribosomal exit tunnel in a reverse orientation relative to the nascent polypeptide chain and make extensive interactions with three distinct regions of the large 50S ribosomal subunit: the A-tRNA binding pocket, the A-site crevice and the upper section of the nascent polypeptide exit tunnel (Figure 1A, B and Supplementary Figure S1). A nearly identical, extended backbone conformation is seen for residues 7–13 of Bac7(1–16) and residues 4–10 of Onc112, Met1 and Pyr, with Arg9 of Bac7(1–16) substituting for Tyr6 of Onc112, Met1 and Pyr (Figure 1B). The structural similarity however does not extend to the N-terminus of Bac7(1–16), where the first six residues adopt a structure that deviates substantially from that of the shorter N-terminus of the insert-derived PrAMPs. Indeed, arginine residues within this region are arranged such that the side chain of Arg6 is sandwiched between the side chains of Arg2 and Arg4 to form a compact, positively charged structure (Figure 1A and B). The binding site of Bac7(1–16) suggests that the additional C-terminal residues of Bac7(1–35) and of the full-length Bac7 (60 residues) would occupy the entire length of the ribosomal tunnel. Consistently, a photocrosslinkable derivative of Bac7(1–35) has been crosslinked to two ribosomal proteins of ∼16 and 25 kDa (19), which we suggest to be L22 and L4, respectively, based on their size and close proximity to the Bac7(1–16) binding site (Supplementary Figure S2). Compared to Onc112 and Met1, additional density for the C-terminal PRPR motif (residues 13–16) of Pyr is observed extending deeper into the tunnel (Figure 1 and Supplementary Figure S1). With the exception of Arg14 for which no density is observed, the PRPR motif is quite well ordered despite not forming any obvious direct interactions with the ribosome.

Bac7 makes extensive interactions with the 50S ribosomal subunit

As with Onc112 (20,21), binding of Bac7(1–16) to the ribosome is accompanied by an induced fit involving 23S rRNA residues A2062, U2506 and U2585 (Supplementary Figure S3A; *E. coli* numbering is used throughout this work for the 23S rRNA), such that the base of this last nucleotide occupies a position that would normally clash with the formylmethionyl moiety of fMet-tRNA$_i^{Met}$ bound to the P-site of an initiation complex (Supplementary Figure S3B). Three modes of interaction are observed between Bac7(1–16) and the large 50S ribosomal subunit (Figure 2A–E).

First, the N-terminal region of Bac7(1–16) forms multiple hydrogen bonds and salt bridges with the A-tRNA binding pocket of the ribosome (Figure 2A and B). In particular, the compact structure formed by Arg2, Arg4 and Arg6 provides a positively charged N-terminal anchor that displaces two magnesium ions from a deep groove lined by 23S rRNA residues C2452, A2453 and G2454 on one side, and residues U2493 and G2494 on the other (Figure 2B). This groove differs from the standard A-form RNA major groove in that it occurs between two unpaired, antiparallel strands of the 23S rRNA. Consequently, the compact arginine structure at the N-terminus of Bac7(1–16) is ideally sized and shaped to fit into this groove and the resulting interaction is likely to be specific in spite of its simple electrostatic nature. Further contacts in this region are likely to increase the specificity of Bac7(1–16) for the ribosome, such as the two hydrogen bonds between the side chain of Arg1 and 23S rRNA residues U2555 and C2556, and four hydrogen bonds between the backbone of Bac7(1–16) residues Arg2-Arg4 and 23 rRNA residues U2492, U2493 and C2573 (Figure 2A).

Second, the unusually high arginine (50%) and proline (37.5%) content of Bac7(1–16) restricts the types of contacts that this peptide can establish with the ribosome. This results in π-stacking interactions between the side chains of Arg2, Arg9, Arg12, Arg14 and Arg16 and exposed bases of 23S rRNA residues C2573, C2452/U2504, C2610, C2586 and A2062, respectively. Additional rigidity within the peptide is provided through the packing of Arg1 against Ile3 and Arg9 against Leu10, and through the compact arginine stack described above (Figure 2C).

Third, numerous possible hydrogen bonds can be established between the backbone of Bac7(1–16) and the ribosome (Figure 2A, D and E), including many indirect interactions via ordered solvent molecules (Figure 2D and E). Many of the water-mediated contacts suggested for *Tth*70S-Bac7 are likely to occur with oncocin, even though the lower resolution of the earlier *Tth*70S-Onc112 structures precluded the modelling of any water molecules (20,21). In addition, interactions such as those between 23S rRNA residue U2506 and the backbone of Bac7(1–16) residues Arg9 and Leu10 were also proposed to occur between the Onc112 peptide and the ribosome (20,21).

Bac7 and Onc112 compete with erythromycin for ribosome binding

The C-terminal residues 12–16 of Bac7(1–16) overlap with the binding site of the macrolide antibiotic erythromycin on the bacterial ribosome (40,41), in particular with the region occupied by the cladinose sugar and part of the lactone ring (Figure 3A). Consistently, we could demonstrate that Bac7(1–16) and Bac7(1–35) efficiently compete with the binding of radiolabelled erythromycin to the 70S ribosome (Figure 3B). Similarly, Onc112 also efficiently competed with erythromycin (Figure 3B), as expected based on the similarity in binding mode with the ribosome for these regions of Onc112 and Bac7 (Figure 1B). In contrast, Bac7(5–35) was a poor competitor of erythromycin (Figure 3B), indicating that the highly cationic N-terminus of Bac7 and its interaction with the A-tRNA binding pocket (Figure 2B) are important for high affinity binding of Bac7 to the ribosome. Indeed, Bac7 derivatives lacking the first four N-terminal residues (RRIR), Bac7(5–35) and Bac7(5–23), exhibit dramatically reduced minimal inhibitory concentrations (MIC) against Gram-negative strains, such as *E. coli*, as well as *Salmonella typhimurium* (6). We note, however, that the internalization of Bac7(5–35) into bacteria is reduced, indicating that the N-terminal RRIR motif also plays an important role for cell penetration (11).

Bac7 allows initiation, but prevents translation elongation

Consistent with the erythromycin binding assays and in agreement with previous results (Figure 4A) (19), we observed that Bac7(1–35) inhibits the production of luciferase with an IC_{50} of 1 μM in an *E. coli in vitro* translation system, similar to MetI and Pyr (Supplementary Figure S1), as well as that observed previously for Onc112 (20,21). Bac7(1–16) was an equally potent inhibitor as Bac7(1–35), consistent with the similar MICs observed for these two derivatives (6,10,11). In contrast, Bac7(5–35) inhibited *in vitro* translation with an IC_{50} of 10 μM, i.e. 10-fold higher than observed for Bac7(1–16) or Bac7(1–35), indicating that the reduced affinity for the ribosome, together with reduced cellular uptake (11), results in the higher MIC of the Bac7(5–35) derivative (6,42).

Next we investigated the mechanism of inhibition by Bac7 using two *in vitro* translation assays. First, we compared the effect of Bac7(1–35) and Bac7(5–35) on the stabilization of disomes formed upon the stalling of ribosomes on a dicistronic mRNA (in this case 2XErmBL mRNA), as measured by sucrose gradient centrifugation (21,38,39). In the absence of inhibitor, the majority of ribosomes are present as 70S monosomes (control in Figure 4B), whereas the presence of erythromycin leads to translational arrest of the ribosomes on both cistrons of the 2XErmBL mRNA, thereby generating the expected disome peaks (Ery in Figure 4B). Consistent with the *in vitro* translation assays (Figure 4A), translation inhibition and thus disome formation was observed in the presence of 10 μM Bac7(1–35), whereas even 100 μM of Bac7(5–35) did not produce significant disomes (Figure 4B). These findings suggest that Bac7(1–35) but not Bac7(5–35) stabilizes an arrested ribosome complex, as observed previously for Onc112 (21).

Second, to monitor the exact site of translation inhibition of the Bac7 derivatives, we employed a toeprinting assay, which uses reverse transcription from the 3′ end of an mRNA to determine the exact location of the ribosomes that are translating it (35). In the absence of in-

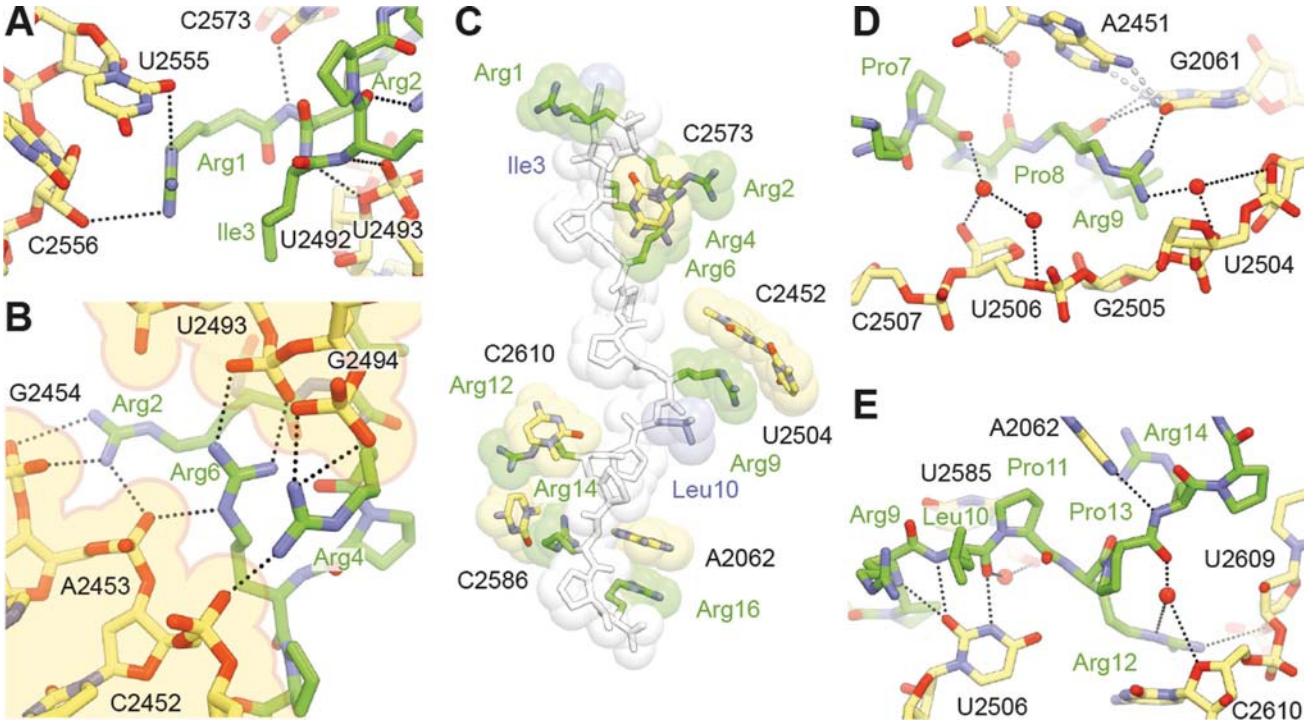

Figure 2. Interactions between Bac7(1–16) and the ribosome. (**A**) Bac7(1–16) (green) makes extensive contacts with the A-site tRNA binding region of the ribosome, in particular (**B**) electrostatic interactions between its N-terminal arginine stack and a deep groove lined by phosphate groups from the 23S rRNA (B). (**C**) π-stacking interactions between arginine side chains (green) of Bac7(1–16) and 23S rRNA bases contribute to much of the binding and are reinforced through further packing against aliphatic side chains (blue). (**D** and **E**) Water-mediated contacts between the peptide and the ribosome are also proposed to occur further down the exit tunnel, in addition to direct hydrogen bonding interactions between the two.

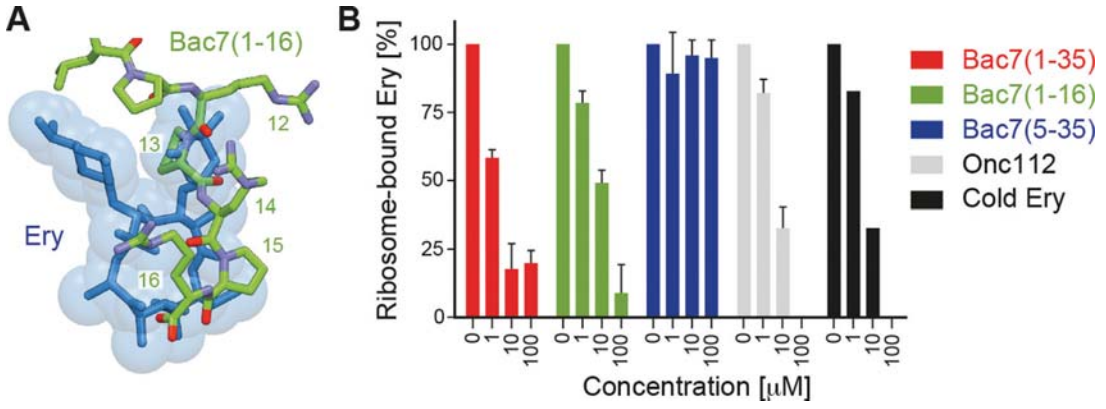

Figure 3. Competition between Bac7 derivatives and erythromycin. (**A**) Superimposition of the binding site of erythromycin (blue) (40,41) with residues 11–16 of Bac7(1–16) (green). (**B**) A filter binding assay was used to monitor competition between radiolabelled [^{14}C]-erythromycin and increasing concentrations (1–100 μM) of Bac7(1–35) (red), Bac7(1–16) (green), Bac7(5–35) (blue), Onc112 (grey) and cold (non-radioactive) erythromycin (ery, black).

hibitor, ribosomes initiated at the AUG start codon of the mRNA, translated through the open reading frame and ultimately became stalled on an isoleucine codon (Figure 4C) due to the omission of isoleucine from the translation mix. In the presence of thiostrepton or clindamycin, ribosomes accumulated at the AUG codon (Figure 4C), since these antibiotics prevent delivery and/or accommodation of aminoacyl-tRNA at the A-site directly following initiation (43). Similar results were observed when using the Bac7(1–35) and Bac7(1–16) derivatives, such that complete inhibition of translation elongation was observed at a peptide concentration of 10 μM (Figure 4C). These findings suggest that like Onc112 (21), Bac7 allows subunit joining and fMet-tRNA$_i^{Met}$ binding, but prevents accommodation of the first aminoacyl-tRNA at the A-site, as suggested by the overlap in the binding site of Bac7 and the CCA-end of an A-tRNA (Figure 4D). Curiously, the toeprint for ribosomes stalled during initiation became weaker at 100 μM of Bac7(1–16) and Bac7(1–35) and the signal for the full-length mRNA became stronger, similar to the effect ob-

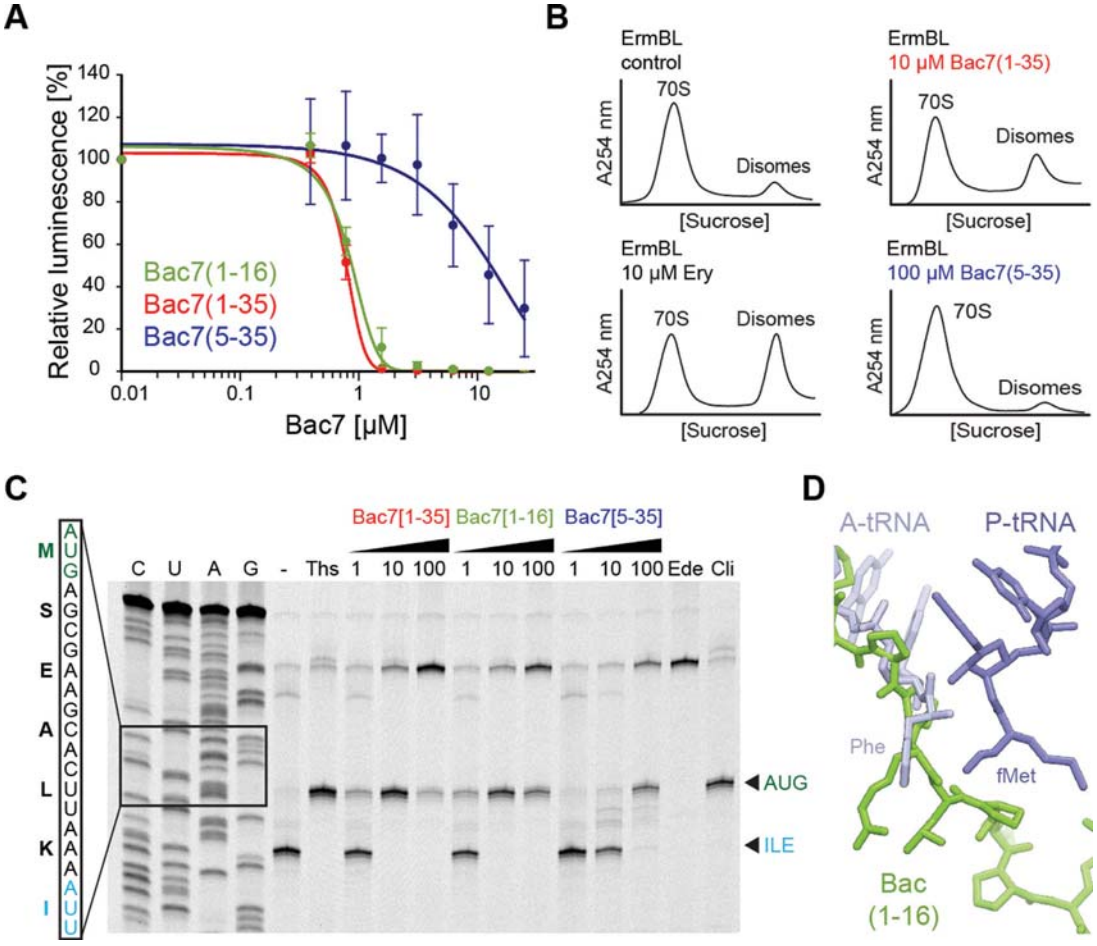

Figure 4. Mechanism of action of Bac7 on the ribosome. (**A**) Effects of increasing concentrations of Bac7 derivatives Bac7(1–16) (green), Bac7(1–35) (red) and Bac7(5–35) (blue) on the luminescence resulting from the *in vitro* translation of firefly luciferase (Fluc) using an *Escherichia coli* lysate-based system. The error bars represent the standard deviation from the mean for triplicate experiments and the luminescence is normalized relative to that measured in the absence of peptide, which was assigned as 100%. (**B**) Sucrose gradient profiles to monitor disome formation from *in vitro* translation of the 2XErmBL mRNA in the absence (control) or presence of 20 μM erythromycin (Ery), 10 μM Bac7(1–35) (red) or 100 μM Bac7(5–35) (blue). (**C**) Toe-printing assay performed in the absence (−) or presence of increasing concentrations (1, 10, 100 μM) of Bac7(1–35), Bac7(1–16) or Bac7(5–35), or 100 μM thiostrepton (Ths), 50 μM edeine (Ede) or 50 μM clindamycin (Cli). Sequencing lanes for C, U, A and G and the sequence surrounding the toe-print bands (arrowed) when ribosomes accumulate at the AUG start codon (green, initiation complex) or the isoleucine codon (blue, stalled elongation complex) are included for reference. (**D**) Structural comparison of Phe-tRNA^{Phe} (slate) in the A-site and fMet-tRNA$_i^{Met}$ in the P-site (blue) (26) with the binding site of Bac7(1–16) (green).

served when the antibiotic edeine was used (Figure 4C). Edeine prevents 70S initiation complex formation by destabilizing fMet-tRNA$_i^{Met}$ binding to the 30S subunit (43). Thus, Bac7 may have a similar effect when high cytosolic concentrations are achieved through active uptake into the cell, possibly due to the presence of non-specific interactions with the ribosome. In contrast to Bac7(1–16) and Bac7(1–35), Bac7(5–35) only stabilized the initiation complex at a much higher concentration (100 μM) (Figure 4C). This is consistent with a reduced affinity of Bac7(5–35) for the ribosome and reinforces the critical role played by the first four residues of Bac7 in its inhibitory activity (Figure 1A) (6,42).

Bac7 inhibits eukaryotic translation *in vitro*

Bac7(1–35) is internalized by mammalian cells (42,44), yet no toxicity has been observed, even at concentrations well above those effective against microbes (12,13,42), raising the question as to whether Bac7 binds to eukaryotic cytosolic ribosomes. A comparison of the binding site of Bac7(1–16) on the bacterial 70S ribosome with the equivalent region of a mammalian 80S ribosome reveals that the rRNA nucleotide sequence is highly conserved. Structurally, the conformation of three 25S rRNA nucleotides, *C4519* (C2573), *U4452* (U2506) and *A3908* (A2602), would be expected to preclude Bac7(1–16) from binding to the mammalian ribosome (Figure 5A). Nevertheless, these nucleotides are highly mobile and adopt different conformations depending on the functional state of the ribosome (26,39,45,46), suggesting that conformational rearrangements of these nu-

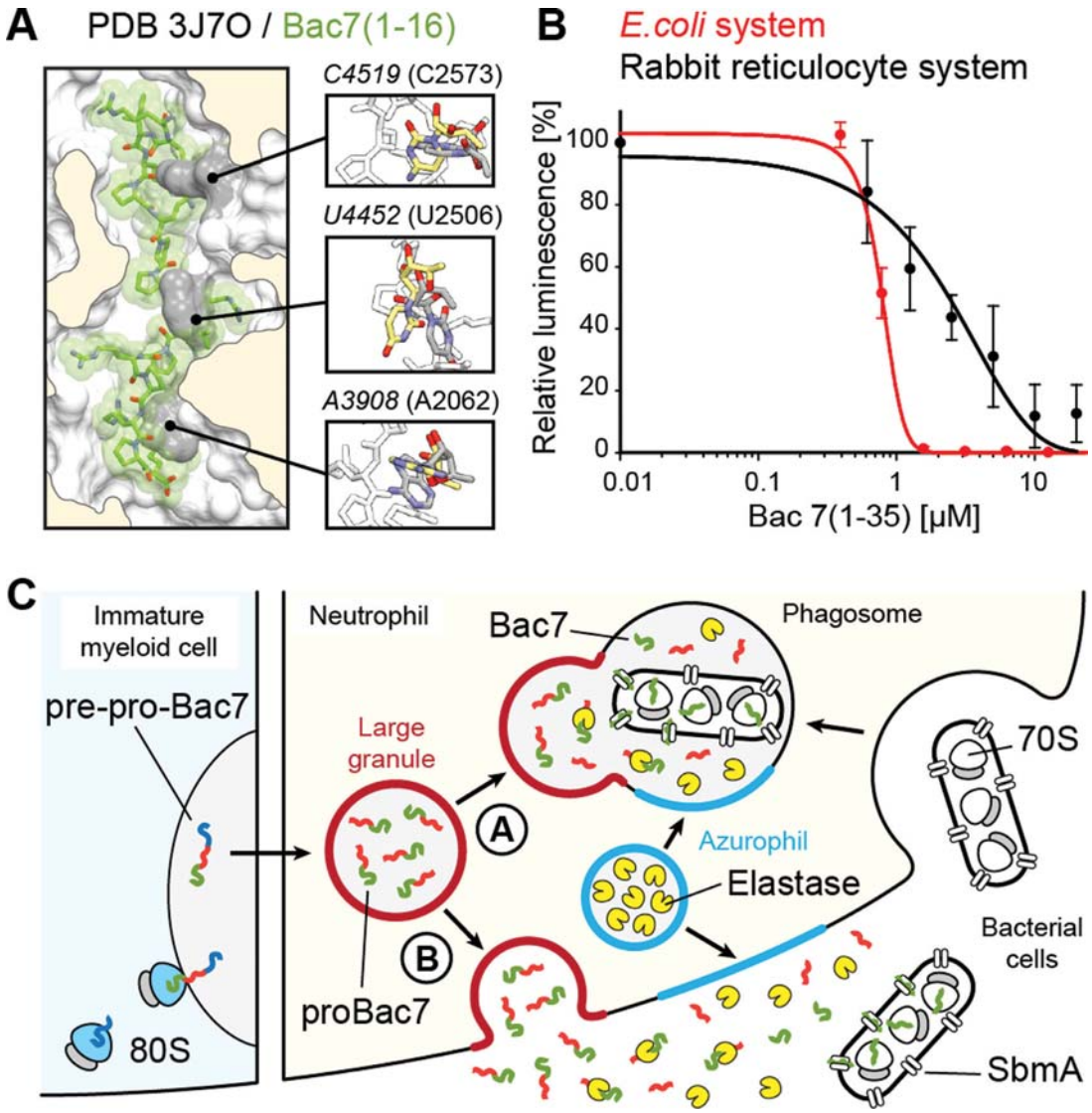

Figure 5. Specificity of Bac7 for bacterial and eukaryotic ribosomes. (**A**) Superimposition of Bac7(1–16) (green) onto a mammalian 80S ribosome (PDB ID: 3J7O) (47) on the basis of the 23S and 25S rRNA chains in the corresponding structures, with inset illustrating three rRNA nucleotides whose conformation differs in the 80S (grey) and *Tth*70S-Bac7 (yellow) structures. (**B**) Effect of increasing concentrations of Bac7(1–35) on the luminescence resulting from the *in vitro* translation of firefly luciferase (Fluc) using an *Escherichia coli* lysate-based system (red) or rabbit reticulocyte-based system (black). The error bars represent the standard deviation from the mean for triplicate experiments and the fluorescence is normalized relative to that measured in the absence of peptide, which was assigned as 100%. (**C**) Model for the targeting of proBac7 to large granules and its processing by elastase to yield active Bac7 peptide. The latter is transported through the bacterial inner membrane by the SbmA transporter and binds within the tunnel of bacterial ribosomes to inhibit translation.

cleotides could allow Bac7(1–16) binding. Indeed, we observed that increasing concentrations of Bac7(1–35) inhibited *in vitro* translation using a rabbit reticulocyte system (Figure 5B). Bac7(1–35) exhibited an IC_{50} of 2.5 μM, only 2.5-fold higher than that observed in the *E. coli in vitro* translation system (Figure 5B). The excellent inhibitory activity of Bac7(1–35) on mammalian ribosomes, combined with its lack of toxicity on mammalian cells (42), would be consistent with a mechanism of internalization via an endocytotic process (42) to ensure that Bac7 minimizes contact with the mammalian cytosolic ribosomes.

DISCUSSION

Our finding that Bac7 is active against eukaryotic translation, together with the current literature, allows us to present a model that explains how and why the mammalian cell prevents the active Bac7 peptide from being present in the cytoplasm (Figure 5C). Bac7 is produced by immature myeloid cells as a pre-pro-Bac7 precursor that is targeted to large granules, where it is stored as pro-Bac7 in differentiated neutrophils (48). The inactive proBac7 is cleaved by elastase, a serine protease that is present in azurophil granules, either upon (A) fusion with the phagosome, or (B) exocytosis and release into the extracellular matrix (Figure

5C) (48,49). The resulting activated Bac7 peptide can then enter into the bacterial cell through the SbmA transporter (10), where it subsequently binds to the ribosome to inhibit translation (Figure 5C) (19). Our structure of the *Tth*70S–Bac7 complex reveals specifically how Bac7 interacts with the bacterial ribosome (Figures 1 and 2) and inhibits translation by allowing initiation but preventing translation elongation (Figure 3). Although the overall mechanism of action of Bac7 is similar to that of insect-derived AMPs like oncocin (20,21), the high arginine content of Bac7 leads to a distinct mode of binding to the ribosome, namely through electrostatic and stacking interactions with the backbone and bases of 23S rRNA nucleotides, respectively (Figure 2C). It will be interesting to see whether such interactions are the basis for the translational arrest that has been observed when the ribosome translates a nascent polypeptide chain bearing positively charged arginine residues (50,51).

ACCESSION NUMBERS

PDB IDs: 5F8K, 5FDU, 5FDV.

SUPPLEMENTARY DATA

Supplementary Data are available at NAR Online.

ACKNOWLEDGEMENT

We thank the staff at the SOLEIL synchrotron (beamlines PROXIMA-2A and PROXIMA-1) for help during data collection and B. Kauffmann and S. Massip at the Institut Européen de Chimie et Biologie for help with crystal freezing and screening.

FUNDING

Agence Nationale pour la Recherche [ANR-14-CE09–0001 to C.A.I., D.N.W.]; Conseil Régional d'Aquitaine [2012-13-01-009 to C.A.I.]; European Union [PCIG14-GA-2013-631479 to C.A.I.]; Deutsche Forschungsgemeinschaft [FOR1805, WI3285/4-1, GRK1721 to D.N.W.]; Fondo Ricerca di Ateneo [FRA2014 to M.S.]; Institut National de la Santé et de la Recherche Médicale Pre-doctoral Fellowship (to A.C.S.); Conseil Régional d'Aquitaine Pre-doctoral Fellowship (to A.C.S.). Funding for open access charge: Institut National de la Santé et de la Recherche Médicale [PCIG14-GA-2013-631479 to C.A.I.].
Conflict of interest statement. None declared.

REFERENCES

1. Brogden,K.A. (2005) Antimicrobial peptides: pore formers or metabolic inhibitors in bacteria? *Nat. Rev. Microbiol.*, **3**, 238–250.
2. Scocchi,M., Tossi,A. and Gennaro,R. (2011) Proline-rich antimicrobial peptides: converging to a non-lytic mechanism of action. *Cell. Mol. Life Sci.*, **68**, 2317–2330.
3. Li,W., Tailhades,J., O'Brien-Simpson,N.M., Separovic,F., Otvos,L. Jr, Hossain,M.A. and Wade,J.D. (2014) Proline-rich antimicrobial peptides: potential therapeutics against antibiotic-resistant bacteria. *Amino Acids*, **46**, 2287–2294.
4. Ebbensgaard,A., Mordhorst,H., Overgaard,M.T., Nielsen,C.G., Aarestrup,F.M. and Hansen,E.B. (2015) Comparative evaluation of the antimicrobial activity of different antimicrobial peptides against a range of pathogenic bacteria. *PLoS One*, **10**, e0144611.
5. Chernysh,S., Cociancich,S., Briand,J.P., Hetru,C. and Bulet,P. (1996) The inducible antibacterial peptides of the Hemipteran insect Palomena prasina: identification of a unique family of proline rich peptides and of a novel insect defensin. *J. Insect. Physiol.*, **42**, 81–89.
6. Benincasa,M., Scocchi,M., Podda,E., Skerlavaj,B., Dolzani,L. and Gennaro,R. (2004) Antimicrobial activity of Bac7 fragments against drug-resistant clinical isolates. *Peptides*, **25**, 2055–2061.
7. Chan,Y.R., Zanetti,M., Gennaro,R. and Gallo,R.L. (2001) Anti-microbial activity and cell binding are controlled by sequence determinants in the anti-microbial peptide PR-39. *J. Invest. Dermatol.*, **116**, 230–235.
8. Frank,R.W., Gennaro,R., Schneider,K., Przybylski,M. and Romeo,D. (1990) Amino acid sequences of two proline-rich bactenecins. Antimicrobial peptides of bovine neutrophils. *J. Biol. Chem.*, **265**, 18871–18874.
9. Tokunaga,Y., Niidome,T., Hatakeyama,T. and Aoyagi,H. (2001) Antibacterial activity of bactenecin 5 fragments and their interaction with phospholipid membranes. *J. Pept. Sci.*, **7**, 297–304.
10. Mattiuzzo,M., Bandiera,A., Gennaro,R., Benincasa,M., Pacor,S., Antcheva,N. and Scocchi,M. (2007) Role of the Escherichia coli SbmA in the antimicrobial activity of proline-rich peptides. *Mol. Microbiol.*, **66**, 151–163.
11. Podda,E., Benincasa,M., Pacor,S., Micali,F., Mattiuzzo,M., Gennaro,R. and Scocchi,M. (2006) Dual mode of action of Bac7, a proline-rich antibacterial peptide. *Biochim. Biophys. Acta*, **1760**, 1732–1740.
12. Benincasa,M., Pelillo,C., Zorzet,S., Garrovo,C., Biffi,S., Gennaro,R. and Scocchi,M. (2010) The proline-rich peptide Bac7 (1–35) reduces mortality from Salmonella typhimurium in a mouse model of infection. *BMC Microbiol.*, **10**, 178.
13. Ghiselli,R., Giacometti,A., Cirioni,O., Circo,R., Mocchegiani,F., Skerlavaj,B., D'Amato,G., Scalise,G., Zanetti,M. and Saba,V. (2003) Neutralization of endotoxin in vitro and in vivo by Bac7(1–35), a proline-rich antibacterial peptide. *Shock*, **19**, 577–581.
14. Krizsan,A., Knappe,D. and Hoffmann,R. (2015) Influence of yjiL and upstream genes on the antibacterial activity of proline-rich antimicrobial peptides overcoming Escherichia coli resistance induced by the missing SbmA transporter system. *Antimicrob. Agents Chemother.*, **59**, 5992–5998.
15. Otvos,L., O,I., Rogers,M.E., Consolvo,P.J., Condie,B.A., Lovas,S., Bulet,P. and Blaszczyk-Thurin,M. (2000) Interaction between heat shock proteins and antimicrobial peptides. *Biochemistry*, **39**, 14150–14159.
16. Czihal,P., Knappe,D., Fritsche,S., Zahn,M., Berthold,N., Piantavigna,S., Müller,U., Van Dorpe,S., Herth,N., Binas,A. *et al.* (2012) Api88 is a novel antibacterial designer peptide to treat systemic infections with multidrug-resistant gram-negative pathogens. *ACS Chem. Biol.*, **7**, 1281–1291.
17. Krizsan,A., Volke,D., Weinert,S., Sträter,N., Knappe,D. and Hoffmann,R. (2014) Insect-derived proline-rich antimicrobial peptides kill bacteria by inhibiting bacterial protein translation at the 70 S ribosome. *Angew. Chem. Int. Ed.*, **53**, 12236–12239.
18. Scocchi,M., Lüthy,C., Decarli,P., Mignogna,G., Christen,P. and Gennaro,R. (2009) The proline-rich antibacterial peptide Bac7 binds to and inhibits in vitro the molecular chaperone DnaK. *Int. J. Pept. Res. Therapeut.*, **15**, 147–155.
19. Mardirossian,M., Grzela,R., Giglione,C., Meinnel,T., Gennaro,R., Mergaert,P. and Scocchi,M. (2014) The host antimicrobial peptide Bac71–35 binds to bacterial ribosomal proteins and inhibits protein synthesis. *Chem. Biol.*, **21**, 1639–1647.
20. Roy,R.N., Lomakin,I.B., Gagnon,M.G. and Steitz,T.A. (2015) The mechanism of inhibition of protein synthesis by the proline-rich peptide oncocin. *Nat. Struct. Mol. Biol.*, **22**, 466–469.
21. Seefeldt,A.C., Nguyen,F., Antunes,S., Perebaskine,N., Graf,M., Arenz,S., Inampudi,K.K., Douat,C., Guichard,G., Wilson,D.N. *et al.* (2015) The proline-rich antimicrobial peptide Onc112 inhibits translation by blocking and destabilizing the initiation complex. *Nat. Struct. Mol. Biol.*, **22**, 470–475.
22. Guida,F., Benincasa,M., Zahariev,S., Scocchi,M., Berti,F., Gennaro,R. and Tossi,A. (2015) Effect of size and N-terminal residue characteristics on bacterial cell penetration and antibacterial activity of the proline-rich peptide Bac7. *J. Med. Chem.*, **58**, 1195–1204.
23. Selmer,M., Dunham,C.M., Murphy,F.V., Weixlbaumer,A., Petry,S., Kelley,A.C., Weir,J.R. and Ramakrishnan,V. (2006) Structure of the

70S ribosome complexed with mRNA and tRNA. *Science*, **313**, 1935–1942.
24. Schmitt,E., Blanquet,S. and Mechulam,Y. (1999) Crystallization and preliminary X-ray analysis of Escherichia coli methionyl-tRNAMetf formyltransferase complexed with formyl-methionyl-tRNAMetf. *Acta Crystallogr. D*, **55**, 332–334.
25. Polikanov,Y.S., Blaha,G.M. and Steitz,T.A. (2012) How hibernation factors RMF, HPF, and YfiA turn off protein synthesis. *Science*, **336**, 915–918.
26. Polikanov,Y.S., Steitz,T.A. and Innis,C.A. (2014) A proton wire to couple aminoacyl-tRNA accommodation and peptide-bond formation on the ribosome. *Nat. Struct. Mol. Biol.*, **21**, 787–793.
27. Kabsch,W. (2010) Xds. *Acta Crystallogr. D Biol. Crystallogr.*, **66**, 125–132.
28. McCoy,A.J., Grosse-Kunstleve,R.W., Adams,P.D., Winn,M.D., Storoni,L.C. and Read,R.J. (2007) Phaser crystallographic software. *J. Appl. Crystallogr.*, **40**, 658–674.
29. Polikanov,Y.S., Melnikov,S.V., Soll,D. and Steitz,T.A. (2015) Structural insights into the role of rRNA modifications in protein synthesis and ribosome assembly. *Nat. Struct. Mol. Biol.*, **22**, 342–344.
30. Chou,F.C., Echols,N., Terwilliger,T.C. and Das,R. (2016) RNA structure refinement using the ERRASER-phenix pipeline. *Methods Mol. Biol.*, **1320**, 269–282.
31. Adams,P.D., Afonine,P.V., Bunkoczi,G., Chen,V.B., Davis,I.W., Echols,N., Headd,J.J., Hung,L.W., Kapral,G.J., Grosse-Kunstleve,R.W. *et al.* (2010) PHENIX: a comprehensive Python-based system for macromolecular structure solution. *Acta Crystallogr. D Biol. Crystallogr.*, **66**, 213–221.
32. Emsley,P. and Cowtan,K. (2004) Coot: model-building tools for molecular graphics. *Acta Crystallogr. D Biol. Crystallogr.*, **60**, 2126–2132.
33. Chen,V.B., Arendall,W.B. 3rd, Headd,J.J., Keedy,D.A., Immormino,R.M., Kapral,G.J., Murray,L.W., Richardson,J.S. and Richardson,D.C. (2010) MolProbity: all-atom structure validation for macromolecular crystallography. *Acta Crystallogr. D Biol. Crystallogr.*, **66**, 12–21.
34. Starosta,A.L., Karpenko,V.V., Shishkina,A.V., Mikolajka,A., Sumbatyan,N.V., Schluenzen,F., Korshunova,G.A., Bogdanov,A.A. and Wilson,D.N. (2010) Interplay between the ribosomal tunnel, nascent chain, and macrolides influences drug inhibition. *Chem. Biol.*, **17**, 504–514.
35. Hartz,D., McPheeters,D.S., Traut,R. and Gold,L. (1988) Extension inhibition analysis of translation initiation complexes. *Methods Enzymol.*, **164**, 419–425.
36. Starosta,A.L., Lassak,J., Peil,L., Atkinson,G.C., Virumäe,K., Tenson,T., Remme,J., Jung,K. and Wilson,D.N. (2014) Translational stalling at polyproline stretches is modulated by the sequence context upstream of the stall site. *Nucleic Acids Res.*, **42**, 10711–10719.
37. Polikanov,Y.S., Starosta,A.L., Juette,M.F., Altman,R.B., Terry,D.S., Lu,W., Burnett,B.J., Dinos,G., Reynolds,K.A., Blanchard,S.C. *et al.* (2015) Distinct tRNA accommodation intermediates observed on the ribosome with the antibiotics hygromycin A and A201A. *Mol. Cell*, **58**, 832–844.
38. Arenz,S., Meydan,S., Starosta,A.L., Berninghausen,O., Beckmann,R., Vazquez-Laslop,N. and Wilson,D.N. (2014) Drug sensing by the ribosome induces translational arrest via active site perturbation. *Mol. Cell*, **56**, 446–452.
39. Arenz,S., Ramu,H., Gupta,P., Berninghausen,O., Beckmann,R., Vazquez-Laslop,N., Mankin,A.S. and Wilson,D.N. (2014) Molecular basis for erythromycin-dependent ribosome stalling during translation of the ErmBL leader peptide. *Nat. Commun.*, **5**, 3501.
40. Bulkley,D., Innis,C.A., Blaha,G. and Steitz,T.A. (2010) Revisiting the structures of several antibiotics bound to the bacterial ribosome. *Proc. Natl. Acad. Sci.*, **107**, 17158–17163.
41. Dunkle,J.A., Xiong,L., Mankin,A.S. and Cate,J.H. (2010) Structures of the Escherichia coli ribosome with antibiotics bound near the peptidyl transferase center explain spectra of drug action. *Proc. Natl. Acad. Sci. U.S.A.*, **107**, 17152–17157.
42. Tomasinsig,L., Skerlavaj,B., Papo,N., Giabbai,B., Shai,Y. and Zanetti,M. (2006) Mechanistic and functional studies of the interaction of a proline-rich antimicrobial peptide with mammalian cells. *J. Biol. Chem.*, **281**, 383–391.
43. Wilson,D.N. (2009) The A-Z of bacterial translation inhibitors. *Crit. Rev. Biochem. Mol. Biol.*, **44**, 393–433.
44. Sadler,K., Eom,K.D., Yang,J.L., Dimitrova,Y. and Tam,J.P. (2002) Translocating proline-rich peptides from the antimicrobial peptide bactenecin 7. *Biochemistry*, **41**, 14150–14157.
45. Schmeing,T.M., Huang,K.S., Strobel,S.A. and Steitz,T.A. (2005) An induced-fit mechanism to promote peptide bond formation and exclude hydrolysis of peptidyl-tRNA. *Nature*, **438**, 520–524.
46. Schuwirth,B.S., Borovinskaya,M.A., Hau,C.W., Zhang,W., Vila-Sanjurjo,A., Holton,J.M. and Cate,J.H. (2005) Structures of the bacterial ribosome at 3.5 A resolution. *Science*, **310**, 827–834.
47. Voorhees,R.M., Fernandez,I.S., Scheres,S.H. and Hegde,R.S. (2014) Structure of the mammalian ribosome-Sec61 complex to 3.4 A resolution. *Cell*, **157**, 1632–1643.
48. Zanetti,M., Litteri,L., Gennaro,R., Horstmann,H. and Romeo,D. (1990) Bactenecins, defense polypeptides of bovine neutrophils, are generated from precursor molecules stored in the large granules. *J. Cell Biol.*, **111**, 1363–1371.
49. Scocchi,M., Skerlavaj,B., Romeo,D. and Gennaro,R. (1992) Proteolytic cleavage by neutrophil elastase converts inactive storage proforms to antibacterial bactenecins. *Eur. J. Biochem.*, **209**, 589–595.
50. Dimitrova,L.N., Kuroha,K., Tatematsu,T. and Inada,T. (2009) Nascent peptide-dependent translation arrest leads to Not4p-mediated protein degradation by the proteasome. *J. Biol. Chem.*, **284**, 10343–10352.
51. Lu,J. and Deutsch,C. (2008) Electrostatics in the ribosomal tunnel modulate chain elongation rates. *J. Mol. Biol.*, **384**, 73–86.

SUPPLEMENTARY ONLINE MATERIALS

for

Structure of the mammalian antimicrobial peptide Bac7(1-16) bound within the exit tunnel of a bacterial ribosome

A. Carolin Seefeldt[1,2,3], Michael Graf[4], Natacha Pérébaskine[1,2,3], Fabian Nguyen[4], Stefan Arenz[4], Mario Mardirossian[5], Marco Scocchi[5], Daniel N. Wilson[4,6,*] and C. Axel Innis[1,2,3,*]

[1] Institut Européen de Chimie et Biologie, University of Bordeaux, Pessac, 33607, France

[2] U1212, Inserm, Bordeaux, 33076, France

[3] UMR[---], CNRS, Bordeaux, 33076, France

[4] Gene Center and Department for Biochemistry, University of Munich, Munich, 81377, Germany

[5] Department of Life Sciences, University of Trieste, Trieste, 34127, Italy

[6] Center for integrated Protein Science Munich (CiPSM), University of Munich, Munich, 81377, Germany

* To whom correspondence should be addressed. Tel: +33 540006149; Fax: +33 540002215; Email: axel.innis@inserm.fr. Correspondence may also be addressed to: wilson@lmb.uni-muenchen.de.

The authors wish it to be known that, in their opinion, the first two authors should be regarded as joint First Authors.

Table S1. X-ray data processing and crystallographic refinement statistics

	Bac7(1-16)	**MetI**	**Pyr**
PDB code	5F8K	5FDU	5FDV
Space group	$P2_12_12_1$	$P2_12_12_1$	$P2_12_12_1$
Unit cell dimensions			
a	209.8 Å	209.7 Å	209.9 Å
b	450.3 Å	448.1 Å	450.1 Å
c	622.2 Å	623.4 Å	622.9 Å
α	90.0°	90.0°	90.0°
β	90.0°	90.0°	90.0°
γ	90.0°	90.0°	90.0°
Data processing			
Resolution	50 Å – 2.8 Å	50 Å – 2.9 Å	50 Å – 2.8 Å
R_{Merge}	51.3% (233.9%)	17.0% (181.0%)	17.8% (229.7%)
I/σI	5.71 (0.95)	11.61 (1.10)	15.99 (1.29)
CC 1/2	95.7 (16.1)	99.7 (34.9)	99.9 (41.1)
Completeness	99.6% (97.6%)	99.6% (99.5%)	100% (100%)
Redundancy	8.3 (8.1)	6.9 (6.7)	13.8 (13.4)
Refinement			
R_{work}/R_{free}	24.8% / 29.2%	18.3% / 23.4%	18.9% / 24.0%
Bond deviations	0.018 Å	0.030 Å	0.029 Å
Angle deviations	1.083°	1.976°	1.942°
Figure of merit	0.80	0.84	0.83
Ramachandran outliers	0.56%	0.95%	0.87%
Favorable backbone	94.3%	92.4%	93.3%

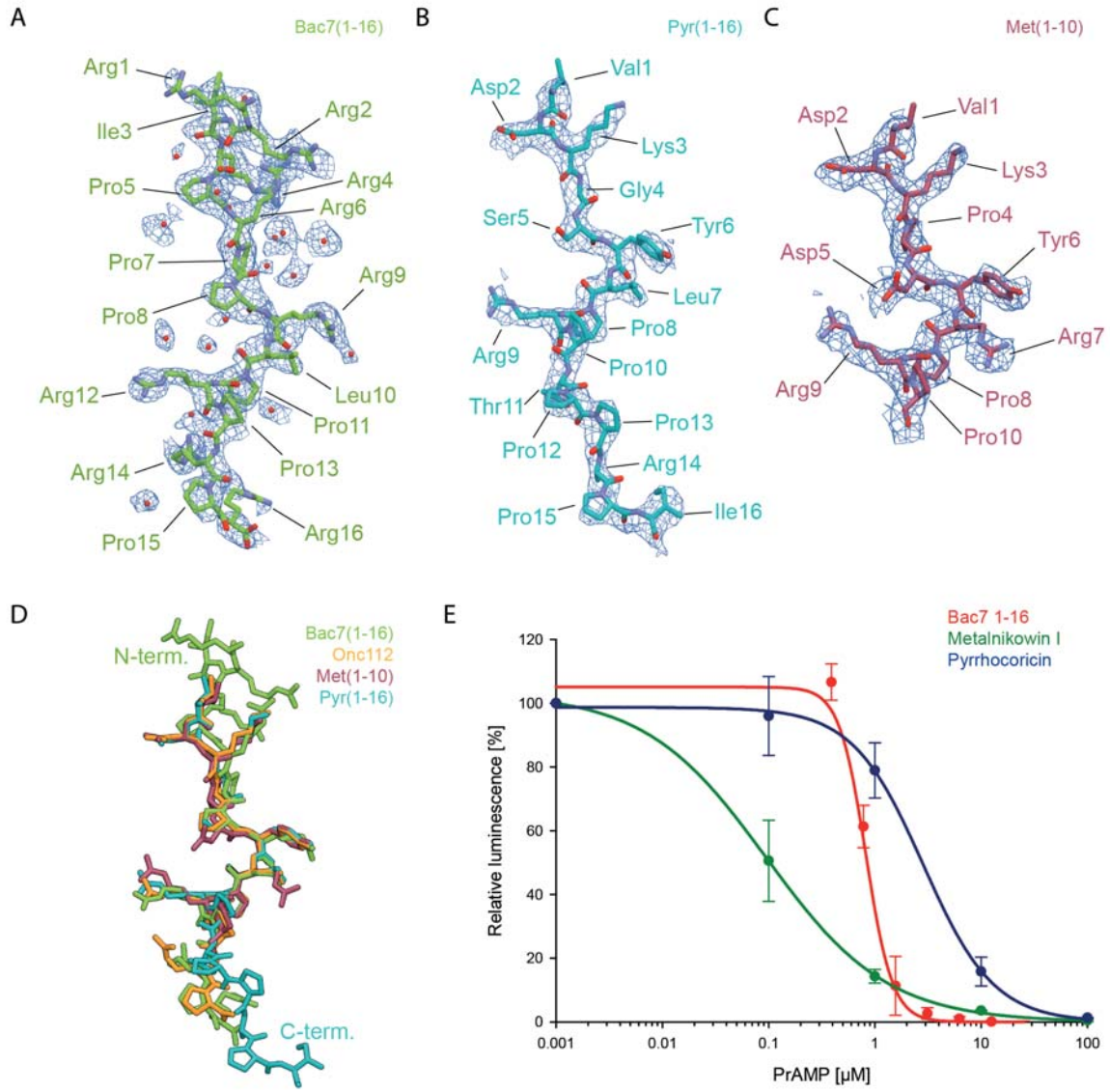

Figure S1. Minimally biased electron density for (A) the Bac7(1-16) peptide (green) and surrounding solvent molecules, as well as the (B) Pyr(1-16) (cyan) and (C) MetI(1-10) (burgundy) peptides. The peptides are shown in the same orientation as in Figure 1A and solvent molecules are displayed as spheres (red). Continuous density for the entire peptide and clear density for the solvent molecules are observed in a minimally biased F_o–F_c difference map contoured at +2.0σ (blue mesh). (D) Superimposition of the Bac7(1-16), Onc112(1-12) (orange), Pyr(1-16) and MetI(1-10) peptides. (E) Effects of increasing concentrations of Bac7(1-16) (red), Metalnikowin I (green) and Pyrrhocoricin (green) on the luminescence resulting from the *in vitro* translation of firefly luciferase (Fluc) using an *E. coli* lysate-based system. The error bars represent the standard deviation from the mean for triplicate experiments and the luminescence is normalized relative to that measured in the absence of peptide, which was assigned as 100%.

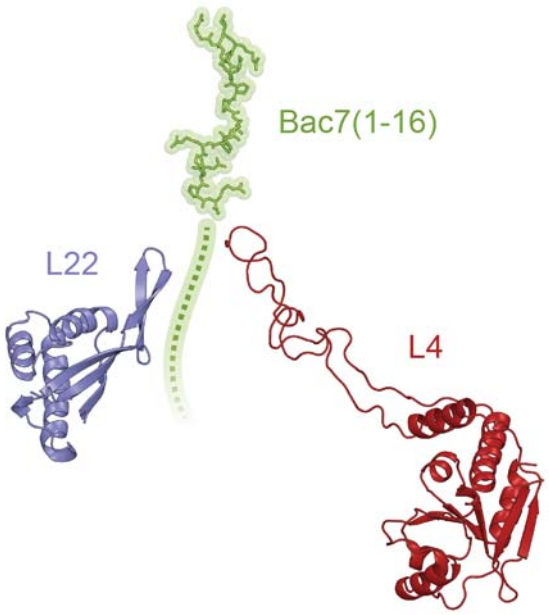

Figure S2. Relative position of the ribosome-bound Bac7(1-16) peptide (green) to the ribosomal proteins L4 (red) and L22 (blue) that reach into the lumen of the ribosomal tunnel. The proposed path for the full-length Bac7 peptide is shown as a dotted green line.

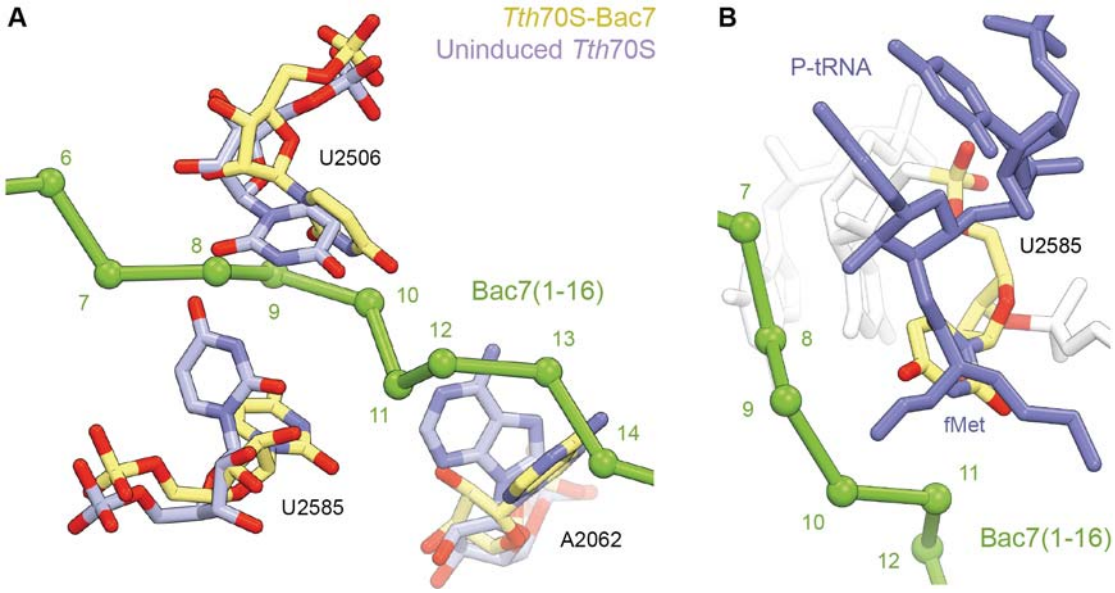

Figure S3. (A) Conformational changes in 23S rRNA nucleotides A2062, U2506 and U2585 that take place upon binding of Bac7(1-16) to the ribosome. Nucleotides from the *Tth*70S-Bac7 structure are shown in yellow, while nucleotides in the Bac7-free or "uninduced" conformation are in blue (1). (B) Clash between the formyl-methionyl moiety of a P-site bound fMet-$tRNA_i^{Met}$ (blue) and 23S rRNA residue U2585 in its Bac7-bound conformation (yellow). Bac7(1-16) is shown as a green Cα-trace in both panels.

SUPPLEMENTARY REFERENCES

1. Jenner, L., Starosta, A.L., Terry, D.S., Mikolajka, A., Filonava, L., Yusupov, M., Blanchard, S.C., Wilson, D.N. and Yusupova, G. (2013) Structural basis for potent inhibitory activity of the antibiotic tigecycline during protein synthesis. *Proceedings of the National Academy of Sciences of the United States of America*, **110**, 3812-3816.

4.2 A novel strategy for the structural characterization of arrested ribosomal complexes featuring short nascent peptides

The second part of this thesis focused on understanding the underlying mechanism of short peptides that mediated nascent chain-dependent translational arrest. Previously, the M+X(+) motif was reported to arrest the ribosome in the presence of erythromycin (Sothiselvam et al., 2014; Sothiselvam et al., 2016) while poly-proline motifs arrest the ribosome without any additional ligands (Doerfel et al., 2013; Ude et al., 2013). However, far no structural information had been obtained.

Previously, long nascent chain-mediated translational arrest peptides, like SecM (Bhushan et al., 2011; Zhang et al., 2015), VemP (Su et al., 2017), MifM (Sohmen et al., 2015), TnaC (Bischoff et al., 2014; Seidelt et al., 2009), ErmBL (Arenz et al., 2016; Arenz et al., 2014b) and ErmCL (Arenz et al., 2014a), have been studied by cryo-EM. The nascent chain-mediated translational arrested ribosome complexes have been obtained using different strategies depending on the length of the arrest peptide. Arrest peptides including SecM, VemP, MifM, and TnaC are long peptides with the N-terminus exiting the ribosomal tunnel and they arrest the ribosome-independent of their N-terminal sequence. The N-terminus was fused to a His_8(H_8)-tag which allowed purification after *in vitro* translation (Sohmen et al., 2015; Su et al., 2017; Zhang et al., 2015) or the purification of the arrest complex from cells (Bischoff et al., 2014). ErmBL and ErmCL are shorter arrest peptides in which the nascent chain does not reach the exit of the ribosomal tunnel and so they cannot be purified using the H_8-tag. To still allow solving the structure, the disome approach was developed (Arenz et al., 2014a; Arenz et al., 2014b). This approach is based on a bicistronic DNA template that encodes two ORFs of the arrest peptide that is added into an *in vitro* translation system. In the absence of the ligand, ribosomes can translate normally resulting in one ribosome per mRNA on average. In the presence of erythromycin, the ribosomes are arrested and so two ribosomes, termed disomes, are bound to the same mRNA molecule. The disomes were separated from the monosomes and through sucrose gradients. Subsequently, RNase H treatment led to the separation of the disomes and the obtained monosomes were used for structure determination (Arenz et al., 2014a; Arenz et al., 2014b).

The original goal of this thesis was to determine the structure of short arrest peptides using X-ray crystallography. For this approach, a high homogeneity of the arrest complex is necessary

to obtain high-resolution information. The approaches used to obtain the ribosomal nascent-chain complexes (RNCs) contain long mRNA fragments that limits the diffraction of the crystals (data unpublished and obtained by Axel Innis while he was in the group of Prof. Thomas Steitz). To overcome limitations of diffraction and to ensure the stoichiometry of the complex, the short arrest peptides can be transferred to the 3'CCA end of a purified tRNA using the flexizyme methodology (Goto et al., 2011), a method that was developed for genomic reprogramming (chapter 1.5). By transferring the arrest peptide directly onto the 3'CCA end of the initiator tRNA, which has a high affinity for the P-site, the length of the mRNA can be reduced significantly. The following figure illustrates how complexes can be formed to study short arrest peptides:

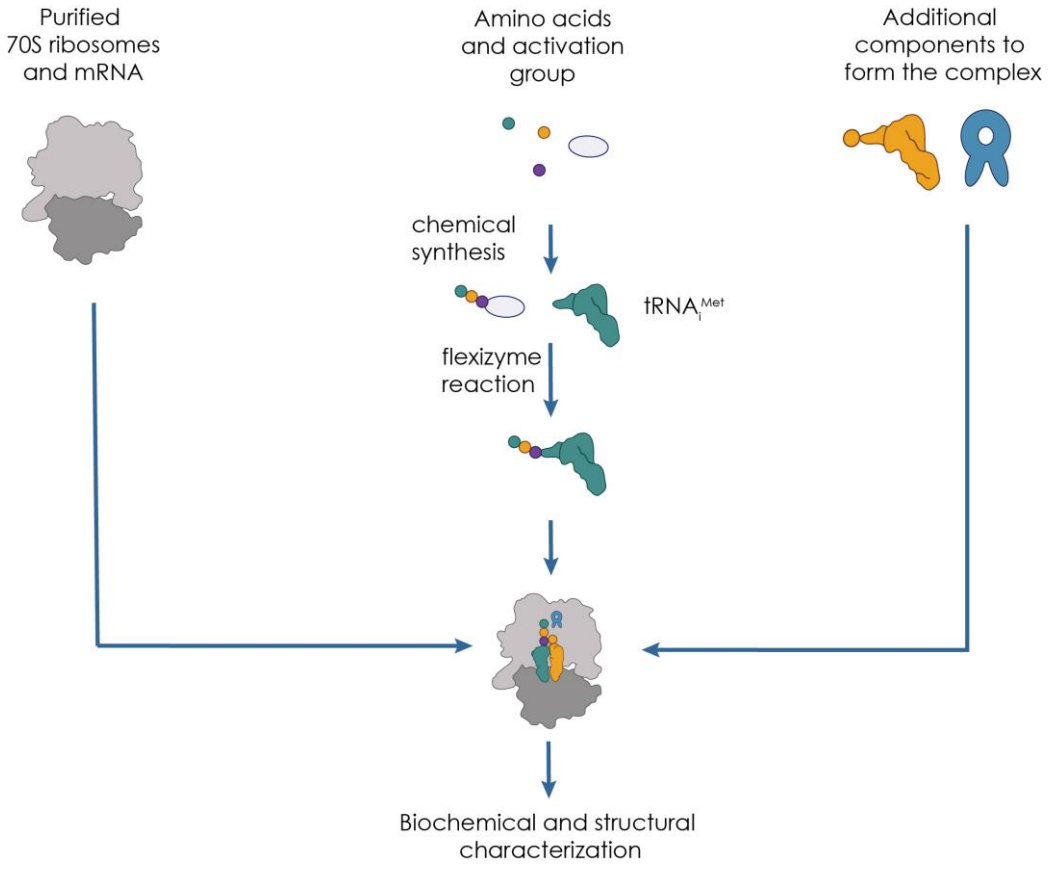

Figure 17: General workflow to study short peptides that mediated nascent chain-dependent translational arrest using the flexizyme methodology. Arrest peptides can be transferred onto the 3' end of purified initiator tRNA. The peptidylated tRNA can be used to form the arrest complex with purified ribosomes.

As 70S *T. thermophilus* ribosome are known to crystallize well and diffract to high resolution, these ribosomes were used for crystallization experiments. For cryo-EM studies, 70S ribosomes from *E. coli* were purified by disassembling them into individual subunits and re-associating

them (Sucrose gradients, supplements Figure 66, Blaha et al., 2000). This strategy ensures the removal of ribosome associated factors and tRNAs and increases further the homogeneity of the complex. A short RNA encoding a Shine-Dalgarno sequence followed by a short open reading frame (Figure 17) and is necessary for peptidyl tRNA binding to the ribosome. The arrest peptides were synthesized and activated chemically by Dr. Caterina Lombardo and Dr. Christophe André from the group of Dr. Gilles Guichard (IECB, Pessac, France) and then transferred via flexizyme reaction onto the 3′ CCA end of the initiator tRNA. The peptidyl-tRNA thus obtained was purified using RP-HPLC. We hypothesized that the high P-site binding affinity of the initiator tRNA is sufficient to force the arrest peptide into the ribosomal exit tunnel. The arrest complex is formed in the presence of additional compounds such as aminoacyl-tRNA or an antibiotic. The stalled complex can then be studied structurally and biochemically. Biochemical assay can be e.g. toeprinting assay, footprinting assay, and puromycin stability assays. The peptide is normally linked via an ester bond to the 3′CCA end of the tRNA and this bond is pH sensitive. However, the ester-linked peptidyl-tRNA can be still used for complex formation to study the RNC with cryo-EM as the sample is frozen directly after complex formation. The recent development of direct detectors and the constant improvement of processing software made it possible to obtain near-atomic resolution structure structures by cryo-EM (Kühlbrandt, 2014). The near-atomic resolution is sufficient to study short arrest peptides and was used to obtain the structure of the MKF-70S *E. coli* ribosome (chapter 4.4).

For X-ray crystallography, crystals were grown for several days at a pH of 7.5 (chapter 3.9) and so the ester bind might hydrolyze during this process. In order to ensure the stoichiometry of the complex, the ester linkage can be replaced by an amide linkage (non-hydrolysable bond) that is pH insensitive and was used in previous studies of the molecular mechanism of peptide bond formation (Polikanov et al., 2014; Voorhees et al., 2009). This tRNA is obtained by exchanging the 3′OH of the tRNA by a 3′NH_2-group (chapter 3.5.4). Attempts to transfer the activated peptides onto 3′NH_2-$tRNA_i^{Met}$ using the flexizyme methodology were so far unsuccessful. Another strategy to introduce the amide bond between the arrest peptide and the tRNA is shown in the following figure:

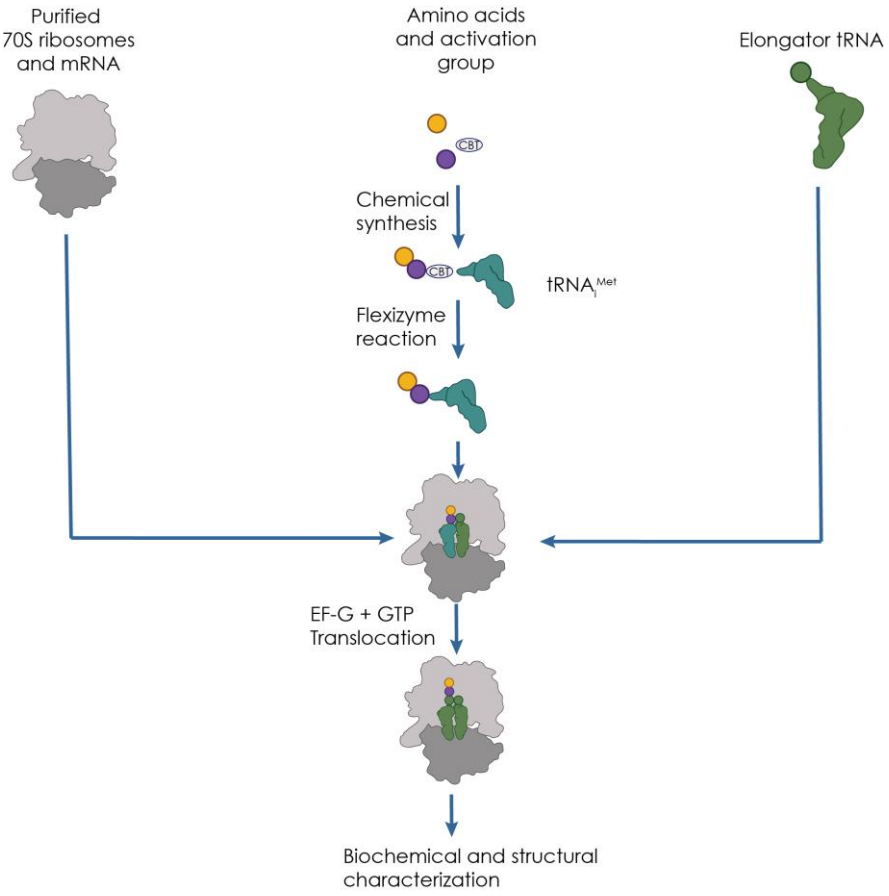

Figure 18: Workflow to obtain the arrest complex using one round of translocation. The pre-arrest complex is formed using peptidyl-tRNA, 70S ribosomes, and elongator tRNA. The arrest complex is obtained after one round of translocation in the presence of EF-G and GTP.

The non-hydrolyzable bond can be introduced using one round of translocation in the presence of the dipeptidyl-tRNA$_i^{Met}$ and a non-hydrolysable aminoacylated elongator tRNA. The aminoacylation reaction can be performed using the corresponding aminoacyl-tRNA synthetase as it was used previously reported (Polikanov et al., 2014; Voorhees et al., 2009). The arrest complex is formed by the addition of EF-G and GTP. Another advantage of the second strategy is that the P-site tRNA within the arrest complex is not tRNA$_i^{Met}$ making the complex more native.

The following chapters include the results obtained to study nascent chain-mediated translational arrest along fM+F(+) in the presence of erythromycin and along consecutive polyprolines and present a novel approach to form arrested complexes using the flexizyme methodology.

4.3 Peptidylation of $tRNA_i^{Met}$ using flexizyme

The flexizymes eFx, dFx, and aFx were generated by *in vitro* transcription as described before (Murakami et al., 2006a). Reaction conditions were tested using a CCA-stem loop, a microhelix. The reaction conditions, including Mg^{2+} concentration and pH, were screened. A higher pH might increase the yield of peptidylated tRNA but includes also the risk of tRNA degradation and depeptidylation. Consequently, the reaction conditions needed to be balanced.

4.3.1 Screening reactivity and time courses

Peptides to study fM+X(+) and polyproline-mediated arrest, were designed applying different rules. Bacterial translation is initiated by initiator tRNA attached to a formylated methionine. Peptides that carried a methionine at the N-terminus were thus formylated in order to mimic the natural substrate. In contrast to this, any other N-terminal amino acid was acetylated to mimic the growing peptide chain and increase the stability of the peptidyl-tRNA. The flexizyme reaction is mainly limited by the solubility of the peptide in aqueous solution (Niwa et al., 2009). The incorporation of positively-charged amino acids such as lysine and arginine increase the solubility of the peptides in water.

Several leaving groups in combination with their corresponding flexizymes were tested in different Mg^{2+} concentrations and pH-values ranging from 6.5 to 8.5. The highest peptidylation capacity was reached with 75 µM eFx and 5 mM AcRP-CBT, AcRA-CBT, AcRD-CBT, and fMK-CBT in a buffer containing 50 mM Bicine-KOH pH 8.5, 50 mM $MgCl_2$, 20% DMSO, 25 µM $tRNA_i^{Met}$. Scale-up reactions were incubated for eight days on ice.

The following figure shows the acidic denaturing PAGE monitoring the daily progress of the reaction:

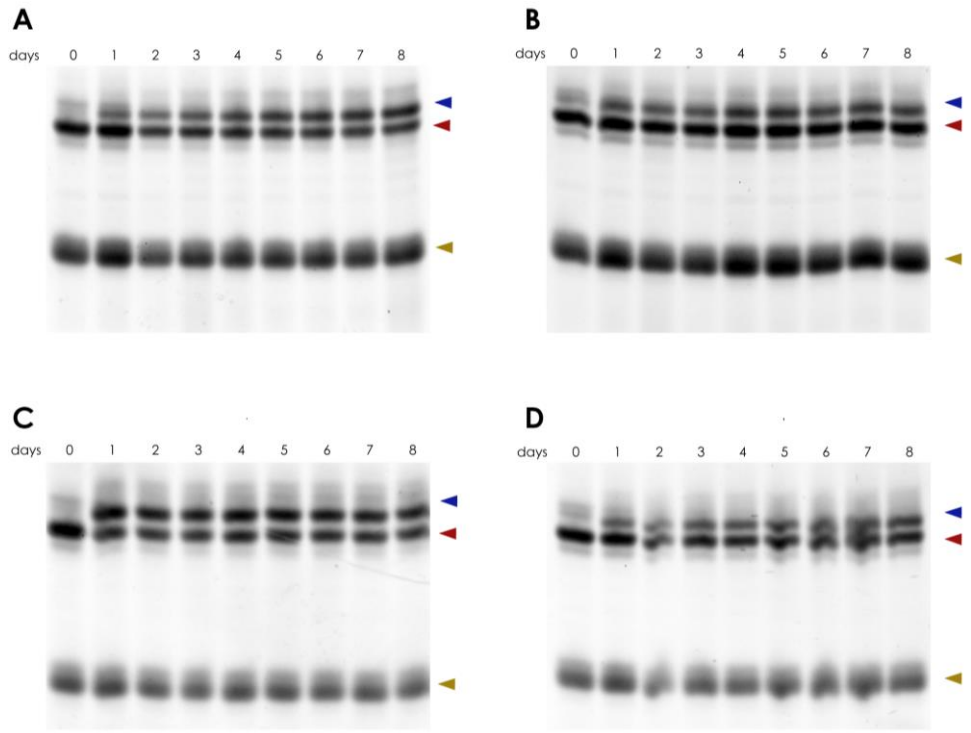

Figure 19: Time course of flexizyme reactions for fMK-CBT (A), AcRP-CBT (B), AcRA-CBT (C) and AcRD-CBT (D) onto $tRNA_i^{Met}$. Time points were taken daily and analyzed by a 12% acidic denaturing PAGE stained with SYBRgold. The blue arrow indicates the peptidylated tRNA, the red one the deaminoacylated $tRNA_i^{Met}$ and the yellow one indicates the band corresponding to eFx. The reaction was performed on ice.

Figure 19 shows that all four peptides can be transferred to a certain degree to the 3' CCA end of $tRNA_i^{Met}$ but their individual reactivity varies depending on the nature of the peptide. The most reactive peptide is AcRA-CBT. The intensity of the AcRA-$tRNA_i^{Met}$ band shows a similar intensity as the band for the deaminoacylated tRNA, meaning a reaction efficiency of approximately 50%. The product is formed within the first day, as indicated by the band corresponding to the peptidyl-tRNA (Figure 19). In contrast to this, the reaction involving AcRP-CBT, AcRD-CBT, and fMK-CBT require a week to obtain a comparable intensity of the band corresponding to the peptidylated tRNA (Figure 19). The reaction was stopped as the intensity of the band corresponding to the product did not increase any more. This might indicate the saturation of the reaction. In addition, further incubation might result in hydrolysis of the peptide and the tRNA. This long reaction time stands in contrast to the reactivity of the fMKF-CME peptide, which reacts within 2 h with a peptidylation efficiency of 100% as shown by Dr. K. Kishore Inampudi, a postdoctoral fellow in the Innis group (PAGE listed in supplemental information Figure 67).

Another strategy to follow the progress of the flexizyme reaction is using a short microhelix as the flexizyme reaction is independent of the body of the tRNA. The time course for following the reaction of tripeptide AcRAP-CME with microhelix and eFx is shown in Figure 20:

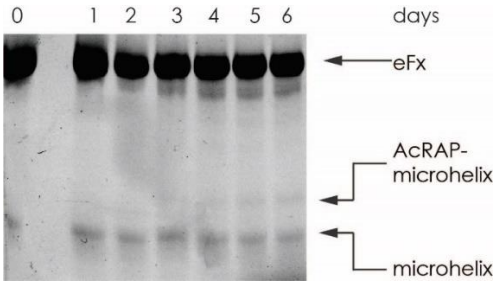

Figure 20: Time course following the peptidylation reaction of AcRAP-CBT peptide with microhelix over six days. The analysis was performed by a 20% acidic denaturing PAGE stained with SYBRgold. The microhelix is smaller than eFx. A band corresponding to the peptidylated product appears after 3 days of reaction on ice.

The first product is visible after three days and increases until the sixth day with a reaction efficiency around 10% (Figure 20). For large scale reactions, the microhelix was replaced by initiator tRNA and incubated for a week on ice before purification as shown in the corresponding PAGE (Figure 22)

4.3.2 Purification of peptidylated $tRNA_i^{Met}$

For the following studies, peptidylated $tRNA_i^{Met}$ was separated from deaminoacylated $tRNA_i^{Met}$ and eFx by RP-HPLC using a C4 column. The deaminoacylated $tRNA_i^{Met}$ has a high affinity for the P-site of the ribosome (Blaha et al., 2009), so the peptidylated tRNA needs to be separated from the unreacted one so that the resulting complex contains little or no deacylated $tRNA_i^{Met}$, which would reduce the occupancy of the peptidyl moiety. In addition, eFx might have a negative effect on crystallization and should thus be removed.

Reactions were stopped by precipitating the RNA using 300 mM $Na(CH_3CO_2)$ pH 5.5/70% Ethanol. To purify the sample was recovered in RP-Buffer (20 mM $NH_4(CH_3CO_2)$, 10 mM $Mg(CH_3CO_2)_2$, 400 mM NaCl) and loaded on a RP-C4-HPLC (see chapter 3.5). The sample was separated using increasing concentrations of methanol (RP buffer B, 40% (v/v) methanol). The gradient was 0-50% RP buffer B over 14 column volumes followed by a steep step from 50-100% buffer B in one column volume. The purification was performed at pH 5.5 in order to

prevent peptide hydrolysis. The chromatograms of this purification are shown in Figure 21 along the corresponding acidic PAGE analysis:

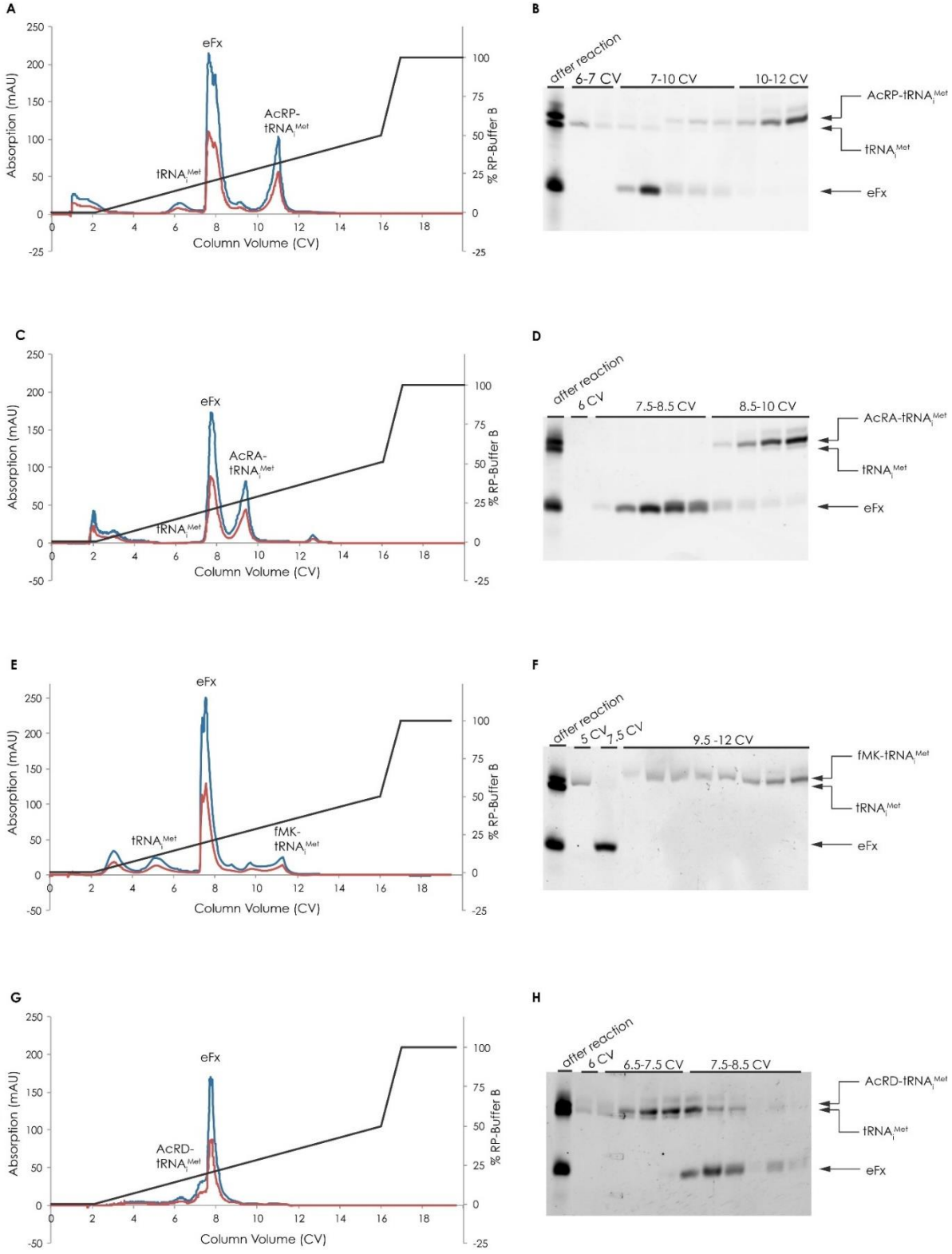

Figure 21: RP-HPLC purification of dipetidylated-tRNA$_i^{Met}$ after flexizyme reaction for 8 days on ice. Elution fractions giving a strong UV signal were analyzed by 12% acidic denaturing PAGE. A, C, E and G show the chromatogram of the purification monitoring the elution profile by measuring the absorption at λ=260 nm (blue)

and λ=280 nm (red). Peaks are labeled depending on their main component as identified by acidic denature PAGE stained with SYBRgold (B, D, F and H)

For the purification of AcRP-tRNA$_i^{Met}$, AcRA-tRNA$_i^{Met}$ and fMK-tRNA$_i^{Met}$ the chromatograms show three or four distinct elution peaks (Figure 21). The first peak elutes before the start of the gradient or at the very beginning of the gradient corresponding to unreacted, activated peptide. The aromatic ring of the CBT leaving group was expected to give a strong UV signal as seen during peptide synthesis. From tRNA$_i^{Met}$ purification (data not shown), the second peak (approx. 4.5 CV) corresponds to deaminoacylated tRNA$_i^{Met}$ which is absent in the AcRA-tRNA (Figure 21, C, D) sample.

The third peak corresponds to eFx (approx. 7.5 CV). The last peaks correspond to the peptidylated tRNA as the peptide increases the hydrophobicity and results in tighter binding to the column material. AcRP-tRNA$_i^{Met}$ (Figure 21A) and AcRA-tRNA$_i^{Met}$ (Figure 7C) elutes over a short number of fractions while the peak corresponding to fMK-tRNA$_i^{Met}$ (Figure 21E) elutes over several fractions. An explanation could be that the lysine side chain might adopt different orientations. In contrast to this, the peptidyl tRNA peak is absent in the chromatogram for AcRD-tRNA$_i^{Met}$ (Figure 21, G, H). In this particular case, the peptide is less hydrophobic as the other ones and co-elutes with eFx. The carboxyl group of the aspartate side chain has a pK_a of 3.64 and is likely to be deprotonated at a pH of 5.5. Consequently, the AcRD-tRNA elutes earlier (Figure 21, G, H). Decreasing the slope of the gradient and reducing the pH of the running buffer resulted in similar elution profiles. Subsequent experiments were performed using AcRP-tRNA$_i^{Met}$ (approx. 80% reaction efficiency), AcRA-tRNA$_i^{Met}$ (approx. 100% reaction efficiency) and fMK-tRNA$_i^{Met}$ (approx. 40% reaction efficiency). The reactivity concluded from the HPLC-profile is in all cases higher than estimated from time courses (Figure 19). Reasons include the partial hydrolysis of the peptide from the tRNA during sample analysis. An explanation could be that the buffer concentration within the loading dye is too low to acidify the reaction buffer (50 mM Bicine-KOH pH 8.5) and partial peptidyl hydrolysis might also occur during heating of the samples prior to loading the PAGE.

The tripeptide AcRAP-CBT was reacted with initiator tRNA in the presence of eFx for one week on ice. Following, the product was purified via C4-RP-HPLC using a modified gradient from 0-80% RP buffer B. The resulting chromatogram is shown in Figure 22:

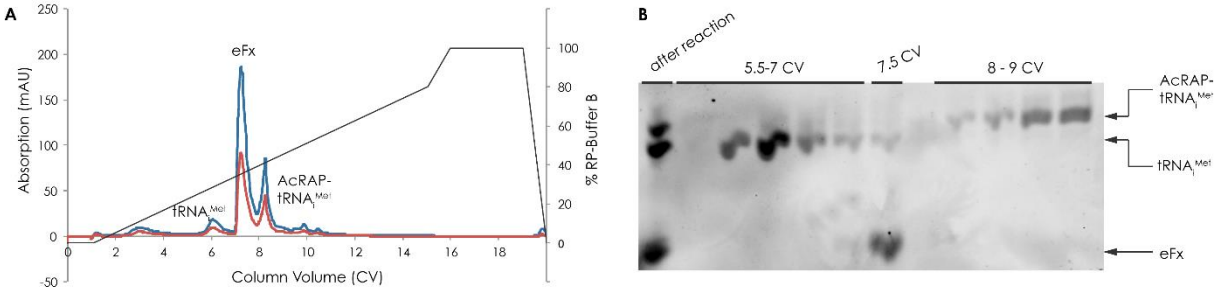

Figure 22: Purification of AcRAP-tRNA$_i^{Met}$ after flexizyme reaction for 7 days on ice by C4-RP-HPLC (A). The elution profile was followed using the absorption profile at ʎ= 260 nm (blue) and ʎ=280 nm (red). Fractions were analyzed by acidic denaturing PAGE (B) stained with SYBRgold.

Figure 22 shows that Ac-RAP-tRNA$_i^{Met}$ can be separated from unreacted initiator tRNA and eFx. Due to its hydrophobic properties, the peptidylated tRNA elutes last and is almost completely separated from the eFx peak. The peptidylation efficiency was estimated to be approximately 80%.

Fractions containing the peptidylated tRNA$_i^{Met}$ were combined. The reverse phase buffer contains 400 mM NaCl, which will interfere with downstream applications e.g. crystallography and *in vitro* protein synthesis. The buffer was exchanged over concentrators into 5 mM $NH_4(CH_3CO_2)$ buffer. The samples were lyophilized followed by resuspension in 20 µL 5 mM $NH_4(CH_3CO_2)$. After concentrating, the sample was analyzed by acidic denaturing PAGE (Figure 23):

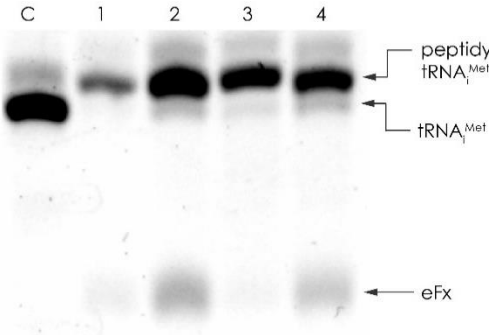

Figure 23: After buffer exchange and lyophilization of the peptidylated tRNAs did not hydrolyze. Lane c shows deaminoacylated initiator tRNA. AcRP-tRNA$_i^{Met}$ (1), AcRA-tRNA$_i^{Met}$ (2), AcRAP-tRNA$_i^{Met}$ (3) and fMKF-tRNA$_i^{Met}$(4) are peptidylated. The analysis was performed by a 12% denaturing acidic PAGE and stained with SYBRgold.

All peptidyl-$tRNA_i^{Met}$ (AcRP-$tRNA_i^{Met}$, AcRA-$tRNA_i^{Met}$, AcRAP-$tRNA_i^{Met}$ and fMK-$tRNA_i^{Met}$,) were still peptidylated after buffer exchange (Figure 23). Samples still contained minor eFx contaminations which were expected not to interfere with downstream applications.

4.4 Investigations of fM+X(+) nascent chain-mediated translational arrest in the presence of erythromycin

4.4.1 Complexes to study fM+X(+) in the presence of erythromycin

Two ribosome profiling studies revealed that ribosomes arrest on +X(+) motifs in the presence of macrolides or ketolides (Davis et al., 2014; Kannan et al., 2014). This motif is also present in the ErmD leader peptide and successive shortening of the arrest peptide led to the identification of the minimal arrest motif MRLR that could be generalized in fM+X(+) (Sothiselvam et al., 2014; Sothiselvam et al., 2016). The underlying mechanism remains unknown. The following figure shows the complex for studying this type of arrest peptide:

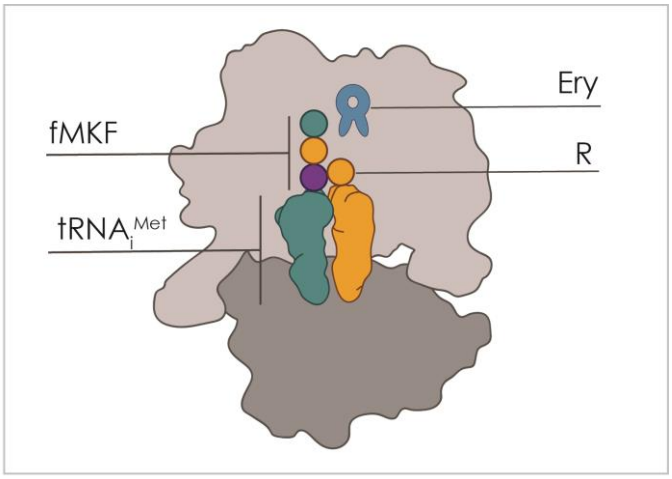

Figure 24: Complex to study fM+X(+)-mediated arrest in the presence of erythromycin. The MKFR sequence was chosen to study this particular arrest.

The sequence variants of this study are fMRF(R) and fMKF(R). The phenylalanine in position 0 is the activated amino acid. Phenylalanine-CME was used to optimize the flexizyme sequences and shows a high reactivity (Goto et al., 2011). Additionally, the aromatic side chain is bulky and would make side chain assignment easier in the event a medium resolution structure was obtained. The lysine in the penultimate position was used as the positively charged residue. Many experiments and toeprints were performed using additionally the MRF(R) sequence but fMR-CBT showed a low peptidylation rate and fMRF-CME was never synthesized and so structural data were obtained studying the fMKF(R) sequence. The methionine was placed in -2 positions as bacterial translation is initiated using fMet-tRNA$_i^{Met}$. The peptide was attached

to $tRNA_i^{Met}$ due to the latter's high affinity for the P-site. Due to its bulky guanidinium group, I chose Arg-$tRNA^{Arg}$ as the incoming aminoacyl-tRNA. This particular tRNA was *in vitro* transcribed and aminoacylated by Dr. Axel Innis while he was in the group of Prof. Thomas Steitz.

For this project, the fMKF-$tRNA_i^{Met}$ was generated and purified by Dr. K. Kishore Inampudi and he used it for X-ray crystallography. I performed the biochemical characterization by toeprinting and structural studies including X-ray crystallography and cryo-EM.

4.4.2 Toeprinting to validate that fM+F(+) arrests the ribosome in the presence of erythromycin

By mutating one position at a time, the MRL(R) motif was generalized to fM+X(+) (Sothiselvam et al., 2016) considering also the published ribosome profiling data that led to the identification of the +X(+) within long nascent chains (Kannan et al., 2014). In contrast to the MRF(R) sequence, arrest induced by the sequences MKFR, MRFK and MKFK, which compared to the MRLR motif encode two substitutions, has not been shown yet. In order to use this sequences for structural studies I therefore first had to show that they could arrest translation in the presence of erythromycin. Toeprinting reactions (chapter 3.9) were performed using DNA templates encoding MRFRI*, MKFRI*, MRFKI* and MKFKI* in the presence or absence of 25 µM erythromycin within the reaction. A PURExpress system (NEB) lacking release factors was used, preventing the release of ribosomes that reached the stop codon, which was expected to yield a toeprint corresponding to ribosomes positioned with their P-site on the preceding isoleucine codon. The following figure illustrates the nascent chain-mediated translational arrest induced by these motifs in the presence of erythromycin:

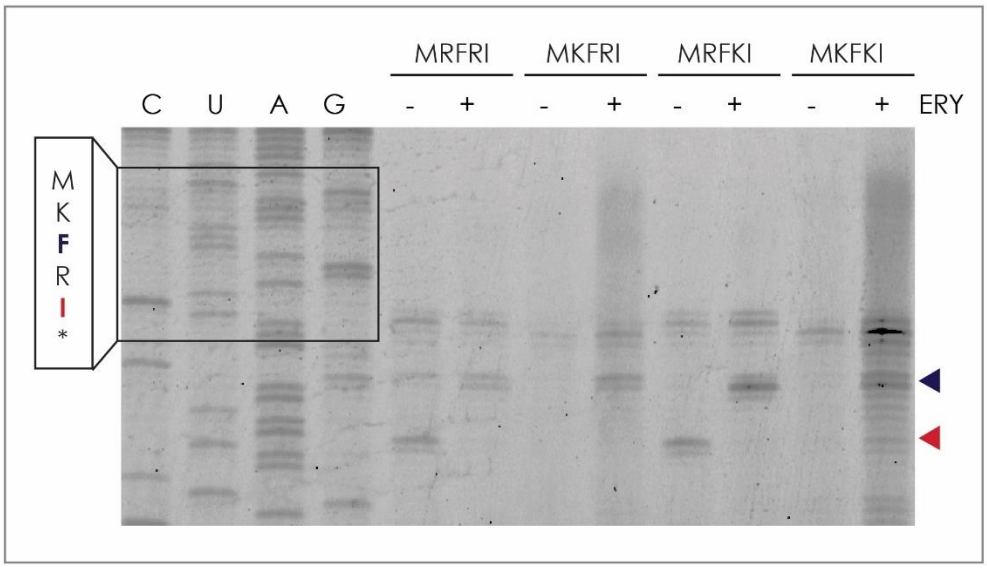

Figure 25: MRFR, MKFR, MRFK and MKFK arrest the *E. coli* ribosome in the presence of erythromycin. Toeprinting reactions were performed using a PURExpress system (NEB) omitting the release factors. Non-arrested ribosomes were not released (red arrow). The arrest site is indicated by the dark blue arrow. The position of the ribosome can be analyzed due to the presence of the sequencing lanes and the fact that the ribosomes cover 16-17 downstream nucleotides counting from the first nucleotide of the P-site.

The toeprint (Figure 25) shows that the ribosome is arrested on the phenylalanine (blue arrow) codon when translating MRFRI, MKFRI, MRFKI, and MKFKI in the presence of erythromycin. Consequently, all four sequences can be used for structural studies. However, sequences encoding at least one arginine codon show a stronger arrest band as sequences encoding two lysine residues. Overall, all sequences tested arrest *E. coli* ribosomes. Since for crystallographic studies complexes were formed with 70S *T. thermophilus* ribosomes, the arrest had to be studied using 70S *T. thermophilus* ribosomes. Earlier studies showed that reconstituted *in vitro* translation systems can be used to study bacterial ribosomes from different species, e.g. *B. subtilis* or *T. thermophilus*, in the presence of *E. coli* translation factors (Chiba et al., 2011; Thompson and Dahlberg, 2004). In the case of 70S *T. thermophilus* ribosomes, the reaction can be enhanced using *T. thermophilus* initiation factors (Thompson and Dahlberg, 2004). Reaction conditions were optimized using the well-characterized arrest peptide ErmDL. The toeprinting reactions were performed starting from a DNA template encoding the wild-type ErmDL sequence (MTHSMRLRSE*) with a final concentration of 2.5 µM 70S ribosomes. The resulting sequencing gel is shown in the following figure:

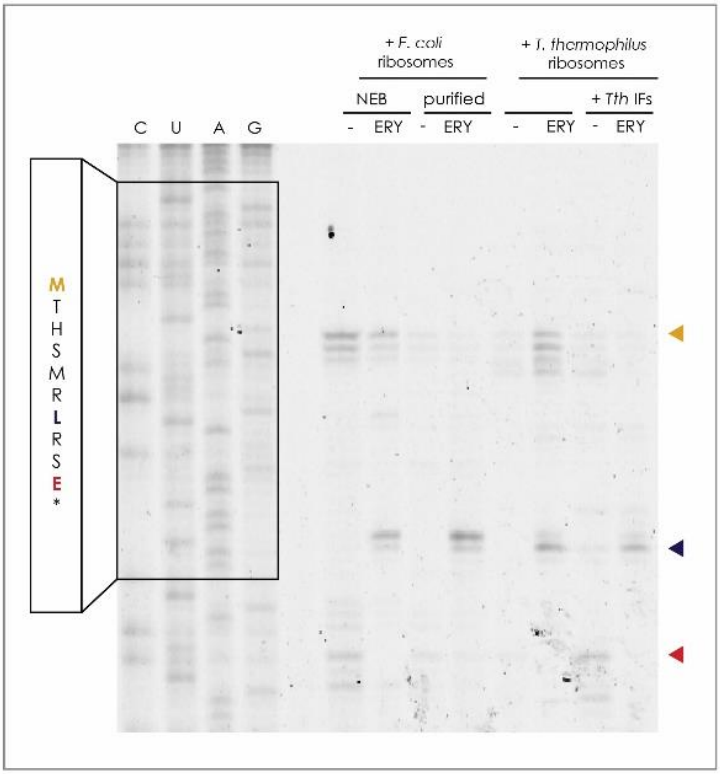

Figure 26: In the presence of erythromycin, ErmDL arrests 70S *T. thermophilus* ribosomes at the same position as the 70S *E. coli* ribosomes. The reaction was performed using a PURExpress system with separated ribosomes and release factors to study the arrest peptide ErmDL in the presence or absence of erythromycin. Reactions were performed using 2.5 µM ribosomes provided from NEB, extracted from *E. coli* KC6 or *T. thermophilus* HB8 cells (chapter 3.6). The reaction was enhanced using 2 µM of IF1, 2 and 3 from *T. thermophilus* purified by Dr. Axel Innis in the Steitz laboratory). The band corresponding to the start codon is indicated by the yellow arrow, the arrest site by the dark blue arrow and the stop codon is indicated by the red arrow.

Figure 26 indicates that in all reactions the ribosomes were arrested at the leucine codon in the presence of erythromycin (dark blue arrow). This indicates that ribosomes purified from *T. thermophilus* HB8 cells can be used to study nascent chain-mediated translational arrest in the custom-made PURExpress system by performing the reaction at 37°C as suggested by published experiments (Thompson et al., 2001). To prevent the arrest of the post-initiation complex, protein synthesis with 70S *T. thermophilus* ribosomes can be enhanced at 37°C through the addition of *T. thermophilus* initiation factors (Thompson and Dahlberg, 2004). The last two lanes show the results of the reaction containing 2 µM of each of the *T. thermophilus* initiation factors. The presence of the *T. thermophilus* initiation factors led to a prominent decrease in 70S *T. thermophilus* ribosomes arrested at the start codon (Figure 26). Subsequent experiments containing 70S *T. thermophilus* ribosomes were performed at 37°C, using a ribosome concentration of 2.5 µM and 2 µM per initiation factor. Crystal structures of 70S

T. thermophilus ribosomes in complex with erythromycin revealed a similar binding mode of the drug as in the 70S *E. coli* ribosome (chapter 1.4.3). As I wanted to determine the structure of the short arrest peptide MRFR in the presence of erythromycin, I wanted to understand how this sequence affects ribosomes from *T. thermophilus*. The optimized conditions given above were used to study nascent chain-mediated translational arrest induced by MRFRI in the presence of erythromycin using 70S *T. thermophilus* ribosomes. The result is shown in the following figure:

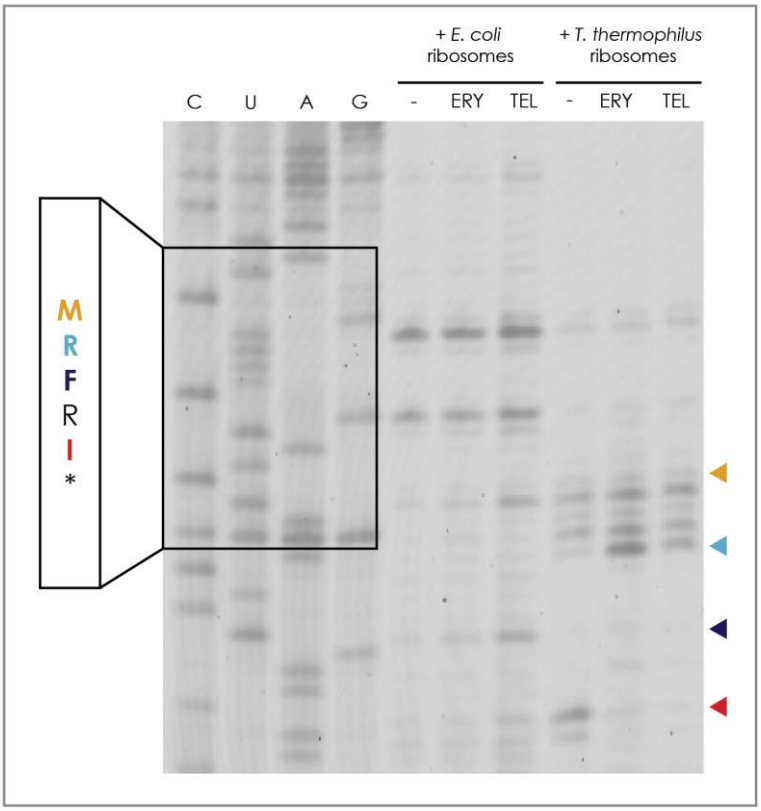

Figure 27: Toeprint of MRFRI in the presence or absence of erythromycin/telithromycin using 70S *T. thermophilus* ribosomes. In the presence of the antibiotic, 70S *T. thermophilus* ribosomes arrest mainly at the second codon (blue arrow). The start codon is indicated by the yellow arrow, arrest site by the dark blue arrow and ribosomes that failed to terminate by the red arrow.

The toeprint assay was performed using the DNA-template encoding MRFRI* (Figure 27). The resulting sequencing-PAGE revealed that the 70S *T. thermophilus* ribosomes arrest on the second codon (blue arrow) and cannot proceed to the third codon to form the arrest complex (dark blue arrow) in the presence of erythromycin. The *T. thermophilus* ribosomes are active as in the absence of erythromycin some ribosomes are arrested at the isoleucine codon. As release factors are omitted these complexes are not released (Figure 27, red arrow). This indicates that

the *T. thermophilus* ribosomes seem to have difficulties translating MR at 37°C in the presence of erythromycin. The presence of erythromycin restricts the PTC and the *T. thermophilus* ribosomes might not be able to overcome this at low temperatures and so the experiment should be repeated using translation factors from *T. thermophilus* allowing to perform the reaction at higher temperatures. For crystallographic studies, this issue might be overcome by forming the complex at a higher temperature or using flexizyme-charged peptide.

4.4.3 Toeprinting: fMKF-tRNA$_i^{Met}$ arrests the ribosome in the presence of erythromycin

fMKF-tRNA$_i^{Met}$ was peptidylated and purified by Dr. K. Kishore Inampudi using the flexizyme eFx and CME activated fMKF. To investigate the stalling activity of the peptide, I performed a toeprinting assay in the presence or absence of erythromycin using a PURExpress (NEB) system without tRNAs, amino acids, and ribosomes.

First attempts to study the incorporation of fMKF-tRNA$_i^{Met}$ by toeprinting were performed using 10 µM fMKF-tRNA$_i^{Met}$ and the total tRNA solution provided by the kit resulting in ribosomes arrested at the initiation codon (data were not shown). The tRNA solution provided by the kit contains total tRNA extracted from cells and used at a concentration of 5 µM end concentration (Shimizu et al., 2001; Shimizu et al., 2005). Additionally, the encoded arginine codon CGG (0.5% in *E. coli* K12) and AGG (0.2% in *E. coli* K12) are both rare codons in *E. coli* K12. the large excess of the initiator tRNA over the rarely represented tRNA^{Arg} resulted propably in a strong signal for the initiation complex but not for the translocated one. The assumption can be made that the amount of the corresponding tRNA is not enough to form the translocated complex that was detectable in toeprinting. To overcome this problem, the experimental set-up was changed to use purified compounds. The initiation complex was pre-formed by incubating 2.5 µM ribosomes with 5 µM mRNA template (coding sequence: MRPPPI, AUG AGG CCG CCG CCG AUC UAA), 10 µM peptidylated-tRNA$_i^{Met}$, 25 µM erythromycin, 20 µM Arg-tRNA^{Arg} and the factor mix, containing all protein factors for the canonical translation cycle, for 5 min at room temperature. Subsequently, solution A$^-$(minus aa, tRNA) provided by the kit, containing nucleotides, was added, allowing complexes that had not been arrested to be translocated (further information are provided in chapter 3.9). The following figure shows the results of these reactions:

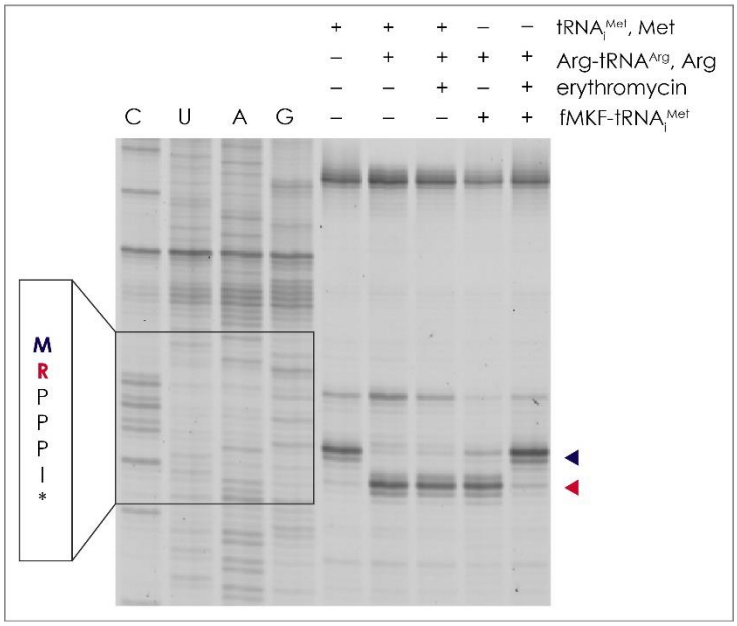

Figure 28 fMKF-tRNA$_i^{Met}$ arrests *E. coli* 70S ribosomes *in vitro* in the presence of erythromycin and Arg-tRNA^{Arg}. The custom-made PURExpress system had separated amino acids, tRNAs and ribosomes All reactions were substituted with *E. coli* ribosomes provided by NEB. The start codon (blue arrow) control reaction (lane 1, first lane after sequencing reaction) contained initiator tRNA$_i^{Met}$ and L-methionine Met. As a translocation control, the two reactions were performed in presence of tRNA$_i^{Met}$, tRNA^{Arg} and their corresponding amino acids in the absence (lane 2) or presence (lane 3) of erythromycin (red arrow). fMKF-tRNA$_i^{Met}$ can translocate in the presence of Arg-tRNA^{Arg} (lane 4). By the addition of erythromycin most ribosomes arrest at the start codon (lane 5).

Figure 28 shows the toeprint to investigate if the arrest complex can be formed using peptidyl-tRNA obtained using flexizyme (Figure 28). The reaction was performed in two steps: the pre-formation of the initiation complex in the presence of peptidyl-tRNA$_i^{Met}$ and Arg-tRNA^{Arg} and translocation by adding GTP to the reaction. During the formation of nascent chain-mediated translational arrest of the fM+X(+) in the presence of erythromycin, the first peptide bond between the methionine and the arginine or lysine needs to be formed. Lane 2 and 3 show a toeprint corresponding to the translocated complex. If the ribosomes are arrested due to the presence of the fMKF peptide in the tunnel, the ribosomes cannot be translocated and remain on the start codon. Therefore, tRNA$_i^{Met}$ is replaced by peptidylated fMKF-tRNA$_i^{Met}$. The toeprint observed in lane 4, corresponding to the reaction without erythromycin shows that ribosomes translocated to the second codon while in the presence of erythromycin the ribosomes remain on the start codon (lane 5). Consequently, the ribosomes in the presence of fMKF-tRNA$_i^{Met}$, Arg-tRNA^{Arg} and erythromycin have undergone drug-dependent translational arrest. However, a less abundant band corresponding to ribosomes that have reached the arginine codon indicates that arrest is not complete. These conditions were used to form the arrest complex

for studying the fMKF(R) in the presence of erythromycin fur further characterization by structural biology methods.

4.4.5 Structural studies of an MKFR-ribosome complex arrested in the presence of erythromycin

Co-crystallization experiments of fMKF-$tRNA_i^{Met}$ with 70S *T. thermophilus* ribosomes in the presence of erythromycin (strategy 1, Figure 17) were performed by Dr. K. Kishore Inampudi. Although he was able to obtain crystals and diffraction data, no density for the peptide could be detected even through clear density for initiator tRNA was visible in a minimally-biased F_o–F_c map obtained from a refinement in which tRNAs were not included in the model. A likely explanation could be that the peptide hydrolyzed during crystallization as the conditions include an incubation time of approximately seven days at 20°C at a pH of 7.5. Similar observations had been made previously by Dr. Axel Innis in the Steitz group.

To address this issue, I performed crystallization experiments starting from the dipeptidyl-tRNA fMK-$tRNA_i^{Met}$ and Phe-NH-$tRNA^{Phe}$ (strategy 2, Figure 18). The pH-sensitive ester bond between the amino acid and the tRNA was replaced by an amide bond. To introduce this bond, the 3'CCA end is removed enzymatically by CCA-adding enzyme in the presence of an excess of pyrophosphate and synthesized again by the same enzyme in the presence of 3'NH_2-ATP, leading to the incorporation of a terminal 3'NH_2-adenosine (Further details chapter 3.5). NH_2-$tRNA^{Phe}$ was aminoacylated with L-phenylalanine using phenylalanyl-tRNA synthetase followed by its purification by RP-HPLC over a C4 column (chapter 3.5). A similar strategy involving fM-NH-$tRNA_i^{Met}$ and F-NH-$tRNA^{Phe}$ had been used previously to study pre-catalysis and post-catalysis states of the 70S *T. thermophilus* ribosome to obtain novel insights into the mechanism of peptide bond formation (Polikanov et al., 2014; Voorhees et al., 2009). This complex was formed to observe if peptide bond formation can occur between the flexizyme-charge peptide and the A-site amino acid which was non-hydrolysable attached to the A-site tRNA. After collecting diffraction data from crystals prepared in this manner, I could see no density that would indicate the presence of aminoacyl-tRNA in the A-site. In contrast, density of deaminoacylated initiator tRNA was detected. An explanation could be that the peptidyl-A-site tRNA has a reduced binding affinity for the A-site and dissociates potentially during crystallization.

However, to form the arrested ribosome complex, the ribosomes have to undergo one round of translocation. Consequently, the complexes were incubated with small amounts of *T. thermophilus* EF-G (1 µM) and 1 mM GTP. This strategy resulted in similar observation as in the data obtained from samples formed without EF-G. An explanation could be that under crystallographic conditions the deaminoacylated tRNA still has a higher binding affinity for the P-site than it does for the E-site. Another explanation could be that the mRNA is too short for proper function of EF-G.

Complexes for cryo-EM were formed using the fMKF-$tRNA_i^{Met}$, 70S *E. coli* ribosomes, erythromycin, mRNA, and Arg-$tRNA^{Arg}$. Peptide hydrolysis was not an issue as the complex is frozen directly after complex formation. Complexes were formed using similar concentrations of mRNA, ribosomes, fMKF-$tRNA_i^{Met}$, Arg-$tRNA^{Arg}$ and erythromycin as used for the toeprinting reactions Subsequently, the sample was diluted to 240-480 nM of ribosomes substituting the dilution buffer with Arg-$tRNA^{Arg}$ (chapter 3.10). The obtained reconstruction is described in the following chapters.

4.4.6 Single particle reconstruction using RELION

Cryo-EM data were collected at the Talos Arctica TEM at the IECB, Bordeaux, France as described in detail in chapter 3.10. The collected micrographs were processed using RELION (Scheres, 2012b; Scheres, 2016). In the first steps, beam-induced movement of the particles was corrected using MotionCorr2 (Zheng et al., 2016; Zheng et al., 2017) followed by CTF correction using CTFFIND4 (Rohou and Grigorieff, 2015). During CTF correction, the exact defocus value, as well as the resolution limit of the micrograph, were determined (further information chapter 3.10). A micrograph and its corresponding CTF is shown in the following figure:

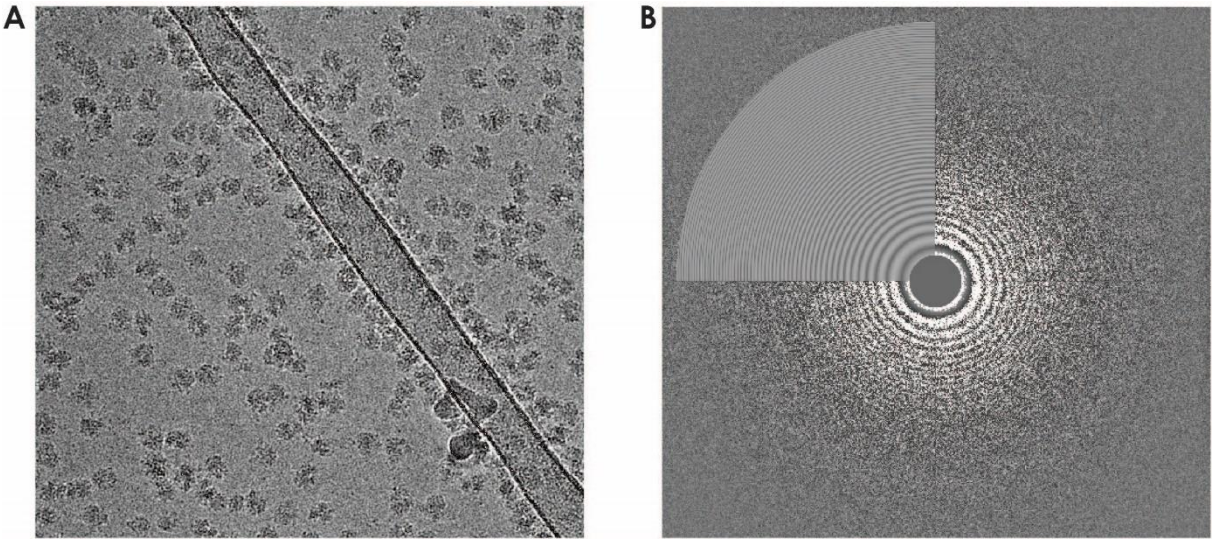

Figure 29: Grids prepared with a ribosome concentration of 480 nM showed a good distribution of particles on micrographs. (A) shows a representative micrograph of the MKF-complex at a magnification of 120 k and a defocus value of 2 µm. (B) shows the corresponding power spectrum after CTF correction. The resolution of this particular micrograph was estimated to be 4.2 Å by CTFFIND4 (Rohou and Grigorieff, 2015).

The ribosomes distribution is even over the micrograph and the ribosomes adopt different orientations (Figure 29). The different orientations are necessary for single particle reconstruction. The concentration was sufficient to have a monolayer of ribosomes. Along the carbon filaments, particles were located too close to each other and excluded during particle picking to avoid bias. For the 3D reconstruction, the defocus value and astigmatism have to be determined. These values are taken into account using the contrast transfer function (CTF). To do so, the program CTFFIND4 (Rohou and Grigorieff, 2015) was used. Figure 29 illustrates the output for one micrograph. The theoretical CTF correlates well with power spectrum calculated from the micrograph. In this particular, the astigmatism is very low. However, one dataset used for the MKF-70S reconstruction was highly astigmatic. The astigmatic angle was taken into account during CTF correction and so the data set was usable for 3D reconstruction.

2000 particles were manually picked and classified into 10 different 2D classes in order to obtain templates for auto-picking. Auto-picking parameters were optimized for each data set (chapter 3.10) Subsequently, the auto-picked particles were classified twice into 100 2D classes (further information 3.10). The classification is used to separate ribosomal particles from artifacts or ribosomes bound to the lacey carbon. The data were collected using lacey carbon grids, which is a support with irregular arrangements. Due to the irregular arrangement of the carbon, some micrographs contained carbon with bound ribosomes, which were mostly

removed during 2D classification. Figure 30 shows the most abundant 2D classes after the second round of 2D-classification:

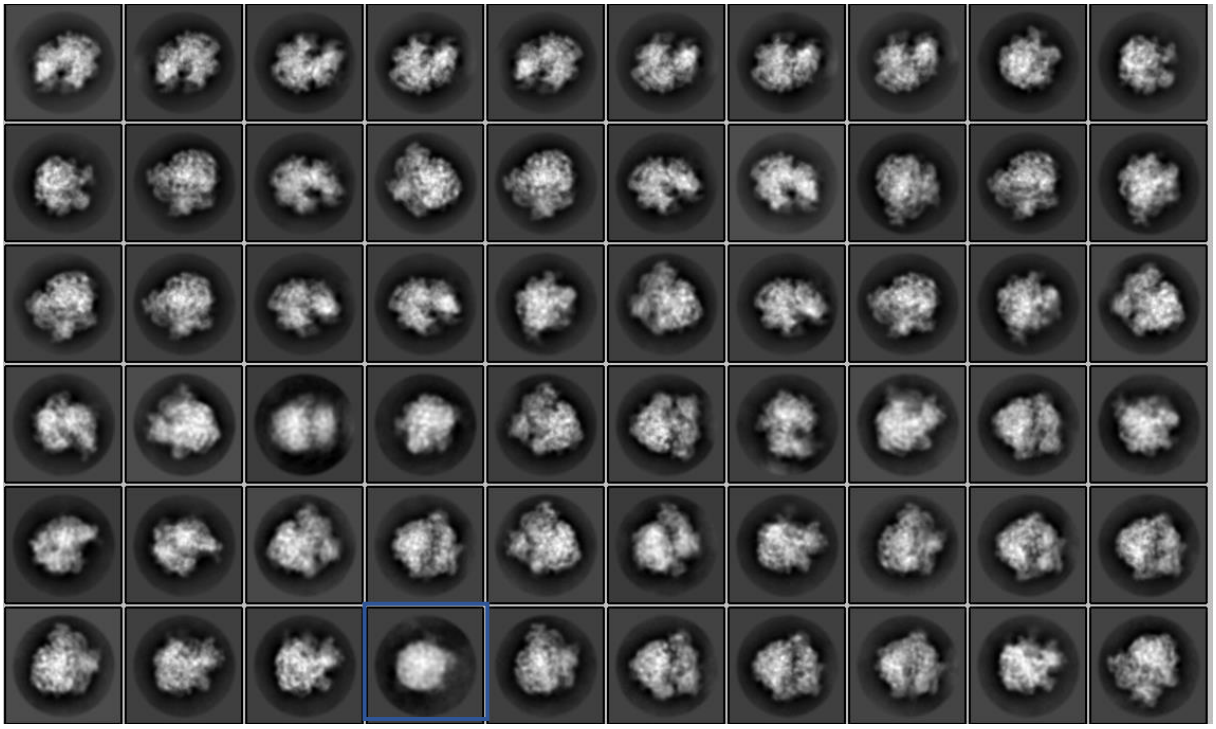

Figure 30: Representative 2D classes of the sample sorted in order of decreasing abundance. The ribosomal particles adopted different orientations. The small and large subunit can be distinguished. The blue box indicates an artificial class that corresponds to an "Einstein-from-noise" class.

Figure 30 shows the representative part of the 2D classification results. The blue box indicates an artificial or "Einstein from noise" class. This class arises from wrongly picked particles. Therefore, they contain only background noise and they appear like blob-like or ghost-like particles (Henderson, 2013; Scheres, 2015, 2016) and were removed for further reconstruction. The 2D classes contained different orientations of the bacterial ribosomes, showing a lot of molecular detail including stalks and subunits. Subsequently, the selected classes were used for 3D auto-refinement to obtain a first initial map. This map is reconstructed from particles with different abundances of the different tRNA. By a masked 3D classification with background subtraction, the particles can be sorted accordingly.

Masked 3D classification is a method to select particles containing information for a specific region by masking out a specific part of the density and classifying the particles accordingly

(Scheres, 2016). For the MKF-70S ribosome structure, the particles were sorted according to their A, P or E-site tRNA occupancy. The resulting distribution is shown in the following figure:

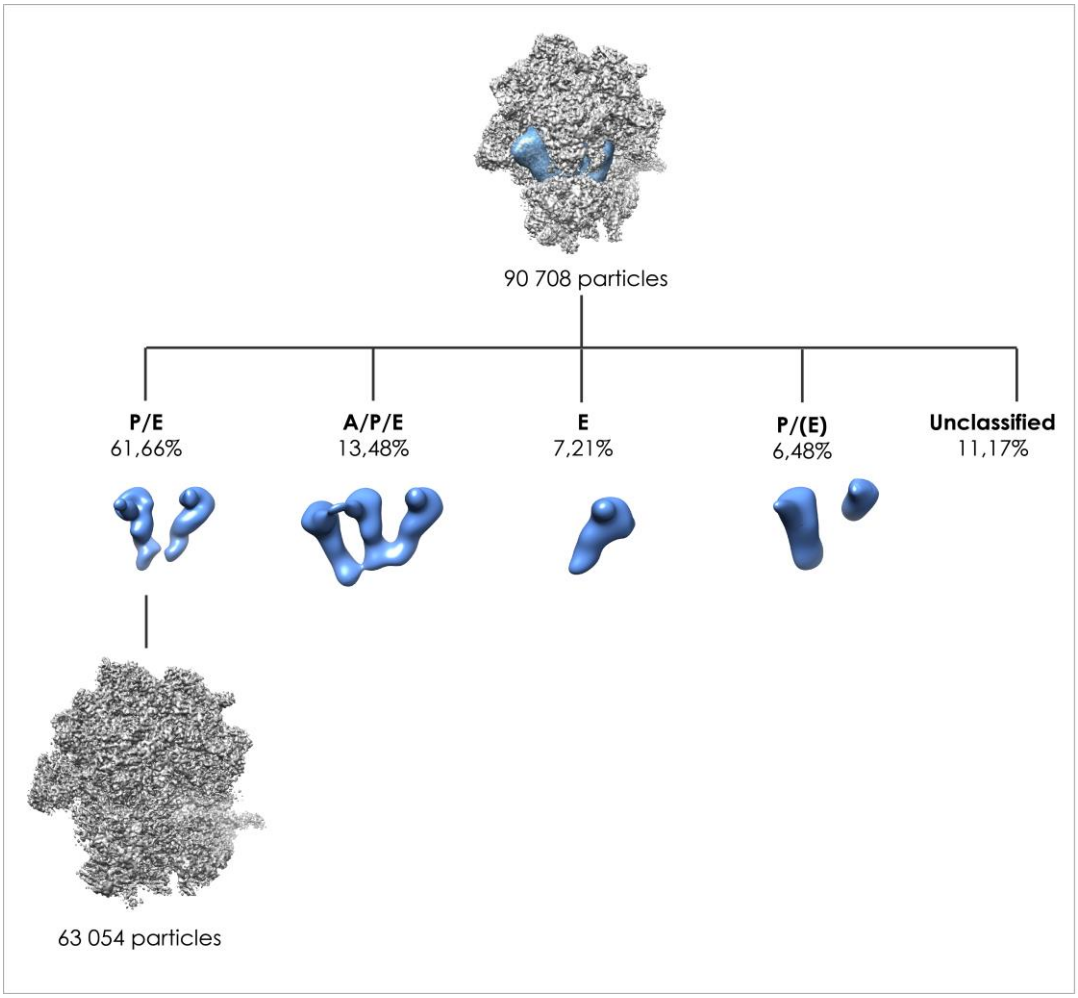

Figure 31: Masked 3D classification sorting according to the occupancy of A-, P- and E-site tRNA. The masked 3D classification identified ten different classes. Six of these ten classes did not contain information for tRNA and labeled as unclassified. The largest class contained P- and E-site tRNA and was used for further reconstruction. Other classes had the following occupied sites APE, E, P with partial E and unclassified. The initial density before classification shows fewer details than the one after masked 3D classification, 3D refinement, movie processing, particle polishing, and postprocessing. The tRNA masks are shown in blue in the initial map.

Figure 31 shows the electron microscopy density after the initial 3D auto-refinement. The map was reconstructed using 90 708 particles. The particles are a mixture of particles containing e.g. one tRNA in P or E-site, two or three tRNAs. These different occupancies influence directly the quality of the map. By using a mask around the tRNA binding sites (blue mask) and subtracting the background, the particles were sorted accordingly into 10 different classes. After evaluating the resulting tRNA maps in chimera, six of these were identified as noise (11.17%). The most abundant class contained a P and an E-site tRNA (61.66%) corresponding to the arrest complex.

These 63 054 particles were used for further reconstruction. The number of particles is sufficient to obtain high-resolution information, as a recent study showed that 30 000 particles are sufficient for near atomic resolution reconstruction of ribosomal particles (Bai et al., 2013).

The second most abundant class (13.48%) had a signal for A-, P-, and E-site tRNA. These particles might correspond to non-arrested ribosomes with the peptide attached to the A-site tRNA, as no EF-G was added to the sample the complex could not translocate. The abundance of this complex corresponds to that observed in the toeprinting experiment which confirmed the arrest (Figure 28). The toeprint was performed in the presence of EF-G. In the sample corresponding to the arrested complex, a faint band for the translocated complex could be observed. To analyze if the APE classified particles correspond to the non-arrested complex the cryo-EM map for those particles could be reconstructed (discussed in chapter 5.2) Other classes contain an E-site tRNA (Class E, 7.21%) and a P-site tRNA with a partially bound E-site tRNA (Class P/(E), 6.48%).

The distribution shows that the arrested complex has a P-site tRNA and an E-site tRNA bound, even if the complex was formed and diluted in the presence of high concentrations of Arg-tRNA^{Arg}. This indicates that the arrest peptide might inhibit the accommodation of this particular tRNA. The abundance of the PE complex in the absence of any complex formation indicates that the strategy to form arrested complexes using the flexizyme methodology to peptidylate tRNA presents a useful tool for structural biology. Nascent chain-mediated translational arrest complexes have been isolated from cells or purified from *in vitro* translation reactions (chapter 4.4.1). The recent structure of TnaC was reconstructed from a sample extracted from cells and the final reconstruction contained only 29% all selected particles (Bischoff et al., 2014). Even if the MKF-70S complex was formed from purified compounds, the toeprinting experiment indicates that the peptidyl-tRNA$_i^{Met}$ can initiate translation in the absence of erythromycin.

After masked 3D classification, the particles were processed using movie refinement and particle polishing to obtain so-called "shiny" particles. Shiny particles were put through another round of 3D auto-refinement using a mask on the 50S subunit as the arrest is taking place in the ribosomal exit tunnel and postprocessing as described in (Scheres, 2016), resulting in the final map. The local resolution distribution and FSC curve (further explanation chapter 3.10) are shown in the following figure:

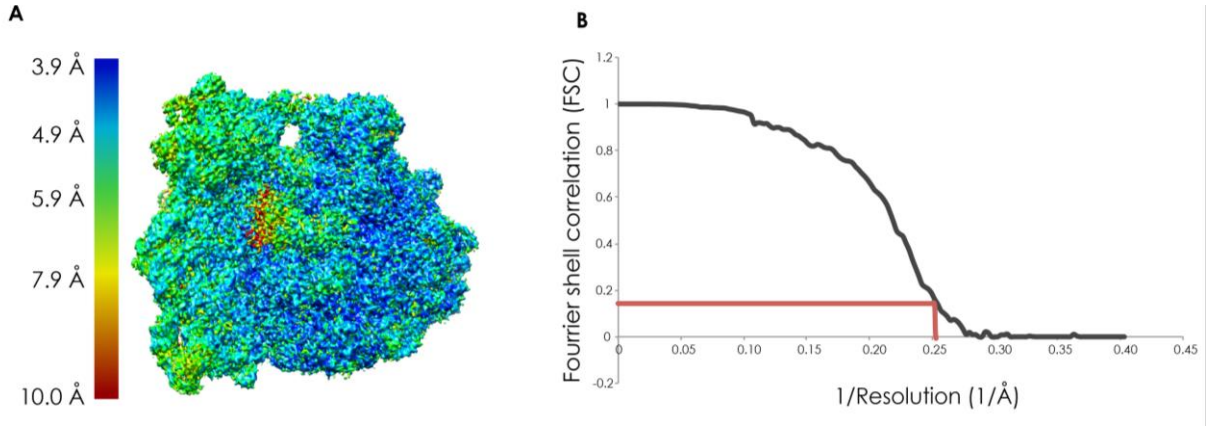

Figure 32: Local resolution distribution and FSC curve. (A) The local resolution distribution is ranging from 3.9-10 Å. The large subunit has a higher resolution than the small subunit as the particles were aligned to the large subunit in the last step of processing. (B) shows the plot of the reciprocal of the resolution to the corresponding the FSC values after gold standard refinement. The resolution cut off was set to FSC=0.143.

The local resolution distribution (Figure 32A) shows that the body of the large subunit has higher resolution on average than the small subunit which was expected as particles were aligned on the 50S subunit. The small subunit shows lower resolution due to its relative mobility to the 50S subunit. Overfitting was prevented by using the gold-standard approach, meaning the data were split into two halves that were refined independently (Henderson et al., 2012; Scheres and Chen, 2012). The Fourier shell correlation (FSC) between the two reconstructions yields a resolution estimate of the reconstruction. The 3.9 Å resolution was determined at an FSC threshold of 0.143 as it is implemented in the RELION refinement (Figure 32, Scheres, 2016; Scheres and Chen, 2012).

4.4.7 Model building, refinement, and validation

The initial model of the 70S *E. coli* ribosome (PDB code: 4U27, Noeske et al., 2014) was rigid-body fitted into the density using the Situs package (Wriggers, 2012) (detailed steps are discussed in chapter 3.10). Afterwards, flexible bases of the 23S rRNA were moved manually into the density using COOT. These bases were A2062, U2506, U2585 and A2602 and are known to adopt specific positions during nascent chain-mediated translational arrest (Arenz et al., 2014a; Arenz et al., 2014b; Bischoff et al., 2014; Gumbart et al., 2012; Sohmen et al., 2015; Su et al., 2017). The model was refined against the electron microscopy density using PHENIX real-space refinement applying base pairing restrains and the high-resolution input model was used a reference model. Figure 33 shows different parts of the ribosome with their corresponding density:

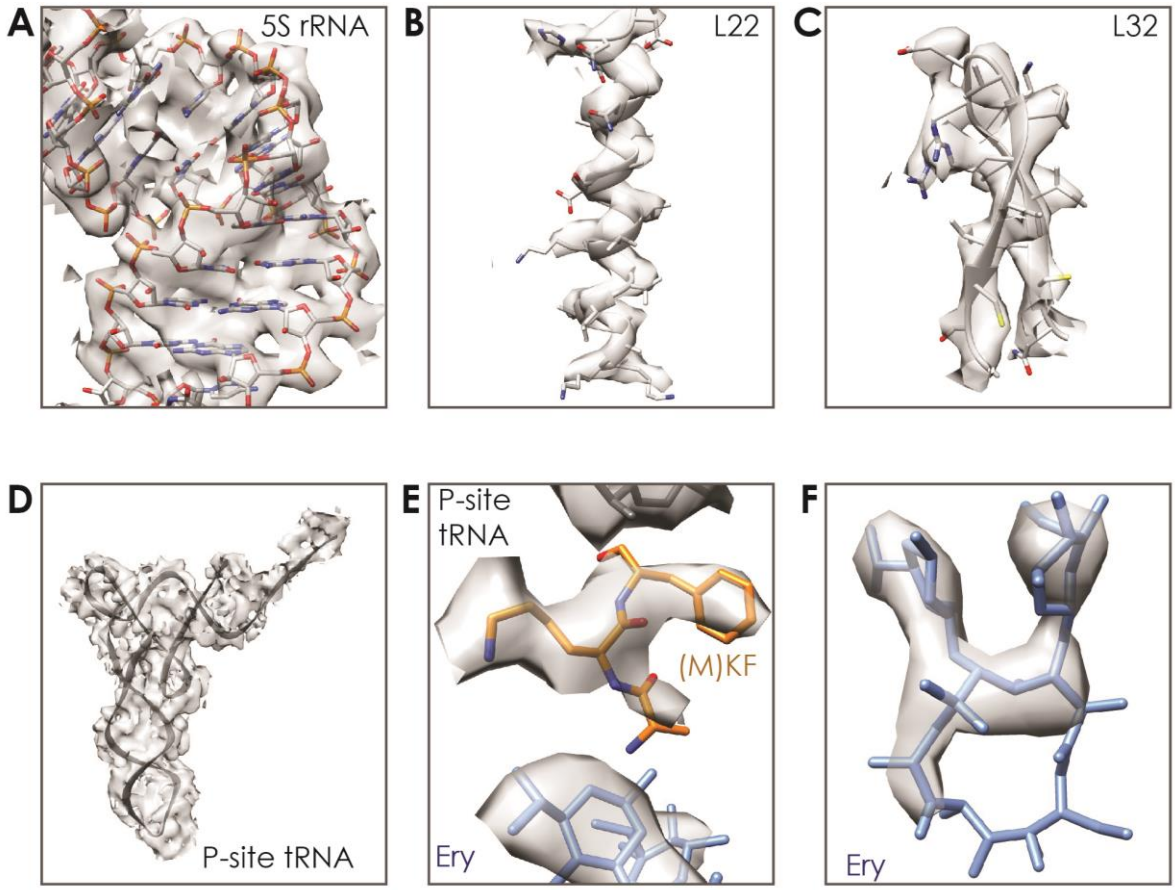

Figure 33: Examples of density display around different parts of the model: (A) 5S rRNA shows no base separation but clear distinction between backbone and base. α-helix the ribosomal protein L22 (B) and β-sheet (C) structure of the ribosomal protein L32 show clear density for side chains even flexible ones like lysine. (D) shows density for the P-site tRNA including a well-defined 3' CCA end. The density corresponding to the arrest peptide includes density for the side chains of phenylalanine and lysine while the methionine side chain appears to be disordered (E). The density corresponding to erythromycin shows clear density for the two sugar moieties and the upper part of the lactone ring (F)**.**

The quality of the density can be further evaluated by interpreting the structural features e.g. secondary structure elements or side chains that can be observed in the density (Figure 33). Figure 33 shows different parts of the ribosome including rRNA and ribosomal proteins. A part of the 5S rRNA is shown in Figure 33A. The density does not show inter-base separation but the phosphate-sugar backbone can be clearly positioned. On the other hand, bases from the two antiparallel strands that are engaged in Watson-Crick base pairing can be clearly distinguished from each other. As a further example, the density for a α-helix of the ribosomal protein L22 and a β-sheet structure of the ribosomal protein L32 (Figure 33 B, C). The density shows the shape of the secondary structure and density for the side chains even for lysine and arginine.

The density of the P-site tRNA (Figure 33D) is well defined. The density corresponding to the fMKF peptide is shown in Figure 33E. Density for the phenylalanine and lysine side chains can be clearly observed. In contrast to this, the methionine side chain is disordered indicating that it might not be necessary for the arrest.

The density of erythromycin clearly indicates the positions of the sugars and the upper part of the lactone ring (Figure 33F). In contrast to X-ray crystallography structures resulting in density for the whole drug (Bulkley et al., 2010; Dunkle et al., 2010), the lower part of the lactone shows no density as observed in previous cryo-EM structure containing erythromycin (Arenz et al., 2014a; Arenz et al., 2014b). This hints that the lactone ring might be more flexible within cryo-EM structures than within crystal structures.

In summary, the electron microscopy density was reconstructed to an average resolution of 3.9 Å. The resolution of the 50S subunit is higher as a 50S mask was used during the last steps of the reconstruction. The density shows clear features corresponding to this resolution such as well-defined secondary structures for nucleic acids and proteins including side chains.

The refinement and model statistics are listed in the following table:

Table 38: Refinement and model statistics single molecular reconstruction.

Data collection	
Particles	63 054
Pixel size (Å)	1.24
Defocus range (μm)	0.5-2.5
Voltage (kV)	200
Electron dose ($e^-/Å^2$)	120 (6.5 per frame)
Model composition	
Protein residues	5617
RNA bases	4633
Refinement	
Resolution (Å, 0.143 FSC)	3.9
Map sharpening B factor ($Å^2$)	-205.652
$FSC_{Average}$	0.91
Validation	
rmsd, bonds	0.02
rmsd, angles	1.24
Rotamers outliers (%)	5.64
Ramachandran outliers (%)	6.38
Ramachandran favored (%)	75.08
Correct sugar puckers (%)	99.31
Good backbone confirmation (%)	83.24
Score	
Clash score, all atoms	3.37

The refinement improved the Ramachandran outliers (input 8.34%) as well as the rotamer outliers (input 21.79%). The refinement is still an ongoing process and needs further improvements including applying, even more, restrains reprocessing the cryo-EM data to possibly increase the resolution and the quality of the density.

4.4.9 Structure interpretation

The complex was formed in the presence of Arg-tRNA^{Arg} a short synthetic mRNA encoding for the amino acid sequence MR. After complex formation, the sample was diluted from 2.5 µM to 240-480 nM. To enhance A-site tRNA binding, the dilution buffer included 20 µM Arg-tRNA^{Arg}. Figure 34 shows the reconstructed density with the P- and E-site tRNAs highlighted:

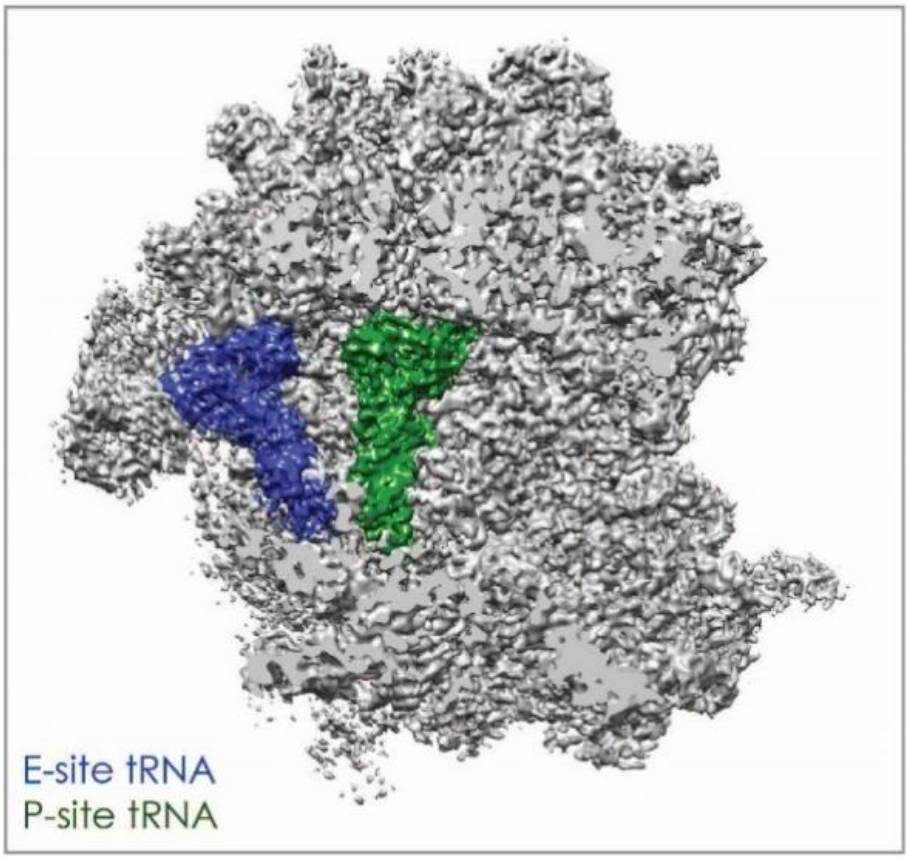

Figure 34: The reconstructed density contains density for P-site (green) and E-site tRNA (dark blue) but no density for an A-site tRNA. The final density was reconstructed from 63 054 particles.

The electron microscopy map contained density for the P-site and E-site tRNAs but no density for the A-site tRNA (Figure 34). The absence of the A-site tRNA can be explained overlying the resulting model with a model containing an A-site tRNA (Figure 35):

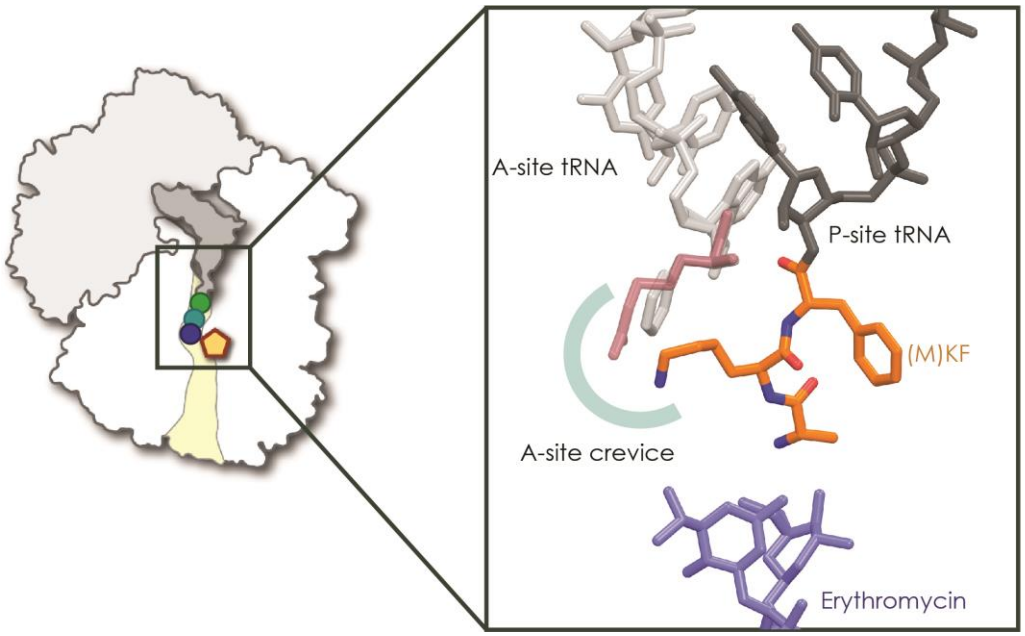

Figure 35: The fMKF-peptide does not form direct contact with the drug while the penultimate lysine side chain points towards the A-site crevice. The MKF peptide is shown in orange and is attached to the P-site tRNA (dark gray) via an ester bond. Erythromycin is shown in blue. The structure was overlaid with a pre-attack structure of the 70S *T. thermophilus* ribosome in complex with Phe-NH-tRNA^{Phe} in the A-site and fMet-NH-tRNA$_i^{Met}$ in the P-site (PDB code: 1VY4, (Polikanov et al., 2014)) to show where the A-site tRNA (light gray) would normally be located. The phenylalanine would come into close proximity to the lysine side chain but would not clash. Replacing the phenylalanine with an arginine residue (raspberry) would bring two long positive charged side chains close to each other and would likely result in static repulsion. Schematic view of the ribosome taken from (Seip and Innis, 2016).

As Figure 35 illustrates, the penultimate lysine side chain (Lys –1) points into the A-site crevice. The overlay with the pre-attack structure of the 70S *T. thermophilus* ribosome in complex with Phe-NH-tRNA^{Phe} in the A-site and fMet-NH-tRNA$_i^{Met}$ in the P-site (PDB code: 1VY4, (Polikanov et al., 2014)) illustrating the location of the A-site tRNA indicates that the Lys –1 side chain would allow the binding with an incoming phenylalanine residue. Toeprinting experiments mutating the A-site tRNA to all canonical amino acids showed that arrest in the presence of erythromycin occurs only if the amino acid is a K, R or W (Sothiselvam et al., 2016). Also replacing the A-site tRNA with an A-site tRNA mimic carrying a positive charge such as e.g. CCA mimics attached to an ornithine, leads to nascent chain-mediated translational arrest (Sothiselvam et al., 2016). Setting this in the context of the structure, an arginine residue in the A-site (raspberry, Figure 35) would bring two residues with long, positively charged side chains close to each other. This would likely result in static repulsion and would explain the absence of the A-site tRNA in the density even though the complex had been formed and diluted into a buffer containing an excess of Arg-tRNA^{Arg}. Thus, ribosome inhibition appears to result from

the inability of the incoming aminoacyl tRNA to fully accommodate into the A-site. A similar inhibition mechanism was observed for the proline-rich antimicrobial peptides (chapter 4.1)

While this explains which step of the translation cycle is blocked, it does not explain how the Lys –1 side chain is made to occupy the A-site crevice. One possible explanation is that it is stabilized in this position by making interactions with the ribosomal tunnel wall but due to the limited resolution hydrogen bonds or salt bridges can at best be suggested by proximity.

Another non-exclusive explanation is that the confined environment within the drug-obstructed tunnel makes it difficult for the Lys –1 side chain to move out of the A-site. To explore this possibility, I will first describe the conformation of various unpaired 23S rRNA residues within the tunnel that are generally known to be involved in the nascent chain-mediated translational arrest and that have been implicated in the inactivation of the PTC. These residues are A2062, A2602, U2585 and U2506 (Arenz et al., 2014a; Arenz et al., 2014b; Bischoff et al., 2014; Su et al., 2017; Vazquez-Laslop et al., 2008).

The position of the base of 23S rRNA residue A2602 in ErmCL or TnaC arrested ribosomes excludes A-site tRNA accommodation and release factor binding (Arenz et al., 2014a; Bischoff et al., 2014). Molecular dynamics studies of erythromycin-bound ribosomes showed that A2602 adopts a specific position rotated 110° from the apo-ribosome position (Sothiselvam et al., 2014). It has been reported from the ErmCL-70S structure and TnaC-70S structure that the base of A2602 adopts a specific conformation that prevents A-site tRNA accommodation or release factor binding, respectively (Arenz et al., 2014a; Bischoff et al., 2014). In the MKF-70S structure, the density for this particular base is very weak, which might indicate that higher resolution information is necessary for this position or A2602 or that it is disordered and has no impact on the absent A-site tRNA. In contrast, the bases U2506, U2585 and A2062 adopt defined conformations in the MKF-70S structure, which differ from their canonical orientation.

U2506 is a universally conserved base and point mutations show a reduction in peptide bond formation but not in peptide release (Youngman et al., 2004). U2506 rotates during A-site tRNA accommodation to rearrange the PTC during the induced fit (Schmeing et al., 2005a). In arrested ribosomal complexes, U2506 was reported in the ErmCL-70S ribosome and VemP-70S ribosome structure to form possible stacking interactions with the peptide chain or to adopt a conformation that would prevent A-site tRNA accommodation (Arenz et al., 2014a; Su

et al., 2017). Figure 36 illustrates that U2506 adopts a different conformation in the MKF-70S structure compared to its position during the different stages of the elongation cycle and during other nascent chain-mediated translational arrest events:

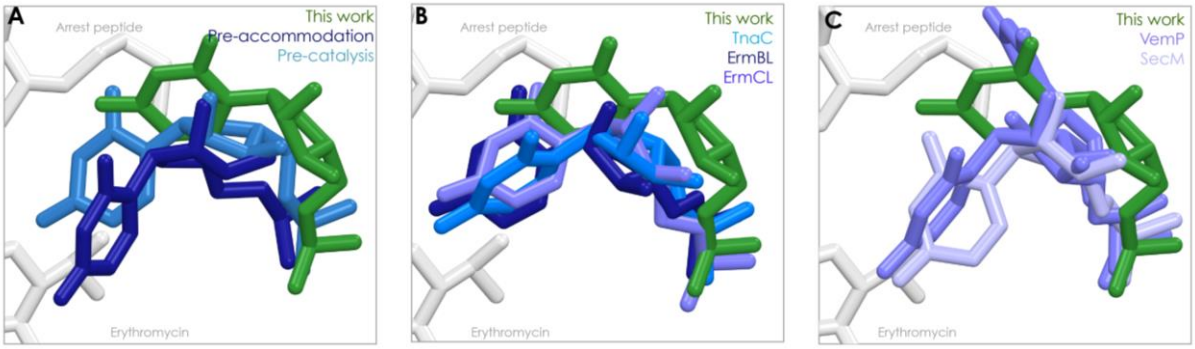

Figure 36: In the MKF-70S *E. coli* structure, U2506 is a universally conserved residue within the PTC that adopts a novel conformation different from one during translational cycle and arrest. (A) position of U2506 during different stages of the elongation cycle (pre-accommodation: PDB code: 1VQ6, pre-catalysis state PDB code: 1VY5), (B) ligand-dependent arrest (ErmBL structure PDB code: 5JTE, TnaC structure PDB code: 4UY8 and ErmCL structure PDB code: 3J7Z). (C) during ligand-independent arrest (SecM arrested ribosomes PDB code: 3JBU and the VemP structure PDB code: 4NWY) U2506 adopts a conformation different from the position in the MKF-70S structure.

In the MKF-70S structure, the base of U2506 is 5.3 Å away from the penultimate lysine side chain making it unlikely to form stacking interactions as it was reported for the ErmCL structure. In this particular structure, the base of U2506 is 3.5 Å away from the ErmCL arrest peptide (Figure 36B, (Arenz et al., 2014a)). U2506 adopts two conformations within the VemP structure that would clash with the accommodation of the A-site tRNA (Figure 36C, (Su et al., 2017)). In the MKF-70S structure, it appears that U2506 is pushed out of its position and adopts a position different from other arrest peptides (Figure 36). In summary, the base of U2506 adopts a defined orientation that is distinct from those reported so far, but it is too far from the nascent peptide to form direct contacts. Consequently, its positioning might be due to the re-arrangement of the PTC.

23S rRNA residue U2585 is universally conserved and is characterized by a highly mobile base, which adopts different positions during peptide bond formation (Schmeing et al., 2005a). During the nascent chain-mediated translational arrest, U2585 can adopt different conformations that differ from its position during the canonical translation cycle as illustrated in Figure 37:

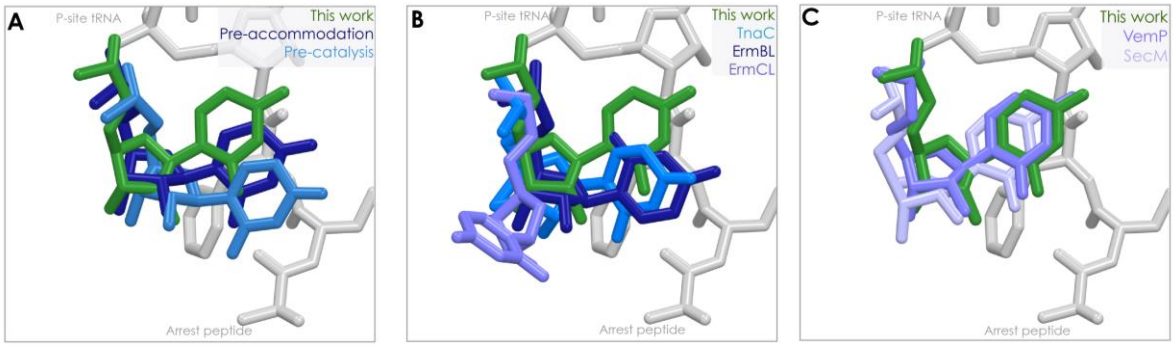

Figure 37: The base of U2585, moving during tRNA accommodation, adopts a specific conformation similar to the one in intrinsic arrested ribosomes. (A) during the canonical translation, U2585 adopts a different conformation due to the presence of tRNAs. The pre-accommodation state (PDB code: 1VQ9) and the post-catalysis state (PDB code: 1VY5) are illustrated. (B) During ligand-dependent arrest, U2585 can differ from the canonical orientation. In the ErmBL (PDB code: 5JTE) and the TnaC structure (PDB code: 4UY8) U2585 points in a similar direction but it is still shifted by a few degrees. In contrast to this, U2582 adopts a specific orientation in the ErmCL structure (PDB code: 3J7Z) preventing A-site tRNA accommodation. (C) In SecM-arrested ribosomes (PDB code: 3JBU) and the VemP structure (PDB code: 4NWY), U2585 adopts a similar conformation as in the MKF-structure.

U2585 adopts different conformation during the translation cycle. In the pre-induced state, it protects the ester bond of the peptidyl-tRNA from hydrolysis. During A-site tRNA accommodation, the base of U2585 moves away from the ester bond of the P-site tRNA towards the 2'OH group of A76 of the P-site tRNA and peptide bond formation can occur (Schmeing et al., 2005a). The position of U2585 differs from the induced and uninduced orientations (Figure 37A) and from the different orientations that it adopts in during arrest along ErmBL, ErmCL or TnaC (Figure 37B). In contrast to this, U2585 adopts a conformation similar to that observed in VemP- or SecM-arrested ribosomes (Figure 37C). In the VemP structure, U2585 adopts this position due to steric hindrance by the helical arrest peptide. Interestingly, the fMKF-peptide would not clash with the conformations of U2585 during the pre-accommodation and pre-catalysis state, so it is forced into this position due to allosteric re-arrangements of the PTC and by stacking interactions of the base of U2585 against the arrest peptide.

Molecular dynamics studies of erythromycin-bound ribosomes suggest that U2585 adopts a specific conformation having a distance of 8.3 Å to the cladinose and 9.6 Å to the desosamine sugar. In the MKF-70Sstructure U2585 is 8.2 Å away from the cladinose sugar and 10-12 Å away from the desosamine sugar. Its conformation in the MKF-structure seems to be similar to its conformation calculated from the molecular dynamics studies restricting the activity of the PTC (Sothiselvam et al., 2014).

Another universally conserved base is 23S rRNA residue A2062, which is located in the tunnel across from the erythromycin binding site (Vazquez-Laslop et al., 2008). This particular base is located in the ribosomal tunnel and is known to adopt different conformations due to the translational state of the ribosome. Ribosomes carrying the point mutations A2062C and A2062U do not arrest when translating the ErmCL peptide in the presence of erythromycin (Vazquez-Laslop et al., 2008). It has been hypothesized that the base of A2062 acts as a sensor for arrest peptides. When the ribosome arrests the base of A2062 re-orientates and might interfere with the base pairing of G2061 with A2451 and induces so a conformational change within the PTC (Vazquez-Laslop et al., 2008). However, this cannot be generalized to all arrest peptides. More recent studies have shown that ErmBL, ErmDL, TnaC and MRL(R) are independent of the chemical properties of the base of A2062 (Sothiselvam et al., 2014; Vázquez-Laslop et al., 2010).

The orientation of the base of A2062 in the MKF-structure in comparison to its position in other structural studies of the bacterial ribosome is shown in Figure 38:

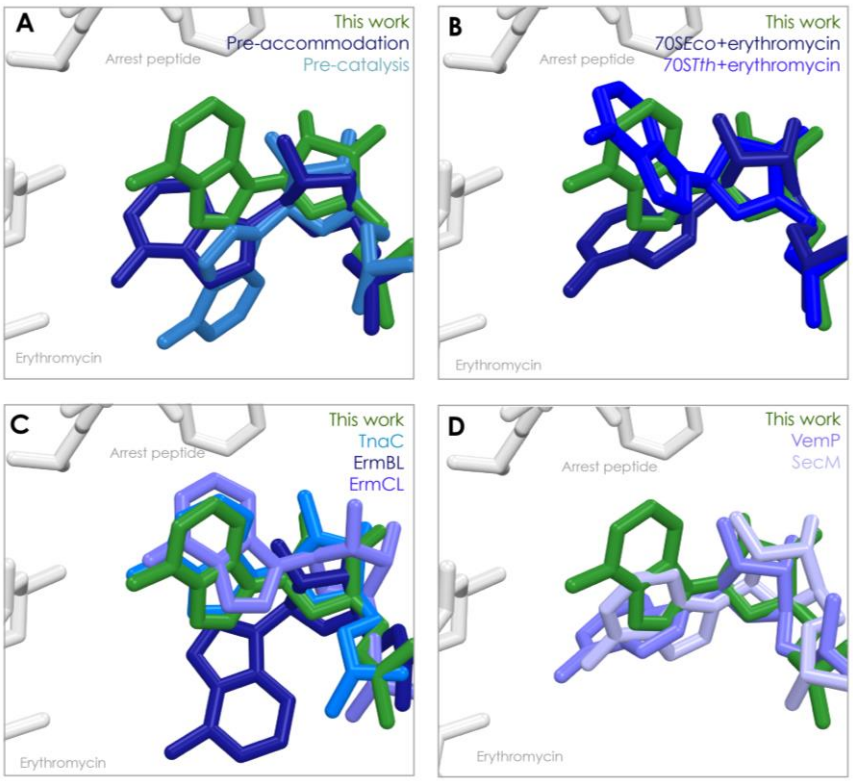

Figure 38: 23S rRNA residue A2062 is a universally conserved base within the ribosomal exit tunnel that acts as a sensor for arrest peptides (Vázquez-Laslop et al., 2010) that points towards the PTC in the MKF-70S structure (green). During pre-accommodation (PDB code: 19VQ) the base of A2062 points towards the lactone ring of the drug, while it points towards the cytoplasm during pre-catalysis, post-catalysis as well as translocation. For simplicity reasons only, the orientation during post-catalysis is shown (PDB code: 1VY5). Comparing the

structures of erythromycin-bound 70S ribosomes of *E. coli* and *T. thermophilus* (B) shows two distinct orientations of A2062. In the 70S *E. coli* ribosome (PDB code: 4V7U), A2062 points towards the cytoplasm, while it points towards the PTC in the 70S *T. thermophilus* ribosome. The comparison of various arrest complexes (C) reveals that the base of A2062 adopts different conformations according to the nature of the arrest peptide. In the ErmBL arrested ribosome (PDB code: 5JTE) the base points towards the cytoplasm, while it points towards the PTC in the ErmCL (PDB code: 3J7Z) and TnaC (PDB code: 4UY8) arrested ribosomes. (D) In SecM-arrested ribosomes (PDB code: 3JBU) the base points in a similar direction as in MFK-70S while in VemP-arrested ribosomes (PDB code: 4NWY) the base points towards the peptidyl transferase center.

In the MKF-70S structure, the density for A2062 was clearly defined and the base was modeled to point towards the PTC (Figure 38). This orientation is different from its orientations during the elongation cycle. During pre-accommodation, A2062 points into the middle of the ribosomal tunnel while it is oriented towards the cytoplasm during peptide bond formation and translocation (Lin et al., 2015; Polikanov et al., 2014; Schmeing et al., 2005a)(Figure 38A for simplicity reasons only shows the post-catalysis orientation, all steps are shown in Figure 64). The erythromycin binding site is located across from A2062. Crystal structures of erythromycin-bound bacterial ribosomes show two distinct positions of A2062. In the 70S *E. coli* ribosome structure, A2062 points towards the cytoplasm while it points towards the PTC in the 70S *T. thermophilus* structure (Figure 38B, (Bulkley et al., 2010)) but is rotated by 90° compared to the MKF-70S structure. This indicates that erythromycin allows two distinct different orientations of the base of A2062.

The base of A2062 was identified to be important in the drug-dependent arrest of ErmCL and it has been shown that is forms direct contacts with the arrest peptide (Arenz et al., 2014a; Vazquez-Laslop et al., 2008). However, the orientation of the base of A2062 in the ErmCL structure points towards the PTC but adopts an orientation similar to the one of the erythromycin bound 70S *T. thermophilus* structure. Biochemical studies have shown that for a number of arrest sequences the chemical properties of the base of A2062 is crucial. Those arrest sequences include ErmCL, ErmAL, and SecM, while ErmBL, TnaC and ErmDL appear to be independent of the chemical properties of the base of A2062 (Vázquez-Laslop et al., 2010). In the ErmBL structure A2062 points towards the cytoplasm. In contrast to this, A2062 in the most recent TnaC structure adopts a similar conformation as observed in the MKF-70S structure (Figure 38C).

In the most recent SecM structure A2062 adopts a slightly different orientation compared to the MKF-70S structure but points towards the PTC, while in the VemP structure the base points into the ribosomal exit tunnel (Figure 38D, (Su et al., 2017; Zhang et al., 2015)).

Like TnaC, it has been shown that MRLR-mediated arrest in the presence of erythromycin is independent of the nature of the A2062 (Sothiselvam et al., 2014). However, molecular dynamics studies of SecM and TnaC arrested ribosomes show a reduction of the flexibility of A2062 (Gumbart et al., 2012). In contrast to ErmCL, the base of A2062 is 4.5 Å away from the backbone of the MKF peptide and consequently cannot form any hydrogen bonding.

In light of the MKF-70S structure, however, it is possible that even though the nature of residue 2062 is not important for the arrest process, the mere presence of a base within the tunnel at this location is sufficient to cause arrest. Indeed, the base of A2062 could prevent the necessary peptide backbone rotation to allow Lys -1out of the A-site crevice, as illustrated in Figure 39.

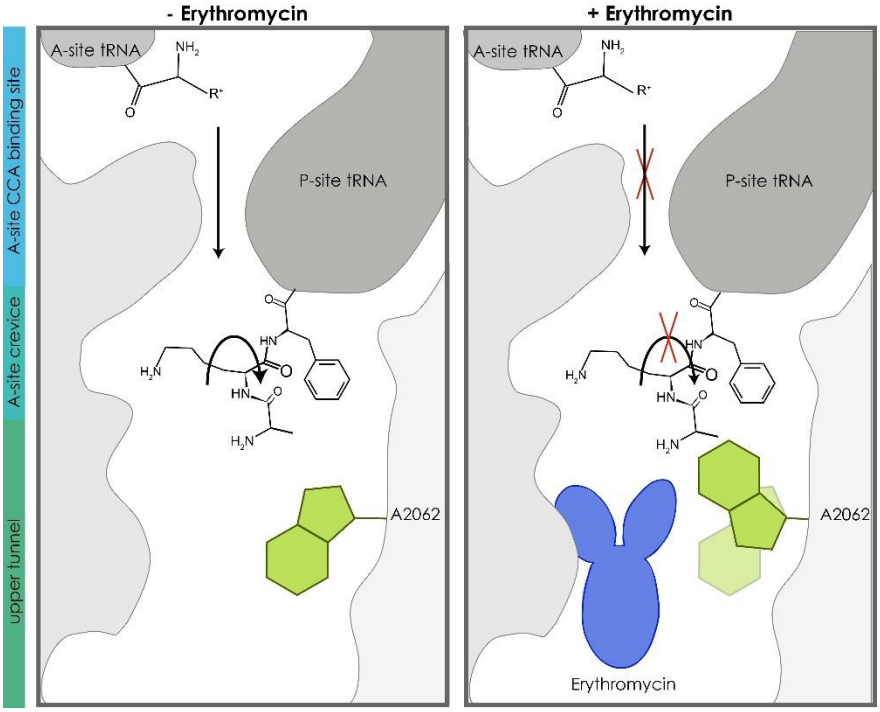

Figure 39: Proposed mechanism of MKF-mediated translational arrest in the presence of erythromycin. In the absence of erythromycin A2062 points towards the cytoplasm. This allows the rotation of the peptide backbone of the MKF peptide and the reorientation of the lysine side chain. Consequently, the following positive A-site tRNA can bind and peptide bond formation can occur. In contrast to this, the presence of erythromycin limits the flexibility of A2062 and in the presence of the peptide this particular base points up towards the PTC. This affects directly the accommodation of the positively charged amino acyl-tRNA and the ribosome undergoes peptide-mediated translational arrest.

In summary, the base of A2062 rotates more easily towards the cytoplasm, thus allowing Lys –1 to leave the A-site crevice in the absence of erythromycin. Consequently, the following amino acyl-tRNA carrying a positive charge can bind and peptide bond formation can occur (Figure 39). In contrast to this, the presence of erythromycin could favor a conformation of A2062 in which the base points towards the PTC. The ribosome arrests when A2062 points towards the PTC inhibiting the reorientation of the arrest peptide and forcing the Lys -1 to point into the A-site crevice. Consequently, the following A-site tRNA carrying a K, R or W side chain cannot bind to the PTC due to steric and static hindrance. The ribosome is arrested due to the prevention of A-site tRNA accommodation (Figure 39).

4.5 Polyproline-mediated arrest

4.5.1 Complexes to study arrest along consecutive proline motifs

Proline is a N-alkylamino acid and its incorporation into the growing peptide chain is slower than that of other canonical amino acids (Muto and Ito, 2008; Pavlov et al., 2009). The ribosome arrests if the mRNA encodes three consecutive prolines. This arrest is released by the translation factor EF-P (Doerfel et al., 2013; Ude et al., 2013). Further studies showed that the amino acid composition in the -2, -1 and +1 positions directly influences the strength of the arrest (Peil et al., 2013; Starosta et al., 2014a). Complexes that I sought to make in order to study this complex using structural biology are summarized in the following figure:

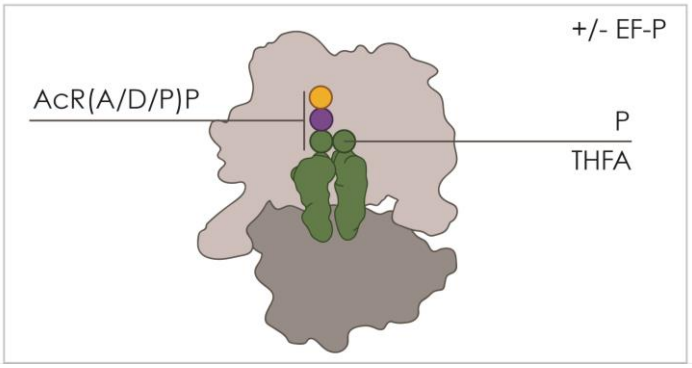

Figure 40: Complexes to study nascent chain-mediated translational arrest along consecutive proline motifs. The -2 position was chosen to be an arginine in order to improve the solubility of the flexizyme substrate. Position -1 can be an alanine or a proline, position 0 is a proline and the incoming amino acid is a proline or its unreactive derivative tetrahydrofuroic-2-acid. All complexes are to be formed in the presence or absence of EF-P.

The experimental design for this project includes the use of AcRP-$tRNA_i^{Met}$, AcRA-$tRNA_i^{Met}$, and AcRAP-$tRNA_i^{Met}$. All peptides can be used to induce strong polyproline mediated arrest (Peil et al., 2013; Starosta et al., 2014a). The incoming amino acid will be proline or tetrahydrofuroic-2-acid (THFA). THFA is a derivative of proline which has instead of the pyrrolyl ring a tetrahaydrofuryl ring, that cannot form a covalent bond with the nascent chain. This will inhibit the release of the polyproline-mediated arrest by EF-P trapping it in a PRE-release state. In doing so, the impact of the modification of EF-P can be studied in detail. For crystallization experiments, 70S *T. thermophilus* ribosomes were used and so far, no data is published about E. coli EF-P binding to the 70S *T. thermophilus* ribosome and so experiments were performed using EF-P from both species.

A recent study showed that the D-loop of $tRNA^{Pro}$ is crucial for EF-P activity (Katoh et al., 2016). Therefore, *E. coli* $tRNA^{Pro}$ had to be purified from cells and prolinylated *in vitro* in order to be used for amino acid delivery. The Pro-$tRNA^{Pro}$ can be used for one round of translocation replacing the initiator tRNA by the $tRNA^{Pro}$ and so the "native" complex can be studied. The complex can be translocated using purified *E. coli* EF-G overexpressed recombinantly (Mikolajka et al., 2011).

4.5.2 $tRNA^{Pro}$ expression and purification

Recent studies showed that the D-loop of $tRNA^{Pro}$ is essential for the function of EF-P (Katoh et al., 2016). In this study, the authors used flexizymes to prolinylate different *in vitro* transcribed tRNAs with varying lengths of the D- loop and base pairing strength depending on the nucleotide composition of the D-stem. To investigate the molecular mechanism of arrest along consecutive prolines structurally, $tRNA^{Pro}$ was isolated from cells to ensure the presence of natural nucleotide modifications. *E. coli* cells have three different genes for $tRNA^{Pro}$, named *proK, proL,* and *proM*. As proK is transcribed as a monocistronic transcript (Mohanty et al., 2016), this $tRNA^{Pro}$ gene was selected for cloning. In addition, the CGG anticodon of *proK* results in $tRNA^{Pro}$ that is incapable of wobble base pairing. Consequently, *proK* is the only $tRNA^{Pro}$ that specifically recognizes the CCG codon.

To obtain large amounts of modified *proK*, two expression strategies were used by cloning the gene into two different types of vectors, as indicated in Figure 41:

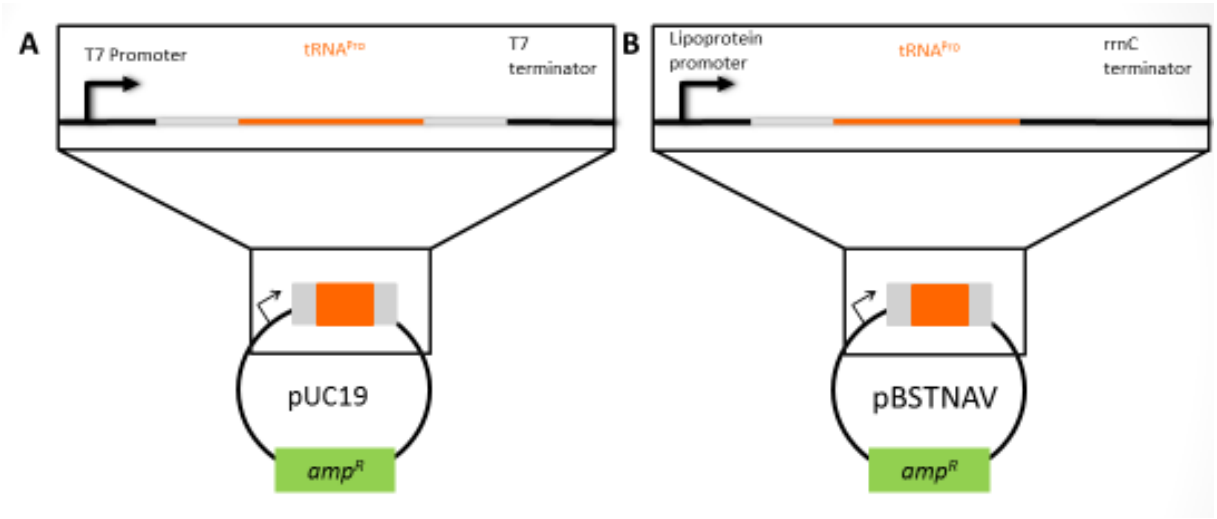

Figure 41: Schematic view of tRNA^{Pro} overexpression strategies using (A) an inducible T7 promoter and *proK* flanking regions (cloned by KK Inampudi) or (B) consecutively overexpression under the control of lipoprotein promoter with optimized flanking regions in pBSTNAV vectors (Meinnel and Blanquet, 1995; Meinnel et al., 1988).

ProK was cloned into the plasmid pUC19 by Dr. K. Kishore Inampudi. As tRNAs are transcribed as longer precursors, the gene was cloned with 8 nt-long flanking regions at the 5′ and 3′ ends, similarly to the native precursor, in order to ensure recognition by processing the enzymes RNase E and RNase P (Mohanty et al., 2016). Transcription was put under the control of a T7-promoter and a T7 terminator. The advantage of using the T7 promoter is that transcription can be finely regulated in response to different concentrations of L-arabinose ranging from 0.01% (w/v) up to 1% (w/v) by using *E. coli* BL21AI cells where the gene for T7 polymerase is under the control of the *araBAD* promoter. Consequently, the tRNA modification machinery should not be saturated, ensuring that tRNA^{Pro} is homogeneously modified.

As a second overexpression strategy, *proK* was cloned into pBSTNAV vectors. Two different variants of the vector were used: pBSTNAV2OK (Meinnel et al., 1988) and pBSTNAV3S (Meinnel and Blanquet, 1995). Both vectors contain optimized flanking regions for RNase P processing. In pBSTNAV3S, the flanking region was optimized for optimal 5′ processing in cases where the first nucleotide of the tRNA is not base-paired, as is the case for tRNA$_i^{Met}$ (Meinnel and Blanquet, 1995; Meinnel et al., 1988). The gene is under the control of the lipoprotein promoter resulting in constitutive overexpression.

4.5.3 Overexpression tests of tRNA^{Pro}

To identify optimal overexpression strategies, pUC19-tRNA^{Pro} was transformed into *E. coli* BL21AI cells while pBSTNAV2OK and pBSTNAV3S with and without the *proK* gene were transformed into the *recA* deficient *E. coli* strains DH5α and HB101. *E. coli* BL21AI transformed with pUC19-tRNA^{Pro} were induced at an OD_{600} of 0.6 with 0.01%, 0.1% and 1 % L-arabinose. Expression levels for each condition were detected by Northern blotting as described in chapter 3.9. The amount of total RNA loaded was normalized based on the optical density of the cell culture.

The following figure shows the Northern blot analysis of tRNA^{Pro} expressed using the pBSTNAV or pUC19-*proK* vector:

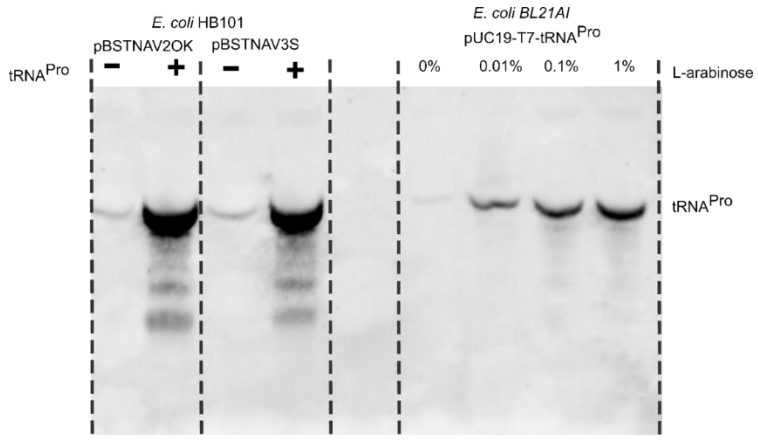

Figure 42: Comparison of the different overexpression strategies using pBSTNAV vectors and pUC19-*proK* vector. The amount of produced is higher using the pBSTNAV vectors compared to expression in the pUC19 vector. In the case of the BL21AI cells, the intensity of the bands correlates to the concentration of L-arabinose used for induction.

As shown in Figure 42, all constructs overexpressed *proK*. The yields for using the pUC19 constructs increase with increasing concentrations of L-arabinose but overexpression of *proK* using pBSTNAV vectors resulted in higher overall yields. Furthermore, the overnight culture using *E. coli* BL21AI reached only a final OD_{600} of 2.6 whereas the overnight culture for *E. coli* HB101 reached a final OD_{600} of 8. Bands detected for the L-arabinose induced expression runs higher compared the bands detected from consecutive expression. An explanation could be that the lanes corresponding to pBSTNAV overexpression were highly overloaded and changed so the overall running behavior and it is not an indication of modification of the tRNA. In addition, slightly differences within the PAGE and during blotting might have had influenced

the running behavior. The higher intensities of the bands on the Northern blot as well as the larger amounts of cells obtained after overnight expression might correspond to higher yields of $tRNA^{Pro}$ for purification. Consequently, pBSTNAV constructs were used for further experiments. As the expression has to be performed in *recA*⁻ strains, pBSTNAV constructs were transformed into *E. coli* DH5α and HB101. The resulting Northern blot is shown in the following figure:

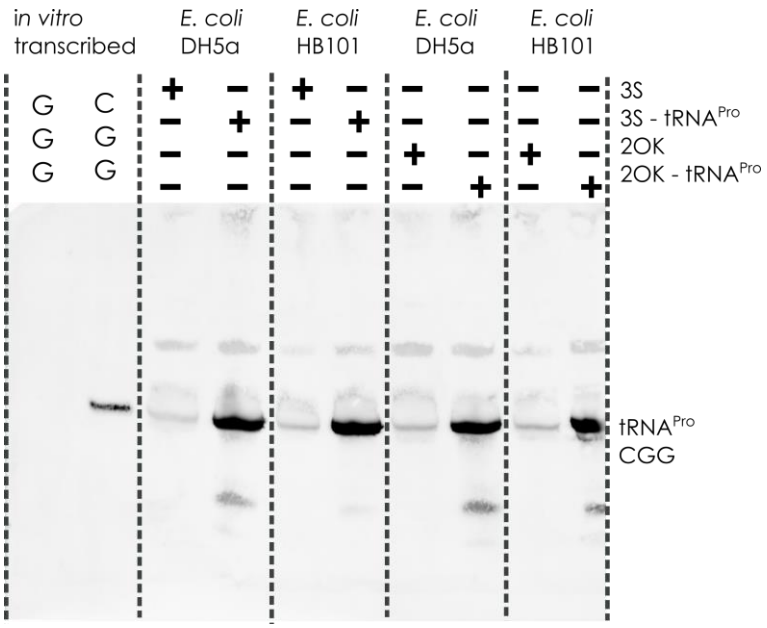

Figure 43: Similar amounts of $tRNA^{Pro}$ in *E. coli* DH5α and HB101 were expressed per cell using the pBSTNAV vectors. Overexpression was tested by Northern blotting using a *proK* specific probe. As a control *proK* and *proM* were transcribed *in vitro* migrating through the gel in a similar fashion as the extracted $tRNA^{Pro}$.

As illustrated in Figure 43 on the left, the probe against *proK* is specific for *proK*, as shown by its inability to detect *proM* in spite of the minor sequence differences within the anticodon loops of the two tRNA species. The right part of the Northern blot (Figure 43) shows that RNA extracted from cells that contain the *proK* plasmids display a higher expression level for $tRNA^{Pro}_{CGG}$ compared to RNA extraction from cells containing the empty plasmid. In addition, the overexpressed appears to be of the correct length as it migrates at the same level as the *in vitro* transcribed tRNA. Furthermore, there is no visible difference in the intensity of the overexpression band between *E. coli* DH5α and HB101. As the overnight culture of HB101 reached an OD_{600} of 8 while the DH5α culture reached only an OD_{600} of 2.8, the *E. coli* HB101 cells were used for large-scale expression. The reason is that the higher cell mass corresponds

directly to higher yields of $tRNA^{Pro}$ and the absence of additional bands corresponding to lower molecular weight RNA species.

4.5.4 $tRNA^{Pro}$ purification

Large-scale expression of $tRNA^{Pro}_{CGG}$ yielded 5 g of cells per 1 L of LB expression culture. Total nucleic acid extraction was performed by acidic phenol-chloroform extraction (chapter 3.5). Genomic DNA, plasmid DNA and long rRNAs were removed using increasing concentrations of isopropanol. Subsequently, the total tRNA sample was deaminoacylated by incubating the extract at 37°C for 2 h at pH 9.0 as the ester bond between the tRNA and amino acid is sensitive to high pH. Using Q-sepharose and RP-C4 HPLC chromatography $tRNA^{Pro}$ was specifically enriched due to its chemical properties (chapter 3.5). Figure 44 shows the different purification steps with the chromatogram and the corresponding Northern blot analysis. For simplicity reasons, the denaturing PAGE is only shown for the Q-sepharose column samples:

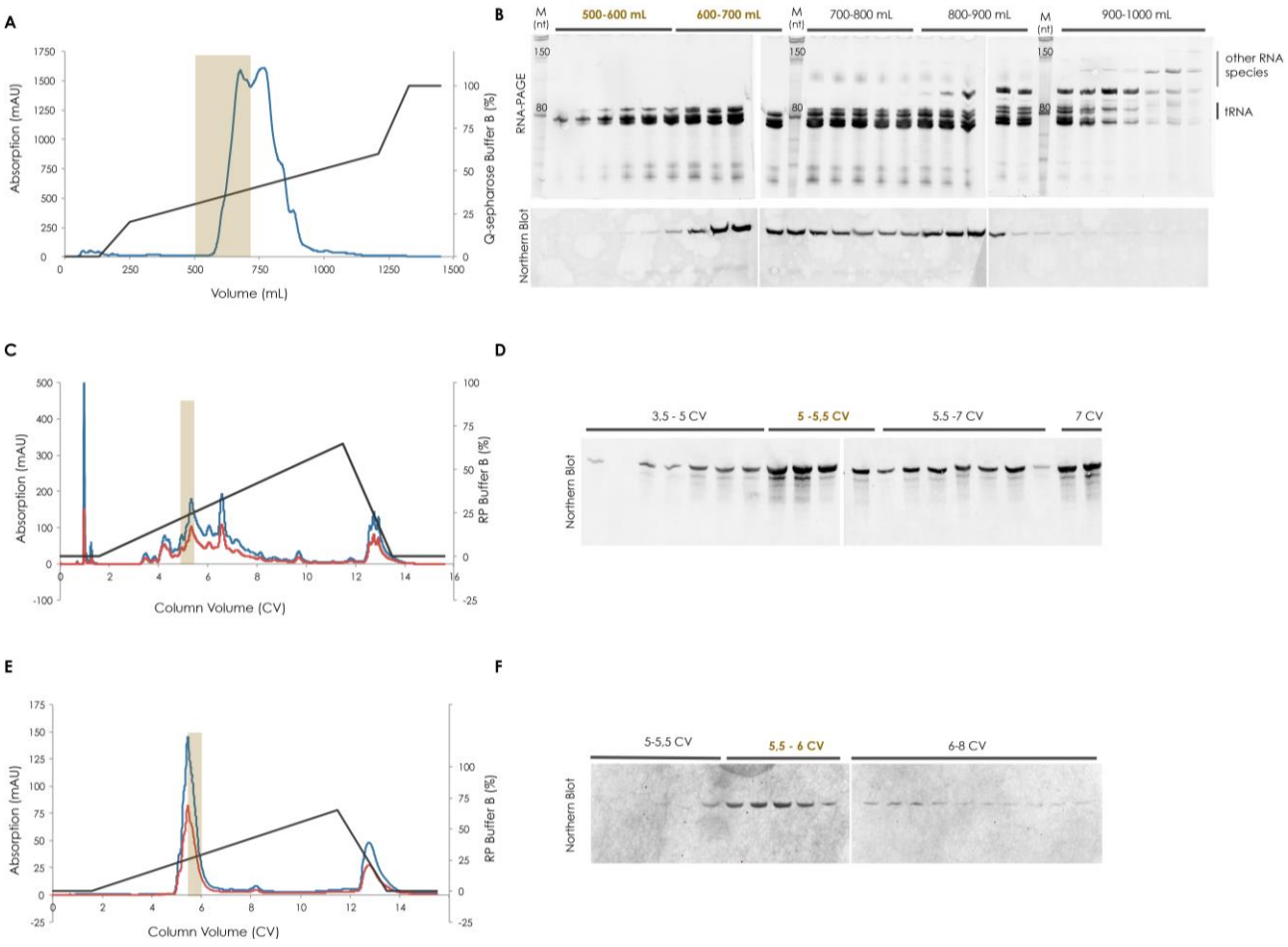

Figure 44: Chromatographic steps of $tRNA^{Pro}$ purification. (A) shows the chromatogram (λ=254 nm blue) of total RNA extract loaded onto a Q-sepharose column and eluted with increasing concentrations of Cl^-. Eluate fractions

were analyzed by denaturing PAGE and Northern blotting. Higher molecular weight RNA species were removed during the purification process. (C) corresponds to the elution chromatogram of RP-C4 HPLC (ʎ= 260 nm blue, ʎ= 280 nm red) of $tRNA^{Pro}$ after prolinylation with ProS. Fractions were analyzed by Northern Blotting (D). Two different peaks could be observed due to incomplete prolinylation. (E) shows the chromatogram of RP-C4 HPLC (ʎ= 260 nm blue, ʎ= 280 nm red) of and the fractions were analyzed by Northern Blotting (F). Pulled fractions are highlighted in yellow and yellow on the Northern Blots. The percentage of buffer B during elution is indicated by the black slope.

Figure 44 summarizes the chromatographic steps of the $tRNA^{Pro}_{CGG}$ purification protocol. The first step includes the removal of higher molecular weight RNA species. Q-sepharose is an anion exchanger that binds negatively charged molecules e.g. RNAs. By increasing concentrations of Cl^- anions, RNA species could be eluted in order of increasing negative charge. Consequently, longer RNA species with greater overall negative charge elute later than the shorter tRNAs. Figure 44A shows the main elution peak with two maxima. The analysis of the fractions indicates that higher molecular weight species begin to co-elute within the second peak (Figure 44B). For further purification, fractions corresponding to an elution volume of 500-700 mL were pooled together and concentrated by ethanol precipitation.

By using proline-tRNA synthetase (ProS) and L-proline, the only $tRNA^{Pro}$ becomes prolinylated, thus altering its chromatographic behavior during reversed phase chromatography. The sample was loaded onto an RP-C4 HPLC column and eluted with an increasing concentration of methanol in the buffer to disrupt hydrophobic interactions. As prolinylation increases the hydrophobicity of $tRNA^{Pro}$, the aminoacylated species elutes at approximately 5-5.5 CVs (Figure 44 C, D, highlighted in yellow) while the deaminoacylated tRNAs elute 0.5 CV later. Consequently, $tRNA^{Pro}$ is specifically enriched during this purification step. The Northern Blot of the prolinylated-tRNA sample (Figure 44D) indicates an additional, strong signal around 7 CV. These fractions were used for a second prolinylation step and re-loaded on the C4-column to exclude that these fractions might be separated from the main proline-$tRNA^{Pro}$ peak due to amino acid hydrolysis. As the peak re-eluted at the same column volume as before (data not shown) it is possible that the sample contains unprocessed precursor $tRNA^{Pro}$ or another longer tRNA that can be detected with the DNA probe used.

From 20 g *E. coli* HB101 cells, 1 mg of $tRNA^{Pro}$ (*proK*) was purified following this protocol. To illustrate the enrichment in the purity of $tRNA^{Pro}$ during the various purification steps samples were analyzed by denaturing PAGE (100 ng per lane) and Northern blotting (1 µg per lane) as shown in Figure 45:

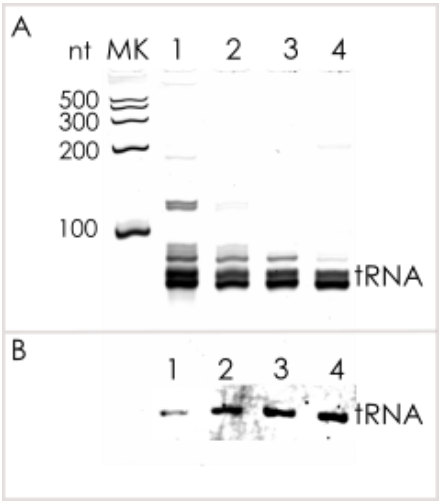

Figure 45: tRNA^{Pro} purification steps analyzed by denaturing PAGE and Northern blotting. (A) denaturing PAGE (100 ng RNA loaded per lane) and (B) Northern blot (loaded RNA 1 µg per lane) using a probe against the tRNA^{Pro} anticodon stem. L corresponds to the Ambion RNA ladder. (1) corresponds to the total small RNA extract, (2) are the pooled fractions from the Q-sepharose column, (3) are the pooled fractions from the C4-RP HPLC run after prolinylation and (4) are the pooled fractions from the C4-RP HPLC run after deaminoacylation. The amount of tRNA^{Pro} increases while the number of impurities decreases.

Figure 45 shows a summary of all purification steps by denaturing PAGE and Northern blotting. For denaturing PAGE, 100 ng RNA were loaded and 1 µg RNA was loaded on the Northern blot to be able to observe tRNA$^{Pro}_{CCG}$ enrichment over the various purification steps. Denaturing PAGE (Figure 45A) confirms that during the different purification steps the intensity of the band corresponding to tRNA^{Pro} (*proK*) is higher while the intensities corresponding to higher molecular weight RNAs decreases but still remains to a certain extent. Indeed, the tRNA^{Pro} sample shows a double band even at the end of the purification procedure, which could correspond to a contamination (approx. 20%) by another tRNA. The Northern blot (Figure 45B) shows that the relative concentration of tRNA^{Pro} increases, as indicated by the progressively greater intensity of the corresponding band over each purification step.

4.5.5 tRNA^{Pro} characterization

After purification, the different methods were used to assess the purity, extent of modification and activity of the purified tRNA^{Pro}. First, the purification and modification state of tRNA^{Pro} was analyzed using native mass spectrometry. To do so, a 10 µM tRNA^{Pro} solution was prepared in such a way as to completely remove Na^+ ions, which interfere with subsequent data interpretation. This was achieved by performing repeated washes with 150 mM $NH_4(CH_3CO_2)$

through centrifugal concentrators. The sample was analyzed by ESI-TOF-MS (electrospray ionization-time of flight – Mass spectrometry). The resulting mass spectrogram is shown in the following figure:

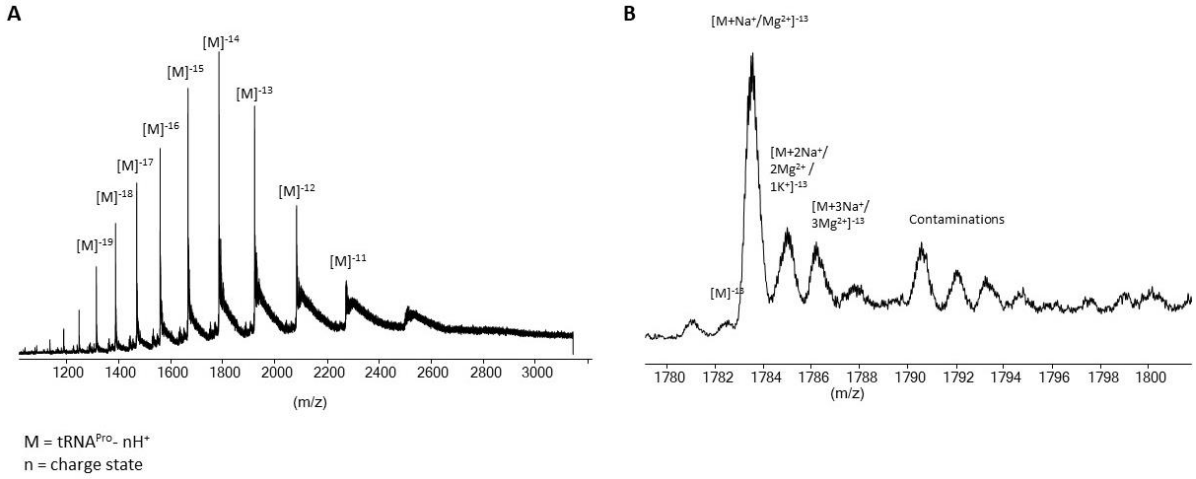

Figure 46: Mass spectrogram from native mass spectrometry of tRNA^{Pro}. M stands for the mass of tRNA^{Pro}-n protons and n correlates to the charge state of the peak. (A) overall spectrum analyzing the distribution of different charged stages (-11: m/z=2267,541, -12: m/z=2078,495, -13: m/z=1918,534, -14: m/z=1781,423, -15: m/z=1662,595, -16: m/z=1558,617, -17: m/z=1466,877, -18: m/z=1385,328, -19: m/z=1312,362) (B) zoomed in view of the -15-charged state. The main peak corresponds to tRNA^{Pro} with an additional Na^+ ion bound (m/z=1782,994), while peaks observed at higher m/z values correspond to contaminations that were observed on the denaturing RNA PAGE.

MODOMICS is a database listing tRNA modifications and the corresponding modification pathways from all kingdoms of life (Bujnicki et al., 2013; Cantara et al., 2011; Dunin-Horkawicz et al., 2006). According to the MODOMICS database, tRNA^{Pro} encoded by *proK* has five different modifications which are present once in the *proK*: dihydrouridine (D, +2 Da), 1-methylguanosine (K, +15 Da), 7-methylguanosine (7, +15 Da), thymine (T, +15 Da) and pseudouridine (P, +0 Da). All modifications except pseudouridine result in a difference in mass compared to the unmodified sequence. The theoretical electrospray series for the unmodified and modified tRNA^{Pro} was calculated using the bioinformatics tool Mongo Oligo calculator (Rozenski et al., 1999) and compared to detected electrospray series. This mass revealed that the sample mainly contained modified tRNA^{Pro} (*proK*) with minor contaminations. Additionally, Figure 46B shows that the main peak corresponds to a cation adduct of the tRNA^{Pro} even though the sample was rigorously washed. The two possible cations are Mg^{2+} (24.3 Da) or Na^+ (23.0 Da) and were both used during tRNA^{Pro} purification. The high charge states detected for the tRNA^{Pro} make a distinction impossible.

The activity of the purified $tRNA^{Pro}$ was verified by toeprinting, using an RNA template that encodes the open reading frame AUG CCG CCG AUC UAA (MPPI*). The reaction was performed in a custom-made PURExpress system devoid of tRNAs, amino acids, release factors and ribosomes (chapter 3.7). This allowed the introduction of the previously purified compounds, including $tRNA^{Pro}$ and initiator tRNA (200 pmol each per reaction). Additionally, the reaction was substituted with 1 nmol of L-Met and L-Pro. The resulting sequencing gel is shown in the following figure:

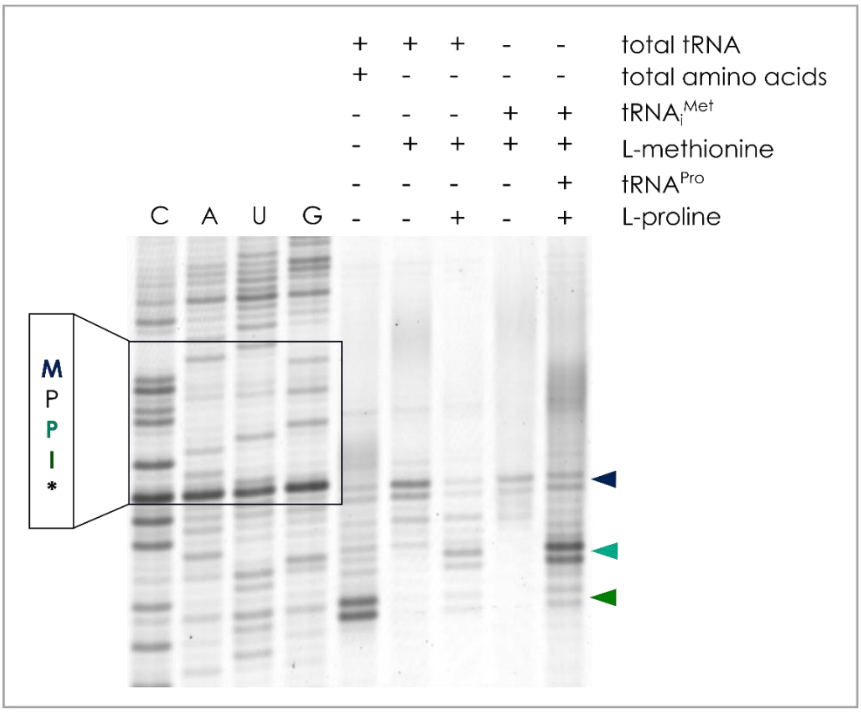

Figure 47: Activity test of purified $tRNA^{Pro}$ using toeprinting (7.5% sequencing TBU-PAGE). The dark blue arrow indicates ribosomes arrested at the start codon, the cyan arrow indicates ribosomes arrested at the third codon and the green arrow indicates unreleased ribosomes. The sample containing purified $tRNA^{Pro}$ shows a clear toeprint for ribosomes stalled on the third codon, indicating active $tRNA^{Pro}$.

Several control reactions (Figure 47) were performed: lane 1 shows the reaction containing total tRNA and all amino acids and as release factors were omitted from the reaction, ribosomes stall when the isoleucine codon is in the P-site and the stop codon is in the A-site (band indicated with the green arrow). Toeprints corresponding to the ribosomes that are arrested at the start codon were loaded in lane 2 and 4 indicated by the dark blue arrow. Lane 2 contains total tRNA with 100 µM L-methionine as the sole amino acid added to the reaction, while in lane 4 total tRNA was replaced by 5 µM $tRNA_i^{Met}$. Lane 3 contains all tRNAs but only the amino acids L-methionine and L-proline, resulting in ribosomes arrested at the third (Pro)

codon (blue arrow). The same pattern is visible in the last lane, which contains the two amino acids (100 µM each), 5 µM $tRNA_i^{Met}$ and 5 µM purified $tRNA^{Pro}$. This indicates that the purified tRNA is recognized by the proline-tRNA synthetase, recognizes the CCG codon and is incorporated into the growing polypeptide chain. The additional band indicated with the cyan arrow corresponds to ribosomes arrested at the stop codon. This indicates that the prior detected impurity might correspond to $tRNA^{Ile}$. Thus, the purified $tRNA^{Pro}$ is active in an *in vitro* translation system.

To summarize, the purified tRNA contains a high proportion of active $tRNA^{Pro}$ with minor contaminations. The latter should subsequently be excluded during the correct decoding of the CCG codon by the ribosome and therefore is unlikely to pose a problem for structural studies.

4.5.6 Purification and activity of Elongation Factor P (EF-P)

Ribosomal arrest along consecutive proline motifs is released by the protein factor EF-P (Doerfel et al., 2013; Ude et al., 2013). Various studies have shown that EF-P needs to be modified post-translationally to be active. EF-P modifying enzyme knockout cells show in a similar phenotype as *efp* knockout cells underlying the importance of the modification (Bullwinkle et al., 2013; Navarre et al., 2010; Park et al., 2012). In *E. coli*, K34 of EF-P is β-lysinylated by the enzymes YjeK (EpmA) and YjeA (EpmB). YjeK converts α-lysine into β-lysine which is then transferred to K34 by YjeA (Bailly and de Crécy-Lagard, 2010; Park et al., 2012). In a third step, this modified residue is hydroxylated by YfcM (EpmC), which is not essential to obtain fully functional EF-P (Peil et al., 2012). In order to purify active, His_6-tagged *E. coli* EF-P, this protein was co-overexpressed with untagged YjeA and YjeK in *E. coli* BL21gold cells as described previously (Peil et al., 2012). The activity of the purified *E. coli* EF-P was tested by toeprinting and the results are shown in Figure 48:

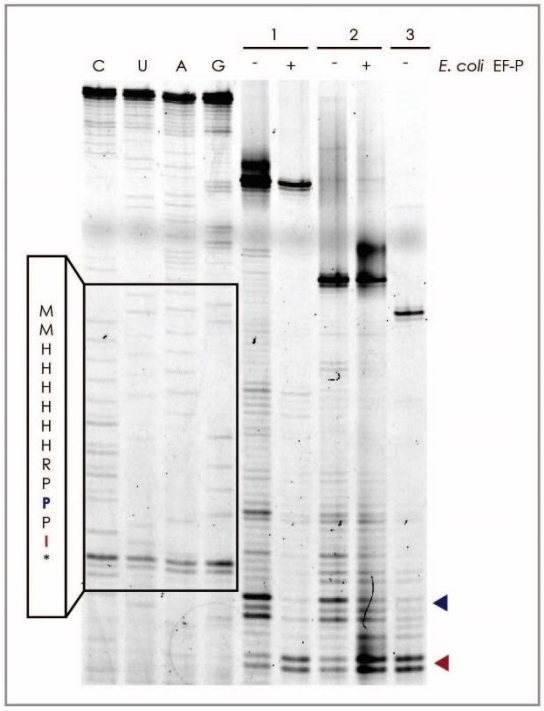

Figure 48: Screening of different toeprinting templates to study polyproline-mediated arrest and its release using purified *E. coli* EF-P. (1) The DNA template codes for MMHHHHHHHRPPPI, (2) MRPPPI and (3) MPPI. (1) and (2) shows polyproline-mediated arrest (dark blue arrow) which is released by an end concentration of 2 µM *E. coli* EF-P resulting in an increase of ribosomes arrested at the isoleucine codon and the stop codon located in the A-site due to the lack of release factors. (3) does not encode an arrest motif, resulting in a toeprint corresponding to non-released ribosomes.

The toeprinting experiment was performed using three different DNA templates to understand if polyproline-mediated arrest is enhanced when the nascent peptide chain has a certain length. The long DNA template encoded MMHHHHHHHRPPPI (1) and the shorter arresting sequence encoded MRPPPI (2). Both sequences contain one arginine followed by three consecutive prolines. This particular motif has been identified to cause strong polyproline-mediated arrest in the absence of EF-P (Starosta et al., 2014a). For both sequences, a toeprint can be detected corresponding to the arrest site in the absence of EF-P (Figure 48, dark blue arrow). Interestingly, the signal corresponding to the polyproline arrest is separated into a triple band with strong bands corresponding to 16 nt and 18 nt spacing between the first nucleotide of the P-site.

In the presence of purified EF-P, the arrest is released, as indicated by the toeprint corresponding to ribosomes located with the stop-codon in the A-site (Figure 48, red arrow). Consequently, the purified EF-P is active. These bands are also observable in the sample without EF-P indicating that the ribosomes can overcome the arrest to a certain extent without

EF-P. The third sequence, MPPI, is a non-arresting sequence and yields a toeprint that corresponds to ribosomes arrested at the stop codon (Figure 48).

4.5.7 Comparison of EF-P from *T. thermophilus* and *E. coli*

Crystallization experiments were performed using 70S *T. thermophilus* ribosomes which are known to give rise to crystals diffracting to high-resolution. So far, no data is published if E. coli EF-P rescues polyproline arrested 70S *T. thermophilus* ribosomes and vice versa. To gain an understanding of the release mechanism of EF-P experiments were performed using EF-P from both species.

As mentioned before, EF-P is post-translationally modified and these modifications are crucial for its activity. Depending on the species, the crucial residue can be a lysine residue (e.g. *E. coli* EF-P) or an arginine residue (e.g. *Pseudomonas aeruginosa* and *T. thermophilus* EF-P). Among prokaryotes, the chemical nature of the modification can differ from β-lysinylation (*E. coli*) to rhamnosylation (*P. aeruginosa*) (Lassak et al., 2015; Park et al., 2012). So far, the existence and nature of the EF-P in *T. thermophilus* remain unknown. The amino acid sequence of *E. coli* and *T. thermophilus* EF-P is not conserved as shown in the following figure:

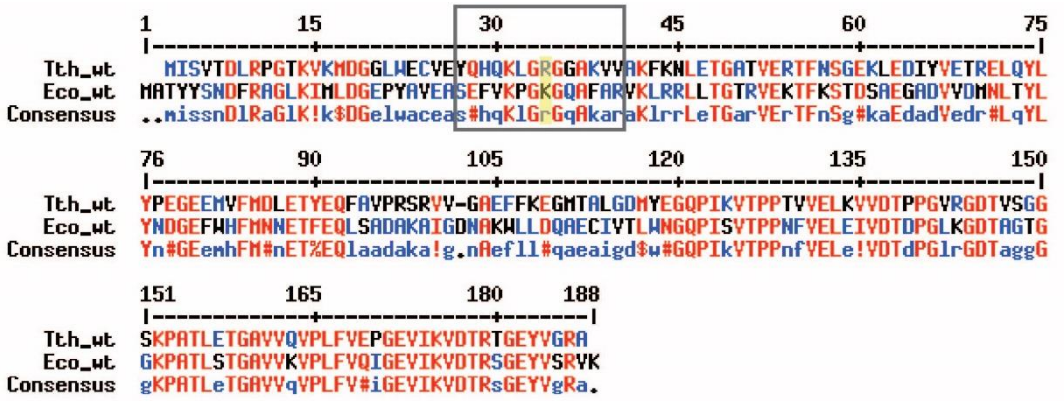

Figure 49: Sequence alignment of *T. thermophilus* EF-P (Tth_wt) and *E. coli* EF-P (Eco_wt). The sequence conservation is low as shown in the consensus line. The important residue is highlighted with a yellow box and the loop region is indicated by the gray box. Alignment was performed using Multalign.

T. thermophilus EF-P was overexpressed and purified from *E. coli* BL21gold cells as published (chapter 3.3, (Blaha et al., 2009)). As *T. thermophilus* EF-P was overexpressed in the absence of modification enzymes and no modification of R32 was reported within the structure of 70S

T. thermophilus in complex with *T. thermophilus* EF-P and tRNA (Blaha et al., 2009), it is safe to assume that the purified *T. thermophilus* EF-P is unmodified. The activity across these two species, *T. thermophilus,* and *E. coli*, was accessed by toeprinting reactions supplemented with 1, 10 or 100 µM EF-P from either species. The resulting gel is shown in the following figure:

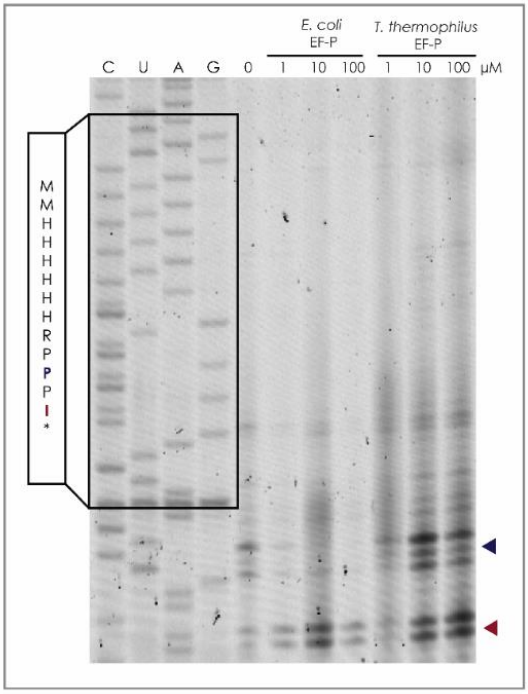

Figure 50: Unmodified *T. thermophilus* EF-P does not release *E. coli* ribosomes arrested on polyproline motifs. Reactions were performed in the absence of EF-P and in the presence of 1, 10 or 100 µM *E. coli* or *T. thermophilus* EF-P. The band indicating an arrested complex is shown by the dark blue arrow and the ribosomes that have reached the isoleucine codon are indicated by the red arrow.

Figure 50 shows that unmodified *T. thermophilus* EF-P does not release 70S *E. coli* ribosomes arrested on polyproline motifs. In contrast to this, *E. coli* EF-P releases the arrested ribosomes even at a concentration as low as 1 µM (Figure 50). It can be hypothesized that the arrest is not released by *T. thermophilus EF-P*, either due to the lack of modification or to the inability of T. thermophilus to bind to the *E. coli* ribosome or both.

The binding affinity of *E. coli* EF-P and *T. thermophilus* EF-P for the 70S *T. thermophilus* ribosome was assessed by crystallography. To do so, complexes containing 70S *T. thermophilus* ribosomes, one of the EF-P homologs and non-hydrolysable fMet-NH-$tRNA_i^{Met}$ and Phe-NH-$tRNA^{Phe}$ (chapter 3.5) were formed and set up for crystallization. The sequence of the D-loop of $tRNA^{Pro}$, which is crucial for EF-P function, is identical to that of the D-loop

sequence of $tRNA_i^{Met}$ (Katoh et al., 2016) and so $tRNA_i^{Met}$ was used for initial crystallization experiments. Crystals could be obtained from co-crystallization experiments for samples containing 20, 50, 100 µM *T. thermophilus* EF-P or 20, 50, 100 µM *E. coli* EF-P. Crystals containing *E. coli* EF-P appeared later and were more fragile than the ones containing *T. thermophilus* EF-P. Crystals containing 50 or 100 µM *E. coli* EF-P concentrations did not diffract to high-resolution (<8 Å) and no diffraction data could, therefore, be collected for these complexes. The obtained data were processed. Restrained crystallographic refinement was performed using a 70S *T. thermophilus* ribosome model lacking tRNAs and flexible ribosomal bases including A2062, U2506, U2585 and A2602 (chapter 3.9). Subsequently, the model from the initial *T. thermophilus* EF-P in complex with the *T. thermophilus* 70S ribosome (PDB code: 4V6A (Blaha et al., 2009)) was used to initially interpret the positive density. The resulting difference map for the factors is shown in the following figure:

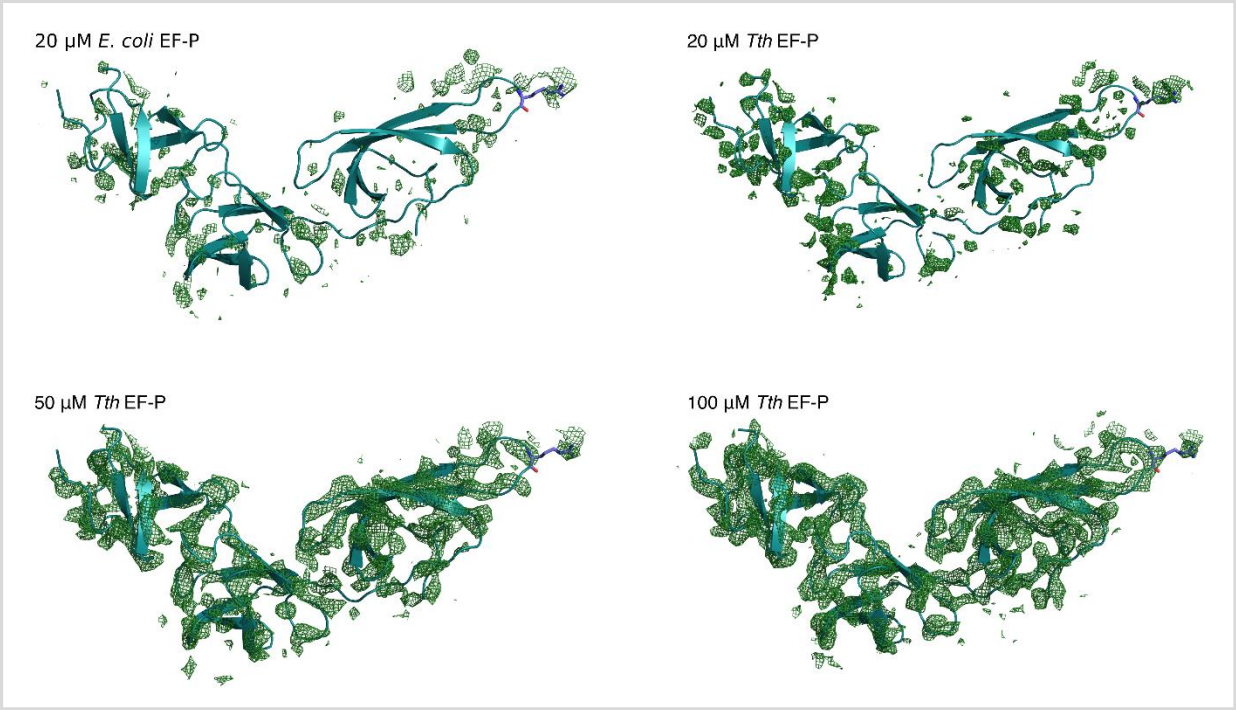

Figure 51: Positive density for minimally biased difference maps (F_o-F_c) of *T. thermophilus* and *E. coli* EF-P. Crystals containing 20 µM *E. coli* EF-P and *T. thermophilus* EF-P show nearly no density for the protein factor when setting the contour level to 2.0 σ while for higher concentrations of *T. thermophilus* EF-P a continuous density for the protein factor appears.

Data obtained from crystals containing 100 µM *T. thermophilus* EF-P resulted in a well-defined positive density. Into this density, the initial *T. thermophilus* EF-P in complex with the 70S *T. thermophilus* ribosome (PDB code: 4V6A (Blaha et al., 2009)) was for rigid-body fitting. The

same model was used to display the positive minimal biased difference map for the other conditions (Figure 51). Complexes co-crystallized in the presence of 20 µM of *E. coli* or *T. thermophilus* EF-P show nearly no density for the factor, which could clearly be seen when higher concentrations of *T. thermophilus* EF-P were used (Figure 51).

In summary, no data could be obtained for *E. coli* EF-P bound to the 70S *T. thermophilus* ribosome and polyproline arrested *E. coli* ribosomes were not released in the presence of unmodified *T. thermophilus* EF-P.

4.5.8 Studies of *T. thermophilus* EF-P mutants containing the flexible loop region from *E. coli* EF-P

One main question of this project was to study the impact of the modification of EF-P on the release of polyproline-mediated arrest. As crystals that were grown in the presence of 70S *T. thermophilus* ribosomes and high concentrations of *E. coli* EF-P, did not diffract to high-resolution and as the modification for *T. thermophilus* EF-P remains unknown, a new strategy was devised to overcome this issue, whereby *T. thermophilus* EF-P was systematically mutated to introduce the amino acid sequence from *E. coli* EF-P that is crucial for the binding of the modification enzymes without disrupting the binding of *T. thermophilus* EF-P to the 70S *T. thermophilus* ribosome. To do so, the structure of *E. coli* EF-P in complex with its modification enzymes ((Yanagisawa et al., 2010), PDB code: 3A5Z) and the crystal structure containing 70S *T. thermophilus* ribosome and *T. thermophilus* EF-P ((Blaha et al., 2009) PDB code: 4V6A) were analyzed in COOT. This led to the design of two different constructs:

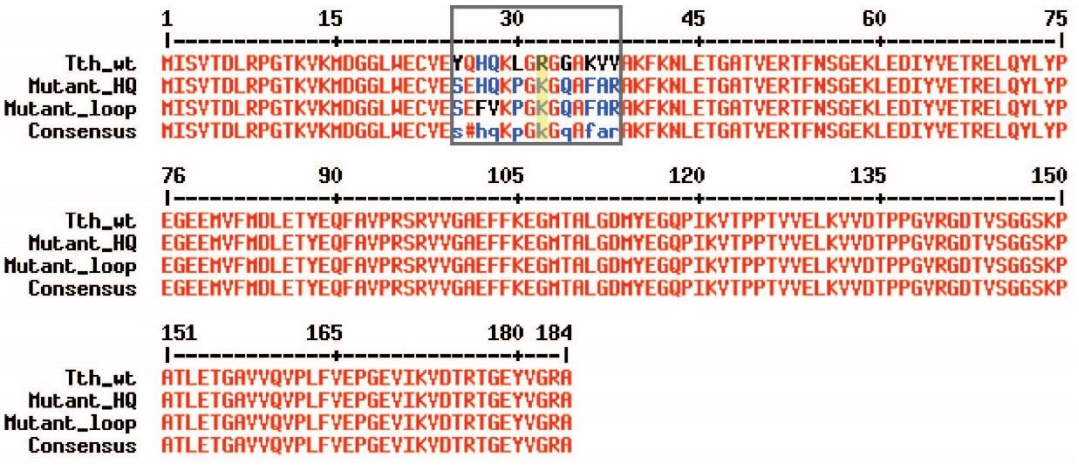

Figure 52: Amino acid sequence alignment of *T. thermophilus* EF-P and the two mutants. Tth_wt shows the *T. thermophilus* EF-P wt sequence while in Mutant_HQ the loop region is replaced by the *E. coli* amino acid sequence except for H27 and Q28 as these two residues seem to form direct contacts with the *T. thermophilus* 70S ribosome. To generate Mutant_loop the whole loop region was replaced with the corresponding amino acid sequence from the *E. coli* EF-P. The potentially modified residue is highlighted in yellow and the mutated loop region is highlighted by the gray box.

The binding site for the *E. coli* modification enzymes is a flexible loop region. The construct titled mutant_loop was generated by replacing the amino acids forming the loop of *T. thermophilus* EF-P with the corresponding *E. coli* sequence. As the amino acids, H27 and Q28, seem to form contacts with the 70S *T. thermophilus* ribosome, a second mutant, titled mutant_HQ, was generated containing the complete amino acid sequence of the *E. coli* loop except for H27 and Q28. The mutants were obtained by site-directed mutagenesis (chapter 3.2) and verified by SANGER sequencing. The mutants were co-overexpressed with the *E. coli* modification enzymes and purified like *T. thermophilus* EF-P. The following figure illustrates the different EF-P variants:

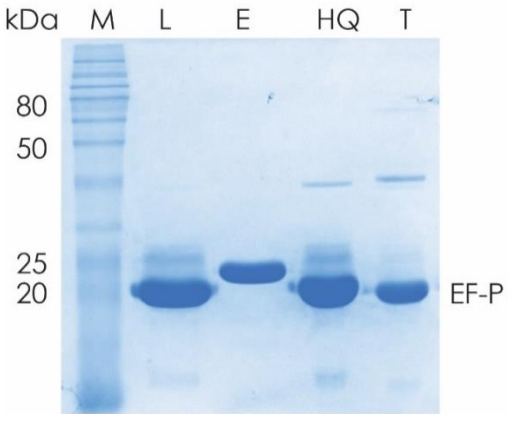

Figure 53: SDS-PAGE showing purified EF-P variants. Mutant_loop (L), *E. coli* EF-P (E), mutant_HQ (HQ) and *T. thermophilus* EF-P analyzed by denaturing protein PAGE, after gel filtration. The protein samples obtained show

high purity. The proteins have a molecular weight of 20.22 kDa for *T. thermophilus* EF-P and its mutants, while the purified *E. coli* EF-P has a molecular weight of 20.5 kDa.

Figure 53 shows the corresponding denaturing protein gel after gel filtration. The mutants show the same molecular weight as the *T. thermophilus* EF-P (Figure 53). The purified proteins show high purity and no degradation after gel filtration due to the lack of additional bands (Figure 53).

The activity of the purified mutants was studied by toeprinting using a PURExpress system lacking release factors. Figure 54 shows the results of this experimental set up:

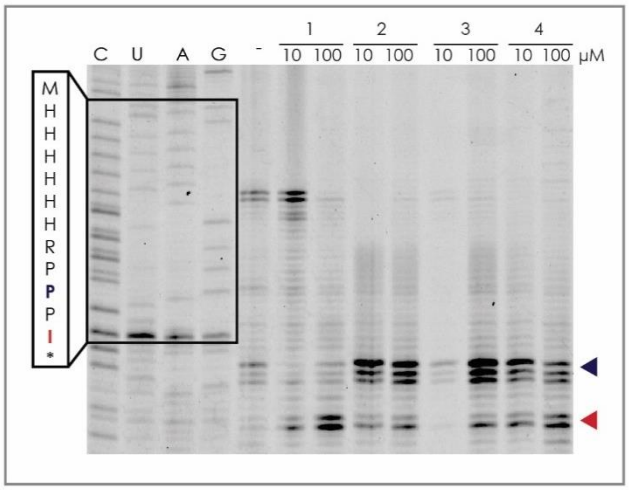

Figure 54: The mutants generated do not release *E. coli* ribosomes arrested at consecutive prolines. The arrest is released in the presence of *E. coli* EF-P (1) but not in the presence of mutant_loop (2), mutant_HQ (3) or *T. thermophilus* WT EF-P. The blue arrow indicates the arrest site while the red arrow corresponds to the isoleucine codon located in the P-site and the stop codon located in the A-site.

E. coli EF-P releases polyproline-mediated arrest while the *T. thermophilus* EF-P and the mutants do not release the arrest (Figure 54). Reasons for this might be that the mutants are not recognized by the modification enzymes or that the mutation of the loop is not sufficient to perform the release of polyproline-arrested 70S *E. coli* ribosome by *T. thermophilus* EF-P. All EF-P mutants were used to set up crystallization drops containing 50 µM of the protein. Although crystals could be obtained, they did not diffract to a high enough resolution (>8 Å) and it was therefore not possible to make assumptions about the binding capacity or modification state of the mutants. Consequently, subsequent experiments were performed using 70S *E. coli* ribosomes and *E. coli* EF-P.

4.5.9 Toeprint to study polyproline-mediated arrest and its release by EF-P

One of the main aims of this project was to obtain the structure of polyproline arrested ribosomes and getting a grounded understanding how the arrest is released by EF-P. As the D-loop of $tRNA^{Pro}$ is crucial for the recognition by EF-P, the reaction was initiated from a dipeptidylated initiator tRNA and so the complex can be formed using strategy 2.

For the poly-proline project, the dipeptides AcRP-CBT and AcRA-CBT, as well as the tripeptide AcRAP-CBT, were used to obtain the corresponding peptidylated initiator tRNA using the flexizyme technique (chapter 4.2). The activity of these peptidyl-$tRNAs_i^{Met}$ was analyzed by toeprinting using a mRNA template that encoded the open reading frame AUG CCG CCG AUC UAA (MPPI*). The mRNA template encodes two proline codons in order to induce stalling only in the presence of dipeptidylated or tripeptidlyted initiator tRNA on the second or first codon, respectively. The reaction was performed using a custom-made PURExpress system (NEB, Ipswich, MA, USA). 10 µM peptidyl-$tRNA_i^{Met}$, 20 µM $tRNA^{Pro}$ and 100 µM L-proline were incubated with 5 µM mRNA, factor mix, and 2.5 µM ribosomes in order to pre-form the complex (5 min at RT). Subsequently, solution A^-(minus aa, tRNA) provided by the kit, containing nucleotides, was added, allowing complexes that had not been arrested to be translocated (further information is provided in chapter 3.9). Certain reactions were supplemented with *E. coli* EF-P in order to allow the release of the arrested complex. The reaction was analyzed on a 7.5% sequencing PAGE and the result is shown Figure 55:

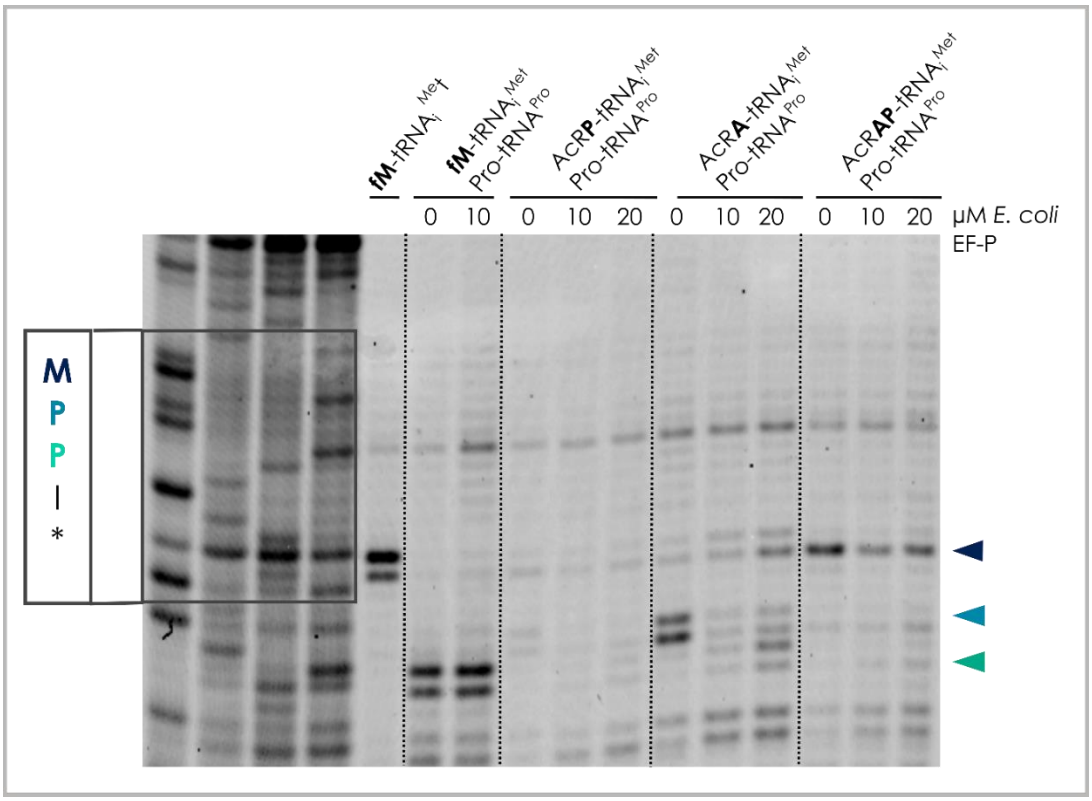

Figure 55: Polyproline-mediated arrest and its release by *E. coli* EF-P was studied using flexizyme-peptidylated tRNAs. The reaction was performed in the custom-made PURExpress. The mRNA template encoded the peptide sequence MPPI. The reaction was performed using 10 µM peptidyl-tRNA$_i^{Met}$ and 20 µM tRNA^{Pro}. Reactions were substituted with 10 and 20 µM *E. coli* EF-P resulting in partial release from the arrest site. The dark blue arrow indicates the start codon equivalent to the arrest complex in the presence of AcRAP-tRNA$_i^{Met}$. The blue arrow indicates the first proline codon, which is equivalent to the arrest site induced by the dipeptidylated tRNAs, including AcRP-tRNA$_i^{Met}$ and AcRA-tRNA$_i^{Met}$ and the cyan arrow indicates the second proline codon equal to the release of the arrest.

The start codon control was performed using 10 µM initiator tRNA and 100 µM L-methionine. The used RNA template encodes for MPPI and ribosomes will not arrest along two consecutive prolines. Consequently, in the presence of tRNA$_i^{Met}$, 100 µM L-methionine, 20 µM tRNA^{Pro} and 100 µM L-proline, the ribosomes translate through both proline codons. Consequently, most ribosomes arrest on the third codon (Figure 55, cyan arrow) due to the absence of tRNA^{Ile}.

AcRP-tRNA$_i^{Met}$ induces a weak arrest complex indicated by a weak double band. The arrest is released by EF-P indicated by a laddering of the double band. AcRA-tRNA$_i^{Met}$ forms a stronger stalling complex (middle blue arrow). In most cases the ribosomes protect 16 to 17 nt (start counting from the first nt of the P-site) (Orelle et al., 2013b). The toeprint generated after initiation with the dipeptidyl-tRNA$_i^{Met}$ has a spacing of 17 to 18 nt. This is consistent with the toeprinting results translating the whole arrest sequence (Figure 48, Figure 56, Figure 50 and

Figure 54). The band corresponding to the polyproline-mediated arrest was split into a triple band corresponding to 16-18 nt (Figure 48, Figure 56, Figure 50 and Figure 54). An explanation could be that the ribosome might adopt a different ratcheting state while being arrested on polyproline motifs. The arrest is released in the presence of *E. coli* EF-P indicated by the release of the arrest band into laddering.

AcRAP-tRNA$_i^{Met}$ carries already the arrest sequence and so the arrest site in the absence of EF-P is the start codon (dark blue arrow Figure 55). Addition of EF-P decreases the intensity of the start codon band indicating partial release of the arrested ribosomes.

Overall, the polyproline-mediated arrest can be characterized in toeprint assays using peptidylated initiator tRNA. The best stalling efficiency and then release by EF-P were observed initiating the reaction with AcRA-tRNA$_i^{Met}$. A reason could be that the proline within the flexizyme-charged peptide potentially has a restricted backbone geometry thus resulting in reduced reactivity compared to the AcRA-tRNA$_i^{Met}$.

In summary, the complex can be formed using the PURExpress system from NEB but the structure remains unknown. As crystals containing high concentrations of *E. coli* EF-P did not diffract and the quality of the cryo-EM map for the MKF-70S structure showed a nice density for the side chains, is promising to obtain a similar result for the polyproline project. The strategy to obtain the complexes are discussed in further detail in the discussion (chapter 5.3).

4.5.10 EF-P does not release other well-characterized nascent chain-mediated translation arrest peptides

A recent *in vivo* study using fluorescently labeled *E. coli* EF-P has shown that EF-P binding events are more frequent than the occurrence of polyproline-mediated translational arrest (Mohapatra et al., 2017) raising the question for other functions of EF-P. Furthermore, an *in vitro* study investigating the effect of miscoding of the P-site tRNA showed that these miscoding events lead to a reduction in the translocation rate that the translocation rate can be enhanced in the presence of EF-P (Alejo and Blanchard, 2017). Both studies illustrate that EF-P might have multiple functions and can bind to ribosomes with empty E-sites (Alejo and Blanchard, 2017; Mohapatra et al., 2017) which appears to be more frequent. In *E. coli*, EF-P is a part of the ribosome rescue system that recognizes and releases stalled ribosomes. Ribosomal stalling can be induced by various factors, including the absence of stop codons, mRNA secondary structures, or amino acid starvation to name only a few examples. The ribosome rescue system is formed by transfer-messenger RNA (tmRNA) and proteins including e.g. RelA and LepA as reviewed by (Giudice and Gillet, 2013). The question whether EF-P might be involved in the release of nascent chain-mediated translational arrested ribosomes stalled by non-polyproline arrest peptides was addressed by performing toeprinting on the well-characterized arrest peptides SecM, TnaC, ErmBL, ErmCL, and ErmDL. The results are shown in Figure 56:

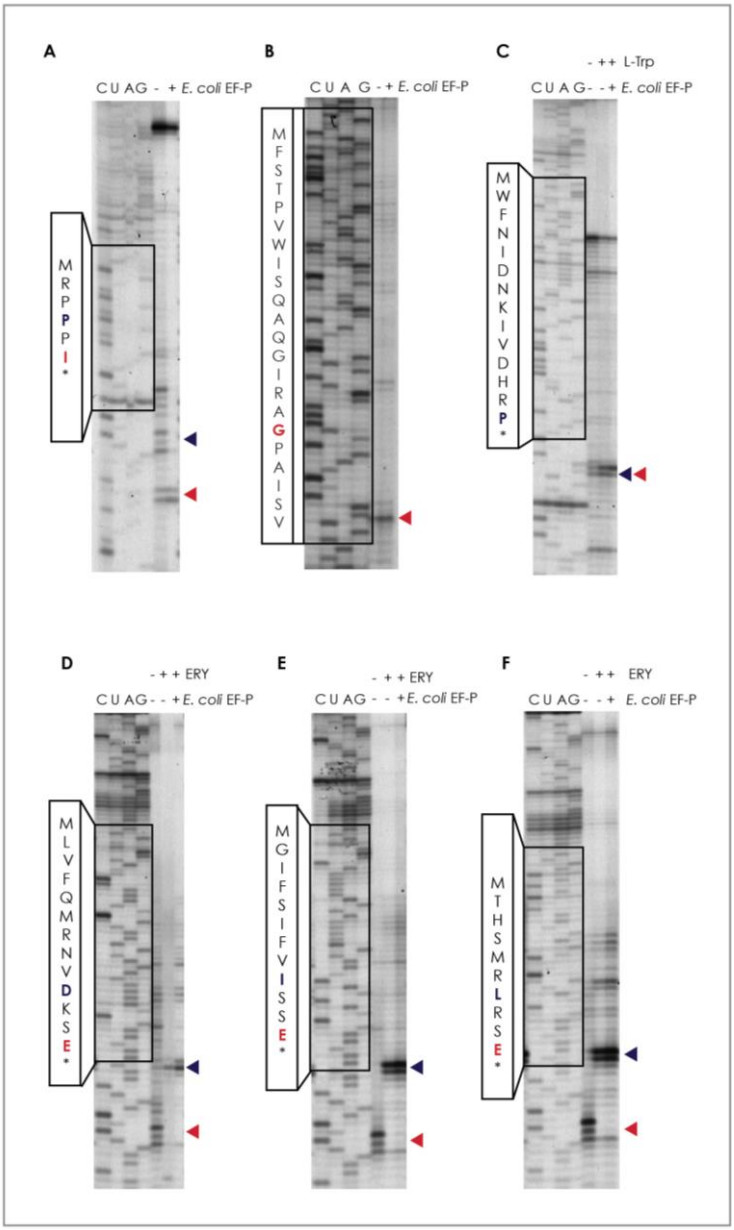

Figure 56: *E. coli* EF-P releases polyproline-mediated arrested ribosomes but does not release ribosomes stalled while translating other well-characterized arrest peptides. *E. coli* EF-P was used to study its activity on (A) Polyproline-mediated arrest, on the ligand-independent arrest peptide SecM (B) and on ligand-dependent arrest sequences including (C) TnaC reaction was supplied with release factors, (D) ErmBL, (E) ErmCL and (F) ErmDL. The toeprint corresponding to the arrested ribosome is indicated by a dark blue arrow and the non-released complexes are indicated by the red arrow.

Figure 56 shows toeprints for several arrest peptides (SecM, TnaC, ErmBL, ErmCL, and ErmDL) in the presence of 2 µM *E. coli* EF-P. In contrast to ligand-dependent arrest sequences, the release mechanism for SecM has been documented. SecM is released by mechanical force applied by the pre-protein translocate SecA (Butkus et al., 2003). Consequently, SecM stalling should not be released by EF-P otherwise the regulation mechanism would not work. The

toeprint experiment (Figure 56B) shows that EF-P does not release SecM arrested ribosomes *in vitro* and is used as a negative control.

In the presence of tryptophan, TnaC arrests when proline codon 24 is located in the P-site and the stop codon is located in the A-site and the release of the peptide is inhibited. To be able to determine arrest conditions from non-arrest conditions the reaction was supplemented with releases factors provided by the kit. On the other hand, the Erm leader peptides arrest ribosomes on internal codons in response to erythromycin. Therefore, release factors could be omitted from the reaction in this case. Ribosomes arrested in the presence of ligands are indicated by dark blue arrows in Figure 56. In all cases, reactions containing EF-P still show a strong signal for the arrested complexes (Figure 56C-E) while ribosomes arrested on polyproline stretches are released (Figure 56A). This means that the arrest peptides SecM, TnaC, ErmBL, ErmCL, and ErmDL are not released by EF-P *in vitro.*

5. Discussion and perspectives

5.1 Proline-rich antimicrobial peptides and implications for further drug development

The combination of structural and biochemical studies led to a deepened understanding of the mechanism of action of the proline-rich antimicrobial peptides Bac7(1-16), Onc112, Met I and Pyr. The peptides bind to the ribosomal exit tunnel in a reverse orientation relative to the nascent peptide chain. Their binding site extends into the PTC, the A-site crevice, and CCA binding pocket. This inhibits the accommodation of the A-site tRNA and thus the transition from initiation towards elongation is also inhibited (Gagnon et al., 2016; Roy et al., 2015; Seefeldt et al., 2016; Seefeldt et al., 2015). A large range of well-characterized antibiotics targeting specifically the PTC and the ribosomal exit tunnel bind to similar regions as PrAMPs, as illustrated in the following figure:

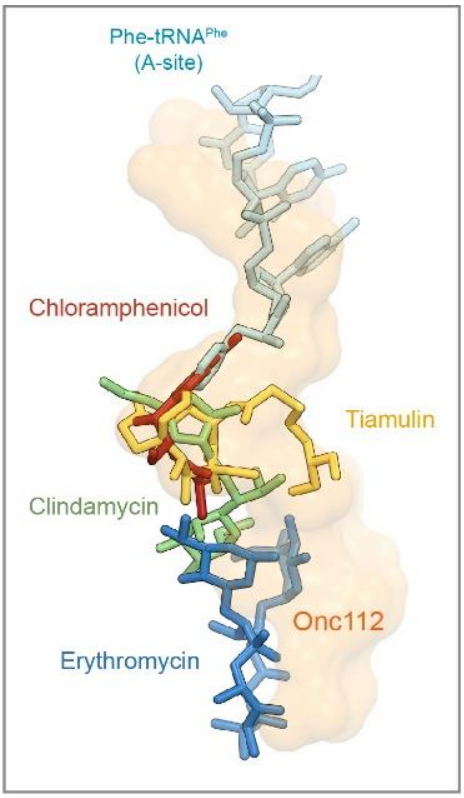

Figure 57: Overlay of the binding sites of Onc112 and clinically used antibiotics. The binding site of Onc112 (orange) overlaps with the binding sites of well-characterized antibiotics. These antibiotics are known to inhibit the transition from initiation to elongation and early elongation. The A-site tRNA is indicated in light blue. The figure is taken from (Seefeldt et al., 2015).

As the binding site of Onc112 overlaps with the binding site of several antibiotics including chloramphenicol and erythromycin (Bulkley et al., 2010; Dunkle et al., 2010), it may be possible to modify PrAMPs in order to increase their binding affinity through additional hydrogen-bonds and stacking interactions. In addition, the elongated fold of the PrAMPs covers a long binding surface and could slow down the appearances of resistance. This strategy is listed as an advantage of synergistic antibiotics as reviewed by (Kohanski et al., 2010). Synergistic antibiotics are pairs of antibiotics acting in concert and therefore enhancing their inhibitory impact. Well-characterized molecules that target the PTC and the upper ribosomal tunnel are streptogramin A and B. These antibiotics are bacteriostatic when used individually, but bactericidal when used together (Vazquez, 1966). The enlarged binding site of two molecules might decrease the rise of resistance (Noeske et al., 2014). Isolated *E. coli* cell lines carrying rRNA mutants that are known to be resistant to antibiotics (e.g. macrolides) were used to determine the minimal inhibitory concentration (MIC) of Bac7 and Onc112 (Gagnon et al., 2016). Cells were carrying the point mutations A2503C and A2059C or the corresponding double mutation. While cells treated with Bac7 were still sensitive to the same concentration of Bac7 (0.75), higher concentrations of Onc112 were necessary to have a similar effect (Gagnon et al., 2016). An explanation could be that the N-terminus of Bac7 anchors the peptide in its binding pocket as it adopts a specific conformation due to stacking interactions with the tunnel bases (Gagnon et al., 2016). In order to increase the binding affinity of the PrAMPs, introducing positively-charged aromatic moieties within the N-terminus might enhance stacking interactions.

Recently published structures of the antimicrobial peptides Api137 and Klebsazolicin in complex with the 70S *E. coli* or *T. thermophilus* ribosomes revealed that these peptides target to the ribosomal exit tunnel (Florin et al., 2017; Metelev et al., 2017). These peptides inhibit early elongation (Metelev et al., 2017) and termination (Florin et al., 2017). The following figure compares their structures to that of Bac7(1-16):

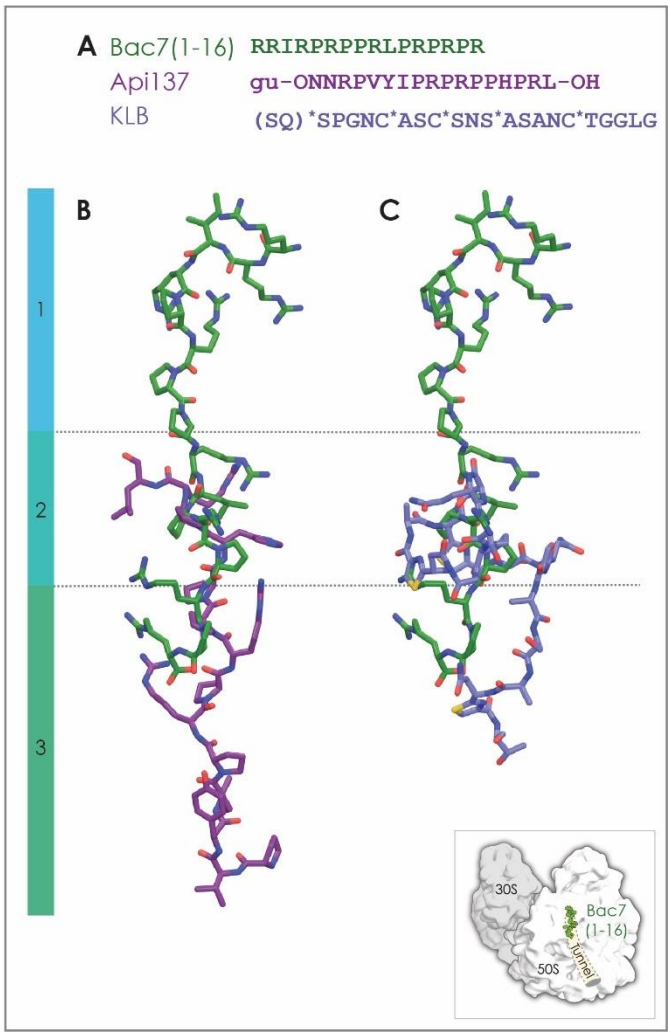

Figure 58: Comparison of the binding sites of Bac7(1-16), Api137 and Klebsazolicin (KLB). (A) The peptides bind to the ribosomal exit tunnel even if they have different sequences and folds (Florin et al., 2017; Metelev et al., 2017; Scocchi et al., 1994). * indicates post-translationally modified residues. Bac7(1-16, green) binds to the A-site tRNA binding pocket (1), the A-site crevice (2) and the upper tunnel. Api137 (B, purple, PDB code: 5O2R) binds to the A-site crevice and reaches further into the ribosomal tunnel (Florin et al., 2017). The post-translational modifications of KLB (C, PDB code: 5W4K) restrict the backbone conformation resulting in a "curled-up" conformation binding from the PTC into the upper tunnel (Metelev et al., 2017). The ribosome is taken from (Seefeldt et al., 2016).

The initial presumed target of PrAMPs such as oncocin or apidaecin was DnaK. Several rounds of *in vitro* drug development led to the derivatives Onc112, Onc72, and Api88 and Api137 ((Knappe et al., 2010; Otvos et al., 2000), discussed in further detail in chapter 1.3). However, cells lacking DnaK remained sensitive to these peptides and Krizsan et al was able to crosslink Api88 to bacterial ribosomes (Krizsan et al., 2014), indicating that the ribosome was the likely target for PrAMPs. These experiments were the starting point of this project and resulted in the structure determination of Onc112 bound to the bacterial ribosome.

Recent biochemical and structural studies showed that Api137 traps the ribosome at the stop codon and prevents the release of the peptide (Florin et al., 2017). In contrast to Bac^{1-16} (Figure 58B), Api137 binds in the same orientation as the nascent peptide chain with the N-terminus pointing towards the cytoplasm. The binding site covers the PTC and reaches further into the upper tunnel compared to $Bac7^{1-16}$ (Florin et al., 2017). Although Api137 and $Bac7^{1-16}$ are both classified as PrAMPs, their binding site, orientation and mechanism of action differ extensively (Figure 58B).

The second peptide Klebsazolicin (KLB) (Metelev et al., 2017). KLB is an antimicrobial peptide produced as a defense mechanism by *K. pneumoniae* by the ribosome and belongs to the microcin class. In contrast to PrAMPs, these bacteriocins are characterized by a high cysteine content. The cysteines are post-translationally modified, resulting in a cyclic backbone with a "curled-up" conformation (Metelev et al., 2017). KLB binds to the PTC and the upper part of the ribosomal exit tunnel (Figure 58B). Biochemical studies confirmed that KLB binding inhibits the translational cycle at the early elongation phase, as indicated by the structure of this peptide in complex with the 70S *T. thermophilus* ribosome (Metelev et al., 2017).

All six peptides, $Bac7^{1-16}$, Onc112, Pyr, Met I, KLB and Api137, have a large variety of different sequences and come from very different organisms, ranging from bacteria to higher vertebrates. All peptides target the PTC, reach into the upper ribosomal exit tunnel and/or reach into the A-site tRNA binding pocket (Florin et al., 2017; Gagnon et al., 2016; Metelev et al., 2017; Roy et al., 2015; Seefeldt et al., 2016; Seefeldt et al., 2015). As recently reviewed in detail for macrolide antibiotics, a major strategy for antibiotic development is to increase bioavailability, through greater drug stability and improved cellular uptake, while enhancing a drug's binding affinity for its target through the chemical modifications (George, 2017). For macrolide antibiotics, modifications include the removal of the cladinose sugar or the attachment of novel side chains to the drug backbone (George, 2017). Similarly, the length of the antimicrobial peptides and their sequence variability opens up a new avenue for drug development. Future objectives will have to include the improvement of the bioavailability and binding affinity of these molecules. This could be achieved by modifying the chemistry of their constituent building blocks, including the use of unusual amino acids and modifications of the backbone, such as the incorporation of β-, γ-, and D-amino acids, as well as urea backbones or peptoids (Pasco et al., 2017).

Bac7, Onc112, Met I, Pyr, KLB and Api137 are active against Gram-negative bacteria due to the presence of the ATP-dependent peptide transporter SbmA (Mattiuzzo et al., 2007; Metelev et al., 2017; Runti et al., 2013). Although SbmA was reported to transport peptides, toxins, peptoids and peptide nucleic acids (PNA) its physiological role remains unknown, mostly due to the absence of a detectable phenotype for the deletion mutants under conditions tested so far (Corbalan et al., 2013). Screening Api137-resistant cells identified mutations within the SbmA transporter, indicating the main limitation for using these peptides as potential drugs (Florin et al., 2017). To overcome this limitation, the uptake of PrAMPs could be coupled to an essential and species-specific transporter system e.g. the Iron-uptake pathway.

In the structures I obtained, the C-terminus of Bac7, Onc112 and Pyr could not be modeled due to the absence of density, indicating that it is disordered within the crystal (Gagnon et al., 2016; Roy et al., 2015; Seefeldt et al., 2016; Seefeldt et al., 2015). C-terminal truncations of Onc112 led *in vivo* to loss of function indicating that it might be a crucial recognition site for cellular uptake (Seefeldt et al., 2015). Since the C-terminus is not important for binding to the ribosome it can be modified in order to avoid the dependency on the SbmA transporter for uptake. As shown recently, introducing a fluorescent label into the PrAMP arasin I does not alter the inhibitory properties of the peptide compared to the unlabeled form (Paulsen et al., 2016). Instead of a fluorescent label a molecule that is recognized specifically by an essential transporter could be introduced into the PrAMP, a method termed “trojan horse” as reviewed in detail (Zgurskaya et al., 2015). An essential transporter that has been used previously is the iron uptake system in bacteria. While Fe^{3+} (Iron) is crucial for bacteria to survive the sources are often limited during infection. To complex Fe^{3+} specifically in the environment and to transport the cation into the cells, bacteria evolved siderophores (Braun and Hantke, 2011). Siderophores represent a large class of molecules with different characteristics and molecular weights ranging from 0.3 to 1 kDa. Previous attempts to introduce siderophores into antibiotics such as chloramphenicol often resulted in loss of function (Page, 2013). In contrast to this, some Streptomyces species have been shown to synthesize siderophore-attached macrolides. Furthermore, some microcins are linked post-translationally to siderophores (Vassiliadis et al., 2010; Vassiliadis et al., 2007) The various siderophores and their corresponding transporters are often species-specific, resulting in narrow-spectrum antibiotics. This opens the possibility of creating PrAMPs that are capable of acting against Gram-positive bacteria, which normally

lack the SbmA transporter. This makes this concept particularly interesting for further rounds of drug development.

In summary, some antimicrobial peptides have been shown to bind to the exit tunnel of bacterial ribosomes and to inhibit the initiation, early elongation or termination steps of translation. Structural data of bacterial ribosomes in complex with these peptides have given us detailed insights into the mechanism of action of PrAMPs, making the structures a solid foundation for further drug development.

5.2 The flexizyme methodology to study nascent chain-mediated translational arrest

The second project of this thesis aimed to study translational arrest mediated by short nascent chains using structure biological methods. Forming the arrest complex by *in vitro* translation requires a long mRNA fragment that can interfere with the crystallization process (personal communication from Axel Innis). In order to avoid this, the arrest peptide was bound directly to the 3'CCA end of the initiator tRNA using the flexizyme methodology (Goto et al., 2011). After the activity of the peptidylated-tRNA was confirmed by toeprinting experiments the arrest complexes were formed for X-ray crystallography. Due to hydrolysis of the ester bond linking the peptide to the tRNA during the crystallization, a second strategy was developed involving the generation of 3'-NH_2-tRNA using previously developed protocols (Polikanov et al., 2014; Voorhees et al., 2009). Attempts to peptidylate a 3'NH_2-tRNA using a flexizyme have not been successful to date.

An alternative strategy to attach the peptide through a non-hydrolysable amide linkage was to add the last amino acid through an additional round of elongation as discussed in detail in chapter 4.2.6. However, resulting crystals revealed no density of the peptide or the A-site tRNA. Reasons could be that the binding affinity of the deaminoacylated $tRNA_i^{Met}$ for the P-site might be too high to be replaced under crystallographic concentrations.

The recent improvement in resolution of structures obtained by cryo-EM has made it possible to study short arrest peptides with this method. The probability of hydrolysis of the ester-linked arrest peptide was reduced as the complex was directly frozen after complex formation.

During the studies of this thesis, two case studies were used to establish a workflow for arrested ribosome complex formation: (i) fM+X(+) mediated arrest in the presence of erythromycin, and (ii) translational arrest along consecutive prolines. Future experiments should focus on the study of the chemical properties of the different amino acids of the arrest peptides to improve or deplete the arresting properties of the peptide as well as the involvement of the peptide backbone in contact formation with the ribosomal residues. The project specific main results are put again into context and perspectives are discussed in the following sections.

5.3 fMKF(R) arrests the 70S *E. coli* ribosome in the presence of erythromycin

fM+X(+) represents a set of short nascent peptides that arrest the bacterial ribosome in the presence of erythromycin (Sothiselvam et al., 2014; Sothiselvam et al., 2016). To study the underlying molecular mechanism, the sequence fMKF(R) was selected as discussed in detail in chapter 4.3. The fMKF(R) arrest sequence had not been shown before to arrest the 70S *E. coli* ribosome. This was shown by toeprinting of the whole ORF and by initiating translation using a fMKF peptidyl moiety attached to initiator tRNA in the presence of the drug.

The structure of the complex was obtained by cryo-EM with an overall resolution of 3.9 Å. The density of the nascent peptide provided information regarding the orientation of two of the three peptide side chains. The advantage of the flexizyme methodology is that it allows peptides composed of non-canonical amino acids to be attached to the 3'CCA end of tRNAs. A previous study investigated the chemical properties of the A-site amino acid necessary for the arrest using tRNA mimics (Sothiselvam et al., 2016). Based on the structure and the previous study, the following modifications can be performed to study the chemical properties of the nascent peptide necessary for the nascent chain mediated translational arrest:

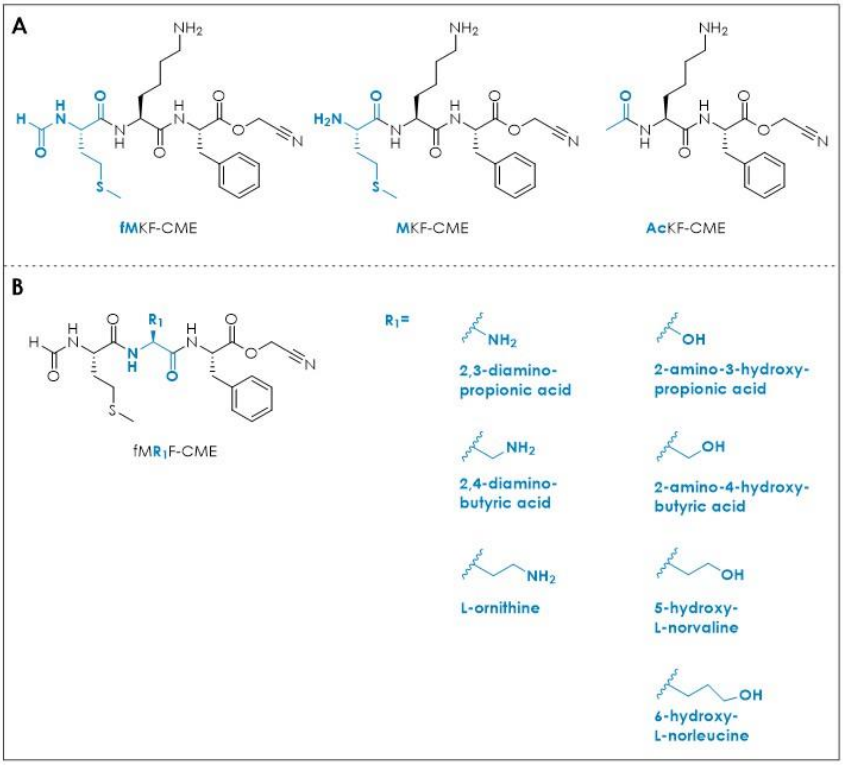

Figure 59: Peptide modifications to get a greater understanding of the chemical properties needed for nascent chain mediated translational arrest. The possible peptide modifications are highlighted in blue. (A) The flexizyme methodology allows translation to be initiated without the N-terminal formyl-group or the N-terminal methionine. (B) To analyze the impact of chain length and the positive charge of the -1 side chain on the arrest, peptides can be synthesized with a shortened side chain at this position or with the amino group replaced by a hydroxyl group.

The methionine side chain was not modeled due to the absence of density. This suggests that the methionine side chain could be disordered and raises the question whether its presence is required for arrest. Bacterial translation is initiated in most cases using fMet-tRNA$_i^{Met}$ as reviewed by ((Laursen et al., 2005), exception listed in chapter 1.1.2.1). Consequently, all toeprinting experiments were performed using the modification listed in Figure 59. One first modification of the fMKF peptide could include the removal of the formyl group to investigate if its presence is important for the arrest. Another peptide could be synthesized replacing the methionine by an acetyl moiety. These modifications can be only introduced using the flexizyme methodology (Figure 59A).

Strikingly, no density could be detected for Arg-tRNA^{Arg} in the A-site even when the dilution buffer was supplemented with this tRNA. As seen in the structure of the fMKF-70S complex, the A-site crevice is blocked by the Lys (-1) side chain. Consequently, the positive charge of the lysine side chain would be in close proximity of the positive charge of the incoming arginine

side chain, resulting in static repulsion. Previously, it has been shown that the positive charge of the A-site amino acid side chain is crucial for arrest, whereas its length is not (Sothiselvam et al., 2016). The same cannot be said for the -1 residue at present. The flexizyme methodology allows us to study the impact of the length and charge of the -1 residue side chain, using the modifications listed in Figure 59B. The need for a particular orientation of the lysine side chain could be verified by replacing this residue with D-lysine. This will force the side chain to adopt the mirrored orientation and thus might prevent arrest in the presence of erythromycin.

The toeprinting experiment to prove the activity of the fMKF-tRNA$_i^{Met}$ (chapter 4.4.3, Figure 28) indicates that even in the presence of erythromycin a certain percentage of ribosomes still translocates to the second codon. Consequently, the arrest strength can be still enhanced. To do so, modification of the -1 side chain to a positively charged aromatic moiety or to an arginine might be enough to enhance the arrest due to potential stacking interactions with the rRNA. In addition, the methionine could be replaced by groups that tend to form stacking interactions, such as aromatic moieties, in order to obtain a higher arrest strength. The arrest strength might be assessed using toeprinting and puromycin sensitivity. Other methionine replacement could include linker side chains to attach the arrest peptide covalently to the macrolide. Previous attempts to peptidylate macrolides included the attachment of long peptide chains (Washington et al., 2014). Another study used chloramphenicol attached to short tri-peptides from *erm* leader peptides including MRL. These peptide-chloramphenicol fusions had an impact on *in vitro* translation comparable to chloramphenicol itself (Mamos et al., 2013). Chemically linking arrest peptides without the tRNA to erythromycin might overcome macrolide resistance as the peptide would extend into the PTC, thus covering a larger binding site in the way synergistic antibiotics do (Noeske et al., 2014).

The current resolution of the MKF-70S structure is 3.9 Å and is thus too low to make assumptions about hydrogen bonding interactions. To investigate the hydrogen bonding of the backbone with the ribosomal residues, the peptide backbone could be modified by N-alkylation of the backbone or replacing each peptide bonds with an ester bond In doing so, the importance of each peptide bond as H-bond donor could be investigated. Other backbone modifications, such as the introduction of urea building blocks or β- and γ-peptides (Pasco et al., 2017) and might influence the folding and orientation of the peptide within the tunnel.

The orientation of the lysine side chain is enhanced by allosteric rearrangement of the 23S rRNA, in particular of bases U2506, U2585, and A2062 which were reported to be crucial for the activity of certain arrest peptides (Koch et al., 2017; Vázquez-Laslop et al., 2011). The orientation of these bases was compared with those in several structures obtained previously, including those of complexes obtained at various stages of the translation cycle or undergoing ligand-dependent or -independent translational arrest. Within the fMKF-70S ribosome structure, U2506 adopts a conformation that is different from that observed in other structures. Furthermore, U2585 adopts a position between pre-accommodation and pre-catalysis that is similar to the conformation observed in the VemP-arrested ribosome (Su et al., 2017) structure and that is stabilized by potential stacking interactions against the peptide.

Strikingly, the base of A2062 adopts a specific orientation which points towards the PTC and appears to be important for the arrest. It has been reported that arrest peptides can be classified into two categories, depending on whether their activity depends on the chemical properties of A2062 or not (Vázquez-Laslop et al., 2011). Ribosomes carrying the A2062C or A2062U point mutations still arrest along the fMRL(R) motif in the presence of erythromycin (Sothiselvam et al., 2014). The fM+X(+) motif was classified as A2062-independent and the conformation of the base of A2062 in the fMKF-70S structure is similar to that observed in the TnaC-70S structure, which is also independent of the chemical properties of A2062 (Bischoff et al., 2014; Sothiselvam et al., 2014; Vázquez-Laslop et al., 2011). Although the nature of the base itself appears not to be important for the arrest process, it is possible that the mere presence of an unpaired base at this position within the tunnel is sufficient to restrict the rotation of the -1 lysine side chain in the presence of erythromycin, thus forcing it to remain within the A-site crevice.

Interestingly, the base of A2062 adopts different orientations within the crystal structures of erythromycin in complex with the 70S ribosomes from *E. coli* or *T. thermophilus*, respectively (Bulkley et al., 2010; Dunkle et al., 2010). An explanation for this discrepancy could be that the binding of erythromycin favors the orientation where the base points towards the PTC but does not entirely preclude the alternative conformation. While translating the fMKF(R) sequence in the presence of erythromycin, the base of A2062 points might frequently point towards the PTC, thus forcing the -1 side chain into the A-site crevice and causing arrest. In contrast to this, if the base points towards to the cytoplasm peptide bond formation can occur and the

ribosome can translocate. This would explain the appearance of a faint band in the toeprinting experiment discussed in chapter 4.4.3 and would make the formation of a stalled complex a stochastic event that is linked to the particular conformation adopted by A2062. Furthermore, the masked 3D classification revealed that 13.48% of the particles, which corresponds to approx. 12 500 particles, contained A-, P- and E-site tRNA (Figure 31) potentially representing those particles that did not arrest and in which the peptide might be connected to the A-site tRNA. Since approximately 30 000 particles are necessary for a high-resolution reconstruction of the ribosome (Bai et al., 2013) including micrographs containing lower resolution data and recollection of new data might result in enough particles to resolve the structure of the potentially non-arrested ribosomes.

Another possibility to assess the role of the bases discussed above is molecular dynamics studies. In a recently published study of the ErmBL arrest peptide, molecular dynamics simulations gave greater insights into the underlying mechanism and mobility of the peptide itself (Arenz et al., 2016). Additionally, biochemical studies to further shed light on the importance of ribosomal bases on the arrest process could include atomic mutagenesis of the ribosome, a method that makes it possible to introduce unnatural bases into or exclude bases from a circularly permutated 23S rRNA. In a recent study using atomic mutagenesis, ribosomes lacking the base of A2062 were generated to study the impact of A2062 on nascent chain-mediated translational arrest along ErmCL in the presence of erythromycin (Koch et al., 2017). Using these ribosomes would give greater insights into the requirements for the base of A2062 since these ribosomes should not arrest when translating M+X(+) motifs, in this case, fMKF(R), in the presence of erythromycin.

In summary, the flexizyme methodology will make it possible to perform further detailed studies to elucidate the arrest mechanism of MRLR. The advantage of the method is the flexibility to investigate the mechanism when using non-natural sequences such as the removal of the N-terminal methionine and the variation of the -1 side chain. Furthermore, the cryo-EM structure solved revealed how the binding of the macrolide to the ribosomal exit tunnel changes the conformation of several bases of the 23S rRNA within the PTC. Additionally, this structure is the first arrest complex that does not bypass the ligand. Further experiments will be necessary to confirm the hypothesized mechanism and to utilize the knowledge obtained for future drug development.

5.4 Polyproline-mediated arrest

Proline is the only N-alkyl amino acid along the canonical amino acids. Kinetics studies have shown that its chemical properties result in low reactivity during peptide bond formation (Pavlov et al., 2009). The translation of consecutive prolines leads to ribosomal arrest that can be released by elongation factor EF-P (Doerfel et al., 2013; Ude et al., 2013).

To investigate polyproline-mediated ribosomal arrest structurally the flexizyme methodology was used to initiate translation with different constructs. Translation reactions initiated with AcRP-$tRNA_i^{Met}$ and AcRA-$tRNA_i^{Met}$ form an arrested complex after one round of translocation that can be released partially in the presence of EF-P (chapter 4,5,9, Figure 56). So far, the underlying mechanism is still unknown and further insights could be obtained by solving the structure of a polyproline arrested ribosome complex The toeprinting reaction was performed using an *in vitro* translation system (Shimizu et al., 2001; Shimizu et al., 2005). The following figure lists all these compounds:

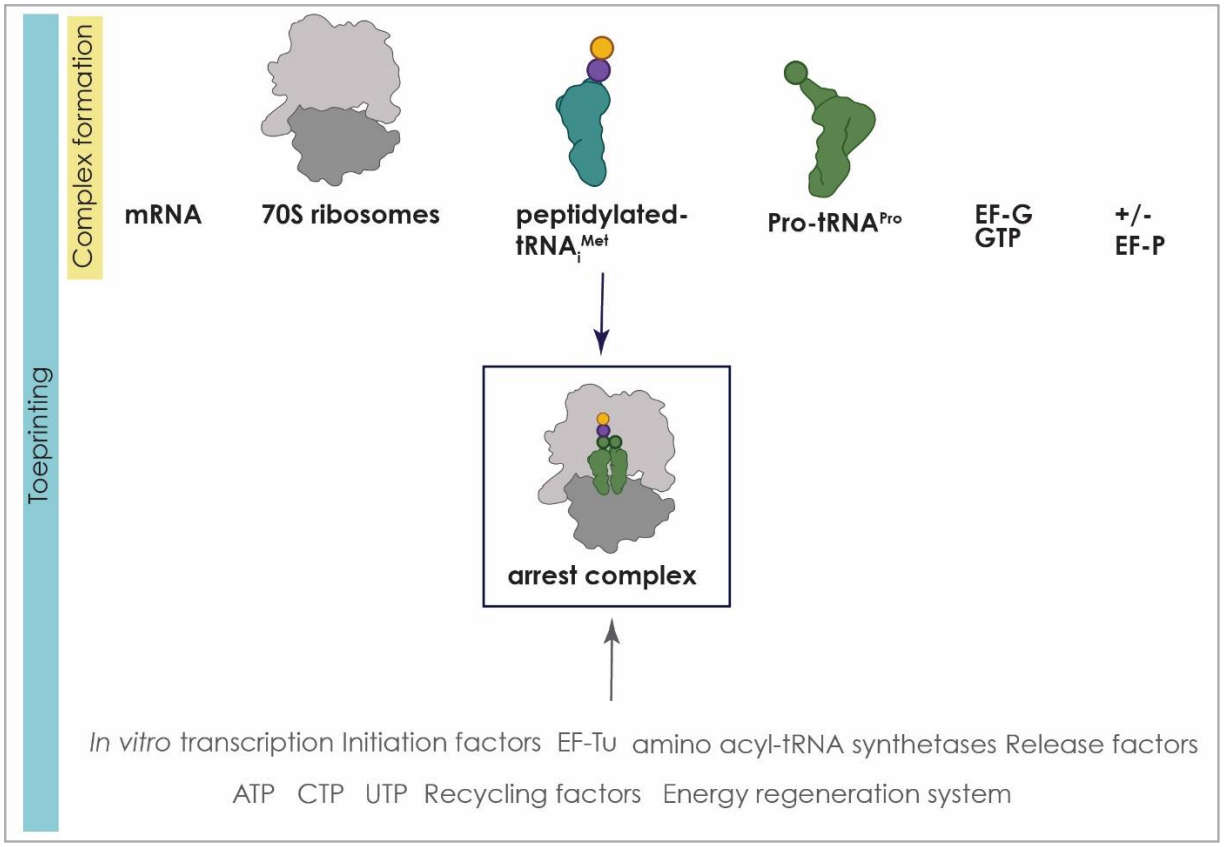

Figure 60: Composition of *in vitro* translation systems for arrested complex formation for structural biology. The toeprint to illustrate the formation of the polyproline-mediated arrest complex, as well as its release by EF-P, was performed in a custom-made PURExpress system (NEB, Ipswich, MA, USA) containing all of the factors needed to perform *in vitro* transcription and translation. To form the arrested complex for structural biology, the reaction mixture was reduced to a minimal set of factors listed in bold, allowing only one round of elongation. EF-P is not provided in the custom-made PURExpress system and was added separately.

The toeprint to illustrate the formation of the arrested complex was performed in a custom-made PURExpress system (NEB, Ipswich, MA, USA) containing all the components listed in Figure 60 but so far, the structure of the polyproline-arrested ribosome in the presence or absence of EF-P has not been solved. In order to form a complex to study polyproline-mediated arrested 70S *E. coli* ribosomes by cryo-EM, the reaction mixture has to be reduced to a minimal set of compounds (listed in bold in Figure 60), while unnecessary factors (e.g. initiation factors or T7 RNAP) can be omitted from the mixture. Optimal conditions for complex formation can be identified using toeprinting (chapter 3.8). Subsequently, these conditions can be used to form the up-scaled reaction for structural studies. The following figure illustrates possible complexes to study the PRE- and POST-release complex of EF-P bound to polyproline-arrested ribosomes:

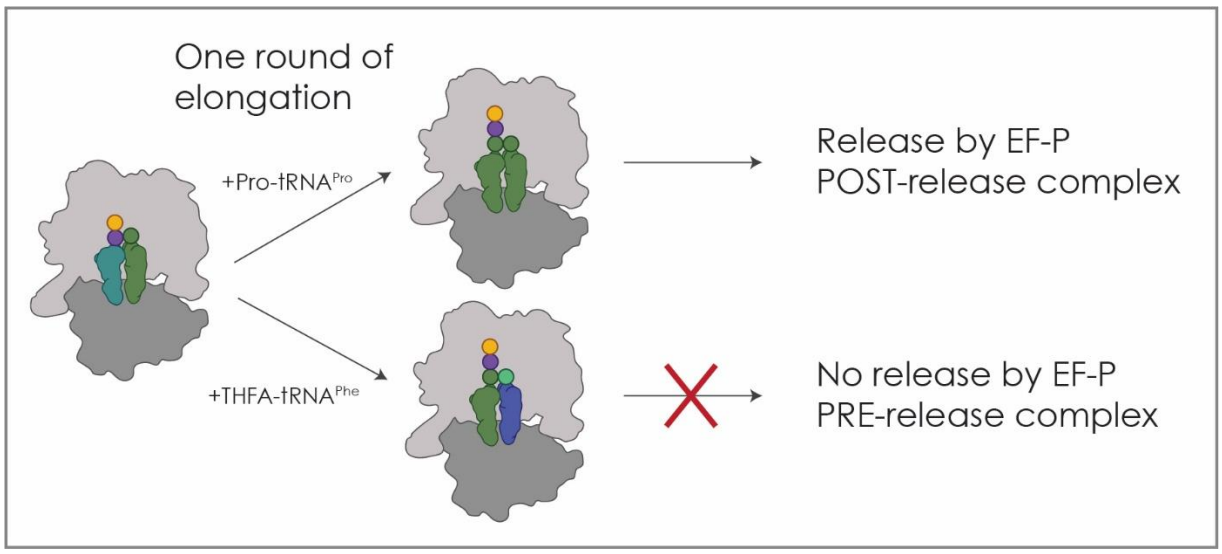

Figure 61: Complexes to study the molecular mechanism of EF-P. The POST-release complex can be studied using Pro-tRNA^{Pro}, as polyproline-mediated translational arrest will be released in the presence of EF-P. The PRE-release complex can be studied by replacing proline with its unreactive analog tetrahydrofuroic-2-acid (THFA). The complex can be formed specifically using the flexizyme methodology to transfer THFA onto e.g. tRNA^{Phe}.

This strategy will allow us to study polyproline-mediated translational arrest in the presence of all compounds that are present in the cell during polyproline-mediated translational arrest. A complex formed with a mRNA encoding MPP allows the binding of AcR(A/P)-tRNA$_i^{Met}$ followed by two Pro-tRNA^{Pro} and the formation of the polyproline-arrested complex. This complex can be released in the presence of EF-P (Doerfel et al., 2013; Peil et al., 2013; Ude et al., 2013). The complex might give insights into the POST-release state.

In order to stabilize the PRE-release state and understand how EF-P releases the arrest, the A-site tRNA can be charged with tetrahydrofuroic-2-acid (THFA), an unreactive derivative of proline (Figure 61). THFA can be activated with CBT or DBE and transferred onto the 3'CCA end of $tRNA^{Phe}$ with the help of the eFx or dFx flexizymes, respectively. Using a mRNA encoding the sequence MPF, it will be possible to direct the binding of THFA-$tRNA^{Phe}$ to the A-site, resulting in potential high homogeneity of the complex. $tRNA^{Phe}$ can be used to study the complex as EF-P seems not to form direct contacts with the A-site tRNA (Blaha et al., 2009) and the nature of the A-site tRNA does not have an impact on EF-P function (Katoh et al., 2016). This strategy will allow us to obtain insights into the state of PRE-release of polyproline-mediated arrest by EF-P.

Furthermore, the flexizyme methodology will allow us to study the effect of chemically modified proline residues. Among all canonical amino acids, proline is the only one able to form *cis* and *trans* peptide bonds within proteins. Binding of EF-P might influence a specific conformation of the pucker. The conformation of the pucker influences directly the isomeric state of the peptide bond as illustrated in the following figure:

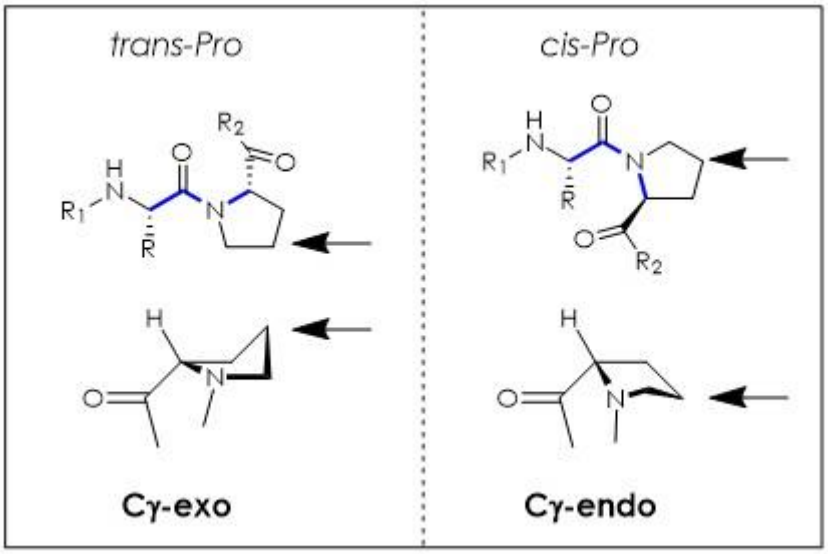

Figure 62: The position of the Cγ-atom influences the isomeric form of the peptide bond. The Cγ atom indicated by the black arrow adopts preferentially its *exo* conformation in a *trans* peptide bond and its *endo* conformation in a *cis* peptide bond (Milner-White et al., 1992; Vitagliano et al., 2001).

The systematic analysis of different protein structures, including collagen, resulted in the assumption that hydroxylation of the Cγ-atom stabilizes its *trans* or *cis* peptide bond by stabilizing the *exo* or *endo* conformation of the pucker, respectively (Figure 62, (Milner-White

et al., 1992; Vitagliano et al., 2001). Introducing modifications of the Cγ atom such as hydroxylation, halogenation or the addition of large aliphatic chains (Pandey et al., 2013) the impact of EF-P on *cis* and *trans* peptide bonds could be investigated in greater detail. This would not only give greater insights into the function of EF-P but might also make it possible to improve the production of peptides composed of cyclic N-alkyl amino acids (CNAs) using the bacterial ribosome. In a recently published study, the flexizyme methodology was employed to produce CNA peptides in bacteria (Kawakami et al., 2013). CNAs are good drug candidates since they display higher membrane permeability compared to other peptides.

In bacteria, EF-P is not essential but crucial for virulence and stress adaptation (Navarre et al., 2010; Zou et al., 2011). Co-crystallization and toeprinting experiments indicate that EF-P does not release arrest across the species tested, meaning that *E. coli* EF-P does not release Polyproline-arrested *T. thermophilus* ribosomes and vice versa. Additionally, introducing the *E. coli* loop sequence into *T. thermophilus* EF-P did not result in a crystal structure and did not relieve polyproline-mediated arrest using toeprinting. Studies have shown that EF-P from various species is modified differently (Bullwinkle et al., 2013; Lassak et al., 2015; Park et al., 2012; Rajkovic et al., 2016). The next figure illustrates the variety of known modifications along prokaryotes:

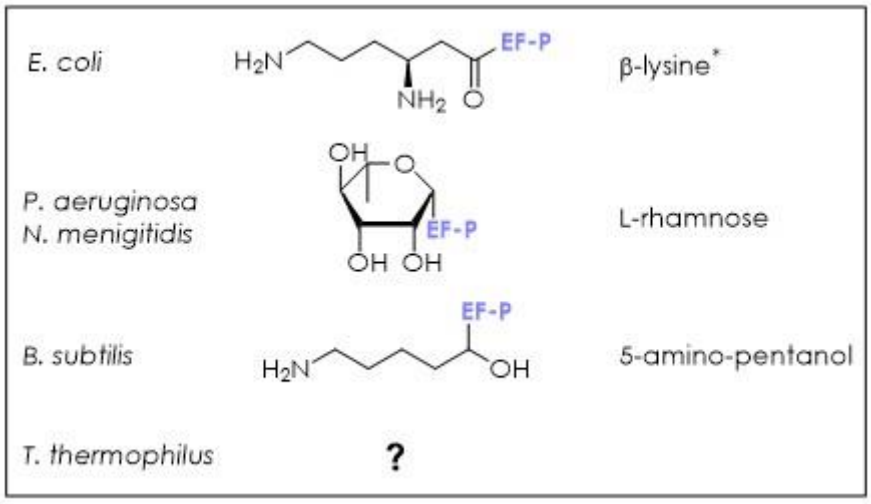

Figure 63: The variety of modifications essential for EF-P activity in different species. In *E. coli* residue K34 needs to be β-lysinylated for EF-P activity. Additionally, K34 is also hydroxylated in a second step (Park et al., 2012; Peil et al., 2012). In *P. aeruginosa* and *N. meningitides*, R32 is rhamnosylated. Recently the modification in *B. subtilis* was identified as 5-amino-pentanol. So far, a potential modification of R32 in *T. thermophilus* remains unknown.

The post-translational modification of the crucial residue of EF-P varies among different prokaryotes (Figure 63), but additional hydrogen bond donors and acceptors are used to possibly enhance interactions with the tRNA. So far, the potential modification of *T. thermophilus* EF-P remains unknown. One of the remaining questions is if a modification of *T. thermophilus* EF-P is necessary for the function of this molecule. This could be investigated by growing *T. thermophilus* under different temperatures and subsequently isolating EF-P via immunoprecipitation to analyze the protein by mass spectrometry as performed previously for EF-P from *E. coli* (Peil et al., 2012; Rajkovic et al., 2016). *T. thermophilus* grows at an optimal temperature of 75°C (Oshima and Imahori, 1974). An explanation could be that 70S *T. thermophilus* ribosomes are not stalled by polyproline motifs or easier overcome the arrest at these high temperatures as the molecules move more. A second explanation includes the unusual high concentrations of polyamines in the cytoplasm, which have been shown to be essential for cell survival. In addition, thermophiles produce species-specific polyamines such as thermine and tetrakis(3-amino-propyl)-ammonium (Oshima, 2007). Furthermore, the addition of polyamines to *in vitro* translation reactions is crucial for the initiation of translation and also enhances the elongation (Uzawa et al., 1993a; Uzawa et al., 1993b). The combination of different polyamines showed a synergistic enhancement of protein production at higher temperatures. Thus *T. thermophilus* EF-P could act as a scaffold to orient polyamines correctly and in doing so release the arrest along consecutive poly-proline motifs. This hypothesis could be toeprinting and co-crystallization experiments using *T. thermophilus* ribosomes in the presence of different polyamines and *T. thermophilus* EF-P.

Species-specific modifications of EF-P, that can range from rhamnosylation to β-lysinylation, demands a large number of different modification enzymes as the chemical properties of the substrate molecules are diverse (Lassak et al., 2015; Park et al., 2012). Understanding the underlying molecular mechanism of different EF-P modifications might result in a better understanding of the species specificities of bacterial ribosomes and this might give rise to species-specific narrow-spectrum antibiotics.

6. Conclusion

My structural studies of the inhibition of bacterial translation by nascent-chain and free peptides resulted in a greater understanding of how these peptides interact with and affect the ribosomal tunnel. Antimicrobial peptides that target the ribosomal exit tunnel are produced as a natural defense mechanism of eukaryotes. The structures obtained can be used for further drug development involving a large number of potential modifications to enhance their uptake by bacteria and their binding affinity for the ribosome. Further steps will also have to include the identification of new sequences and their characterization.

In addition, short arrest peptides can be bound directly to the 3′ CCA end of tRNAs using the flexizyme technology, for further structural or biochemical characterization. This allows to study the impact of non-canonical amino acids and non-natural backbones on peptide bond formation and on nascent chain mediated translational arrest. An increased understanding of the determinants of nascent chain-mediated translational arrest will ultimately result in a better understanding of the bacterial ribosome. This will allow the development of new scaffolds for novel antibiotics. Further experiments using the flexizyme methodology and the knowledge obtained during this work will provide information about the reactivity and incorporation of non-natural amino acids for example D-amino acids using the bacterial ribosome as a production machinery.

7. Résumé français

7.1 Général

Les ribosomes bactériens sont de grands complexes ribonucléoprotéiques constitués d'une petite sous-unité 30S et d'une grande sous-unité 50S, qui catalysent la réaction de traduction de l'information codée par l'ARN messager (ARNm) en protéines (Monro, 1967; Ogle et al., 2003; Schmeing and Ramakrishnan, 2009). La formation de la liaison peptidique elle-même est indépendante de l'énergie et est catalysée par l'ARN ribosomal (ARNr) dans le «peptidyl transferase center » (PTC) alors que des étapes comme l'initiation, la livraison d'ARNs, la translocation et la dissociation des sous-unités requièrent un apport d'énergie et certains facteurs protéiques (Schmeing and Ramakrishnan, 2009). Au sein du PTC, la chaîne peptidique naissante traverse le tunnel de sortie du ribosome par la sous-unité 50S (Nissen et al., 2000). Le ribosome constitue l'une des principales cibles des antibiotiques de par son rôle central dans les processus cellulaires (Wilson, 2009). En raison de la prévalence croissante des bactéries multirésistantes, le développement de nouveaux antibiotiques est rapidement devenu une priorité de santé publique (Wilson, 2014). Certains peptides peuvent inhiber la traduction bactérienne, soit en tant que peptides libres produits lors des mécanismes de défense contre d'autres organismes tels que les peptides antimicrobiens riches en proline (PrAMPs), soit lors de leur propre traduction (peptides d'arrêt traductionnel médié par la chaîne naissante).

7.2 Peptides antimicrobiens riches en proline (PrAMPs)

La première partie de cette thèse a consisté à la compréhension du mécanisme sous-jacent de l'inhibition de la traduction bactérienne par des peptides antimicrobiens riches en proline. Ces peptides sont produits par le système immunitaire inné des insectes et des mammifères (Otvos, 2002). Les PrAMP sont des agents puissants contre les bactéries à coloration Gram négative et ont fait l'objet d'études visant à améliorer leurs propriétés en tant que potentiels agents antibactériens. Les séquences peptidiques montrent une teneur élevée en prolines et au moins un motif Pro-Arg-Pro qui conduit à une conformation désordonnée du peptide en solution (Otvos et al., 2000). Le chaperon DnaK a été identifié comme une cible présumée (Otvos et al., 2000). Cependant, de récentes études ont montré que les cellules dépourvues de *dnaK* ne sont pas résistantes à certaines PrAMP provenant d'insectes comme les oncocines dérivées de la punaise tuberculée (*Oncopeltus faciatus*) ou de l'apidaecine des abeilles (*Apis vespidae*)

(Krizsan et al., 2014). Ces peptides peuvent en effet être attachés aux ribosomes bactériens et inhiber la synthèse des protéines *in vitro*. D'autres études ont montré que la bacténécine-7 PrAMP provenant de mammifères (Bac7, *Bos taurus*) se lie également aux ribosomes bactériens et inhibe la traduction *in vitro* (Mardirossian et al., 2014).

Le mécanisme d'action moléculaire sous-jacent des PrAMPs était encore inconnu lorsque j'ai résolu les structures cristallines du ribosome *Thermus thermophilus* 70S en complexe avec les PrAMPs Onc112, Bac7$^{1-16}$, Pyrrhocoricin (Pyr) et Metalnikowin I (Met I). La résolution se situe entre 2,8 Å et 3,2 Å. En comparaison à la chaîne peptidique naissante en croissance, le PrAMP se lie dans une orientation inverse au sein du tunnel de sortie du ribosome. Un réseau de potentielles liaisons hydrogènes ajouté à l'interaction d'empilement du peptide avec des résidus ribosomaux stabilisent les peptides dans le tunnel de sortie, leur conférant une structure adéquate (Gagnon et al., 2016; Roy et al., 2015; Seefeldt et al., 2016; Seefeldt et al., 2015).

A partir du site de liaison qui chevauche l'aminoacyl-ARNt entrant, nous pouvons supposer que les PrAMP inhibent la transition entre l'initiation et l'allongement. Afin de répondre à cette hypothèse, des études biochimiques ont été réalisées par nos collaborateurs issus du groupe du Prof. Daniel N Wilson (Gene Center, (Munich maintenant Université de Hambourg)) via des expériences de toeprinting, des tests disome et des tests de synthèse protéique acellulaire et ainsi confirmer le mécanisme proposé. Nos études ont montré que les PrAMP inhibent spécifiquement la transition de l'initiation à l'élongation et déstabilisent le complexe post-initiation (Seefeldt et al., 2016; Seefeldt et al., 2015).

Le travail a été publié en parallèle des travaux du groupe du professeur Thomas A. Steitz, ce qui a permis de confirmer nos résultats (Gagnon et al., 2016; Roy et al., 2015).

7.3 L'arrêt de la traduction induit par le peptide naissant

Le sujet de la deuxième partie de cette thèse était d'acquérir la compréhension du mécanisme moléculaire des courts peptides d'arrêt. L'arrêt de la traduction médiée par la chaîne naissante se produit lorsque cette dernière est capable d'interagir avec la paroi du tunnel du ribosome et entraîne un réarrangement au sein du centre de la peptidyl-transférase (Ito and Chiba, 2013; Seip and Innis, 2016; Wilson et al., 2016). Les raisons de l'arrêt peuvent être simplement la composition en acides aminés du peptide naissant, ajouté à la présence d'un ligand ou l'incorporation d'acides aminés non naturels (Ito and Chiba, 2013; Seip and Innis, 2016; Wilson

et al., 2016). Les longs peptides d'arrêt comme les peptides TnaC (Bischoff et al., 2014; Seidelt et al., 2009) et Erm (Arenz et al., 2016; Arenz et al., 2014a; Arenz et al., 2014b)ont été étudiés par cryo-EM, tandis que les mécanismes d'arrêt des peptides courts incluant les motifs polyproline ainsi que le motif fM+X(+) arrêtent le ribosome en présence d'érythromycine.

Pour mieux comprendre le mécanisme moléculaire sous-jacent des peptides d'arrêt courts, des structures à haute résolution sont nécessaires, mais il est difficile d'obtenir un échantillon homogène suite à la traduction *in vitro*. Ceux-ci peuvent être obtenus par cristallographie aux rayons X en utilisant des ribosomes 70S provenant dans notre cas de *T. thermophilus* ou par microscopie cryogénique en utilisant des ribosomes 70S d'*Escherichia coli*.

Pour obtenir des cristaux hautement diffractants, le complexe ne doit contenir que de courts fragments d'ARNm. Ainsi, des complexes ne peuvent pas être formés en utilisant une réaction de traduction *in vitro* car l'ARNm codant chevauche un contact cristallin et limite ainsi la diffraction (Axel Innis, communication personnelle). Une solution pour assurer la formation d'une liaison stoechiométrique de l'ARNt peptidyle au ribosome et d'augmenter l'homogénéité du complexe pourrait être de charger un peptide chimiquement synthétisé directement sur l'ARNt. Pour obtenir l'ARNt peptidylé, l'approche flexyzyme a été employée, reposant sur le pouvoir catalytique d'un petit ribozyme afin de former une liaison ester entre le peptide chimiquement activé et l'extrémité CCA de l'ARNt (Goto et al., 2011). Dans l'étape suivante, l'ARNt peptidylé a été purifié par chromatographie HPLC. Et les peptides ont été synthétisés par le Dr. Caterina Lombardo et le Dr. Christophe André. Par cette méthode, les fragments des peptides d'arrêt ont été spécifiquement chargés sur l'$ARNt_i^{Met}$ initiateur. Les ARNt peptidylés ont été caractérisés en utilisant des méthodes biologiques biochimiques et structurales.

La méthode que nous présentons peut-être appliquée à un grand nombre de peptides d'arrêt courts, y compris des peptides contenant des acides aminés non naturels dans le but d'acquérir une meilleure compréhension de la spécificité du ribosome.

7.3.1 M+X(+) arrête le ribosome bactérien en présence d'érythromycine

L'arrêt du ribosome peut être utilisé pour réguler l'expression des gènes dans les cellules. Pour ce faire, le peptide d'arrêt agit comme un capteur pour détecter la présence d'un médicament comme l'érythromycine ou d'un métabolite, comme par exemple le tryptophane. Le gène de résistance à l'érythromycine (*ermD*) code pour une méthyltransférase qui méthyle la base A2058 de l'ARNr 23S dans le tunnel ribosomal, empêchant ainsi la liaison du médicament. Les

ribosomes modifiés de cette manière sont moins efficaces que les ribosomes non modifiés, par conséquent, l'expression du gène de résistance doit être étroitement régulée. En amont du gène *ermD*, un peptide leader ErmDL court est codé pour réguler l'expression de la méthyltransférase (Hue and Bechhofer, 1992).

Différents peptides leaders impliqués dans la régulation des gènes de résistance à l'érythromycine ont été identifiés et caractérisés. Le raccourcissement systématique de la séquence peptidique ErmDL a conduit à l'identification de la séquence de décrochage minimale MRL(R) (Sothiselvam et al., 2014). La mutagenèse systématique des séquences (Sothiselvam et al., 2016) couplée aux données de ribosome profiling obtenues en traitant *E. coli* et *Staphyluscoccus aureus* avec l'érythromycine, la télithromycine et l'azithromycine ont montré que ce motif peut être généralisé à +X(+) (Davis et al., 2014; Kannan et al., 2014). Le peptide d'arrêt est si court qu'il atteint à peine le site de liaison du médicament.

Au cours de cette thèse, la séquence MKF(R) a été choisie pour d'autres études. Ce faisant, le Dr. K. Kishore Inampudi (ancien PostDoc dans le laboratoire) a spécifiquement chargé le peptide MKF (méthionine-lysine-phénylalanine) sur l'ARNt méthylé en utilisant la méthodologie du flexizyme (Goto et al., 2011). J'ai évalué l'activité de cet ARNt peptidylé par des expériences de toeprinting en présence et en absence d'érythromycine confirmant l'arrêt du complexe formé par la chaîne naissante.

Aucune structure n'a pu être obtenue en utilisant la cristallographie aux rayons X car le peptide a été hydrolysé pendant le processus de cristallisation. J'ai donc déterminé la structure du MKF arrêté sur le ribosome d'*E. coli* 70S en formant le complexe en présence de ribosomes 70S purifiés, de MKF-tRNAiMet, d'Arg -tRNAArg, et d'érythromycine par cryo-EM. Basé sur la structure obtenue, le réarrangement allostérique des résidus ARNr 23S ainsi que l'absence de l'ARNt du site A, le mécanisme suivant a pu être proposé: En l'absence d'érythromycine, la base A2062 tourne plus facilement vers le cytoplasme, permettant donc à la Lys -1 de quitter la crevasse du site A. Par conséquent, l'amino-acyl-ARNt suivant et portant une charge positive peut se lier, permettant la formation de la liaison peptidique. En revanche, la présence d'érythromycine pourrait favoriser une conformation de A2062 dans laquelle la base pointe vers le PTC. Le ribosome s'arrête lorsque la base d'A2062 de l'ARNr 23S pointe vers le PTC inhibant la réorientation du peptide d'arrêt et forçant le Lys -1 à pointer dans la crevasse du site A. Par conséquent, l'ARNt de site A suivant portant une chaîne latérale K, R ou W ne peut

pas se lier au PTC en raison de l'encombrement stérique et statique. Le ribosome est arrêté en raison de la prévention de l'accommodation de l'ARNt du site A.

7.3.2 L'arrêt médié par la polyproline est soulagé par le facteur d'élongation P

Plusieurs études ont montré que la vitesse de formation de la liaison peptidique est réduite lorsque le ribosome incorpore la proline par rapport à la vitesse d'incorporation des autres acides aminés (Muto and Ito, 2008; Pavlov et al., 2009). La proline est, d'un point de vue chimique, un N-alkylaminoacide (iminoacide), ce qui entraîne une alcalinité plus élevée par rapport aux autres acides aminés canoniques et une probabilité plus élevée d'obtenir un groupe α-imino protoné à un pH physiologique (Pavlov et al., 2009). De plus, la proline est le seul acide aminé canonique qui peut former à la fois des liaisons peptidiques trans et cis, conduisant à des replis possibles au sein des hélices α.

De récentes études *in vitro* et *in vivo* ont montré que trois prolines consécutives conduisent à un arrêt du ribosome (Doerfel et al., 2013; Ude et al., 2013). De nombreux gènes importants pour le fitness de la bactérie contiennent des séquences de polyproline, comme par exemple le gène codant la valinyl-tRNA synthetase (*valS*) (Starosta et al., 2014b). Les ribosomes bactériens arrêtés peuvent être libérés lors de la traduction par le facteur d'élongation P (EF-P) (Doerfel et al., 2013; Ude et al., 2013). La même observation a été faite pour le facteur d'initiation des homologues eucaryotes 5A (eIF5A) (Gutierrez et al., 2013). Une autre étude protéomique utilisant le marquage isotopique stable d'acides aminés en culture cellulaire (SILAC) sur des cellules *Δefp* a montré que le nombre de gènes EF-P dépendants n'est pas seulement limité à une séquence PPP (Peil et al., 2013; Starosta et al., 2014a). Une analyse plus approfondie utilisant des systèmes de rapporteurs *in vivo* et des essais de traduction *in vitro* ont permis d'identifier la diversité de séquences arrêtant en l'absence de EF-P. Pour obtenir une fonction complète, EF P doit être modifié après traduction (Bullwinkle et al., 2013; Navarre et al., 2010). La modification peut varier en fonction de l'espèce bactérienne du sucre jusqu'à la lysine (Bullwinkle et al., 2013; Lassak et al., 2015). Les cellules bactériennes dépourvues d'*efp* ou de ses enzymes de modification présentent le même phénotype et sont moins en forme et moins virulentes (Navarre et al., 2010). Cela fait de l'EF-P une cible intéressante pour les antibiotiques. Cependant, jusqu'à présent, le mécanisme sous-jacent de l'arrêt de la traduction médié par le motif polyproline ainsi que son soulagement par EF P reste inconnu.

Pour obtenir de plus amples informations sur le mécanisme sous-jacent, EF-P a été purifié comme publié précédemment et son activité a été évaluée par des expériences de toeprinting. En utilisant la cristallographie aux rayons X, il aurait pu être montré que l'EF-P de *E. coli* ne se lie pas aux ribosomes de *T. thermophilus* 70S dans des conditions cristallographiques. Il a été montré précédemment que *E. coli* EF-P reconnaît la boucle D de $tRNA^{Pro}$ (Katoh et al., 2016). Pour obtenir une compréhension approfondie du mécanisme sous-jacent, une partie de ce projet consistait à purifier l'ARNt pro à partir d'extraits cellulaires. La pureté a été déterminée à environ 80% par spectrométrie de masse et son activité a été prouvée par toeprinting. Pour étudier l'arrêt médié par le motif polyproline, AcRA-$ARNt_i^{Met}$, AcRP-$ARNt_i^{Met}$ et AcRAP-$ARNt_i^{Met}$ ont été obtenus en utilisant la méthodologie du flexizyme. J'ai évalué l'activité des peptidyl-ARNt par toeprinting en présence et en absence d'EF-P d'*E. coli* montrant la formation et la libération du complexe d'arrêt. Les expériences futures permettront de trouver des conditions optimales de formation des complexes dans le but de résoudre la structure par cryo-EM.

7.4 Conclusion

Les connaissances obtenues ont permis de mieux comprendre comment la formation de liaisons peptidiques peut être inhibée de manière spécifique et pourrait conduire au développement de nouveaux antibiotiques hautement spécifiques ciblant le ribosome bactérien.

8. References

Adams, P.D., Afonine, P.V., Bunkóczi, G., Chen, V.B., Davis, I.W., Echols, N., Headd, J.J., Hung, L.-W., Kapral, G.J., and Grosse-Kunstleve, R.W. (2010). PHENIX: a comprehensive Python-based system for macromolecular structure solution. Acta Crystallographica Section D: Biological Crystallography *66*, 213-221.

Afonine, P.V., Headd, J.J., Terwilliger, T.C., and Adams, P.D. (2013). Computational Crystallography Newsletter *4*, 23.

Agrawal, R.K., Heagle, A.B., Penczek, P., Grassucci, R.A., and Frank, J. (1999). EF-G-dependent GTP hydrolysis induces translocation accompanied by large conformational changes in the 70S ribosome. Nature Structural & Molecular Biology *6*, 643-647.

Agrawal, R.K., Penczek, P., Grassucci, R.A., and Frank, J. (1998). Visualization of elongation factor G on the Escherichia coli 70S ribosome: the mechanism of translocation. Proceedings of the National Academy of Sciences *95*, 6134-6138.

Agrawal, R.K., Penczek, P., Grassucci, R.A., Li, Y., Leith, A., Nierhaus, K.H., and Frank, J. (1996). Direct Visualization of A-, P-, and E-Site Transfer RNAs in the *Escherichia coli* Ribosome. Science *271*, 1000-1002.

Aguilar, M.-I. (2004). Reversed-Phase High-Performance Liquid Chromatography. In HPLC of Peptides and Proteins: Methods and Protocols, M.-I. Aguilar, ed. (Totowa, NJ: Springer New York), pp. 9-22.

Alejo, J.L., and Blanchard, S.C. (2017). Miscoding-induced stalling of substrate translocation on the bacterial ribosome. Proceedings of the National Academy of Sciences *114*, E8603-E8610.

Alexieva, Z., Duvall, E.J., Ambulos, N.P., Kim, U.J., and Lovett, P.S. (1988). Chloramphenicol induction of cat-86 requires ribosome stalling at a specific site in the leader. Proceedings of the National Academy of Sciences *85*, 3057-3061.

Altschul, S.F., Gish, W., Miller, W., Myers, E.W., and Lipman, D.J. (1990). Basic local alignment search tool. Journal of molecular biology *215*, 403-410.

Alwine, J.C., Kemp, D.J., and Stark, G.R. (1977). Method for detection of specific RNAs in agarose gels by transfer to diazobenzyloxymethyl-paper and hybridization with DNA probes. Proceedings of the National Academy of Sciences of the United States of America *74*, 5350-5354.

An, G., Glick, B.R., Friesen, J.D., and Ganoza, M.C. (1980). Identification and quantitation of elongation factor EF-P in *Escherichia coli* cell-free extracts. Canadian journal of biochemistry *58*, 1312-1314.

Antoun, A., Pavlov, M.Y., Andersson, K., Tenson, T., and Ehrenberg, M. (2003). The roles of initiation factor 2 and guanosine triphosphate in initiation of protein synthesis. The EMBO Journal *22*, 5593-5601.

Antoun, A., Pavlov, M.Y., Lovmar, M., and Ehrenberg, M. (2006a). How Initiation Factors Maximize the Accuracy of tRNA Selection in Initiation of Bacterial Protein Synthesis. Molecular Cell *23*, 183-193.

Antoun, A., Pavlov, M.Y., Lovmar, M., and Ehrenberg, M. (2006b). How initiation factors tune the rate of initiation of protein synthesis in bacteria. The EMBO Journal *25*, 2539-2550.

Arenz, S., Bock, L.V., Graf, M., Innis, C.A., Beckmann, R., Grubmüller, H., Vaiana, A.C., and Wilson, D.N. (2016). A combined cryo-EM and molecular dynamics approach reveals the mechanism of ErmBL-mediated translation arrest. *7*, 12026.

Arenz, S., Meydan, S., Starosta, A.L., Berninghausen, O., Beckmann, R., Vázquez-Laslop, N., and Wilson, D.N. (2014a). Drug sensing by the ribosome induces translational arrest via active site perturbation. Molecular cell *56*, 446-452.

Arenz, S., Ramu, H., Gupta, P., Berninghausen, O., Beckmann, R., Vázquez-Laslop, N., Mankin, A.S., and Wilson, D.N. (2014b). Molecular basis for erythromycin-dependent ribosome stalling during translation of the ErmBL leader peptide. Nature communications *5*.

Arenz, S., and Wilson, D.N. (2016). Bacterial Protein Synthesis as a Target for Antibiotic Inhibition. Cold Spring Harbor perspectives in medicine *6*, a025361.

Bai, X.-C., Fernandez, I.S., McMullan, G., and Scheres, S.H. (2013). Ribosome structures to near-atomic resolution from thirty thousand cryo-EM particles. Elife *2*, e00461.

Bailly, M., and de Crécy-Lagard, V. (2010). Predicting the pathway involved in post-translational modification of elongation factor P in a subset of bacterial species. Biology direct *5*, 3.

Ban, N., Beckmann, R., Cate, J.H., Dinman, J.D., Dragon, F., Ellis, S.R., Lafontaine, D.L., Lindahl, L., Liljas, A., and Lipton, J.M. (2014). A new system for naming ribosomal proteins. Current opinion in structural biology *24*, 165-169.

Ban, N., Nissen, P., Hansen, J., Moore, P.B., and Steitz, T.A. (2000). The complete atomic structure of the large ribosomal subunit at 2.4 Å resolution. Science *289*, 905-920.

Barat, C., Datta, P.P., Raj, V.S., Sharma, M.R., Kaji, H., Kaji, A., and Agrawal, R.K. (2007). Progression of the ribosome recycling factor through the ribosome dissociates the two ribosomal subunits. Molecular cell *27*, 250-261.

Beringer, M., Adio, S., Wintermeyer, W., and Rodnina, M. (2003). The G2447A mutation does not affect ionization of a ribosomal group taking part in peptide bond formation. RNA *9*, 919-922.

Beringer, M., Bruell, C., Xiong, L., Pfister, P., Bieling, P., Katunin, V.I., Mankin, A.S., Böttger, E.C., and Rodnina, M.V. (2005). Essential Mechanisms in the Catalysis of Peptide Bond Formation on the Ribosome. Journal of Biological Chemistry *280*, 36065-36072.

Berisio, R., Harms, J., Schluenzen, F., Zarivach, R., Hansen, H.A., Fucini, P., and Yonath, A. (2003). Structural insight into the antibiotic action of telithromycin against resistant mutants. Journal of bacteriology *185*, 4276-4279.

Bertani, G. (1951). Studies on Lysogenesis I.: The Mode of Phage Liberation by Lysogenic *Escherichia coli*. Journal of bacteriology *62*, 293.

Bhushan, S., Gartmann, M., Halic, M., Armache, J.-P., Jarasch, A., Mielke, T., Berninghausen, O., Wilson, D.N., and Beckmann, R. (2010). α-Helical nascent polypeptide chains visualized within distinct regions of the ribosomal exit tunnel. Nature structural & molecular biology *17*, 313.

Bhushan, S., Hoffmann, T., Seidelt, B., Frauenfeld, J., Mielke, T., Berninghausen, O., Wilson, D.N., and Beckmann, R. (2011). SecM-stalled ribosomes adopt an altered geometry at the peptidyl transferase center. PLoS biology *9*, e1000581.

Bieling, P., Beringer, M., Adio, S., and Rodnina, M.V. (2006). Peptide bond formation does not involve acid-base catalysis by ribosomal residues. Nature structural & molecular biology *13*, 423-428.

Bischoff, L., Berninghausen, O., and Beckmann, R. (2014). Molecular basis for the ribosome functioning as an L-tryptophan sensor. Cell reports *9*, 469-475.

Blaha, G., Stanley, R.E., and Steitz, T.A. (2009). Formation of the first peptide bond: the structure of EF-P bound to the 70S ribosome. Science *325*, 966-970.

Blaha, G., Stelzl, U., Spahn, C.M., Agrawal, R.K., Frank, J., and Nierhaus, K.H. (2000). Preparation of functional ribosomal complexes and effect of buffer conditions on tRNA positions observed by cryo-electron microscopy. Methods in enzymology *317*, 292-309.

Blattner, F.R., Plunkett, G., Bloch, C.A., Perna, N.T., Burland, V., Riley, M., Collado-Vides, J., Glasner, J.D., Rode, C.K., Mayhew, G.F.*, et al.* (1997). The Complete Genome Sequence of Escherichia coli K-12. Science *277*, 1453-1462.

Böttger, E.C., Springer, B., Prammananan, T., Kidan, Y., and Sander, P. (2001). Structural basis for selectivity and toxicity of ribosomal antibiotics. EMBO reports *2*, 318-323.

Braun, V., and Hantke, K. (2011). Recent insights into iron import by bacteria. Current opinion in chemical biology *15*, 328-334.

Brenner, S., Barnett, L., Katz, E., and Crick, F. (1967). UGA: a third nonsense triplet in the genetic code. Nature *213*, 449-450.

Brenner, S., Stretton, A., and Kaplan, S. (1965). Genetic code: the 'nonsense'triplets for chain termination and their suppression. Nature *206*, 994-998.

Brockmann, H., and Henkel, W. (1950). Pikromycin, ein neues Antibiotikum aus Actinomyceten. Naturwissenschaften *37*, 138-139.

Brückner, R., and Matzura, H. (1985). Regulation of the inducible chloramphenicol acetyltransferase gene of the *Staphylococcus aureus* plasmid pUB112. The EMBO journal *4*, 2295.

Bujnicki, J., Machnicka, M., Milanowska, K., Oglou, O., Purta, E., Piatkowski, P., Kurkowska, M., Olchowik, A., Rother, K., and Helm, M. (2013). Modomics: a database of RNA modification pathways. The Febs Journal *280*, 41.

Bulkley, D., Innis, C.A., Blaha, G., and Steitz, T.A. (2010). Revisiting the structures of several antibiotics bound to the bacterial ribosome. Proceedings of the National Academy of Sciences *107*, 17158-17163.

Bullwinkle, T.J., Zou, S.B., Rajkovic, A., Hersch, S.J., Elgamal, S., Robinson, N., Smil, D., Bolshan, Y., Navarre, W.W., and Ibba, M. (2013). (R)-β-lysine-modified elongation factor P functions in translation elongation. Journal of Biological Chemistry *288*, 4416-4423.

Butkus, M.E., Prundeanu, L.B., and Oliver, D.B. (2003). Translocon "pulling" of nascent SecM controls the duration of its translational pause and secretion-responsive secA regulation. Journal of bacteriology *185*, 6719-6722.

Calhoun, K.A., and Swartz, J.R. (2006). Total amino acid stabilization during cell-free protein synthesis reactions. Journal of Biotechnology *123*, 193-203.

Cantara, W.A., Crain, P.F., Rozenski, J., McCloskey, J.A., Harris, K.A., Zhang, X., Vendeix, F.A., Fabris, D., and Agris, P.F. (2011). The RNA modification database, RNAMDB: 2011 update. Nucleic acids research *39*, D195-D201.

Carter, A.P., Clemons, W.M., Brodersen, D.E., Morgan-Warren, R.J., Hartsch, T., Wimberly, B.T., and Ramakrishnan, V. (2001). Crystal structure of an initiation factor bound to the 30S ribosomal subunit. Science *291*, 498-501.

Casteels, P., Ampe, C., Rivière, L., DAMME, J., Elicone, C., Fleming, M., JACOBS, F., and Tempst, P. (1990). Isolation and characterization of abaecin, a major antibacterial response peptide in the honeybee (*Apis mellifera*). The FEBS Journal *187*, 381-386.

Cayama, E., Yépez, A., Rotondo, F., Bandeira, E., Ferreras, A.C., and Triana-Alonso, F.J. (2000). New chromatographic and biochemical strategies for quick preparative isolation of tRNA. Nucleic Acids Research *28*, e64-e64.

Celma, M., Monro, R., and Vazquez, D. (1971). Substrate and antibiotic binding sites at the peptidyl transferase centre of *E. coli* ribosomes: Binding of UACCA-Leu to 50 S subunits. FEBS letters *13*, 247-251.

Chao, F.-C. (1957). Dissociation of macromolecular ribonucleoprotein of yeast. Archives of biochemistry and biophysics *70*, 426-431.

Chen, C., Cui, X., Beausang, J.F., Zhang, H., Farrell, I., Cooperman, B.S., and Goldman, Y.E. (2016). Elongation factor G initiates translocation through a power stroke. Proceedings of the National Academy of Sciences of the United States of America *113*, 7515-7520.

Chen, V.B., Arendall, W.B., Headd, J.J., Keedy, D.A., Immormino, R.M., Kapral, G.J., Murray, L.W., Richardson, J.S., and Richardson, D.C. (2010). MolProbity: all-atom structure validation for macromolecular crystallography. Acta Crystallographica Section D: Biological Crystallography *66*, 12-21.

Chen, Y., Feng, S., Kumar, V., Ero, R., and Gao, Y.-G. (2013). Structure of EF-G–ribosome complex in a pretranslocation state. Nat Struct Mol Biol *20*, 1077-1084.

Chernysh, S., Cociancich, S., Briand, J.-P., Hetru, C., and Bulet, P. (1996). The inducible antibacterial peptides of the Hemipteran insect Palomena prasina: Identification of a unique family of proline-rich peptides and of a novel insect defensin. Journal of Insect Physiology *42*, 81-89.

Chiba, S., and Ito, K. (2012). Multisite ribosomal stalling: a unique mode of regulatory nascent chain action revealed for MifM. Molecular cell *47*, 863-872.

Chiba, S., and Ito, K. (2015). MifM Monitors Total YidC Activities of *Bacillus subtilis*, Including That of YidC2, the Target of Regulation. Journal of Bacteriology *197*, 99-107.

Chiba, S., Kanamori, T., Ueda, T., Akiyama, Y., Pogliano, K., and Ito, K. (2011). Recruitment of a species-specific translational arrest module to monitor different cellular processes. Proceedings of the National Academy of Sciences *108*, 6073-6078.

Chiba, S., Lamsa, A., and Pogliano, K. (2009). A ribosome–nascent chain sensor of membrane protein biogenesis in *Bacillus subtilis*. The EMBO Journal *28*, 3461-3475.

Cho, H.-J., Hyun, J.-K., Kim, J.-G., Jeong, H.S., Park, H.N., You, D.-J., and Jung, H.S. (2013). Measurement of ice thickness on vitreous ice embedded cryo-EM grids: investigation of

optimizing condition for visualizing macromolecules. Journal of Analytical Science and Technology *4*, 7.

Chou, F.-C., Echols, N., Terwilliger, T.C., and Das, R. (2016). RNA Structure Refinement using the ERRASER-Phenix pipeline. Methods in molecular biology (Clifton, NJ) *1320*, 269-282.

Cociancich, S., Dupont, A., Hegy, G., Lanot, R., Holder, F., Hetru, C., Hoffmann, J., and Bulet, P. (1994). Novel inducible antibacterial peptides from a hemipteran insect, the sap-sucking bug *Pyrrhocoris apterus*. Biochemical Journal *300*, 567-575.

Corbalan, N., Runti, G., Adler, C., Covaceuszach, S., Ford, R.C., Lamba, D., Beis, K., Scocchi, M., and Vincent, P.A. (2013). Functional and Structural Study of the Dimeric Inner Membrane Protein SbmA. Journal of Bacteriology *195*, 5352-5361.

Corpet, F. (1988). Multiple sequence alignment with hierarchical clustering. Nucleic acids research *16*, 10881-10890.

Crick, F. (1970). Central Dogma of Molecular Biology. Nature *227*, 561-563.

Crick, F.H. (1958). On protein synthesis. Symposia of the Society for Experimental Biology *12*, 138-163.

Crick, F.H., Barnett, L., Brenner, S., and Watts-Tobin, R.J. (1961). General nature of the genetic code for proteins. Nature *192*, 1227-1232.

Cruz-Vera, L.R., Rajagopal, S., Squires, C., and Yanofsky, C. (2005). Features of ribosome-peptidyl-tRNA interactions essential for tryptophan induction of tna operon expression. Molecular cell *19*, 333-343.

Cruz-Vera, L.R., Yang, R., and Yanofsky, C. (2009). Tryptophan inhibits Proteus vulgaris TnaC leader peptide elongation, activating tna operon expression. Journal of bacteriology *191*, 7001-7006.

Dallas, A., and Noller, H.F. (2001). Interaction of translation initiation factor 3 with the 30S ribosomal subunit. Molecular cell *8*, 855-864.

Darken, M.A. (1964). Puromycin inhibition of protein synthesis. Pharmacological Reviews *16*, 223-243.

Davis, A.R., Gohara, D.W., and Yap, M.-N.F. (2014). Sequence selectivity of macrolide-induced translational attenuation. Proceedings of the National Academy of Sciences *111*, 15379-15384.

DeLano, W. (2010). The PyMOL Molecular Graphics System. San Carlos, CA: DeLano Scientific; 2002 (Accessed 6/25/2007. Available at http://www. pymol, org).

Dever, T.E., Gutierrez, E., and Shin, B.-S. (2014). The hypusine-containing translation factor eIF5A. Critical reviews in biochemistry and molecular biology *49*, 413-425.

Diaconu, M., Kothe, U., Schlünzen, F., Fischer, N., Harms, J.M., Tonevitsky, A.G., Stark, H., Rodnina, M.V., and Wahl, M.C. (2005). Structural basis for the function of the ribosomal L7/12 stalk in factor binding and GTPase activation. Cell *121*, 991-1004.

Dock-Bregeon, A.-C., Sankaranarayanan, R., Romby, P., Caillet, J., Springer, M., Rees, B., Francklyn, C.S., Ehresmann, C., and Moras, D. (2000). Transfer RNA–Mediated Editing in Threonyl-tRNA Synthetase: The Class II Solution to the Double Discrimination Problem. Cell *103*, 877-884.

Doerfel, L.K., Wohlgemuth, I., Kothe, C., Peske, F., Urlaub, H., and Rodnina, M.V. (2013). EF-P is essential for rapid synthesis of proteins containing consecutive proline residues. Science *339*, 85-88.

Doerfel, L.K., Wohlgemuth, I., Kubyshkin, V., Starosta, A.L., Wilson, D.N., Budisa, N., and Rodnina, M.V. (2015). Entropic contribution of elongation factor P to proline positioning at the catalytic center of the ribosome. Journal of the American Chemical Society *137*, 12997-13006.

Dorman, C.J., and Foster, T.J. (1985). Posttranscriptional regulation of the inducible nonenzymatic chloramphenicol resistance determinant of IncP plasmid R26. Journal of bacteriology *161*, 147-152.

Dorner, S., Panuschka, C., Schmid, W., and Barta, A. (2003). Mononucleotide derivatives as ribosomal P-site substrates reveal an important contribution of the 2′-OH to activity. Nucleic Acids Research *31*, 6536-6542.

Dorner, S., Polacek, N., Schulmeister, U., Panuschka, C., and Barta, A. (2002). Molecular aspects of the ribosomal peptidyl transferase. Biochemical Society Transactions *30*, 1131-1137.

Dunin-Horkawicz, S., Czerwoniec, A., Gajda, M.J., Feder, M., Grosjean, H., and Bujnicki, J.M. (2006). MODOMICS: a database of RNA modification pathways. Nucleic acids research *34*, D145-D149.

Dunkle, J.A., Xiong, L., Mankin, A.S., and Cate, J.H. (2010). Structures of the *Escherichia coli* ribosome with antibiotics bound near the peptidyl transferase center explain spectra of drug action. Proceedings of the National Academy of Sciences *107*, 17152-17157.

Ebel, J., Giegé, R., Bonnet, J., Kern, D., Befort, N., Bollack, C., Fasiolo, F., Gangloff, J., and Dirheimer, G. (1973). Factors determining the specificity of the tRNA aminoacylation reaction: Non-absolute specificity of tRNA-aminoacyl-tRNA synthetase recognition and particular importance of the maximal velocity. Biochimie *55*, 547-557.

Emsley, P., and Cowtan, K. (2004). Coot: model-building tools for molecular graphics. Acta Crystallographica Section D: Biological Crystallography *60*, 2126-2132.

Epand, R.M., and Vogel, H.J. (1999). Diversity of antimicrobial peptides and their mechanisms of action. Biochimica et Biophysica Acta (BBA)-Biomembranes *1462*, 11-28.

Erlacher, M.D., Lang, K., Shankaran, N., Wotzel, B., Hüttenhofer, A., Micura, R., Mankin, A.S., and Polacek, N. (2005). Chemical engineering of the peptidyl transferase center reveals an important role of the 2′-hydroxyl group of A2451. Nucleic acids research *33*, 1618-1627.

Erlacher, M.D., Lang, K., Wotzel, B., Rieder, R., Micura, R., and Polacek, N. (2006). Efficient ribosomal peptidyl transfer critically relies on the presence of the ribose 2 ′-OH at A2451 of 23S rRNA. Journal of the American Chemical Society *128*, 4453-4459.

Fernandez-Leiro, R., and Scheres, S.H.W. (2017). A pipeline approach to single-particle processing in RELION. Acta Crystallographica Section D *73*, 496-502.

Fischer, N., Konevega, A.L., Wintermeyer, W., Rodnina, M.V., and Stark, H. (2010). Ribosome dynamics and tRNA movement by time-resolved electron cryomicroscopy. Nature *466*, 329-333.

Florin, T., Maracci, C., Graf, M., Karki, P., Klepacki, D., Berninghausen, O., Beckmann, R., Vazquez-Laslop, N., Wilson, D.N., Rodnina, M.V.*, et al.* (2017). An antimicrobial peptide that inhibits translation by trapping release factors on the ribosome. Nat Struct Mol Biol *24*, 752-757.

Frank, J., and Agrawal, R.K. (2000). A ratchet-like inter-subunit reorganization of the ribosome during translocation. Nature *406*, 318-322.

Frank, J., Zhu, J., Penczek, P., and Li, Y. (1995). A model of protein synthesis based on cryo-electron microscopy of the E. coli ribosome. Nature *376*, 441.

Fraser, T.H., and Rich, A. (1973). Synthesis and Aminoacylation of 3′-Amino-3′-deoxy Transfer RNA and Its Activity in Ribosomal Protein Synthesis. Proceedings of the National Academy of Sciences of the United States of America *70*, 2671-2675.

Fredrick, K., and Noller, H.F. (2003). Catalysis of Ribosomal Translocation by Sparsomycin. Science *300*, 1159-1162.

Freistroffer, D.V., Pavlov, M.Y., MacDougall, J., Buckingham, R.H., and Ehrenberg, M. (1997). Release factor RF3 in E. coli accelerates the dissociation of release factors RF1 and RF2 from the ribosome in a GTP-dependent manner. The EMBO journal *16*, 4126-4133.

Gabashvili, I.S., Gregory, S.T., Valle, M., Grassucci, R., Worbs, M., Wahl, M.C., Dahlberg, A.E., and Frank, J. (2001). The polypeptide tunnel system in the ribosome and its gating in erythromycin resistance mutants of L4 and L22. Molecular cell *8*, 181-188.

Gagnon, M.G., Roy, R.N., Lomakin, I.B., Florin, T., Mankin, A.S., and Steitz, T.A. (2016). Structures of proline-rich peptides bound to the ribosome reveal a common mechanism of protein synthesis inhibition. Nucleic acids research, gkw018.

Gao, Y.-G., Selmer, M., Dunham, C.M., Weixlbaumer, A., Kelley, A.C., and Ramakrishnan, V. (2009). The Structure of the Ribosome with Elongation Factor G Trapped in the Posttranslocational State. Science *326*, 694-699.

Gasteiger, E., Gattiker, A., Hoogland, C., Ivanyi, I., Appel, R.D., and Bairoch, A. (2003). ExPASy: the proteomics server for in-depth protein knowledge and analysis. Nucleic Acids Research *31*, 3784-3788.

George, D.P. (2017). The Macrolide Antibiotic Renaissance. British Journal of Pharmacology, n/a-n/a.

Giudice, E., and Gillet, R. (2013). The task force that rescues stalled ribosomes in bacteria. Trends in biochemical sciences *38*, 403-411.

Glick, B.R., Chládek, S., and Ganoza, M.C. (1979). Peptide Bond Formation Stimulated by Protein Synthesis Factor EF-P Depends on the Aminoacyl Moiety of the Acceptor. The FEBS Journal *97*, 23-28.

Glick, B.R., and Ganoza, M.C. (1975). Identification of a soluble protein that stimulates peptide bond synthesis. Proceedings of the National Academy of Sciences *72*, 4257-4260.

Goldstein, J.L., and Caskey, C.T. (1970). Peptide Chain Termination: Effect of Protein S on Ribosomal Binding of Release Factors. Proceedings of the National Academy of Sciences *67*, 537-543.

Gong, F., Ito, K., Nakamura, Y., and Yanofsky, C. (2001). The mechanism of tryptophan induction of tryptophanase operon expression: tryptophan inhibits release factor-mediated cleavage of TnaC-peptidyl-tRNAPro. Proceedings of the National Academy of Sciences *98*, 8997-9001.

Gong, F., and Yanofsky, C. (2002). Analysis of tryptophanase operon expression in vitro accumulation of TnaC-peptidyl-tRNA in a release factor 2-depleted S-30 extract prevents Rho factor action, simulating induction. Journal of Biological Chemistry *277*, 17095-17100.

Goto, Y., Katoh, T., and Suga, H. (2011). Flexizymes for genetic code reprogramming. Nature protocols *6*, 779-790.

Goto, Y., Murakami, H., and Suga, H. (2008). Initiating translation with D-amino acids. RNA *14*, 1390-1398.

Goto, Y., and Suga, H. (2009). Translation Initiator tRNA charged with exotic peptides. Journal of the American Chemical Society *131*, 2.

Gryczan, T.J., Grandi, G., Hahn, J., Grandi, R., and Dubnau, D. (1980). Conformational alteration of mRNA structure and the posttranscriptional regulation of erythromycin-induced drug resistance. Nucleic Acids Research *8*, 6081-6097.

Gu, Z., Harrod, R., Rogers, E.J., and Lovett, P.S. (1994). Anti-peptidyl transferase leader peptides of attenuation-regulated chloramphenicol-resistance genes. Proceedings of the National Academy of Sciences *91*, 5612-5616.

Gu, Z., Rogers, E., and Lovett, P. (1993). Peptidyl transferase inhibition by the nascent leader peptide of an inducible *cat* gene. Journal of bacteriology *175*, 5309-5313.

Guillerez, J., Lopez, P.J., Proux, F., Launay, H., and Dreyfus, M. (2005). A mutation in T7 RNA polymerase that facilitates promoter clearance. Proceedings of the National Academy of Sciences *102*, 5958-5963.

Gumbart, J., Schreiner, E., Wilson, D.N., Beckmann, R., and Schulten, K. (2012). Mechanisms of SecM-mediated stalling in the ribosome. Biophysical journal *103*, 331-341.

Gupta, P., Kannan, K., Mankin, A.S., and Vázquez-Laslop, N. (2013). Regulation of gene expression by macrolide-induced ribosomal frameshifting. Molecular cell *52*, 629-642.

Gupta, P., Liu, B., Klepacki, D., Gupta, V., Schulten, K., Mankin, A.S., and Vazquez-Laslop, N. (2016). Nascent peptide assists the ribosome in recognizing chemically distinct small molecules. Nat Chem Biol *12*, 153-158.

Gürel, G., Blaha, G., Moore, P.B., and Steitz, T.A. (2009). U2504 Determines the Species Specificity of the A-site Cleft Antibiotics. The Structures of Tiamulin, Homoharringtonine and Bruceantin Bound to the Ribosome. Journal of molecular biology *389*, 146-156.

Gutierrez, E., Shin, B.-S., Woolstenhulme, C.J., Kim, J.-R., Saini, P., Buskirk, A.R., and Dever, T.E. (2013). eIF5A promotes translation of polyproline motifs. Molecular cell *51*, 35-45.

Hagel, L. (2001). Gel-Filtration Chromatography. In Current Protocols in Molecular Biology (John Wiley & Sons, Inc.).

Hager, A.J., Pollard, J.D., and Szostak, J.W. (1996). Ribozymes: aiming at RNA replication and protein synthesis. Chemistry & biology, 8.

Hanahan, D. (1983). Studies on transformation of *Escherichia coli* with plasmids. Journal of molecular biology *166*, 557-580.

Hanahan, D. (1985). Techniques for transformation of *E. coli*. DNA cloning *1*, 109-135.

Hansen, A., Schäfer, I., Knappe, D., Seibel, P., and Hoffmann, R. (2012). Intracellular toxicity of proline-rich antimicrobial peptides shuttled into mammalian cells by the cell-penetrating peptide penetratin. Antimicrobial agents and chemotherapy *56*, 5194-5201.

Hartman, M.C., Josephson, K., Lin, C.-W., and Szostak, J.W. (2007). An expanded set of amino acid analogs for the ribosomal translation of unnatural peptides. PLoS One *2*, e972.

Hartman, M.C., Josephson, K., and Szostak, J.W. (2006). Enzymatic aminoacylation of tRNA with unnatural amino acids. Proceedings of the National Academy of Sciences of the United States of America *103*, 4356-4361.

Hartz, D., McPheeters, D.S., Traut, R., and Gold, L. (1988). [27] Extension inhibition analysis of translation initiation complexes. Methods in enzymology *164*, 419-425.

Henderson, R. (2013). Avoiding the pitfalls of single particle cryo-electron microscopy: Einstein from noise. Proceedings of the National Academy of Sciences *110*, 18037-18041.

Henderson, R., Sali, A., Baker, M.L., Carragher, B., Devkota, B., Downing, K.H., Egelman, E.H., Feng, Z., Frank, J., and Grigorieff, N. (2012). Outcome of the first electron microscopy validation task force meeting. Structure *20*, 205-214.

Hoagland, M.B., Stephenson, M.L., Scott, J.F., Hecht, L.I., and Zamecnik, P.C. (1958). A soluble ribonucleic acif intermediate in protein synthesis. Journal of Biological Chemistry *231*, 241-257.

Horinouchi, S., Byeon, W., and Weisblum, B. (1983). A complex attenuator regulates inducible resistance to macrolides, lincosamides, and streptogramin type B antibiotics in Streptococcus sanguis. Journal of bacteriology *154*, 1252-1262.

Horinouchi, S., and Weisblum, B. (1980). Posttranscriptional modification of mRNA conformation: mechanism that regulates erythromycin-induced resistance. Proceedings of the National Academy of Sciences *77*, 7079-7083.

Hue, K., and Bechhofer, D.H. (1992). Regulation of the macrolide-lincosamide-streptogramin B resistance gene ermD. Journal of bacteriology *174*, 5860-5868.

Hur, G.H., Vickery, C.R., and Burkart, M.D. (2012). Explorations of catalytic domains in non-ribosomal peptide synthetase enzymology. Natural Product Reports *29*, 1074-1098.

Ibba, M., Curnow, A.W., and Söll, D. (1997). Aminoacyl-tRNA synthesis: divergent routes to a common goal. Trends in biochemical sciences *22*, 39-42.

Ibba, M., Söll, and Dieter (1999). Quality Control Mechanisms During Translation. Science *286*, 1893-1897.

Ingolia, N.T., Ghaemmaghami, S., Newman, J.R., and Weissman, J.S. (2009). Genome-wide analysis in vivo of translation with nucleotide resolution using ribosome profiling. science *324*, 218-223.

Ishii, E., Chiba, S., Hashimoto, N., Kojima, S., Homma, M., Ito, K., Akiyama, Y., and Mori, H. (2015). Nascent chain-monitored remodeling of the Sec machinery for salinity adaptation of marine bacteria. Proceedings of the National Academy of Sciences *112*, E5513-E5522.

Ito, K., and Chiba, S. (2013). Arrest peptides: cis-acting modulators of translation. Annual review of biochemistry *82*, 171-202.

Iwane, Y., Hitomi, A., Murakami, H., Katoh, T., Goto, Y., and Suga, H. (2016). Expanding the amino acid repertoire of ribosomal polypeptide synthesis via the artificial division of codon boxes. Nature chemistry.

Jin, H., Kelley, A.C., Loakes, D., and Ramakrishnan, V. (2010). Structure of the 70S ribosome bound to release factor 2 and a substrate analog provides insights into catalysis of peptide release. Proceedings of the National Academy of Sciences *107*, 8593-8598.

Jin, H., Kelley, A.C., and Ramakrishnan, V. (2011). Crystal structure of the hybrid state of ribosome in complex with the guanosine triphosphatase release factor 3. Proceedings of the National Academy of Sciences *108*, 15798-15803.

Johansson, M., Chen, J., Tsai, A., Kornberg, G., and Puglisi, Joseph D. (2014). Sequence-Dependent Elongation Dynamics on Macrolide-Bound Ribosomes. Cell Reports *7*, 1534-1546.

Jühling, F., Mörl, M., Hartmann, R.K., Sprinzl, M., Stadler, P.F., and Pütz, J. (2009). tRNAdb 2009: compilation of tRNA sequences and tRNA genes. Nucleic acids research *37*, D159-D162.

Jünemann, R., Wadzack, J., Triana-Alonso, F.J., Bittner, J., Caillet, J., Meinnel, T., Vanatalu, K., and Nierhaus, K.H. (1996). In vivo deuteration of transfer RNAs: overexpresssion and large-scale purification of deuterated specific tRNAs. Nucleic acids research *5*, 7.

Kabsch, W. (2010). XDS. Acta Crystallographica Section D *66*, 125-132.

Kannan, K., Kanabar, P., Schryer, D., Florin, T., Oh, E., Bahroos, N., Tenson, T., Weissman, J.S., and Mankin, A.S. (2014). The general mode of translation inhibition by macrolide antibiotics. Proceedings of the National Academy of Sciences *111*, 15958-15963.

Kannan, K., and Mankin, A.S. (2011). Macrolide antibiotics in the ribosome exit tunnel: species-specific binding and action. Annals of the New York Academy of Sciences *1241*, 33-47.

Kannan, K., Vázquez-Laslop, N., and Mankin, A.S. (2012). Selective protein synthesis by ribosomes with a drug-obstructed exit tunnel. Cell *151*, 508-520.

Karimi, R., Pavlov, M.Y., Buckingham, R.H., and Ehrenberg, M. (1999). Novel roles for classical factors at the interface between translation termination and initiation. Molecular cell *3*, 601-609.

Katoh, T., Wohlgemuth, I., Nagano, M., Rodnina, M.V., and Suga, H. (2016). Essential structural elements in $tRNA^{Pro}$ for EF-P-mediated alleviation of translation stalling. Nature communications *7*.

Katz, L., and Ashley, G.W. (2005). Translation and protein synthesis: macrolides. Chemical reviews *105*, 499-528.

Katz, L., Brown, D., Boris, K., and Tuan, J. (1987). Expression of the macrolide-lincosamide-streptogramin-B-resistance methylase gene, ermE, from *Streptomyces erythraeus* in *Escherichia coli* results in N 6-monomethylation and N 6, N 6-dimethylation of ribosomal RNA. Gene *55*, 319-325.

Kawakami, T., Ishizawa, T., and Murakami, H. (2013). Extensive Reprogramming of the Genetic Code for Genetically Encoded Synthesis of Highly N-Alkylated Polycyclic Peptidomimetics. Journal of the American Chemical Society *135*, 12297-12304.

Kim, S.W., Li, Z., Moore, P.S., Monaghan, A., Chang, Y., Nichols, M., and John, B. (2010). A sensitive non-radioactive northern blot method to detect small RNAs. Nucleic Acids Research *38*, e98-e98.

Klaholz, B.P., Pape, T., Zavialov, A.V., Myasnikov, A.G., Orlova, E.V., Vestergaard, B., Ehrenberg, M., and van Heel, M. (2003). Structure of the *Escherichia coli* ribosomal termination complex with release factor 2. Nature *421*, 90-94.

Knappe, D., Piantavigna, S., Hansen, A., Mechler, A., Binas, A., Nolte, O., Martin, L.L., and Hoffmann, R. (2010). Oncocin (VDKPPYLPRPRPPRRIYNR-NH2): a novel antibacterial peptide

optimized against gram-negative human pathogens. Journal of medicinal chemistry *53*, 5240-5247.

Knappe, D., Zahn, M., Sauer, U., Schiffer, G., Sträter, N., and Hoffmann, R. (2011). Rational Design of Oncocin Derivatives with Superior Protease Stabilities and Antibacterial Activities Based on the High-Resolution Structure of the Oncocin-DnaK Complex. Chembiochem *12*, 874-876.

Koch, M., Willi, J., Pradère, U., Hall, J., and Polacek, N. (2017). Critical 23S rRNA interactions for macrolide-dependent ribosome stalling on the ErmCL nascent peptide chain. Nucleic acids research, 12.

Kohanski, M.A., Dwyer, D.J., and Collins, J.J. (2010). How antibiotics kill bacteria: from targets to networks. Nature Reviews Microbiology *8*, 423-435.

Konan, K.V., and Yanofsky, C. (1997). Regulation of the *Escherichia coli tna* operon: nascent leader peptide control at the tnaC stop codon. Journal of bacteriology *179*, 1774-1779.

Korostelev, A., Asahara, H., Lancaster, L., Laurberg, M., Hirschi, A., Zhu, J., Trakhanov, S., Scott, W.G., and Noller, H.F. (2008). Crystal structure of a translation termination complex formed with release factor RF2. Proceedings of the National Academy of Sciences *105*, 19684-19689.

Korostelev, A.A. (2011). Structural aspects of translation termination on the ribosome. RNA *17*, 1409-1421.

Krizsan, A., Volke, D., Weinert, S., Sträter, N., Knappe, D., and Hoffmann, R. (2014). Insect-Derived Proline-Rich Antimicrobial Peptides Kill Bacteria by Inhibiting Bacterial Protein Translation at the 70S Ribosome. Angewandte Chemie International Edition *53*, 12236-12239.

Kühlbrandt, W. (2014). The resolution revolution. Science *343*, 1443-1444.

Kurland, C.G. (1960). Molecular characterization of ribonucleic acid from Escherichia coli ribosomes. Journal of Molecular Biology *2*, 83-91.

Lang, K., Erlacher, M., Wilson, D.N., Micura, R., and Polacek, N. (2008). The role of 23S ribosomal RNA residue A2451 in peptide bond synthesis revealed by atomic mutagenesis. Chemistry & biology *15*, 485-492.

Lassak, J., Keilhauer, E.C., Fürst, M., Wuichet, K., Gödeke, J., Starosta, A.L., Chen, J.-M., Søgaard-Andersen, L., Rohr, J., and Wilson, D.N. (2015). Arginine-rhamnosylation as new strategy to activate translation elongation factor P. Nature chemical biology *11*, 266-270.

Laurberg, M., Asahara, H., Korostelev, A., Zhu, J., Trakhanov, S., and Noller, H.F. (2008). Structural basis for translation termination on the 70S ribosome. Nature *454*, 852-857.

Laursen, B.S., Sørensen, H.P., Mortensen, K.K., and Sperling-Petersen, H.U. (2005). Initiation of Protein Synthesis in Bacteria. Microbiology and Molecular Biology Reviews *69*, 101-123.

Lee, N., Bessho, Y., Wei, K., Szostak, J.W., and Suga, H. (2000). Ribozyme-catalyzed tRNA aminoacylation. Nature Structural & Molecular Biology *7*, 28-33.

Legrand, P. (2017). XDSME: XDS Made Easier. GitHub repository.

Leney, A.C., and Heck, A.J. (2017). Native mass spectrometry: what is in the name? Journal of The American Society for Mass Spectrometry *28*, 5-13.

Leung, E.K.Y., Suslov, N., Tuttle, N., Sengupta, R., and Piccirilli, J.A. (2011). The mechanism of peptidyl transfer catalysis by the ribosome. Annual review of biochemistry *80*, 527-555.

Lewis, K. (2013). Platforms for antibiotic discovery. Nat Rev Drug Discov *12*, 371-387.

Li, M.Z., and Elledge, S.J. (2012). SLIC: a method for sequence-and ligation-independent cloning. Gene Synthesis: Methods and Protocols, 51-59.

Lin, J., Gagnon, M.G., Bulkley, D., and Steitz, T.A. (2015). Conformational changes of elongation factor G on the ribosome during tRNA translocation. Cell *160*, 219-227.

Lohse, P.A., and Szostak, J.W. (1996). Ribozyme-catalysed amino-acid transfer reactions. Nature *381*, 442.

Lu, J., and Deutsch, C. (2005). Folding zones inside the ribosomal exit tunnel. Nature structural & molecular biology *12*, 1123-1129.

Maden, B., Traut, R., and Monro, R. (1968). Ribosome-catalysed peptidyl transfer: the polyphenylalanine system. Journal of molecular biology *35*, 333-345.

Malkin, L.I., and Rich, A. (1967). Partial resistance of nascent polypeptide chains to proteolytic digestion due to ribosomal shielding. Journal of molecular biology *26*, 329-346.

Mamos, P., Krokidis, M.G., Papadas, A., Karahalios, P., Starosta, A.L., Wilson, D.N., Kalpaxis, D.L., and Dinos, G.P. (2013). On the use of the antibiotic chloramphenicol to target polypeptide chain mimics to the ribosomal exit tunnel. Biochimie *95*, 1765-1772.

Mardirossian, M., Grzela, R., Giglione, C., Meinnel, T., Gennaro, R., Mergaert, P., and Scocchi, M. (2014). The host antimicrobial peptide Bac7 1-35 binds to bacterial ribosomal proteins and inhibits protein synthesis. Chemistry & biology *21*, 1639-1647.

Martínez, A.K., Gordon, E., Sengupta, A., Shirole, N., Klepacki, D., Martinez-Garriga, B., Brown, L.M., Benedik, M.J., Yanofsky, C., Mankin, A.S.*, et al.* (2014). Interactions of the TnaC nascent peptide with rRNA in the exit tunnel enable the ribosome to respond to free tryptophan. Nucleic acids research *42*, 1245-1256.

Mattiuzzo, M., Bandiera, A., Gennaro, R., Benincasa, M., Pacor, S., Antcheva, N., and Scocchi, M. (2007). Role of the *Escherichia coli* SbmA in the antimicrobial activity of proline-rich peptides. Molecular microbiology *66*, 151-163.

Mcguire JM, Bunch RL, Anderson RC, Boaz HE, Flynn EH, Powell HM, and JW, S. (1952). Ilotycin, a new antibiotic. Schweiz MedWochenschr *82*, 2.

McNicholas, P., Salavati, R., and Oliver, D. (1997). Dual regulation of Escherichia coli secA translation by distinct upstream elements. Journal of molecular biology *265*, 128-141.

Mechulam, Y., Guillon, L., Yatime, L., Blanquet, S., and Schmitt, E. (2007). Protection-based assays to measure aminoacyl-tRNA binding to translation initiation factors. Methods in enzymology *430*, 265-281.

Meinnel, T., and Blanquet, S. (1995). Maturation of pre-tRNAfMet by Escherichia coli RNase P is specified by a guanosine of the 5′-flanking sequence. Journal of Biological Chemistry *270*, 15908-15914.

Meinnel, T., Mechulam, Y., and Fayat, G. (1988). Fast purification of a functional elongator tRNAmet expressed from a synthetic gene in vivo. Nucleic acids research *16*, 8095.

Melnikov, S., Mailliot, J., Rigger, L., Neuner, S., Shin, B.S., Yusupova, G., Dever, T.E., Micura, R., and Yusupov, M. (2016a). Molecular insights into protein synthesis with proline residues. EMBO reports, e201642943.

Melnikov, S., Mailliot, J., Shin, B.-S., Rigger, L., Yusupova, G., Micura, R., Dever, T.E., and Yusupov, M. (2016b). Crystal structure of hypusine-containing translation factor eIF5A bound to a rotated eukaryotic ribosome. Journal of molecular biology *428*, 3570-3576.

Menninger, J.R. (1995). Mechanism of inhibition of protein synthesis by macrolide and lincosamide antibiotics. Journal of basic and clinical physiology and pharmacology *6*, 229-250.

Menninger, J.R., and Otto, D. (1982). Erythromycin, carbomycin, and spiramycin inhibit protein synthesis by stimulating the dissociation of peptidyl-tRNA from ribosomes. Antimicrobial agents and Chemotherapy *21*, 811-818.

Metelev, M., Osterman, I.A., Ghilarov, D., Khabibullina, N.F., Yakimov, A., Shabalin, K., Utkina, I., Travin, D.Y., Komarova, E.S., Serebryakova, M.*, et al.* (2017). Klebsazolicin inhibits 70S ribosome by obstructing the peptide exit tunnel. Nat Chem Biol *13*, 1129-1136.

Mikolajka, A., Liu, H., Chen, Y., Starosta, Agata L., Márquez, V., Ivanova, M., Cooperman, Barry S., and Wilson, Daniel N. (2011). Differential Effects of Thiopeptide and Orthosomycin Antibiotics on Translational GTPases. Chemistry & Biology *18*, 589-600.

Milner-White, E.J., Bell, L.H., and Maccallum, P.H. (1992). Pyrrolidine ring puckering in cis and trans-proline residues in proteins and polypeptides: Different puckers are favoured in certain situations. Journal of Molecular Biology *228*, 725-734.

Miyazaki, K. (2003). Creating random mutagenesis libraries by megaprimer PCR of whole plasmid (MEGAWHOP). Directed evolution library creation: methods and protocols, 23-28.

Miyazaki, K. (2011). 17 MEGAWHOP Cloning: A Method of Creating Random Mutagenesis Libraries via Megaprimer PCR of Whole Plasmids. Methods in enzymology *498*, 399.

Moazed, D., and Noller, H.F. (1987). Chloramphenicol, erythromycin, carbomycin and vernamycin B protect overlapping sites in the peptidyl transferase region of 23S ribosomal RNA. Biochimie *69*, 879-884.

Moffatt, B.A., and Studier, F.W. (1987). T7 lysozyme inhibits transcription by T7 RNA polymerase. Cell *49*, 221-227.

Mohanty, B.K., and Kushner, S.R. (2006). The majority of *Escherichia coli* mRNAs undergo post-transcriptional modification in exponentially growing cells. Nucleic Acids Research *34*, 5695-5704.

Mohanty, B.K., Petree, J.R., and Kushner, S.R. (2016). Endonucleolytic cleavages by RNase E generate the mature 3′ termini of the three proline tRNAs in *Escherichia coli.* Nucleic Acids Research *44*, 6350-6362.

Mohapatra, S., Choi, H., Ge, X., Sanyal, S., and Weisshaar, J.C. (2017). Spatial Distribution and Ribosome-Binding Dynamics of EF-P in Live *Escherichia coli*. mBio *8*.

Monro, R.E. (1967). Catalysis of peptide bond formation by 50S ribosomal subunits from Escherichia coli. Journal of molecular biology *26*, 147-151.

Mullis, K.B., Erlich, H.A., Arnheim, N., Horn, G.T., Saiki, R.K., and Scharf, S.J. (1987). Process for amplifying, detecting, and/or-cloning nucleic acid sequences (Google Patents).

Munro, J.B., Altman, R.B., O'Connor, N., and Blanchard, S.C. (2007). Identification of two distinct hybrid state intermediates on the ribosome. Molecular cell *25*, 505-517.

Murakami, H., Ohta, A., Ashigai, H., and Suga, H. (2006a). A highly flexible tRNA acylation method for non-natural polypeptide synthesis. Nature Methods *3*.

Murakami, H., Ohta, A., Goto, Y., Sako, Y., and Suga, H. (2006b). Flexizyme as a versatile tRNA acylation catalyst and the application for translation. Paper presented at: Nucleic Acids Symposium Series (Oxford Univ Press).

Murakami, H., Saito, H., and Suga, H. (2003). A versatile tRNA aminoacylation catalyst based on RNA. Chemistry & biology *10*, 655-662.

Murphy, E. (1985). Nucleotide sequence of ermA, a macrolide-lincosamide-streptogramin B determinant in *Staphylococcus aureus*. Journal of bacteriology *162*, 633-640.

Muto, H., and Ito, K. (2008). Peptidyl-prolyl-tRNA at the ribosomal P-site reacts poorly with puromycin. Biochemical and biophysical research communications *366*, 1043-1047.

Muto, H., Nakatogawa, H., and Ito, K. (2006). Genetically encoded but nonpolypeptide prolyl-tRNA functions in the A site for SecM-mediated ribosomal stall. Molecular cell *22*, 545-552.

Nakatogawa, H., and Ito, K. (2001). Secretion monitor, SecM, undergoes self-translation arrest in the cytosol. Molecular cell *7*, 185-192.

Nakatogawa, H., and Ito, K. (2002). The ribosomal exit tunnel functions as a discriminating gate. Cell *108*, 629-636.

Nakatogawa, H., Murakami, A., Mori, H., and Ito, K. (2005). SecM facilitates translocase function of SecA by localizing its biosynthesis. Genes & development *19*, 436-444.

Nakayama, I. (1984). Macrolides in clinical practice. Macrolide antibiotics Academic Press, Orlando, Fla, 261-300.

Navarre, W.W., Zou, S.B., Roy, H., Xie, J.L., Savchenko, A., Singer, A., Edvokimova, E., Prost, L.R., Kumar, R., and Ibba, M. (2010). PoxA, yjeK, and elongation factor P coordinately modulate virulence and drug resistance in *Salmonella enterica*. Molecular cell *39*, 209-221.

Nilsson, O.B., Hedman, R., Marino, J., Wickles, S., Bischoff, L., Johansson, M., Müller-Lucks, A., Trovato, F., Puglisi, J.D., and O'Brien, E.P. (2015). Cotranslational protein folding inside the ribosome exit tunnel. Cell reports *12*, 1533-1540.

Nissen, P., Hansen, J., Ban, N., Moore, P.B., and Steitz, T.A. (2000). The structural basis of ribosome activity in peptide bond synthesis. Science *289*, 920-930.

Nissen, P., Kjeldgaard, M., Thirup, S., and Polekhina, G. (1995). Crystal structure of the ternary complex of Phe-tRNAPhe, EF-Tu, and a GTP analog. Science *270*, 1464.

Niwa, N., Yamagishi, Y., Murakami, H., and Suga, H. (2009). A flexizyme that selectively charges amino acids activated by a water-friendly leaving group. Bioorganic & medicinal chemistry letters *19*, 3892-3894.

Noeske, J., Huang, J., Olivier, N.B., Giacobbe, R.A., Zambrowski, M., and Cate, J.H.D. (2014). Synergy of Streptogramin Antibiotics Occurs Independently of Their Effects on Translation. Antimicrobial Agents and Chemotherapy *58*, 5269-5279.

Noller, H.F. (1993). Peptidyl transferase: protein, ribonucleoprotein, or RNA? Journal of Bacteriology *175*, 5297-5300.

Nureki, O., Vassylyev, D.G., Tateno, M., Shimada, A., Nakama, T., Fukai, S., Konno, M., Hendrickson, T.L., Schimmel, P., and Yokoyama, S. (1998). Enzyme structure with two catalytic sites for double-sieve selection of substrate. Science *280*, 578-582.

Ogle, J.M., Carter, A.P., and Ramakrishnan, V. (2003). Insights into the decoding mechanism from recent ribosome structures. Trends in biochemical sciences *28*, 259-266.

Oliver, D., Norman, J., and Sarker, S. (1998). Regulation of *Escherichia coli secA* by Cellular Protein Secretion Proficiency Requires an Intact Gene X Signal Sequence and an Active Translocon. Journal of Bacteriology *180*, 5240-5242.

Orelle, C., Carlson, S., Kaushal, B., Almutairi, M.M., Liu, H., Ochabowicz, A., Quan, S., Pham, V.C., Squires, C.L., and Murphy, B.T. (2013a). Tools for characterizing bacterial protein synthesis inhibitors. Antimicrobial agents and chemotherapy *57*, 5994-6004.

Orelle, C., Szal, T., Klepacki, D., Shaw, K.J., Vazquez-Laslop, N., and Mankin, A.S. (2013b). Identifying the targets of aminoacyl-tRNA synthetase inhibitors by primer extension inhibition. Nucleic acids research, gkt526.

Oshima, T. (2007). Unique polyamines produced by an extreme thermophile, Thermus thermophilus. Amino Acids *33*, 367-372.

Oshima, T., and Imahori, K. (1974). Description of *Thermus thermophilus* (Yoshida and Oshima) comb. nov., a nonsporulating thermophilic bacterium from a Japanese thermal spa. International Journal of Systematic and Evolutionary Microbiology *24*, 102-112.

Ostorhazi, E., Nemes-Nikodem, E., Knappe, D., and Hoffmann, R. (2014). *In vivo* activity of optimized apidaecin and oncocin peptides against a multiresistant, KPC-producing *Klebsiella pneumoniae* strain. Protein and peptide letters *21*, 368-373.

Otvos, J., Laszlo (2002). The short proline-rich antibacterial peptide family. Cellular and Molecular Life Sciences *59*, 1138-1150.

Otvos, L. (2005). Antibacterial peptides and proteins with multiple cellular targets. Journal of Peptide Science *11*, 697-706.

Otvos, L., O, I., Rogers, M.E., Consolvo, P.J., Condie, B.A., Lovas, S., Bulet, P., and Blaszczyk-Thurin, M. (2000). Interaction between heat shock proteins and antimicrobial peptides. Biochemistry *39*, 14150-14159.

Page, M.G. (2013). Siderophore conjugates. Annals of the New York Academy of Sciences *1277*, 115-126.

Palade, G.E. (1955). A small particulate component of the cytoplasm. The Journal of Biophysical and Biochemical Cytology *1*, 59-68.

Pandey, A.K., Naduthambi, D., Thomas, K.M., and Zondlo, N.J. (2013). Proline Editing: A General and Practical Approach to the Synthesis of Functionally and Structurally Diverse Peptides. Analysis of Steric versus Stereoelectronic Effects of 4-Substituted Prolines on Conformation within Peptides. Journal of the American Chemical Society *135*, 4333-4363.

Pape, T., Wintermeyer, W., and Rodnina, M.V. (1998). Complete kinetic mechanism of elongation factor Tu-dependent binding of aminoacyl-tRNA to the A site of the E.coli ribosome. The EMBO Journal *17*, 7490-7497.

Park, J.-H., Johansson, H.E., Aoki, H., Huang, B.X., Kim, H.-Y., Ganoza, M.C., and Park, M.H. (2012). Post-translational modification by β-lysylation is required for activity of Escherichia coli elongation factor P (EF-P). Journal of Biological Chemistry *287*, 2579-2590.

Pasco, M., Dolain, C., and Guichard, G. (2017). Foldamers in Medical Chemistry. In Comprehensive Supramolecular Chemistry II, J. Atwood, ed. (Oxford: Elsevier), pp. 89-125.

Passmore, L.A., and Russo, C.J. (2016). Chapter Three - Specimen Preparation for High-Resolution Cryo-EM. In Methods in Enzymology, R.A. Crowther, ed. (Academic Press), pp. 51-86.

Paulsen, V.S., Mardirossian, M., Blencke, H.-M., Benincasa, M., Runti, G., Nepa, M., Haug, T., Stensvåg, K., and Scocchi, M. (2016). Inner membrane proteins YgdD and SbmA are required for the complete susceptibility of *Escherichia coli* to the proline-rich antimicrobial peptide arasin 1 (1–25). Microbiology *162*, 601-609.

Pavlov, M.Y., Freistroffer, D.V., MacDougall, J., Buckingham, R.H., and Ehrenberg, M. (1997). Fast recycling of *Escherichia coli* ribosomes requires both ribosome recycling factor (RRF) and release factor RF3. The EMBO Journal *16*, 4134-4141.

Pavlov, M.Y., Watts, R.E., Tan, Z., Cornish, V.W., Ehrenberg, M., and Forster, A.C. (2009). Slow peptide bond formation by proline and other N-alkylamino acids in translation. Proceedings of the National Academy of Sciences *106*, 50-54.

Peil, L., Starosta, A.L., Lassak, J., Atkinson, G.C., Virumäe, K., Spitzer, M., Tenson, T., Jung, K., Remme, J., and Wilson, D.N. (2013). Distinct XPPX sequence motifs induce ribosome stalling, which is rescued by the translation elongation factor EF-P. Proceedings of the National Academy of Sciences *110*, 15265-15270.

Peil, L., Starosta, A.L., Virumäe, K., Atkinson, G.C., Tenson, T., Remme, J., and Wilson, D.N. (2012). Lys34 of translation elongation factor EF-P is hydroxylated by YfcM. Nature chemical biology *8*, 695-697.

Petry, S., Weixlbaumer, A., and Ramakrishnan, V. (2008). The termination of translation. Current opinion in structural biology *18*, 70-77.

Pettersen, E.F., Goddard, T.D., Huang, C.C., Couch, G.S., Greenblatt, D.M., Meng, E.C., and Ferrin, T.E. (2004). UCSF Chimera—a visualization system for exploratory research and analysis. Journal of computational chemistry *25*, 1605-1612.

Petty, K.J. (2001). Metal-Chelate Affinity Chromatography. In Current Protocols in Molecular Biology (John Wiley & Sons, Inc.).

Polacek, N., Gaynor, M., Yassin, A., and Mankin, A.S. (2001). Ribosomal peptidyl transferase can withstand mutations at the putative catalytic nucleotide. Nature *411*, 498.

Polikanov, Y.S., Melnikov, S.V., Söll, D., and Steitz, T.A. (2015a). Structural insights into the role of rRNA modifications in protein synthesis and ribosome assembly. Nature structural & molecular biology *22*, 342-344.

Polikanov, Y.S., Starosta, A.L., Juette, M.F., Altman, R.B., Terry, D.S., Lu, W., Burnett, B.J., Dinos, G., Reynolds, K.A., and Blanchard, S.C. (2015b). Distinct tRNA accommodation intermediates observed on the ribosome with the antibiotics hygromycin A and A201A. Molecular cell *58*, 832-844.

Polikanov, Y.S., Steitz, T.A., and Innis, C.A. (2014). A proton wire to couple aminoacyl-tRNA accommodation and peptide-bond formation on the ribosome. Nature structural & molecular biology *21*, 787-793.

Pulk, A., and Cate, J.H.D. (2013). Control of Ribosomal Subunit Rotation by Elongation Factor G. Science *340*.

Rajkovic, A., Hummels, K.R., Witzky, A., Erickson, S., Gafken, P.R., Whitelegge, J.P., Faull, K.F., Kearns, D.B., and Ibba, M. (2016). Translation Control of Swarming Proficiency in Bacillus subtilis by 5-Amino-pentanolylated Elongation Factor P. Journal of Biological Chemistry *291*, 10976-10985.

Ramaswamy, K., Saito, H., Murakami, H., Shiba, K., and Suga, H. (2004). Designer ribozymes: programming the tRNA specificity into flexizyme. Journal of the American Chemical Society *126*, 11454-11455.

Ramu, H., Mankin, A., and Vazquez-Laslop, N. (2009). Programmed drug-dependent ribosome stalling. Molecular microbiology *71*, 811-824.

Ramu, H., Vázquez-Laslop, N., Klepacki, D., Dai, Q., Piccirilli, J., Micura, R., and Mankin, A.S. (2011). Nascent peptide in the ribosome exit tunnel affects functional properties of the A-site of the peptidyl transferase center. Molecular cell *41*, 321-330.

Razi, A., Britton, R.A., and Ortega, J. (2017). The impact of recent improvements in cryo-electron microscopy technology on the understanding of bacterial ribosome assembly. Nucleic Acids Research *45*, 1027-1040.

Ringquist, S., Shinedling, S., Barrick, D., Green, L., Binkley, J., Stormo, G.D., and Gold, L. (1992). Translation initiation in *Escherichia coli:* sequences within the ribosome-binding site. Molecular Microbiology *6*, 1219-1229.

Roberts, M.C. (2008). Update on macrolide–lincosamide–streptogramin, ketolide, and oxazolidinone resistance genes. FEMS microbiology letters *282*, 147-159.

Roberts, M.C., Sutcliffe, J., Courvalin, P., Jensen, L.B., Rood, J., and Seppala, H. (1999). Nomenclature for macrolide and macrolide-lincosamide-streptogramin B resistance determinants. Antimicrobial Agents and Chemotherapy *43*, 2823-2830.

Rodnina, Marina V., and Wintermeyer, W. (2011). The ribosome as a molecular machine: the mechanism of tRNA–mRNA movement in translocation. Biochemical Society Transactions *39*, 658-662.

Rohou, A., and Grigorieff, N. (2015). CTFFIND4: Fast and accurate defocus estimation from electron micrographs. Journal of structural biology *192*, 216-221.

Roy, R.N., Lomakin, I.B., Gagnon, M.G., and Steitz, T.A. (2015). The mechanism of inhibition of protein synthesis by the proline-rich peptide oncocin. Nature structural & molecular biology *22*, 466-469.

Rozenski, J. (1999). Mongo Oligo Mass Calculator v2. 06.

Rozenski, J., Crain, P.F., and McCloskey, J.A. (1999). The RNA modification database: 1999 update. Nucleic Acids Research *27*, 196-197.

Runti, G., Lopez Ruiz, M.d.C., Stoilova, T., Hussain, R., Jennions, M., Choudhury, H.G., Benincasa, M., Gennaro, R., Beis, K., and Scocchi, M. (2013). Functional Characterization of SbmA, a

Bacterial Inner Membrane Transporter Required for Importing the Antimicrobial Peptide Bac7(1-35). Journal of Bacteriology *195*, 5343-5351.

Saiki, R., Gelfand, D., Stoffel, S., Scharf, S., Higuchi, R., Horn, G., Mullis, K., and Erlich, H. (1988). Primer-directed enzymatic amplification of DNA with a thermostable DNA polymerase. Science *239*, 487-491.

Saito, H., Kourouklis, D., and Suga, H. (2001a). An in vitro evolved precursor tRNA with aminoacylation activity. The EMBO Journal *20*, 1797-1806.

Saito, H., and Suga, H. (2002). Outersphere and innersphere coordinated metal ions in an aminoacyl-tRNA synthetase ribozyme. Nucleic acids research *30*, 5151-5159.

Saito, H., Watanabe, K., and Suga, H. (2001b). Concurrent molecular recognition of the amino acid and tRNA by a ribozyme. RNA *7*, 1867-1878.

Sanger, F., and Coulson, A.R. (1975). A rapid method for determining sequences in DNA by primed synthesis with DNA polymerase. Journal of Molecular Biology *94*, 441-448.

Sanger, F., Nicklen, S., and Coulson, A.R. (1977). DNA sequencing with chain-terminating inhibitors. Proceedings of the National Academy of Sciences *74*, 5463-5467.

Scheres, S.H. (2012a). A Bayesian view on cryo-EM structure determination. Journal of molecular biology *415*, 406-418.

Scheres, S.H. (2012b). RELION: implementation of a Bayesian approach to cryo-EM structure determination. Journal of structural biology *180*, 519-530.

Scheres, S.H.W. (2010). Maximum-likelihood methods in cryo-EM. Part II: application to experimental data. Methods in enzymology *482*, 295-320.

Scheres, S.H.W. (2015). Semi-automated selection of cryo-EM particles in RELION-1.3. Journal of structural biology *189*, 18.

Scheres, S.H.W. (2016). Chapter Six - Processing of Structurally Heterogeneous Cryo-EM Data in RELION. In Methods in Enzymology, R.A. Crowther, ed. (Academic Press), pp. 125-157.

Scheres, S.H.W., and Chen, S. (2012). Prevention of overfitting in cryo-EM structure determination. Nature Methods *9*, 2.

Schlunzen, F., Zarivach, R., Harms, J., Bashan, A., Tocilj, A., Albrecht, R., Yonath, A., and Franceschi, F. (2001). Structural basis for the interaction of antibiotics with the peptidyl transferase centre in eubacteria. Nature *413*, 814-821.

Schmeing, M.T., Huang, K.S., Strobel, S.A., and Steitz, T.A. (2005a). An induced-fit mechanism to promote peptide bond formation and exclude hydrolysis of peptidyl-tRNA. Nature *438*, 520-524.

Schmeing, T.M., Huang, K.S., Kitchen, D.E., Strobel, S.A., and Steitz, T.A. (2005b). Structural insights into the roles of water and the 2′ hydroxyl of the P site tRNA in the peptidyl transferase reaction. Molecular cell *20*, 437-448.

Schmeing, T.M., Huang, K.S., Strobel, S.A., and Steitz, T.A. (2005c). An induced-fit mechanism to promote peptide bond formation and exclude hydrolysis of peptidyl-tRNA. Nature *438*, 520-524.

Schmeing, T.M., and Ramakrishnan, V. (2009). What recent ribosome structures have revealed about the mechanism of translation. Nature *461*, 1234-1242.

Schmeing, T.M., Seila, A.C., Hansen, J.L., Freeborn, B., Soukup, J.K., Scaringe, S.A., Strobel, S.A., Moore, P.B., and Steitz, T.A. (2002). A pre-translocational intermediate in protein synthesis observed in crystals of enzymatically active 50S subunits. Nature Structural & Molecular Biology *9*, 225-230.

Schmeing, T.M., Voorhees, R.M., Kelley, A.C., Gao, Y.-G., Murphy, F.V., Weir, J.R., and Ramakrishnan, V. (2009). The crystal structure of the ribosome bound to EF-Tu and aminoacyl-tRNA. Science *326*, 688-694.

Schmidt, C., Becker, T., Heuer, A., Braunger, K., Shanmuganathan, V., Pech, M., Berninghausen, O., Wilson, D.N., and Beckmann, R. (2015). Structure of the hypusinylated eukaryotic translation factor eIF-5A bound to the ribosome. Nucleic acids research, gkv1517.

Schmidt, E., and Schimmel, P. (1994). Mutational isolation of a sieve for editing in a transfer RNA synthetase. Science-AAAS-Weekly Paper Edition-including Guide to Scientific Information *264*, 265-266.

Schmitt, E., Blanquet, S., and Mechulam, Y. (1999). Crystallization and preliminary X-ray analysis of *Escherichia coli* methionyl-tRNAMetf formyltransferase complexed with formyl-methionyl-tRNAMetf. Acta Crystallographica Section D: Biological Crystallography *55*, 332-334.

Schneider, M., and Dorn, A. (2001). Differential infectivity of two Pseudomonas species and the immune response in the milkweed bug, *Oncopeltus fasciatus* (Insecta: Hemiptera). Journal of invertebrate pathology *78*, 135-140.

Schuwirth, B.S., Borovinskaya, M.A., Hau, C.W., Zhang, W., Vila-Sanjurjo, A., Holton, J.M., and Cate, J.H.D. (2005). Structures of the bacterial ribosome at 3.5 Å resolution. Science *310*, 827-834.

Scocchi, M., Romeo, D., and Zanetti, M. (1994). Molecular cloning of Bac7, a proline-and arginine-rich antimicrobial peptide from bovine neutrophils. FEBS letters *352*, 197-200.

Seefeldt, A.C., Graf, M., Pérébaskine, N., Nguyen, F., Arenz, S., Mardirossian, M., Scocchi, M., Wilson, D.N., and Innis, C.A. (2016). Structure of the mammalian antimicrobial peptide Bac7 (1–16) bound within the exit tunnel of a bacterial ribosome. Nucleic acids research, gkv1545.

Seefeldt, A.C., Nguyen, F., Antunes, S., Pérébaskine, N., Graf, M., Arenz, S., Inampudi, K.K., Douat, C., Guichard, G., Wilson, D.N*., et al.* (2015). The proline-rich antimicrobial peptide Onc112 inhibits translation by blocking and destabilizing the initiation complex. Nature structural & molecular biology *22*, 470-475.

Seidelt, B., Innis, C.A., Wilson, D.N., Gartmann, M., Armache, J.-P., Villa, E., Trabuco, L.G., Becker, T., Mielke, T., and Schulten, K. (2009). Structural insight into nascent polypeptide chain–mediated translational stalling. Science *326*, 1412-1415.

Seip, B., and Innis, C.A. (2016). How Widespread is Metabolite Sensing by Ribosome-Arresting Nascent Peptides? Journal of Molecular Biology *428*, 2217-2227.

Selmer, M., Dunham, C.M., Murphy, F.V., Weixlbaumer, A., Petry, S., Kelley, A.C., Weir, J.R., and Ramakrishnan, V. (2006). Structure of the 70S *Tth* Ribosome Complexed with mRNA and tRNA. Science *313*, 1935-1942.

Shimizu, Y., Inoue, A., Tomari, Y., Suzuki, T., Yokogawa, T., Nishikawa, K., and Ueda, T. (2001). Cell-free translation reconstituted with purified components. Nature biotechnology *19*, 751-755.

Shimizu, Y., Kanamori, T., and Ueda, T. (2005). Protein synthesis by pure translation systems. Methods *36*, 299-304.

Shine, J., and Dalgarno, L. (1974). The 3'-terminal sequence of Escherichia coli 16S ribosomal RNA: complementarity to nonsense triplets and ribosome binding sites. Proceedings of the National Academy of Sciences *71*, 1342-1346.

Sievers, A., Beringer, M., Rodnina, M.V., and Wolfenden, R. (2004). The ribosome as an entropy trap. Proceedings of the National Academy of Sciences of the United States of America *101*, 7897-7901.

Simonetti, A., Marzi, S., Billas, I.M., Tsai, A., Fabbretti, A., Myasnikov, A.G., Roblin, P., Vaiana, A.C., Hazemann, I., and Eiler, D. (2013). Involvement of protein IF2 N domain in ribosomal subunit joining revealed from architecture and function of the full-length initiation factor. Proceedings of the National Academy of Sciences *110*, 15656-15661.

Sohmen, D., Chiba, S., Shimokawa-Chiba, N., Innis, C.A., Berninghausen, O., Beckmann, R., Ito, K., and Wilson, D.N. (2015). Structure of the Bacillus subtilis 70S ribosome reveals the basis for species-specific stalling. *6*, 6941.

Sørensen, M.A., Kurland, C., and Pedersen, S. (1989). Codon usage determines translation rate in Escherichia coli. Journal of molecular biology *207*, 365-377.

Sothiselvam, S., Liu, B., Han, W., Ramu, H., Klepacki, D., Atkinson, G.C., Brauer, A., Remm, M., Tenson, T., Schulten, K.*, et al.* (2014). Macrolide antibiotics allosterically predispose the ribosome for translation arrest. Proceedings of the National Academy of Sciences *111*, 9804-9809.

Sothiselvam, S., Neuner, S., Rigger, L., Klepacki, D., Micura, R., Vázquez-Laslop, N., and Mankin, A.S. (2016). Binding of macrolide antibiotics leads to ribosomal selection against specific substrates based on their charge and size. Cell reports *16*, 1789-1799.

Speyer, J.F., Lengyel, P., Basilio, C., Wahba, A.J., Gardner, R.S., and Ochoa, S. (1963). Synthetic polynucleotides and the amino acid code. Paper presented at: Cold Spring Harbor Symposia on Quantitative Biology (Cold Spring Harbor Laboratory Press).

Stalmans, S., Wynendaele, E., Bracke, N., Knappe, D., Hoffmann, R., Peremans, K., Polis, I., Burvenich, C., and De Spiegeleer, B. (2014). Blood-brain barrier transport of short proline-rich antimicrobial peptides. Protein and peptide letters *21*, 399-406.

Starosta, A.L., Lassak, J., Peil, L., Atkinson, G.C., Virumäe, K., Tenson, T., Remme, J., Jung, K., and Wilson, D.N. (2014a). Translational stalling at polyproline stretches is modulated by the sequence context upstream of the stall site. Nucleic acids research *42*, 10711-10719.

Starosta, A.L., Lassak, J., Peil, L., Atkinson, G.C., Woolstenhulme, C.J., Virumäe, K., Buskirk, A., Tenson, T., Remme, J., and Jung, K. (2014b). A conserved proline triplet in Val-tRNA synthetase and the origin of elongation factor P. Cell reports *9*, 476-483.

Studier, F.W., and Moffatt, B.A. (1986). Use of bacteriophage T7 RNA polymerase to direct selective high-level expression of cloned genes. Journal of Molecular Biology *189*, 113-130.

Su, T., Cheng, J., Sohmen, D., Hedman, R., Berninghausen, O., von Heijne, G., Wilson, D.N., and Beckmann, R. (2017). The force-sensing peptide VemP employs extreme compaction and secondary structure formation to induce ribosomal stalling. eLife *6*, e25642.

Suga, H., Cowan, J.A., and Szostak, J.W. (1998a). Unusual metal ion catalysis in an acyl-transferase ribozyme. Biochemistry *37*, 10118-10125.

Suga, H., Lohse, P.A., and Szostak, J.W. (1998b). Structural and kinetic characterization of an acyl transferase ribozyme. Journal of the American Chemical Society *120*, 1151-1156.

Svidritskiy, E., Ling, C., Ermolenko, D.N., and Korostelev, A.A. (2013). Blasticidin S inhibits translation by trapping deformed tRNA on the ribosome. Proceedings of the National Academy of Sciences *110*, 12283-12288.

Tartof, K.D., and Hobbs, C.A. (1987). Improved media for growing plasmid and cosmid clones. Bethesda Res Lab Focus *9*, 12.

Taubman, S.B., Jones, N.R., Young, F.E., and Corcoran, J.W. (1966). Sensitivity and resistance to erythromycin in *Bacillus subtilis* 168: The ribosomal binding of erythromycin and chloramphenicol. Biochimica et Biophysica Acta (BBA) - Nucleic Acids and Protein Synthesis *123*, 438-440.

Tenson, T., Lovmar, M., and Ehrenberg, M. (2003). The mechanism of action of macrolides, lincosamides and streptogramin B reveals the nascent peptide exit path in the ribosome. Journal of molecular biology *330*, 1005-1014.

Thomas, P.S. (1980). Hybridization of denatured RNA and small DNA fragments transferred to nitrocellulose. Proceedings of the National Academy of Sciences of the United States of America *77*, 5201-5205.

Thompson, J., and Dahlberg, A.E. (2004). Testing the conservation of the translational machinery over evolution in diverse environments: assaying *Thermus thermophilus* ribosomes and initiation factors in a coupled transcription–translation system from *Escherichia coli*. Nucleic acids research *32*, 5954-5961.

Thompson, J., Kim, D.F., O'Connor, M., Lieberman, K.R., Bayfield, M.A., Gregory, S.T., Green, R., Noller, H.F., and Dahlberg, A.E. (2001). Analysis of mutations at residues A2451 and G2447 of 23S rRNA in the peptidyltransferase active site of the 50S ribosomal subunit. Proceedings of the National Academy of Sciences *98*, 9002-9007.

Tomasinsig, L., Skerlavaj, B., Papo, N., Giabbai, B., Shai, Y., and Zanetti, M. (2006). Mechanistic and Functional Studies of the Interaction of a Proline-rich Antimicrobial Peptide with Mammalian Cells. Journal of Biological Chemistry *281*, 383-391.

Tourigny, D.S., Fernández, I.S., Kelley, A.C., and Ramakrishnan, V. (2013). Elongation Factor G Bound to the Ribosome in an Intermediate State of Translocation. Science *340*.

Traut, R., and Monro, R. (1964). The puromycin reaction and its relation to protein synthesis. Journal of molecular biology *10*, 63-72.

Trobro, S., and Åqvist, J. (2005). Mechanism of peptide bond synthesis on the ribosome. Proceedings of the National Academy of Sciences of the United States of America *102*, 12395-12400.

Tsai, A., Kornberg, G., Johansson, M., Chen, J., and Puglisi, Joseph D. (2014). The Dynamics of SecM-Induced Translational Stalling. Cell Reports *7*, 1521-1533.

Tu, D., Blaha, G., Moore, P.B., and Steitz, T.A. (2005). Structures of MLS B K antibiotics bound to mutated large ribosomal subunits provide a structural explanation for resistance. Cell *121*, 257-270.

Ude, S., Lassak, J., Starosta, A.L., Kraxenberger, T., Wilson, D.N., and Jung, K. (2013). Translation elongation factor EF-P alleviates ribosome stalling at polyproline stretches. Science *339*, 82-85.

Uzawa, T., Hamasaki, N., and Oshima, T. (1993a). Effects of Novel Polyamines on Cell-Free Polypeptide Synthesis Catalyzed by Thermus thermophilus HB8 Extract. The Journal of Biochemistry *114*, 478-486.

Uzawa, T., Yamagishi, A., Ueda, T., Chikazumi, N., Watanabe, K., and Oshlma, T. (1993b). Effects of Polyamines on a Continuous Cell-Free Protein Synthesis System of an Extreme Thermophile, *Thermus thermophilus*. The Journal of Biochemistry *114*, 732-734.

Valle, M., Sengupta, J., Swami, N.K., Grassucci, R.A., Burkhardt, N., Nierhaus, K.H., Agrawal, R.K., and Frank, J. (2002). Cryo-EM reveals an active role for aminoacyl-tRNA in the accommodation process. The EMBO Journal *21*, 3557-3567.

Vassiliadis, G., Destoumieux-Garzón, D., Lombard, C., Rebuffat, S., and Peduzzi, J. (2010). Isolation and Characterization of Two Members of the Siderophore-Microcin Family, Microcins M and H47. Antimicrobial Agents and Chemotherapy *54*, 288-297.

Vassiliadis, G., Peduzzi, J., Zirah, S., Thomas, X., Rebuffat, S., and Destoumieux-Garzón, D. (2007). Insight into Siderophore-Carrying Peptide Biosynthesis: Enterobactin Is a Precursor for Microcin E492 Posttranslational Modification. Antimicrobial Agents and Chemotherapy *51*, 3546-3553.

Vázquez-Laslop, N., Klepacki, D., Mulhearn, D.C., Ramu, H., Krasnykh, O., Franzblau, S., and Mankin, A.S. (2011). Role of antibiotic ligand in nascent peptide-dependent ribosome stalling. Proceedings of the National Academy of Sciences *108*, 10496-10501.

Vazquez-Laslop, N., Thum, C., and Mankin, A.S. (2008). Molecular mechanism of drug-dependent ribosome stalling. Molecular cell *30*, 190-202.

Vázquez-Laslop, N., Ramu, H., Klepacki, D., Kannan, K., and Mankin, A.S. (2010). The key function of a conserved and modified rRNA residue in the ribosomal response to the nascent peptide. The EMBO journal *29*, 3108-3117.

Vazquez, D. (1966). Studies on the Mode of Action of the Streptogramin Antibiotics. Microbiology *42*, 93-106.

Vitagliano, L., Berisio, R., Mastrangelo, A., Mazzarella, L., and Zagari, A. (2001). Preferred proline puckerings in cis and trans peptide groups: implications for collagen stability. Protein Sci *10*, 2627-2632.

Voorhees, R.M., Weixlbaumer, A., Loakes, D., Kelley, A.C., and Ramakrishnan, V. (2009). Insights into substrate stabilization from snapshots of the peptidyl transferase center of the intact 70S ribosome. Nature structural & molecular biology *16*, 528-533.

Voss, N.R., Gerstein, M., Steitz, T.A., and Moore, P.B. (2006). The Geometry of the Ribosomal Polypeptide Exit Tunnel. Journal of Molecular Biology *360*, 893-906.

Wallin, G., and Åqvist, J. (2010). The transition state for peptide bond formation reveals the ribosome as a water trap. Proceedings of the National Academy of Sciences *107*, 1888-1893.

Washington, A.Z., Benicewicz, D.B., Canzoneri, J.C., Fagan, C.E., Mwakwari, S.C., Maehigashi, T., Dunham, C.M., and Oyelere, A.K. (2014). Macrolide-Peptide Conjugates as Probes of the Path of Travel of the Nascent Peptides through the Ribosome. ACS Chemical Biology *9*, 2621-2631.

Weinger, J.S., Parnell, K.M., Dorner, S., Green, R., and Strobel, S.A. (2004). Substrate-assisted catalysis of peptide bond formation by the ribosome. Nature structural & molecular biology *11*, 1101.

Weixlbaumer, A., Jin, H., Neubauer, C., Voorhees, R.M., Petry, S., Kelley, A.C., and Ramakrishnan, V. (2008). Insights into translational termination from the structure of RF2 bound to the ribosome. Science *322*, 953-956.

Weixlbaumer, A., Petry, S., Dunham, C.M., Selmer, M., Kelley, A.C., and Ramakrishnan, V. (2007). Crystal structure of the ribosome recycling factor bound to the ribosome. Nature structural & molecular biology *14*, 733.

Williams, A. (2001). Overview of Conventional Chromatography. In Current Protocols in Protein Science (John Wiley & Sons, Inc.).

Wilson, D.N. (2009). The A–Z of bacterial translation inhibitors. Critical reviews in biochemistry and molecular biology *44*, 393-433.

Wilson, D.N. (2011). On the specificity of antibiotics targeting the large ribosomal subunit. Annals of the New York Academy of Sciences *1241*, 1-16.

Wilson, D.N. (2014). Ribosome-targeting antibiotics and mechanisms of bacterial resistance. Nature Reviews Microbiology *12*, 35-48.

Wilson, D.N., Arenz, S., and Beckmann, R. (2016). Translation regulation via nascent polypeptide-mediated ribosome stalling. Current opinion in structural biology *37*, 123-133.

Wilson, D.N., and Nierhaus, K.H. (2005). Ribosomal Proteins in the Spotlight. Critical Reviews in Biochemistry and Molecular Biology *40*, 243-267.

Wilson, D.N., Schluenzen, F., Harms, J.M., Starosta, A.L., Connell, S.R., and Fucini, P. (2008). The oxazolidinone antibiotics perturb the ribosomal peptidyl-transferase center and effect tRNA positioning. Proceedings of the National Academy of Sciences *105*, 13339-13344.

Wimberly, B.T., Brodersen, D.E., Clemons, W.M., Morgan-Warren, R.J., Carter, A.P., Vonrhein, C., Hartsch, T., and Ramakrishnan, V. (2000). Structure of the 30S ribosomal subunit. Nature *407*, 327-339.

Woolstenhulme, C.J., Guydosh, N.R., Green, R., and Buskirk, A.R. (2015). High-precision analysis of translational pausing by ribosome profiling in bacteria lacking EFP. Cell reports *11*, 13-21.

Woolstenhulme, C.J., Parajuli, S., Healey, D.W., Valverde, D.P., Petersen, E.N., Starosta, A.L., Guydosh, N.R., Johnson, W.E., Wilson, D.N., and Buskirk, A.R. (2013). Nascent peptides that block protein synthesis in bacteria. Proceedings of the National Academy of Sciences *110*, E878-E887.

Wriggers, W. (2012). Conventions and workflows for using Situs. Acta Crystallographica Section D: Biological Crystallography *68*, 344-351.

Xiao, H., Murakami, H., Suga, H., and Ferré-D'Amaré, A.R. (2008). Structural basis of specific tRNA aminoacylation by a small *in vitro* selected ribozyme. Nature *454*, 358-361.

Yanagisawa, T., Sumida, T., Ishii, R., Takemoto, C., and Yokoyama, S. (2010). A paralog of lysyl-tRNA synthetase aminoacylates a conserved lysine residue in translation elongation factor P. Nat Struct Mol Biol *17*, 1136-1143.

Youngman, E.M., Brunelle, J.L., Kochaniak, A.B., and Green, R. (2004). The active site of the ribosome is composed of two layers of conserved nucleotides with distinct roles in peptide bond formation and peptide release. Cell *117*, 589-599.

Yutin, N., Puigbò, P., Koonin, E.V., and Wolf, Y.I. (2012). Phylogenomics of Prokaryotic Ribosomal Proteins. PLOS ONE *7*, e36972.

Zahn, M., Berthold, N., Kieslich, B., Knappe, D., Hoffmann, R., and Sträter, N. (2013). Structural studies on the forward and reverse binding modes of peptides to the chaperone DnaK. Journal of molecular biology *425*, 2463-2479.

Zahn, M., Kieslich, B., Berthold, N., Knappe, D., Hoffmann, R., and Strater, N. (2014). Structural identification of DnaK binding sites within bovine and sheep bactenecin Bac7. Protein and peptide letters *21*, 407-412.

Zanetti, M., Litteri, L., Gennaro, R., Horstmann, H., and Romeo, D. (1990). Bactenecins, defense polypeptides of bovine neutrophils, are generated from precursor molecules stored in the large granules. The Journal of Cell Biology *111*, 1363-1371.

Zavialov, A.V., Buckingham, R.H., and Ehrenberg, M. (2001). A posttermination ribosomal complex is the guanine nucleotide exchange factor for peptide release factor RF3. Cell *107*, 115-124.

Zgurskaya, H.I., López, C.A., and Gnanakaran, S. (2015). Permeability barrier of Gram-negative cell envelopes and approaches to bypass it. ACS infectious diseases *1*, 512-522.

Zhang, J., Pan, X., Yan, K., Sun, S., Gao, N., and Sui, S.-F. (2015). Mechanisms of ribosome stalling by SecM at multiple elongation steps. elife *4*, e09684.

Zheng, S., Palovcak, E., Armache, J.-P., Cheng, Y., and Agard, D. (2016). Anisotropic correction of beam-induced motion for improved single-particle electron cryo-microscopy. bioRxiv, 061960.

Zheng, S.Q., Palovcak, E., Armache, J.-P., Verba, K.A., Cheng, Y., and Agard, D.A. (2017). MotionCor2: anisotropic correction of beam-induced motion for improved cryo-electron microscopy. Nature methods *14*.

Zhong, P., and Shortridge, V. (2001). The emerging new generation of antibiotic: ketolides. Current Drug Targets-Infectious Disorders *1*, 125-131.

Zhou, J., Lancaster, L., Donohue, J.P., and Noller, H.F. (2013). Crystal Structures of EF-G–Ribosome Complexes Trapped in Intermediate States of Translocation. Science *340*.

Zou, S.B., Roy, H., Ibba, M., and Navarre, W.W. (2011). Elongation factor P mediates a novel post-transcriptional regulatory pathway critical for bacterial virulence. Virulence *2*, 147-151.

9. Curriculum vitae

Education

05/2014 – Present *Institut européen de Chemie et Biologie (IECB), Pessac, France*
PhD thesis under the supervision of Dr. Axel Innis
"Inhibition of bacterial protein synthesis by nascent chain and free peptides."

02/2014 *Ludwig Maximilian University (LMU), Munich, Germany*
Graduation Master of Science (final grade 1.14, very good)

10/2011 – 02/2014 *LMU, Munich, Germany*
Master studies in Biochemistry (Major subject 1), Cell biology (major subject 2) and Structural Biology (Minor subject)

08/2013 – 02/2014 *Gene center, Munich, Germany*
Master thesis under the supervision of Dr. Daniel Wilson
"Studies of non-canonical translation factors, EF-P, YeiP and LepA"

08/2012 – 01/2013 *University of California Riverside (UCR), Riverside, USA*
Research lab course under the supervision of Dr. Gregor Blaha
"Cloning, Expression and Protein purification of SpoT from β- and γ-Proteobacteria."

04/ – 05/2012 *Biocenter, LMU, Munich, Germany*
Research lab course under the supervision of Prof. Angelika Boettger
"BrdU in the whole animal/ SAHM and the differentiation of Nematocytes/ Regneration of transgenic β-catenin animals *Hydra vulgaris*"

09/2011 *LMU, Munich, Germany*
Graduation: Bachelor of Science (final grade 2.01, good)

10/2008 – 09/2011 *LMU, Munich, Germany*
Bachelor studies in Chemistry and Biochemistry with specialization on Biochemistry and Physical Chemistry
Bachelor thesis under the supervision of Prof. Patrick Cramer
"Cloning, expression and purification of the capping enzyme Cet1 and Ceg1 (*Saccharomyces cerevisiae*)"

07/2008 *Hebel-Gymnasium, Schwetzingen, Germany*
Abitur (university entrance diploma) Award for excellent performance in the Chemistry Final Exam of the Society of German Chemists (GDCh) (final grade 1.5; very good)

Professional experience:

Participation at the BCA-CCP4 summer school at the Diamond Synchrotron in Didcot, UK (21st-26th August 2016) to deepen knowledge about X-ray crystallography and related bioinformatic tools

Head of the organization committee for the "9th Young Scientist Symposium" at the Institute Européen de la Chimie et Biologie, Pessac, France (26th – 27th May 2016) International annual conference, aiming for interaction of Young Scientists.

Member of the organization committee for the "8th Young Scientist Symposium" at the Institute Européen de la Chimie et Biologie, Pessac, France (21st – 22nd May 2015)

Teaching assistant in mathematics, biochemistry and cell biology

Active member in the student council of the LMU Chemistry Department (working field Biochemistry)

Publications

Peer-reviewed:

Graf, M., Mardirossian, M., Nguyen, F., **Seefeldt, A.C**., Guichard, G., Scocchi, M., Innis, C.A., Wilson, D.N. (2017). Proline-rich antimicrobial peptides targeting protein synthesis. *Nat Prod Rep.* doi:10.1039/C7NP00020K

Seefeldt AC, Graf M, Pérébaskine N, Nguyen F, Arenz S, Mardirossian M, Scocchi M, Wilson DN, Innis CA: Structure of the mammalian antimicrobial peptide Bac7(1-16) bound within the exit tunnel of a bacterial ribosome. *Nucleic Acids Res*. 2016 Mar 18;44(5):2429-38. PDB codes: 5F8K, 5FDU, 5FDV

Seefeldt AC, Nguyen F, Antunes S, Pérébaskine N, Graf M, Arenz S, Inampudi KK, Douat C, Guichard G, Wilson DN, Innis CA: The proline-rich antimicrobial peptide Onc112 inhibits translation by blocking and destabilization of the initiation complex. *Nat Struct Mol Biol.* 2015 Jun;22(6):470-5. PDB code: 4ZER
(Highlighted in "This week in Microbiology": http://www.microbeworld.org/podcasts/this-week-in-microbiology/archives/1923-twim-105-real-bugs-with-legs)

Münder S, Tischer S, Grundhuber M, Büchels N, Bruckmeier N, Eckert S, **Seefeldt CA**, Prexl A, Käsbauer T, Böttger A: Notch-signalling is required for head regeneration and tentacle patterning in hydra*. Dev Biol.* 2013 Sep 5.

Non-refereed articles

A Carolin Seefeldt and Britta Seip. Kurze Peptide regulieren die Aktivität bakterieller Ribosomen. Biospektrum der Wissenschaft, in press. (2017)

Conferences contributions:

A Carolin Seefeldt, K Kishore Inampudi, Caterina Lombardo, Christophe André, Thomas A Steitz, Gilles Guichard and C Axel Innis
Using the flexizyme methodology to study translational arrest mediated by short peptides
Poster communication at the Proteins Synthesis and Translational Control meeting, EMBL, Heidelberg, Germany (September 2017)

A Carolin Seefeldt, Fabian Nguyen, Michael Graf, Stéphanie Antunes, Natacha Pérébaskine, Stefan Arenz, K Kishore Inampudi, Mario Mardirossian, Céline Douat, Marco Scocchi, Gilles Guichard, Daniel N Wilson and C Axel Innis
The proline-rich antimicrobial peptides Bac7, Onc112, Pyr and MetI inhibit translation by blocking and destabilizing the initiation complex
Oral communication at the 10th Young Scientist Symposium at the IECB, Pessac, France, (May 2017)
Poster communication at the Ribosome structure and function 2016, EMBO meeting, Strasbourg, France, (July 2016)
Oral communication at the 10ièmes Journées de l'Association bordelaise de Cristallographie, Bordeaux, France (June 2016)
Poster communication at the 8th RNA symposium, IECB, Bordeaux, France (June 2016), awarded with 3rd prize for poster communication

A Carolin Seefeldt, Fabian Nguyen, Stéphanie Antunes, Natacha Pérébaskine, Michael Graf, Stefan Arenz, K Kishore Inampudi, Céline Douat, Gilles Guichard, Daniel N Wilson and C Axel Innis
The proline-rich antimicrobial peptide Onc112 inhibits translation by blocking and destabilizing the initiation complex
Poster communication at the Proteins Synthesis and Translational Control meeting, EMBL, Heidelberg, Germany (September 2015)
Oral communication at the 7th RNA workshop, IECB, Bordeaux, France (June 2015)

10. Supplemental information

10.1 DNA primer lists

Table 39:Primer list for aminoacyl-tRNA synthetase cloning

Name	Sequence	Plasmid	Organism	Restriction enzymes
EF-P_thermus_FW	CCGCGCGGCAGCCATATGATCAGCGTGACGG	pMKE2	*T. thermuphilus*	NdeI, NcoI
EF-P_Thermus_RV:	GTGCTCGAGTGCGGCCCTAGGCCCGGCCCAC	pMKE2	*T. thermuphilus*	NdeI, NcoI
TrpRS_FW_1	GGAGATATATCC**ATG**ACTAAGCCCATCGTTTTTAGTG	pBAT4	*E. coli*	NdeI, NcoI
TrpRS_RV_1	AGCTTATGCATGCGGTTAgtggtggtggtggtggtgCGGCTTCGCCACAAAAC	pBAT4	*E. coli*	NdeI, NcoI
asnS_For1	GGAGATATATCC**ATG**ATGcaccaccaccaccaccaccacATGAGCGTTGTGCCTG	pBAT4	*E. coli*	NdeI, NcoI
asnS_Rev1	AGCTTATGCATGCGGTTAGAAGCTGGCGTTACG	pBAT4	*E. coli*	NdeI, NcoI
aspS_FV	GGAGATATATCC**ATG**CGTACAGAATATTGTG	pBAT4	*E. coli*	NdeI, NcoI
aspS_RV	AGCTTATGCATGCGGTTAgtggtggtggtggtggtgGTTATTCTCAGCCTTC	pBAT4	*E. coli*	NdeI, NcoI
glyS_RS FV1	GGAGATATATCC**ATG**CAAAAGTTTGATACCAGG	pBAT4	*E. coli*	NdeI, NcoI
glyRS_RV 1	AGCTTATGCATGCGGTTAgtggtggtggtggtggtgTTGCAACAGCGAAATATC	pBAT4	*E. coli*	NdeI, NcoI
Arg_FW NEW	GGAGATATATCC**ATG**ATGcaccaccaccaccaccaccacGTGAATATTCAGGCTC	pBAT4	*E. coli*	NdeI, NcoI
ARG RV NEW	AGCTTATGCATGCGGTTACATACGCTCTAC	pBAT4	*E. coli*	NdeI, NcoI

Table 40: DNA primers for mutagenesis for *T. thermophilus* EF-P

Name	Sequence
TthEFP_complete_ecoliloop_FW :	CGGC CTT TGG GAG TGC GTG GAG AGT GAA TTC GTA AAA CCG GGT AAA GGC CAG GCA TTT GCT CGC
TthEFP_complete_ecoliloop_RV:	CCGTGGCCCCCGTCTCCAGGTTCTTGAACTTGGCGCGAGCAAATGCCTGGCCTTTACCCGGTTTTACGAATTCACT
Ecoli loop HQ FW	GGC CTT TGG GAG TGC GTG GAG AGT GAA CAC CAG AAA CCG GGT AAA GGC CAG GCA TTT GCT CGC
Ecoli loop HQ RV:	CAGGTTCTTGAACTTGGCGCGAGCAAATGCCTGGCCTTTACCCGGTTTCTGGTGTTCACT

Table 41: DNA primers for tRNA cloning

Name	Sequence	Plasmid	Restriction enzyme
tRNAPro_CGG_NAV2-FWshort:	AACTTTGTGTAATACCGG	pBSTNAV2OK	EcoRI, PstI
tRNAPro_CGG_NAV2-FW1:	CTTTGTGTAATACCGGTGATTGGCGCAGCCTGGTAGCG	pBSTNAV2OK	EcoRI, PstI
tRNAPro_CGG_NAV2-Rev2:	ACCTCCGACCCCTTCGTCCCGAACGAAGTGCGCTACCAGGCTG	pBSTNAV2OK	EcoRI, PstI
tRNAPro_CGG_NAV2-FW2:	GGGGTCGGAGGTTCGAATCCTCTATCACCGACCA	pBSTNAV2OK	EcoRI, PstI
tRNAPro_CGG_NAV2-Rev2:	CTTTCGCTAAGATCTGCAGTGGTCGGTGATAGAGG	pBSTNAV2OK	EcoRI, PstI
tRNAPro_CGG_NAV2-Revshort	CTTTCGCTAAGATCTGC	pBSTNAV2OK	EcoRI, PstI
tRNAPro_CGG_NAV3-FW1:	GTGTAATACTTGTAACGCCGGTGATTGGCGCAGCCTGGTAGCG	pBSTNAV3OK	SacII, PstI
tRNAPro_CGG_NAV3-FW1_short	GTGTAATACTTGTAACGCC	pBSTNAV3OK	SacII, PstI
Puc19 T7 promotor RV	TATAGTGAGTCGTATTAgATTCACTGGCCGTCG	pUC19	EcoRI, HindIII
PUC19 T7 terminator FW	CTAGCATAACCCCTTGGGGCCTCTAAACGGGTCTTGAGGGGTTTTTTGAAGCTTGGCGTAATCATGG	pUC19	EcoRI, HindIII
WtRNA FV T7prom	CGACTCACTATAGccctaattAGGGGCGTAGTTCAATTG	pUC19	EcoRI, HindIII
WtRNA RV beg	CGGTTTTGGAGACCGGTGCTCTACCAATTGAACTACGC	pUC19	EcoRI, HindIII
WtRNA FV end	CGGTCTCCAAAACCGGGTGTTGGGAGTTCGAGTCTCTCCGCCCC	pUC19	EcoRI, HindIII
WtRNA RV T7term	CAAGGGGTTATGCTAGggatgatttcTGGCAGGGGCGGAGAGAC	pUC19	EcoRI, HindIII

Table 42: DNA Primer for toeprinting templates

Name	DNA sequence	Amino acid sequence
PURE_fwd_short:	CGATCGAATTCTAATACGACTCACTATAG	
PURE_fragment1_fwd:	CGATCGAATTCTAATACGACTCACTATAGGGCTTAAGTATAAGGAGGAAAAAATATG	
TP_frag2_rev	CTTGCCTGCGCACGAAGAGTACGGATGTTGTTCAGAGTCAGTTATTATTCGCT	
TP_frag2_NV_rev	GGTTATAATGAATTTTGCTTATTAACCTTGCCTGCGCACG	
TP_rev_short	GGTTATAATGAATTTTGCTT	
TP_ermAL_ORF	GgaggaaaaaatatgtgcaccagtatcgcagtagtaAGCGAATAATAACTGACTCTG	MCTSIAVVSE*
TP_ermBL_ORF	GgaggaaaaaatatgttggtattccaaatgcgtaatgtagataaaAGCGAATAATAACTGACTCTG	MLVFQMRNVDKSE*
TP_ermCL_ORF	GgaggaaaaaatatgggcatttttagtatttttgtaatcagcAGCGAATAATAACTGACTCTG	MGIFSIFVISSE*
TP_ermDL_ORF	Ggaggaaaaaatatgacacactcaatgagacttcgt AGCGAATAATAACTGACTCTG	MTHSMRLRSE*
TP_secM_template	GgaggaaaaaatatgTTCAGCACGCCC GTC TGG ATAAGCCAGGCGCAAGGCATC CGT GCT GGC CCTGCGATCTCGGTGTAtaaTAA CTG ACT CTGAACAACATCCGTACTCTT CGT GCG CAGGCAAGGTTAATAAGCAA AAT TCA TTA TAACC	MFSTPVWISQAQGIRAGPAISV
TP_MRFRI_AGG	GgaggaaaaaatatgaggTTaggatcTAATAACTGACTCTG	MRFRI*
TP_MKFRI_AGG	GgaggaaaaaatatgaagTTTaggatcTAATAACTGACTCTG	MKFRI*
TP_MRFKI_AGG	GgaggaaaaaatatgaggTTTaagatcTAATAACTGACTCTG	MRFKI*
TP_MKFKI	GgaggaaaaaatatgaagTTTaagatcTAATAACTGACTCTG	MKFKI*
TP_MFRI_AGG	GgaggaaaaaatatgTTTaggatcTAATAACTGACTCTG	MFRI*
TP_MHHHHHHRPPPI_AGG	GgaggaaaaaatatgATGCATCATCATCATCATCACCGTCCGCCGCCGATCTAATAACTGACTCTG	MHHHHHHRPPPI*
TP_MRPPPI_AGG	Ggaggaaaaaatatgaggccgccgccgatctaataactgactctg	MRPPPI*

Name	DNA sequence	Amino acid sequence
TP_MRI_AGG	Ggaggaaaaaatatgaggatctaataactgactctg	MRI*
TP_MKFRI_AGG	Ggaggaaaaaatatgaaatttaggatctaataactgactctg	MKFRI*
T7 prom	ATTAATACGACTCACTATAGGG	
T7-SD-AUG_MFR	ATTAATACGACTCACTATAGGGatataaggaggaaaaCatatgTTTCGT	
ORF1 RV_MFRI	GATGTTGTTCAGAGTTTAGATACGAAAcatatGtttttctttcc	
ORF 2 FW_MFRI	ACTCTGAACAACATCCGTACTCTTCGTGCCG	
ORF3 RV NV1	GGTTATAATGAATTTTGCTTATTAACCTTGCCTGCGCACGAAGAGTACG	
NV1 RV	GGTTATAATGAATTTTGCTTATTAAC	
T7SD_MRFRI_CCTFw	ATTAATACGACTCACTATAGGGatataaggaggaaaaCatatgAGGTTTA	
TP_MRFRI_CCTRv	GATGTTGTTCAGAGTTTAGATCCTAAACCTcatatGtttc	

DNA primers to generate the flexizyme DNA templates were used as published previously. Following to DNA template generation, the construct was large scale (10 mL reaction) *in vitro* transcribed (Goto et al. 2011).

10.2 Canonical base orientations

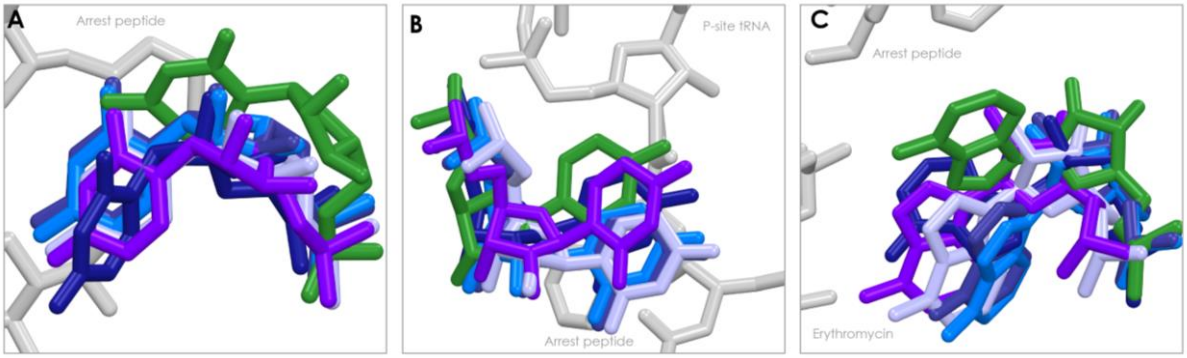

Figure 64: Additional conformations of U2506 (A), U2585 (B) and A2062 (C) during pre-accommodation, catalysis and translocation. The conformation of the different bases for the MKF-70S structure is shown in green. Bases from the structure of the pre-accommodation state has the PDB code: 1VQ6 and is shown in density. Bases from the Pre (PDB code: 1VY4) and Post catalysis state (PDB code: 1VY5) are shown in marine and slate, respectively. Bases from the structure of the Pre- (PDB code: 4WPO) and Post-translocation (4WQY) are shown in light blue and purple respectively. The bases adopt in all cases different orientations than in the MKF-70S structure

10.3 tRNA^{Pro} modifications

proK is the only tRNA^{Pro} which is listed in the MODOMICS database. Modifications include the two standard modifications pseudouridine and dihydrouridine. Other modifications include methylations of the bases. The modifications are listed in the following figure:

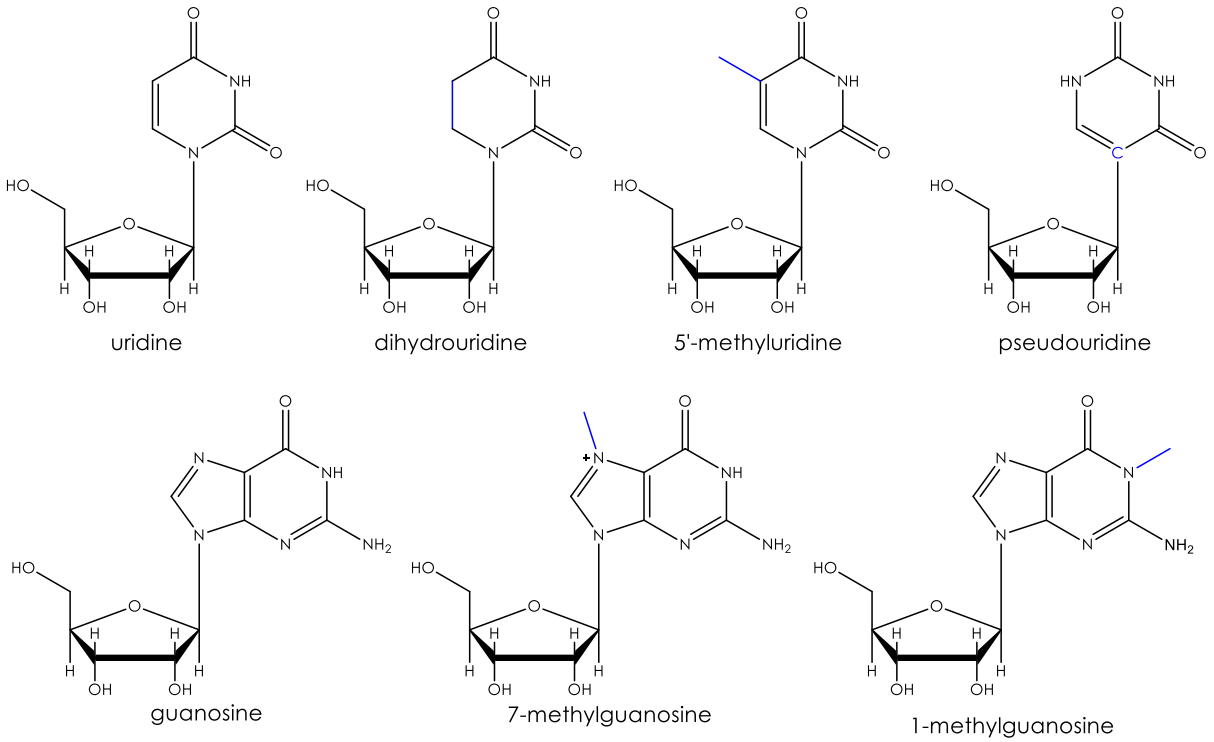

Figure 65: Base modification found in *proK*. Differences are highlighted in blue. Dihydrouridine, thymine (5-methyluridine) and pseudouridine are derrived from uridine. 7-methylguanosine and 1-methylguanosine are modified guanosine bases. Modifications were listed on the MODONOMICS database.

10.4 Ribosome purification

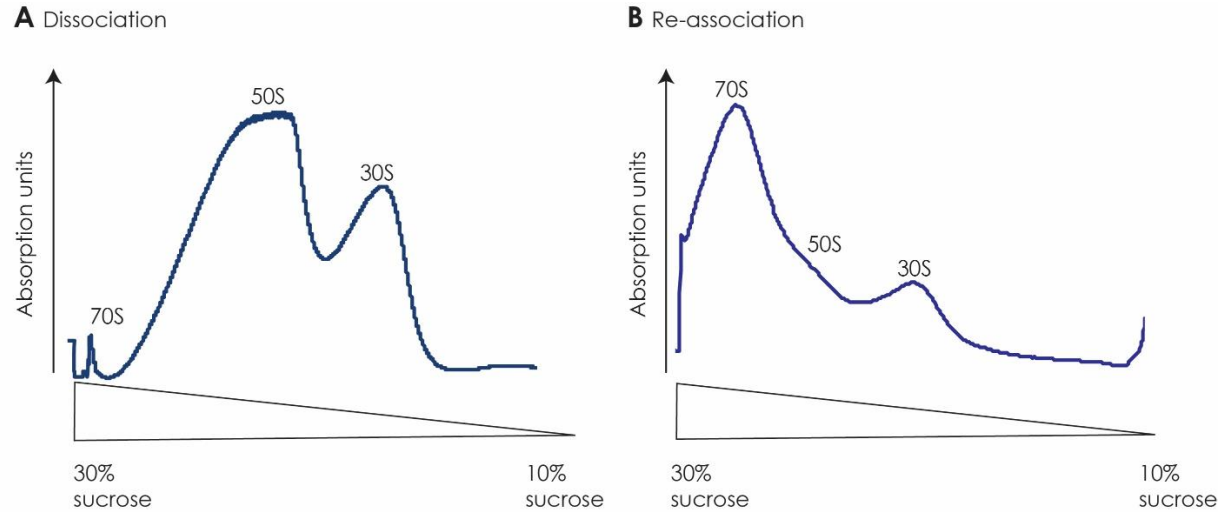

Figure 66: Sucrose gradients of the 70S *E. coli* ribosome purification. Ribosomes were purified by sucrose gradients. The ribosomes were dissociated by reducing the Mg^{2+} ion concentration and the subunits were purified by sucrose gradients (A). Subsequently, the ribosomes were re-assembled and the 70S peak was taken (Blaha et al., 2000).

10.5 MKF-CME flexizyme reaction

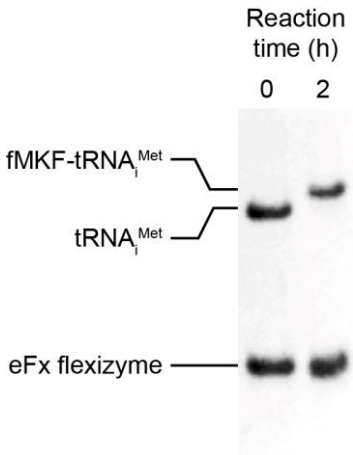

Figure 67: fMKF-CME flexizyme reaction performed by Dr. K. Kishore Inampudi. After 2h reaction on ice the initiator tRNA is peptidylated.

10.6 Protein purifications

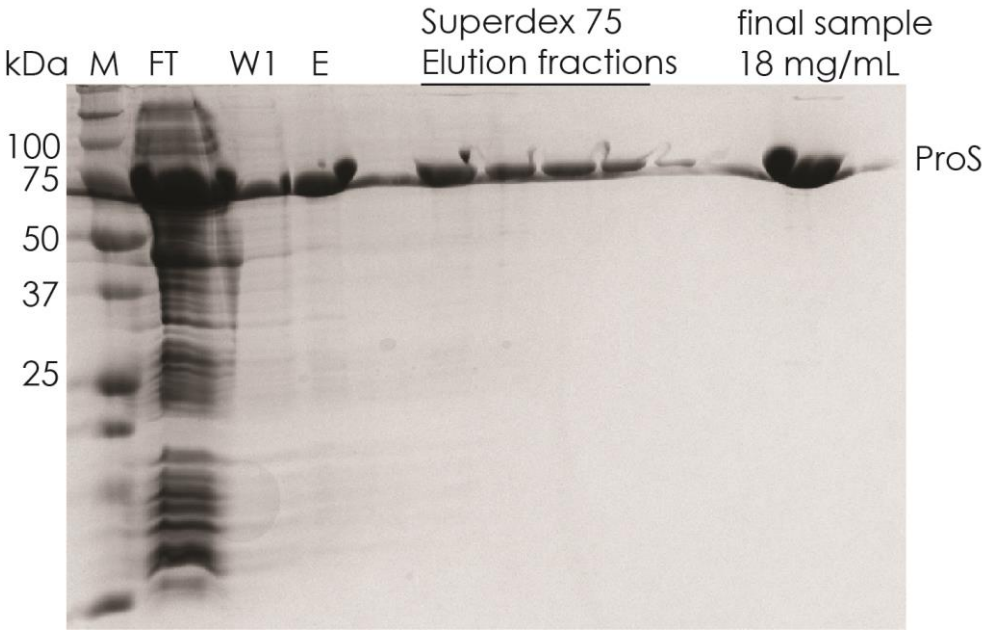

Figure 68: ProS purification steps analyzed by SDS-PAGE. M stands for Marker, FT for flow through, W1 for the last washing step, E for the elution fractions from the Co^{2+}-NTA column. Next samples correspond to the elution fractions from the gel filtration. The final sample was concentrated to a final concentration of 18 mg/mL.

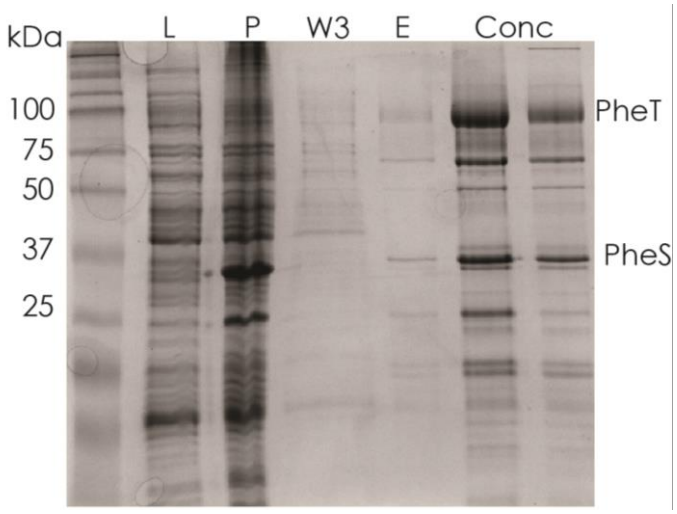

Figure 69: PheST purification steps analyzed by SDS-PAGE. M stands for Marker, FT for flow through, W3 for the last washing step, E for the elution fractions from the Ni^{2+}-NTA column. The buffer was exchanged over concentrators and samples were taken throughout this step (Conc).

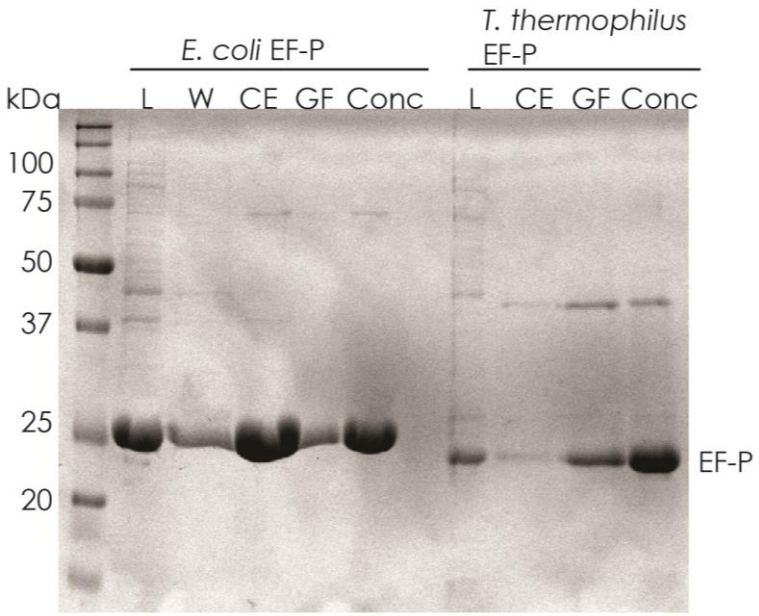

Figure 70: *E. coli* and *T. thermophilus* EF-P purification steps analyzed by SDS-PAGE. L stands for lysis, W for the last washing step, CE stands for elution fraction from Co^{2+}-NTA column, GF stand for pulled fractions from gel filtration and Conc corresponds to the sample taken after concentrating the sample to 20 mg/mL and before flash freezing.

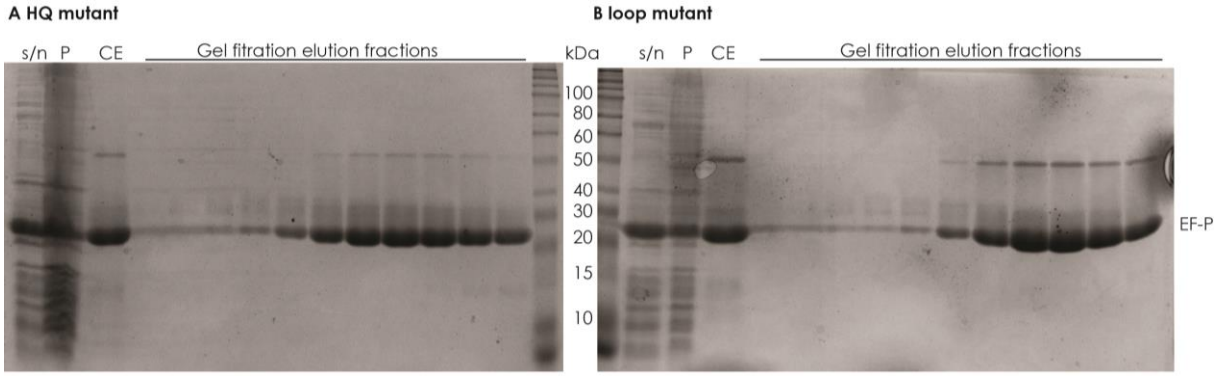

Figure 71: Purification of the *T. thermophilus* mutants by SDS-PAGE. s/n stands for supernatant, P stands for pellet, CE stands for elution fraction from Co^{2+}-NTA column. Next lanes, correspond to the elution fractions of the corresponding gel filtration

10.7 Sequencing results

Sequencing results were analyzed using the alignment tool Multalign.

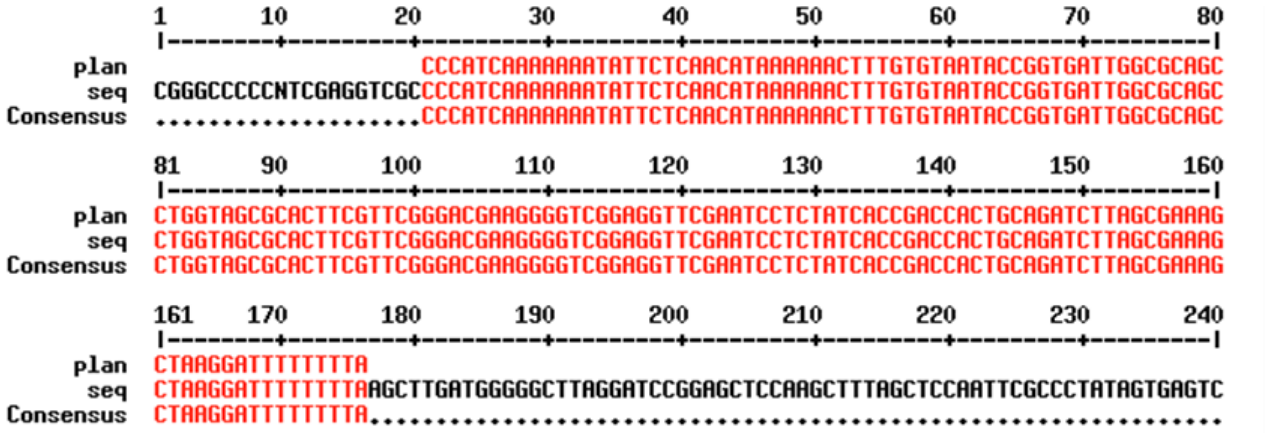

Figure 72: Sequencing results for proK-pBSTNAV2OK

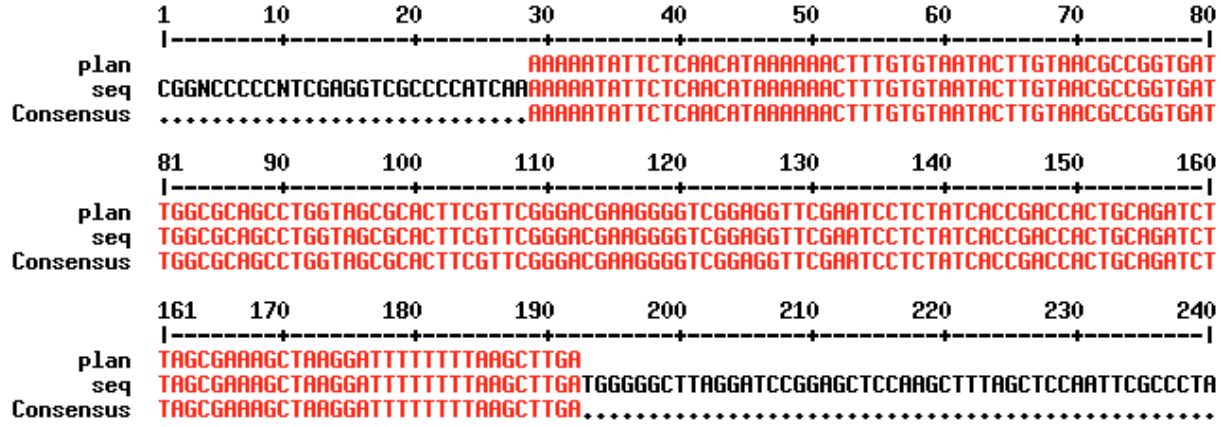

Figure 73: Sequencing results for tRNA^{Pro} into pBSTNAV3S vector.

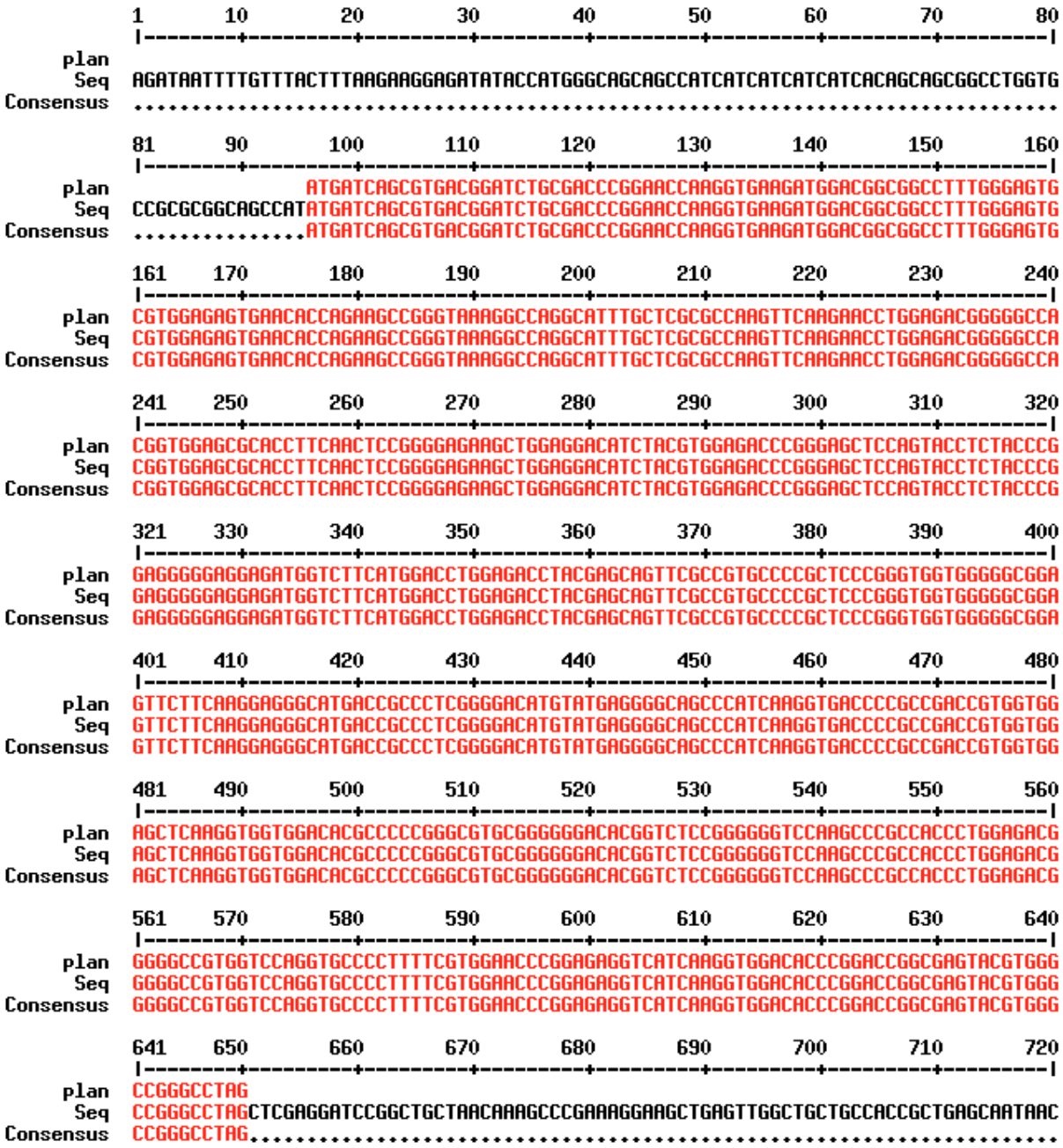

Figure 74: sequencing result of *Tth* EF-P HQ mutant

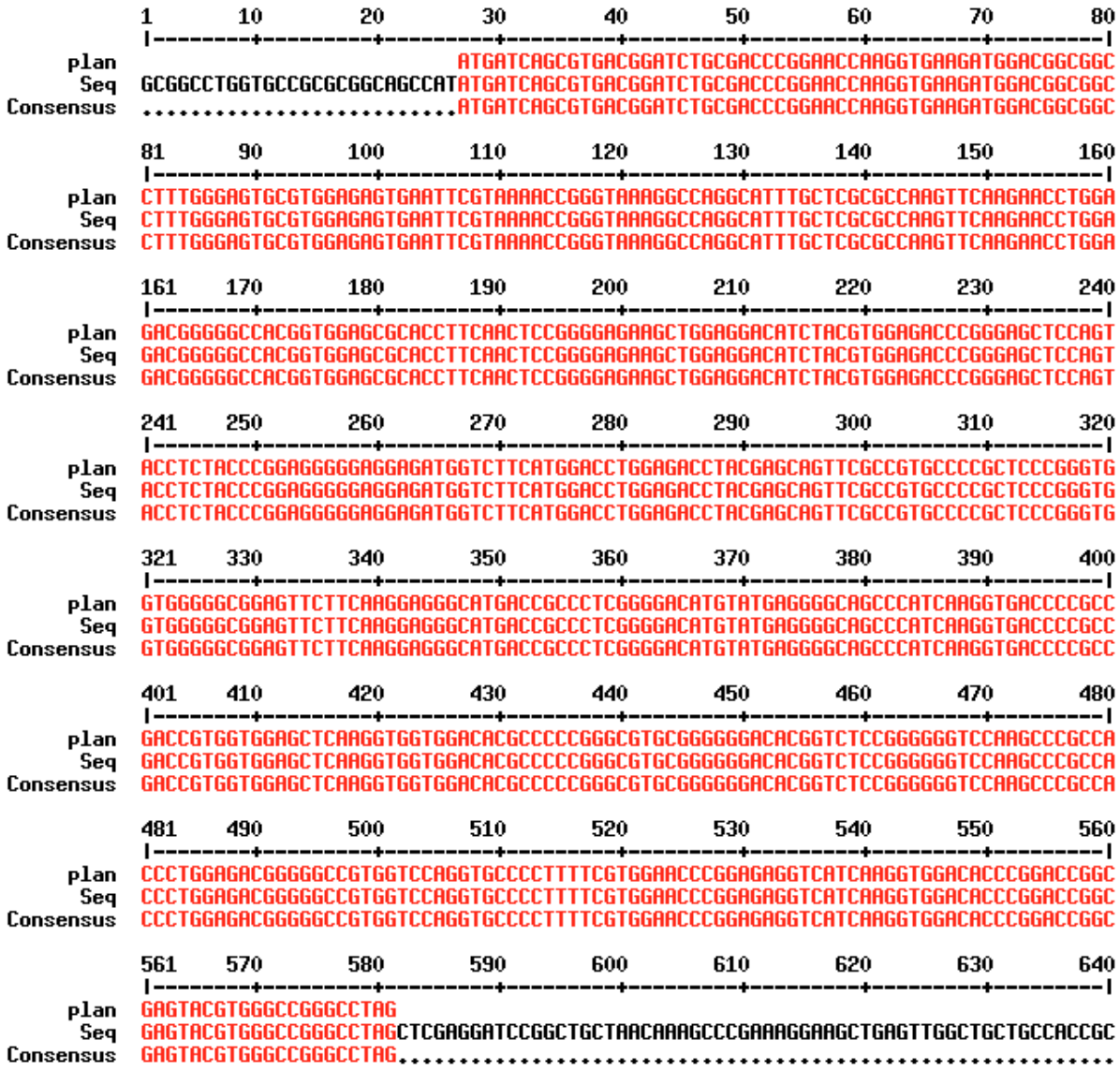

Figure 75: Sequencing result from mutagenesis to generate *Tth* EF-P mutant incl ecoli loop.

10.8 Purity of flexizyme compounds

The following analysis were performed, written and kindly provided by Dr. Christophe André

Formyl-Met-Arg-DBE•HCl (CA 1-192)

General procedure for the synthesis of 3,5-dinitrobenzyl ester was used from Formyl-Met-Arg(Pbf)-OH (150 mg, 0.26 mmol) to led to the titled activated ester peptide as a white solid *lyophilisate* (38 mg, 28 %).

HPLC: t_R = 5.57 min; **MS (ESI+)**: (m/z) = 514.1335 $[M+H]^+$

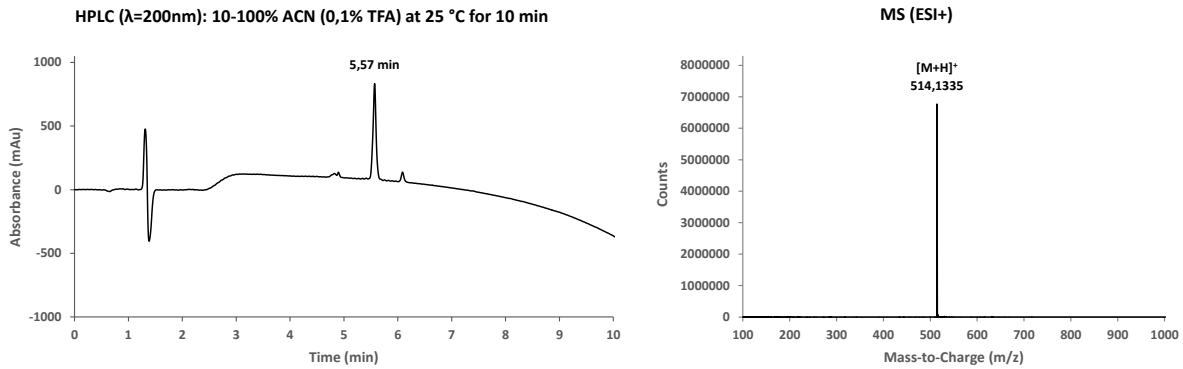

Acetyl-Arg-Pro-DBE•HCl (CA 1-194)

General procedure for the synthesis of 3,5-dinitrobenzyl ester was used from Acetyl-Arg(Pbf)-Pro-OH (150 mg, 0.27 mmol) to led to the titled activated ester peptide as a white solid *lyophilisate* (13 mg, 10 %).

HPLC: t_R = 5.21 min; **MS (ESI+)**: (*m/z*) = 494.1591 $[M+H]^+$

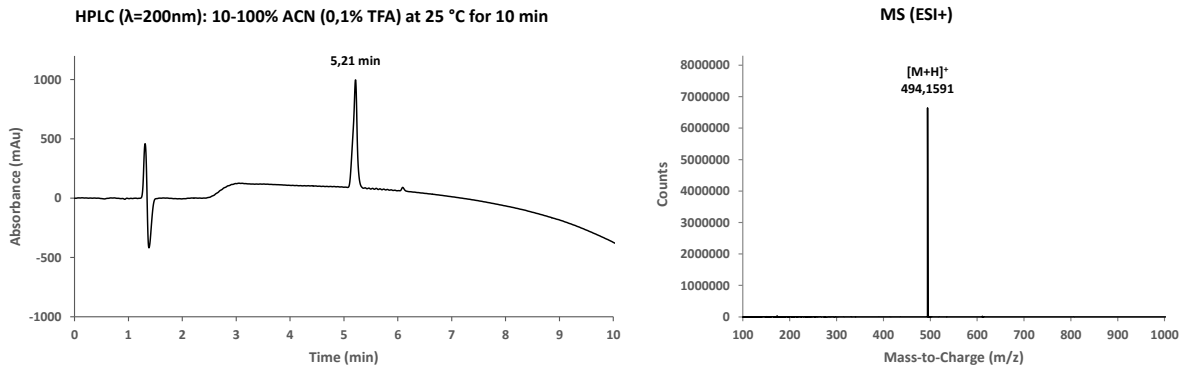

Formyl-Met-Arg-CBT•HCl (CA 2-(8)16)

General procedure for the synthesis of 4-chlorobenzyl thioester was used from Formyl-Met-Arg(Pbf)-OH (150 mg, 0.26 mmol) to led to the titled activated thioester peptide as a white solid *lyophilisate* (39 mg, 31 %).

HPLC: t_R = 6.25 min; **MS (ESI+)**: (*m/z*) = 474.1005 $[M+H]^+$

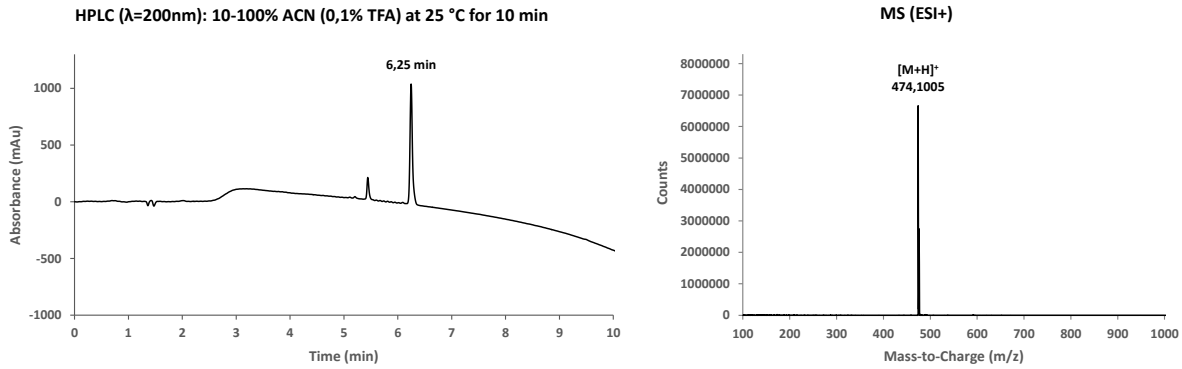

Acetyl-Arg-Pro-CBT•HCl (CA 2-(12)20)

General procedure for the synthesis of 4-chlorobenzyl thioester was used from Acetyl-Arg(Pbf)-Pro-OH (150 mg, 0.26 mmol) to led to the titled activated thioester peptide as a white solid *lyophilisate* (19 mg, 16 %).

HPLC: t_R = 5.84 min; **MS (ESI+)**: (*m/z*) = 454.1295 $[M+H]^+$

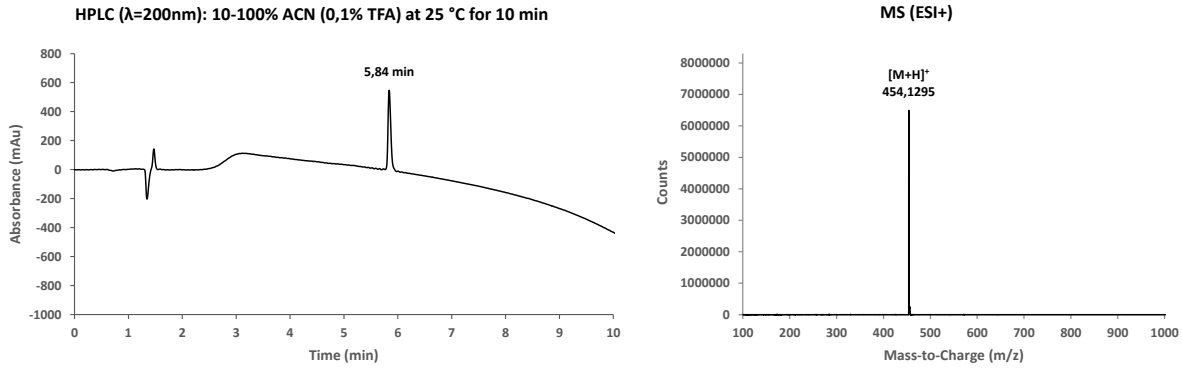

Acetyl-Arg-Asp-CBT•HCl (CA 2-144)

General procedure for the synthesis of 4-chlorobenzyl thioester was used from Acetyl-Arg(Pbf)-Asp(tBu)-OH (100 mg, 0.16 mmol) to led to the titled activated thioester peptide as a white solid *lyophilisate* (28 mg, 38 %).

HPLC: t_R = 4.86 min; **MS (ESI+)**: (*m/z*) = 472.1047 $[M+H]^+$

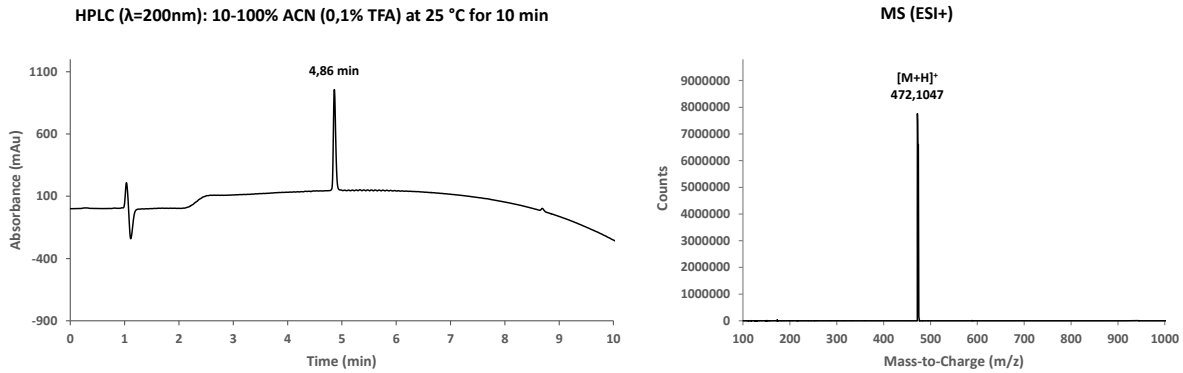

Acetyl-Arg-Ala-CBT•HCl (CA 3-48)

General procedure for the synthesis of 4-chlorobenzyl thioester was used from Acetyl-Arg(Pbf)-Ala-OH (200 mg, 0.31 mmol) to led to the titled activated thioester peptide as a white solid *lyophilisate* (44 mg, 33 %).

HPLC: t_R = 5.20 min; **MS (ESI+)**: (*m/z*) = 428.0727 $[M+H]^+$

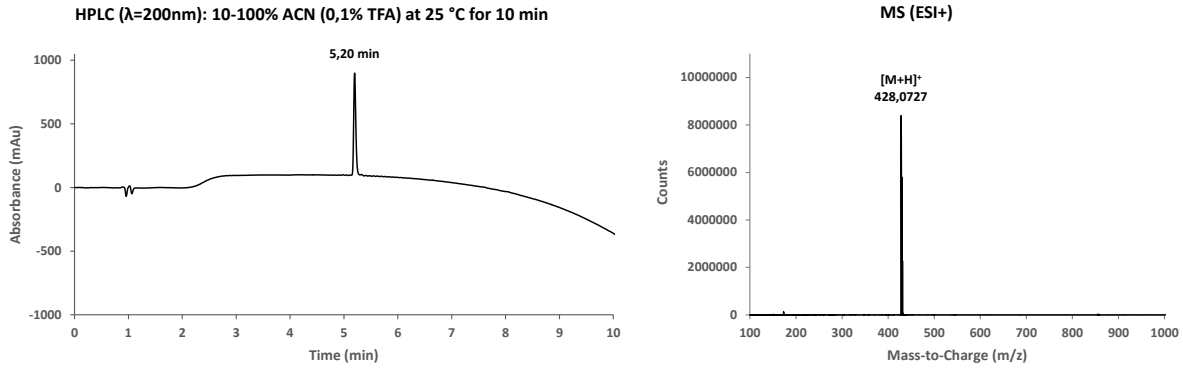

Formyl-Met-Lys-CBT•HCl (CA 3-60)

General procedure for the synthesis of 4-chlorobenzyl thioester was used from Formyl-Met-Lys(Boc)-OH (200 mg, 0.49 mmol) to led to the titled activated thioester peptide as a white solid *lyophilisate* (54 mg, 25 %).

HPLC: t_R = 5.77 min; **MS (ESI+)**: (*m/z*) = 446.0484 $[M+H]^+$

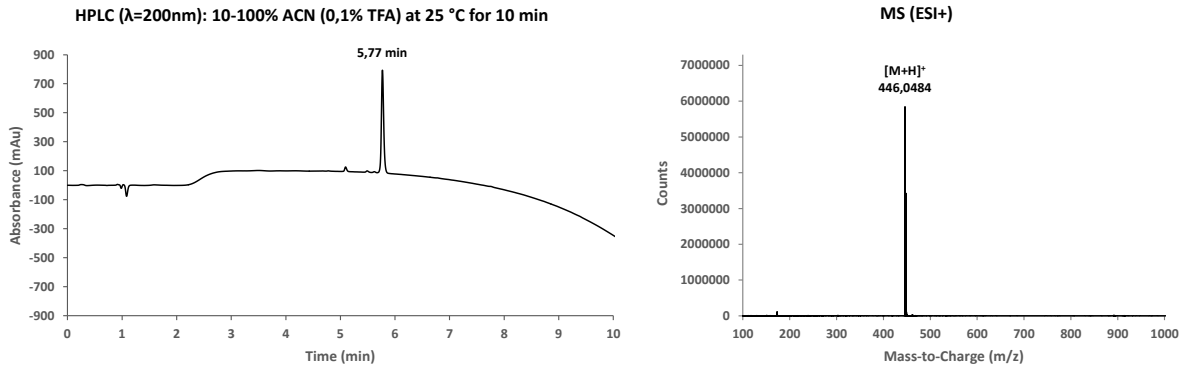

Acetyl-Arg-Ala-Pro-CBT•HCl (CA 3-102)

General procedure for the synthesis of 4-chlorobenzyl thioester was used from Acetyl-Arg(Pbf)-Ala-Pro-OH (200 mg, 0.31 mmol) to led to the titled activated thioester peptide as a white solid *lyophilisate* (31 mg, 19 %).

HPLC: t_R = 5.47 min; **MS (ESI+)**: (*m/z*) = 252.1155 $[M+H]^+$

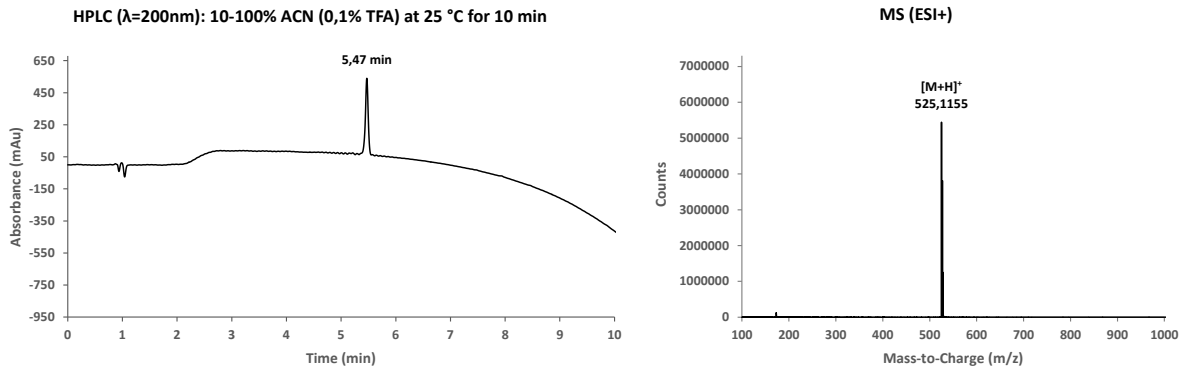

Acetyl-Arg-Asp-Pro-CBT•HCl (CA 3-104)

General procedure for the synthesis of 4-chlorobenzyl thioester was used from Acetyl-Arg(Pbf)-Asp(tBu)-Pro-OH (200 mg, 0.27 mmol) to led to the titled activated thioester peptide as a white solid *lyophilisate* (27 mg, 17 %).

HPLC: t_R = 5.06 min; **MS (ESI+)**: (*m/z*) = 569.0996 $[M+H]^+$

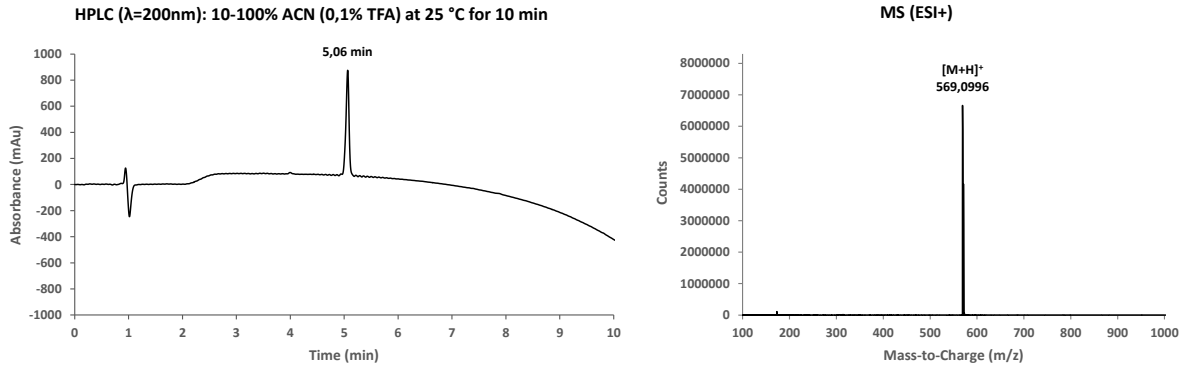

Formyl-Met-Lys-Phe-CME•TFA (CA 4-104)

General procedure for the synthesis of cyanomethyl ester was used from Formyl-Met-Lys(Boc)-Phe-OH (150 mg, 0.27 mmol) to led to the titled activated ester peptide as a white solid *lyophilisate* (37 mg, 28 %).

HPLC: t_R = 4.31 min; **MS (ESI+)**: (*m/z*) = 492.2331 $[M+H]^+$

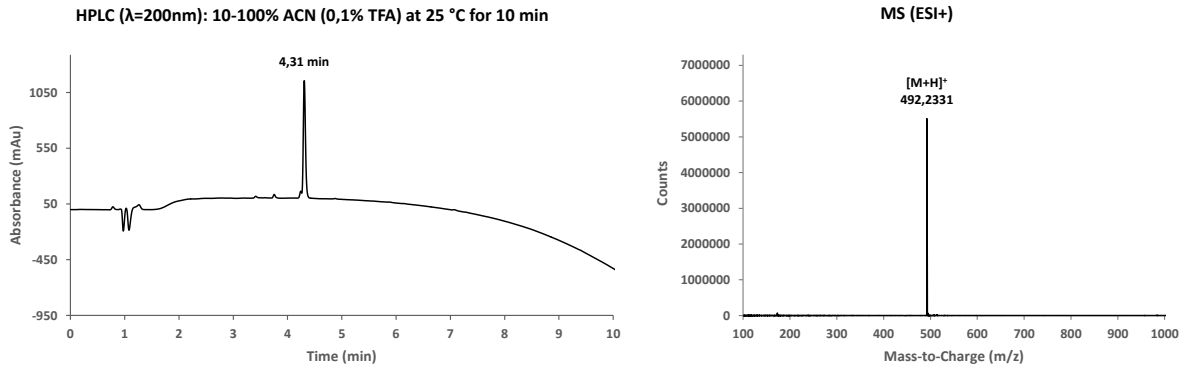

Acetyl-Lys-Phe-CME•TFA (CA 4-112)

General procedure for the synthesis of cyanomethyl ester was used from Acetyl-Lys(Boc)-Phe-OH (150 mg, 0.34 mmol) to led to the titled activated ester peptide as a white solid *lyophilisate* (36 mg, 28 %).

HPLC: t_R = 3.65 min; **MS (ESI+)**: (*m/z*) = 375.2104 $[M+H]^+$

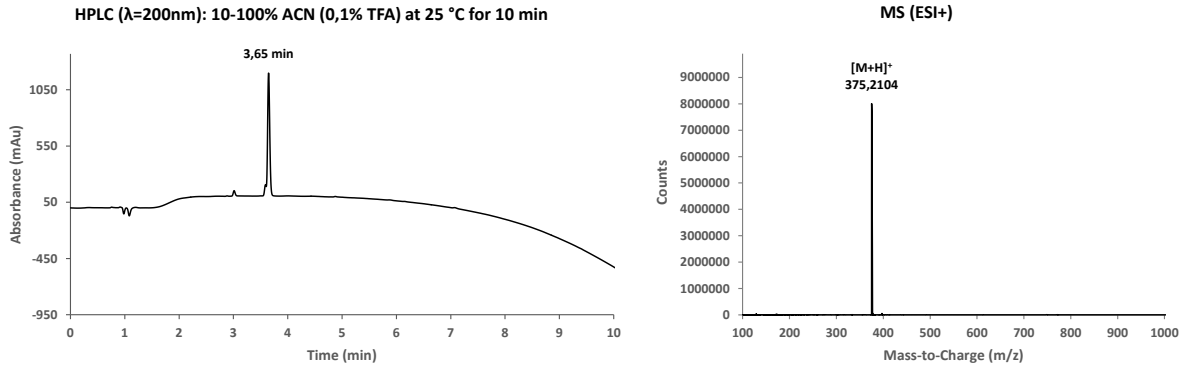

Formyl-Met-Orn-Phe-CME•TFA (CA 4-114)

General procedure for the synthesis of cyanomethyl ester was used from Formyl-Met-Orn(Boc)-Phe-OH (150 mg, 0.28 mmol) to led to the titled activated ester peptide as a white solid *lyophilisate* (47 mg, 35 %).

HPLC: t_R = 4.28 min; **MS (ESI+)**: (m/z) = 478.1809 $[M+H]^+$

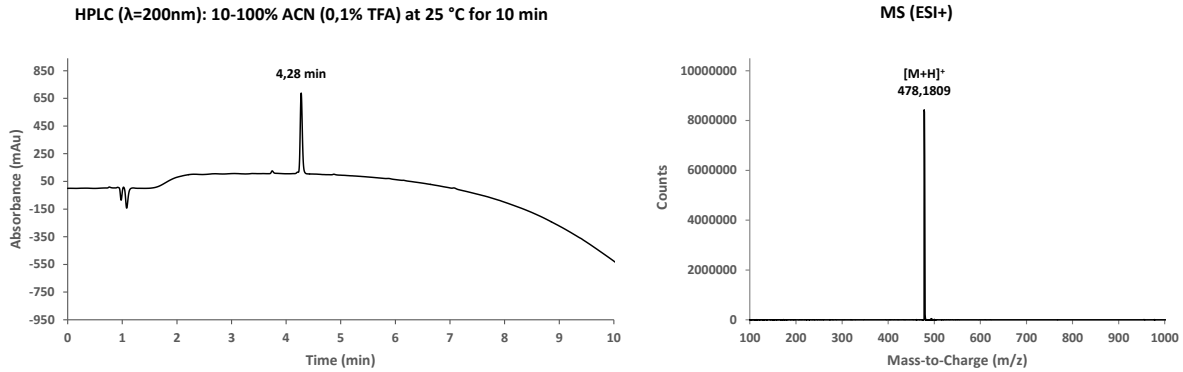

H-Met-Lys-Phe-CME•TFA (CA 4-116)

General procedure for the synthesis of cyanomethyl ester was used from Boc-Met-Lys(Boc)-Phe-OH (150 mg, 0.24 mmol) to led to the titled activated ester peptide as a white solid *lyophilisate* (16 mg, 14 %).

HPLC: t_R = 3.79 min; **MS (ESI+)**: (*m/z*) = 464.1888 $[M+H]^+$

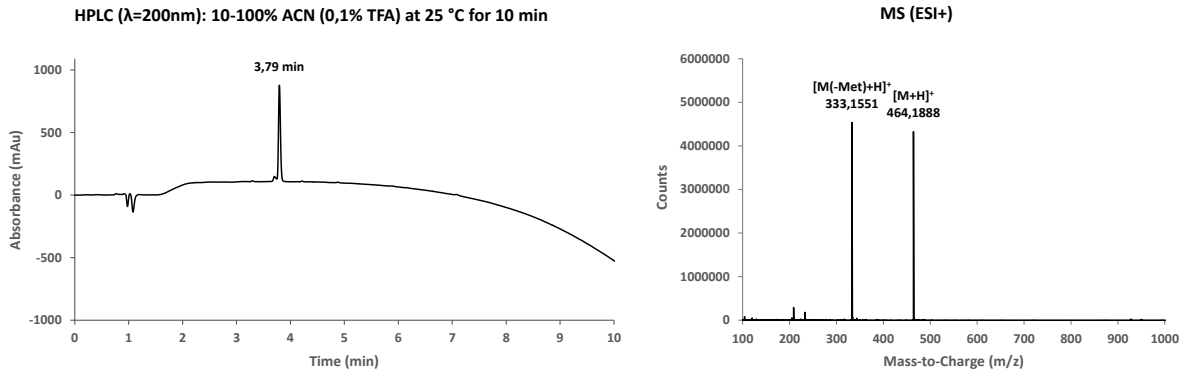

Formyl-Met-Lys-Phe-CBT•HCl (CA 4-142)

General procedure for the synthesis of 4-chlorobenzyl thioester was used from Formyl-Met-Lys(Boc)-Phe-OH (150 mg, 0.27 mmol) to led to the titled activated thioester peptide as a white solid *lyophilisate* (62 mg, 39 %).

HPLC: t_R = 6.49 min; **MS (ESI+)**: (*m/z*) = 593.1595 $[M+H]^+$

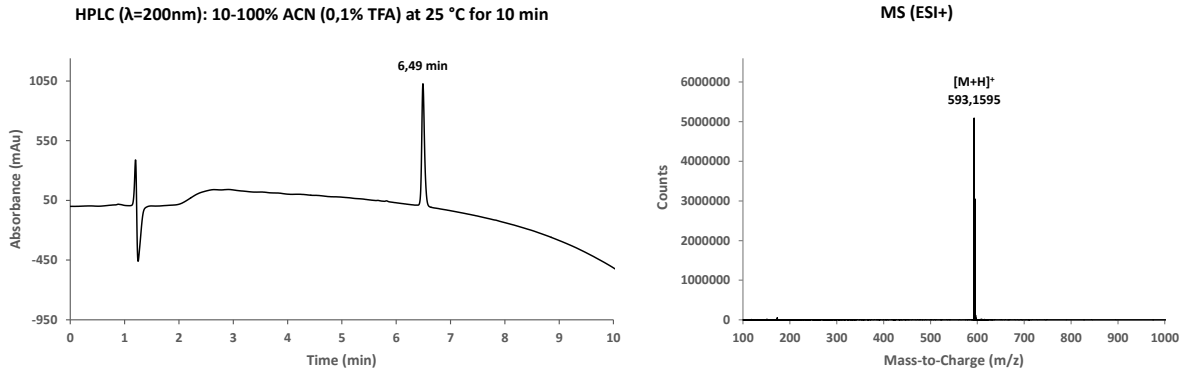

Formyl-Met-Orn-Phe-CBT•HCl (CA 4-144)

General procedure for the synthesis of 4-chlorobenzyl thioester was used from Formyl-Met-Orn(Boc)-Phe-OH (150 mg, 0.28 mmol) to led to the titled activated thioester peptide as a white solid *lyophilisate* (44 mg, 27 %).

HPLC: t_R = 6.51 min; **MS (ESI+)**: (*m/z*) = 579.1505 $[M+H]^+$

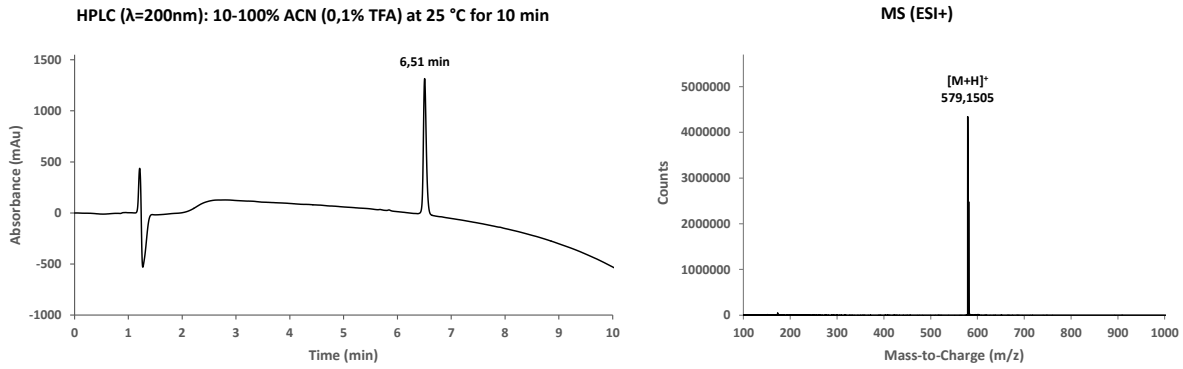

H-Met-Lys-Phe-CBT•HCl (CA 4-146)

General procedure for the synthesis of 4-chlorobenzyl thioester was used from Boc-Met-Lys(Boc)-Phe-OH (150 mg, 0.24 mmol) to led to the titled activated thioester peptide as a white solid *lyophilisate* (46 mg, 34 %).

HPLC: t_R = 5.81 min; **MS (ESI+)**: (*m/z*) = 565.1642 $[M+H]^+$

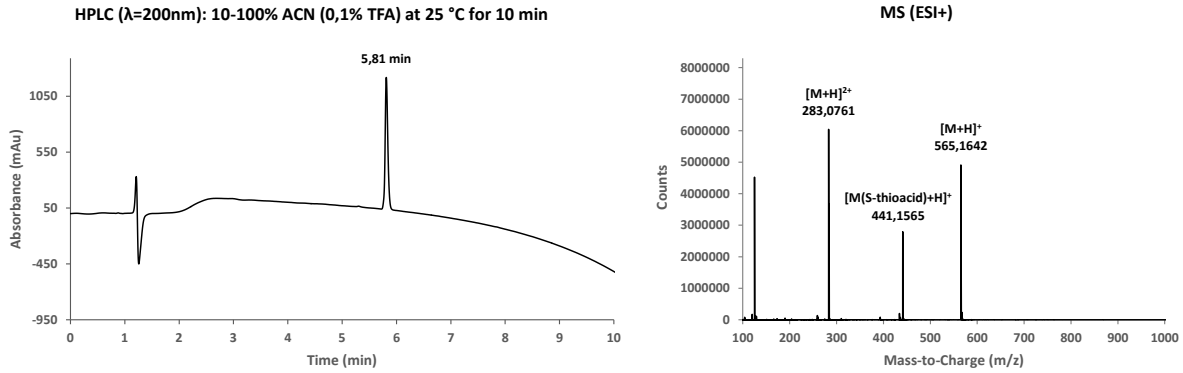

Acetyl-Lys-Phe-CBT•HCl (CA 4-148)

General procedure for the synthesis of 4-chlorobenzyl thioester was used from Acetyl-Lys(Boc)-Phe-OH (120 mg, 0.28 mmol to led to the titled activated thioester peptide as a white solid *lyophilisate* (56 mg, 43 %).

HPLC: t_R = 6.15 min; **MS (ESI+)**: (*m/z*) = 476.1411 $[M+H]^+$

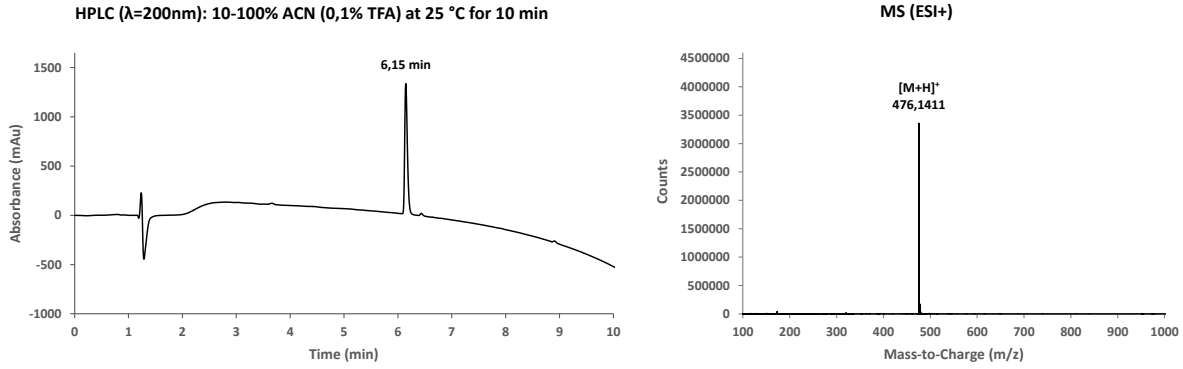

Inhibition du ribosome bactérien par les peptides naissants et antimicrobiens

Le ribosome bactérien (70S) catalyse la formation de la liaison peptidique et représente une cible majeure pour les antibiotiques. Le peptide synthétisé passe à travers le tunnel de sortie de la sous-unité 50S du ribosome avant d'être libéré dans le cytoplasme. Des peptides spécifiques peuvent inhiber la traduction en agissant en *cis* (peptides naissants) ou en *trans* (peptides antimicrobiens riches en proline, PrAMPs) sur ce tunnel.
Il a été montré que les PrAMPs inhibent la synthèse des protéines en se liant au ribosome 70S. Au cours de ma thèse, j'ai résolu les structures cristallines de quatre PrAMPs en complexe avec le ribosome 70S. J'ai ainsi pu révéler que tous ces peptides recouvrent le centre peptidyl transferase (PTC) et se lient avec le tunnel dans une orientation inverse par rapport au peptide naissant. J'ai aussi pu conclure que les PrAMPs inhibent la traduction en bloquant la transition de la phase d'initiation vers l'élongation.
L'arrêt de la traduction induit par le peptide naissant se produit lorsqu'un peptide naissant interagit avec le tunnel, entraînant l'inactivation du PTC. L'arrêt peut être uniquement dû à la séquence du peptide ou peut nécessiter un co-inducteur, tel un antibiotique. Les mécanismes d'action des peptides d'arrêt courts (motifs polyproline ou M+X(+)) restent inconnus. Afin d'étudier ces peptides de manière biochimique et structurale, j'ai formé des complexes ribosomaux bloqués avec un peptidyl-ARNt d'arrêt préparé à l'aide d'un ribozyme appelé flexizyme. J'ai ainsi pu obtenir une structure par cryo-EM d'un 70S bloqué par un motif M+X(+) en présence d'érythromycine et de formuler un modèle expliquant l'inactivation allostérique du PTC.

Antibiotiques, ribosome, biologie structurale, peptides d'arrêt

Inhibition of the bacterial ribosome by nascent chain and free peptides

The bacterial (70S) ribosome catalyzes peptide bond formation and represents a major target for antibiotics. The synthesized peptide passes through the exit tunnel of the large ribosomal subunit before it is released into the cytoplasm. Specific peptides can inhibit translation by acting in *cis* (nascent peptide) or in *trans* (proline-rich antimicrobial peptides; PrAMPs) due to interactions with the tunnel.
PrAMPs were reported to inhibit protein biosynthesis and bind to the 70S ribosome. During my thesis, I solved the crystal structures of four different PrAMPs in complex with the bacterial ribosome, revealing that all peptides cover the peptidyl transferase center (PTC) and bind in a reverse orientation within the exit tunnel relative to a nascent chain. From this, I concluded that PrAMP binding inhibits the transition from initiation towards elongation.
Nascent chain-mediated translational arrest occurs when a nascent peptide interacts with the exit tunnel, leading to the rearrangement and inactivation of the PTC. Arrest can be solely due to the peptide's sequence or may require a small molecule co-inducer, such as a drug. The underlying mechanisms of action for short arrest peptides (polyproline or M+X(+) motifs) remain unknown. In order to study these short arrest peptides biochemically and structurally, I adopted a strategy to form arrested ribosomal complexes through the direct addition of the arrest peptidyl moiety to $tRNA_i^{Met}$ with the help of a small ribozyme known as flexizyme. I was able to solve the cryo-EM structure of a ribosome arrested by an M+X(+) motif in the presence of erythromycin and to propose a model for the allosteric inactivation of the PTC.

Antibiotics, ribosomes, nascent-chain mediated translational arrest, structure biology

Inserm U1212, CNRS UMR 5320
2, Rue Robert Escarpit, 33607 Pessac